Matrix Manipulation to Study ECC Behaviour

Gao Song

Thesis presented in partial fulfilment of the requirement for the degree of

Master of Science in Engineering at the university of Stellenbosch

Study leader: Prof G.P.A.G van Zijl

April 2005

Declaration

I, the undersigned, hereby declare that the work contained in this thesis is my own original work ,except where specifically acknowledged in the text, and that I have not previously in its entirety or in part submitted it at any university for a degree.

Signature…….

Date…….

Synopsis

As a fibre reinforced material, engineered cementitious composite (ECC) has tough, strain-hardening behaviour in tension despite containing low volumes of fibres. This property can be brought about by developments in fibre, matrix and interfacial properties.

Poly Vinyl Alcohol (PVA) fibre has been developed in recent years for ECC, due to its high tensile strength and elasticity modulus. However, the strong interfacial bond between fibre surface and matrix is a challenge for its application. This study focuses on the tailoring of matrix and fibre/matrix interfacial properties by cement replacement with fly ash (FA) and Ground Granulated Corex Slagment (GGCS).

In this study the direct tensile test, three point bending test, micro-scale analysis, such as X-Ray Fluorescence Spectrometry analysis (XRF), Scanning Electron Microscope (SEM), are employed to investigate the influence of cement replacement, aging, Water/Binder (W/B) ratio, workability on ECC behaviour.

This study has successfully achieved the aim that cement replacement by FA and GGCS helps to improve the fibre/matrix interfacial properties and therefore enhances the ECC tensile behaviour. Specifically, a high volume FA-ECC has stable high tensile strain capacity at the age of 21 days. This enables a constant matrix design for the investigation of other matrix influences. The Slag-ECC has a higher tensile strength but lower tensile strain capacity. The combination of FA and GGCS, moderate tensile strength and strain capacity is achieved Both tensile tests and Micro-scale analyses infer that the high volume FA-ECC has an adhesive type fibre/matrix interfacial interaction, as opposed to the cohesive type of normal PVA fibre-ECC.

The different tensile behaviour trend of steel fibre-ECC and PVA fibre-ECC with the FA content is presented and discussed in this research.

The investigations of aging influence indicate that the high volume FA-ECC has a beneficial effect on the properties of the composite at an early stage. However, at a high age, it has some difficulty to undergo multiple cracking and then leads to the reduction of tensile strain capacity. The modified mix design is made with the combination of FA and GGCS, which successfully increases the interfacial bond and, thereby, improves the shear transfer to reach the matrix crack strength. Therefore, an improved high age tensile behaviour is achieved.

The W/B and fresh state workability influence investigations show that the W/B can hardly affect the tensile strain at early age. However, the workability influences on composite tensile strain significantly, because of the influence on fibre dispersion.

Other investigations with regard to the hybrid fibre influences, the comparison of bending behaviours between extruded plate and cast plate, the relation between bending MOR and tensile stress, and the relation between compression strength and tensile strength contribute to understand ECC behaviour.

.

Samevatting

As ‘n veselversterkte materiaal, het ontwerpte sementbasis saamgestelde materiale, taai vervormingsverhardingseienskappe in trek, ten spyte van lae veselinhoud. Hierdie eienskap word bewerkstellig, deur ontwikkelings in vesel, matriks en tussenveselbindingseienskappe.

Poli-Viniel Alkohol (PVA) vesels is ontwikkel vir ECC, as gevolg van die hoë trekkrag en hoë modulus van hierdie veseltipe. Die sterk binding tussen die PVA-veseloppervlak en die matriks is egter ‘n uitdaging vir sy toepassing. Hierdie studie fokus op die skep van gunstige matriks en vesel/matriks tussenvesel-bindingseienskappe deur sement te vervang met vlieg-as (FA) en slagment (GGCS).

In hierdie navorsing is direkte trek-toetse, drie-punt-buigtoetse, mikro-skaal analise (soos die X-straal ‘Fluorescence Spectrometry’ analise (XRF) en Skanderende Elektron Mikroskoop (SEM)) toegepas. Hierdie metodes is gebruik om die invloed van sementvervanging, veroudering, water/binder (W/B)-verhouding en werkbaarheid op die meganiese gedrag van ECC te ondersoek.

Die resultate van hierdie navorsing toon dat sementvervanging deur FA en GGCS help om die vesel/matriks tussenveselbindingseienskappe te verbeter. Dus is die ECC-trekgedrag ook verbeter. Veral ‘n hoë volume FA-ECC het stabiele hoë trekvervormingskapasiteit op ‘n ouderdom van 21 dae. Dit bewerkstellig ‘n konstante matriksontwerp vir die navorsing van ander matriks invloede.
Die Slag-ECC het ‘n hoër treksterkte, maar laer trekvervormingskapasiteit.

Deur die kombinasie van FA en GGCS word hoë treksterkte, sowel as gematigde vervormbaarheid in trek verkry. Beide trektoetse en mikro-skaal analise dui aan dat die hoë volume FA-ECC ‘n adhesie-tipe vesel/matriks tussenvesel-bindingsinteraksie het, teenoor die ‘kohesie-tipe van normale PVA vesel-ECC.

Die verskille in trekgedrag van staalvesel-ECC en PVA vesel-ECC ten opsigte van die FA-inhoud is ondersoek en word bespreek in die navorsing.

Die navorsing toon verder dat die hoë volume FA-ECC goeie meganiese eienskappe het op ‘n vroeë ouderdom. Op hoër ouderdom word minder krake gevorm, wat ‘n verlaging in die trekvervormingskapasiteit tot gevolg het. Met die kombinasie van FA en GGCS, word die vesel-matriksverband verhoog, waardeur ‘n verbetering in die skuifoordrag tussen vesel en matriks plaasvind. Verbeterde hoë omeganiese gedrag word daardeur tot stand gebring.

Navorsing ten opsigte van die invoed van die W/B en werkbaarheid dui daarop dat die W/B

slegs geringe invloed het op die trekvormbaarheid, terwyl die werkbaarheid ‘n dominerende rol speel in hierdie verband.

Verdere studies sluit in die invloed van verskillende vesels, die vergelyking van die buigingsgedrag van geëkstueerde plate en gegote plate, die verhouding tussen buigsterkte en treksterkte, en die verhouding tussen druksterkte en treksterkte dra by tot beter begrip van die gedrag van ECC.

Acknowledgement

The experience of my master's study at University of Stellenbosch in South Africa, from January of 2003 – April of 2005, was unforgettable and enriching.

I would like to thank the following people:

Prof. G.P.A.G. Van Zijl for the supervision of my study and thesis. I really appreciate that Prof. Van Zijl leaded me into this academics field and let me be the member of the ECC research group, as well as for his trust and understanding with regard to the difficulties and frustration attached to the completion of my thesis. Many ideas of this thesis sourced from the meet with Prof. Van zijl. I also appreciate the offer by Prof. Van zijl for leading me to attend the conferences in Italy and the overseas study trip. It was enjoyable and content. I appreciate all the trouble Prof. Van zijl went thought in organising the experimental programme.

Prof. J.V. Retief for his lecture and kindly help of my thesis when I meet the frustration in the experimental data treatment.

Dr. P. Maincon for his lecture and elicitations for my study. It is pleasant to discuss with Maincon since his erudition.

Dr. G.C. Van Rooyen for his lecture of the informatics and many interest tutorials,

Mr. W. P. Boshoff for his work to design the set of the test system and kindly help when I meet the difficulties in the research project. Boshoff also lead me go through stellenbosch make me homefelt to stay in Stellenosch.

Mrs. Mary lotter for her many meticulous helps during my two years study in Stellebnbosch.

A. Layman for his many helps in the experimental projects from serving the sand to weight most materials and preparing my experiments.

Common symbols table

σ_M	First crack stress
σ_u	Ultimate stress
ε_M	First crack strain
ε_U	Ultimate strain
ε_F	Strain capacity
W/B	Water binder ratio
S/B	Sand binder ratio
VA/B	Viscous agent binder ratio
R/C	Reinforced concrete
J_{tip}	Composite crack tip toughness
J_b'	Complementary bridging energy
MOR	Moment of rupture
R.H	Relative humidity
g	Snubbing factor
τ	Interfacial bond strength
β	Fibre slip-hardening coefficient
V_f	Fibre content
V_f^{crit}	Critical fibre content
L_f	Fibre length
d_f	Fibre diameter
G_d	The fibre/matrix chemical bond
FA	Fly ash
GGCS	Ground Granulated Corex Slag

Content table

Chapter 1
Introduction

The properties of normal cementitious materials have been well studied and developed. One of the problems of cementitious materials is the inherently brittle failure resulting from tensile and impact loading. Therefore, fibre is employed as a reinforcing material in cementitious materials. The main use of fibre in cementitious materials is for the sake of enhancing the resistance and toughness in tension and shear. The contribution of fibre reinforcement to building materials can be traced back to the beginning of human civilisation when horsehair or straw were mixed into the mud for bricks and straw mats were used for housing construction in the Far East 4000 years ago. Modern fibre reinforced cementitious materials have been analysed since the 1960's.

In the last decade, a new group of fibre reinforced cementitious composite (FRC), namely Engineered Cementitious Composite (ECC), a class of microstructurally tailored FRC, has been developed. This class of FRC exhibits tough, strain-hardening behaviour in tension, despite containing low volumes of fibres. These properties were brought about by developments in fibre, matrix and processing technology. In addition, the importance of the interaction between these fibres and the matrix, governed by the fibre/matrix interface has been recognised, leading to interface modification techniques to engineer the desired properties. Whereas work in the early 90's focussed on fibre volumes (V_f) of 5% or more, or on the use of expensive, high modulus fibre, for instance high modulus polyethylene fibres, at eight times or more the cost of Poly Vinyl Alcohol (PVA) fibres and steel fibre, the new approach is to tailor the surface of the fibres with an oiling agent (Li et al., 2001).

The present work is focussed on development of matrix and interface properties. It follows Li (1992), who introduced the terminology of "Performance Driven Design Approach (PDDA)". The aim of PDDA is to form the relationship between the structural requirements and the material performance. The material's optimisation can be practise to achieve the targeted composite performance and therefore the particular application required.

As a hydrophilic fibre, PVA fibre has a strong chemical bond with surrounding hydrated cement. This, as well as its filament microstructure, causes breaking of fibres rather than fibres pulling out from the matrix. When fibres break, stress re-distribution leads to progressive fibre breakage in a section, causing abrupt, brittle failure of the section in tension as a whole. However, it is well known that Coulomb-friction type behaviour maintains a resistance despite the initial chemical bond, or adhesion, being lost. This type of behaviour between fibre and matrix is preferable, as all resistance is not lost at a fibre after exceeding the virgin strength limit, hence enabling stress transfer to surrounding fibres to restore global

equilibrium with external loads. The mechanism to activate such a response is slippage, or pull-out of fibre from the matrix.

In this study a different way of achieving such pull-out behaviour is investigated. At the same time, it is aimed to reduce the cost of ECC, by using cement replacement in the form of fly ash (FA) and ground granulated Corex slag (GGCS). It attempts to exploit the spherical geometry of FA to modify the fibre-matrix interface, to enable fibre pull-out. To overcome the low strength development rate when FA is used to replace cement, slag is added.

The research focuses on the influence of the varied type and content of cement replacement on ECC performance. The investigation is based on the tensile behaviours. Direct tensile, as well as three point bending responses and micro-scale analyses, such as SEM analysis and XRF analysis are employed. Of particular interest for this study is also the sensitivities of this kind of ECC material, such as aging influence, matrix W/B influence, fresh state workability influence, etc.

Chapter 2 introduces the survey of state-of-the-art theory, which involves the definition of fibre reinforced materials, the performance driven design approach, correlative terminologies, the basic theoretical requirement for ECC performance achievement, the role of the materials, influences on ECC performance, and the application concept. Chapter 3 introduces the experimental program and method, also specifying the materials used in the present research. Next, Chapter 4 describes the experimental procedures.

Chapter 5 presents the experimental results of the research, including the PVA fibre ECC series tests, steel fibre ECC series mixes and sensitivity investigation tests. Contrasting tensile behaviour trends between PVA fibre ECC and steel fibre ECC with FA contents will be presented and discussed in this chapter.

Chapter 6 investigates the tailoring of matrix and fibre/matrix interfacial properties by cement replacement with FA and GGCS. The matrix properties have an influence not only on composite tensile strength but also on multiple crack development. The tensile strain capacity is controlled by the magnitude between matrix crack tip toughness J_{tip} and the fibre commentary bridging energy J_b'. The latter is controlled by fibre/matrix interfacial properties. The major parameters controlling the interfacial properties are fibre/matrix chemical bond G_d, the frictional force τ, and fibre slip-hardening β. The investigation of the tailoring of interfacial properties is based on our understanding of these three parameters.

Chapter 7 describes an important influence on ECC in practical application, namely aging. The investigation involves ECC mix with pure fly ash and the combination of GGCS and fly ash. The relationship between fibre/matrix interfacial properties and ECC performance is described in order to explain the varied high age properties.

Chapter 8 presents the influence of the properties of the matrix water binder ratio (W/B) and fresh state rheology on ECC tensile behaviours. The W/B influences only on tensile strength, but not the strain capacity, if the fresh state workability remains uniform. On the other hand, the workability has a significant influence on ECC strain capacity through its influence on the fibre distribution.

Chapter 9 introduces four facts contributory to understanding ECC properties. They are the hybrid fibre-ECC investigations, the ratio of bending MOR and tensile stress, the comparison of bending behaviours between cast specimens and piston–extruded specimens, and the relation between specimen compression strength and ultimate tensile stress.

Chapter 10 present the conclusions of this research.

Chapter 2
Review of theory

Before discussing the specific experimental program and results, it is imperative to introduce some background knowledge from the current level of understanding of ECC. It is also important to be acquainted with investigations carried out by other researchers relating to the current research. This chapter encompasses information pertaining to terminology, design method of Engineered Cementitious Composites (ECC), property principles of ECC and some application principles of ECC.

Review of the theoretical research, which follows, is based on the literature study.

2.1 Useful terminology

Fibre Reinforced Cementitious Composite (FRCC) as a type of material has been developed for more than 40 years. The idea of ECC was developed since 1993 (JCI-DFRCC Committee, 2003). There are certainly some specific definitions and terminology that need to be introduced to distinguish ECC from normal FRCC.

2.1.1 Classification of FRCC (Fibre Reinforced Cementitious composite)

There are various systems of classification of FRCC. For instance, Shah suggested two categories of fibre reinforced cementitious composite, which are: conventional cast materials and High Performance Fibre Reinforced Cementitious Composites (HPFRCC). The former is a kind of material with a small fibrous bulk, less than 2% by volume, and improved post-crack ductility. The HPFRCC is produced by specialized techniques based on analysis and characterized by elasticity, strain hardening, and post-peak softening (Shah et al., 2004).

The JCI-DFRCC Committee defines the several classes of fibre reinforced cementitious composite, including FRCC, DFRCC, HFRCC, and ECC. The present research inclines toward this method of definition. The definitions of some chief FRC classes will be introduced as follows:

FRCC (Fibre Reinforced Cementitious composite) is the holistic definition of the entire class of fibre reinforced cementitious composites. It includes DFRCC, HPFRCC, ECC and other fibre reinforced cementitious composites (JCI-DFRCC Committee, 2003). The development of steel fibre reinforced concrete began in the 1960s and expanded. Polymeric fibres were

used in the 1970s, glass fibre in the 1980s, and carbon fibre started to draw much attention in the early 1990s (Li, 2002). Normal FRCC shows crack localizing in direct tension.

DFRCC (Ductile Fibre Reinforced Cementitious Composites) is a class of FRCC that is characterized by multiple cracking in bending or both bending and tension, strain softening or hardening, and slightly ductile response. DFRCC has unique and multipurpose structural applications, such as damage reduction, damage tolerance, energy absorption, crack distribution, deformation compatibility, and delamination resistance (JCI-DFRCC Committee1, 2003).

HPFRCC (High Performance Fibre Reinforced Cementitious Composites) is a class of DFRCC material, which displays ductile response, multiple cracks and strain hardening in tension as well as bending (JCI-DFRCC Committee1, 2003). High performance means that high strength, high ductility, high durability, specialized processing or interfacial tailoring techniques are employed. The distinguishing criteria that differentiate it from a normal FRC are the high tensile strain capacity, minimized fibre content, and limited crack width (Li, 2003 and Shah et al., 2004).

ECC (Engineered Cementitious Composites) is a new class of HPFRCC. There are various HPFRCC such as ECC, Cardifrc, and SIFCON (JCI-DFRCC Committee, 2003) that have been investigated. Li started investigating ECC material in 1993 and suggested that ECC exhibits pseudo strain hardening with a strain capacity of more than 3%, in spite of the relatively low fibre content of 2% to 3% by volume (JCI-DFRCC Committee, 2003), which is kept low for the sake of processibility. This means ECC can easily employ typical mixing and casting techniques, and thereby reduce costs. The important difference between HPFRC and ECC is that ECC contains just enough bulk of material, especially fibre to achieve the minimized performance requirement, which normally will be defined by its various application purposes. ECC materials are typically developed for applications in large material volume usage by the cost sensitive construction industry.

As a kind of new material, ECC materials are characterized by various properties for various application purposes. So there are actually various definitions of ECC property requirements and mix design, such as fibre content 2%-3% (JCI-DFRCC Committee, 2003), with ductility ranging from 3% to 6%.

In the present research, ECC is defined as a kind of FRCC material that exhibits tough, strain-hardening behaviour in tension, and tensile strain capacity larger than 3 %.

In the present research, some specific ECC materials are also defined herein, including FA-ECC, Slag-ECC and FA & Slag-ECC, which are series ECC mixes with a large fraction by mass of Fly Ash (FA), Ground Granulated Corex Slag (GGCS), and the combination of FA and GGCS as cement replacements respectively.

Since ECC is an important HPFRC material type, the high performance and other characteristics of ECC will be introduced in subsequent sections below.

Various HPFRCCs such as SIFCON and Ductal will not be introduced because they are

irrelevant to the present research.

A comparison between FRC, HPFRCC and ECC is made in Table 2.1.

Table 2.1 Comparisons between FRC, HPFRCC and ECC (Li, 2002)

	FRC	Common HPFRC	ECC
Composite Design Methodology	NA	Use high V_f	Micromechanics based, minimized V_f for cost and processibility
Fibre	Any type V_f usually< 2%; d_f (steel) about 500um	Mostly steel, V_f usually > 5%; d_f About 150um	Tailored, polymer fibre most suitable; V_f usually < 2%; d_f < 50um
Matrix	Coarse aggregates used	Fine aggregates used	Controlled for matrix toughness and initial flaw size; fine sand used
Interface	Not controlled	Not controlled	G and τ controlled
Tensile behaviour	Strain softening	Strain hardening	Strain hardening
Tensile strain capacity	0.1%	<1.5%	>3%; 8% demonstrated
Crack width	Unlimited	Typically several hundred um, unlimited for ε >1.5%	Typically <100um during strain-hardening
Processing	Self-compaction demonstrated; Extrudability demonstrated	Self-compaction impossible due to high V_f often requiring high frequency vibration Extrudability demonstrated	Self-compaction demonstrated; Extrudability demonstrated

2.1.2 Characteristics of ECC

Strain hardening/pseudo strain hardening and strain softening: As a specific terminology, strain hardening/ pseudo strain hardening describes a phenomenon where tensile stress increases consecutively even after first cracking. However, strain-hardening of ECC is different from metallic materials, so the terminology pseudo strain hardening is used instead. If transmitted tensile stress reduces after first crack, it is described as strain softening. This phenomena are illustrated in Figure 2.1.

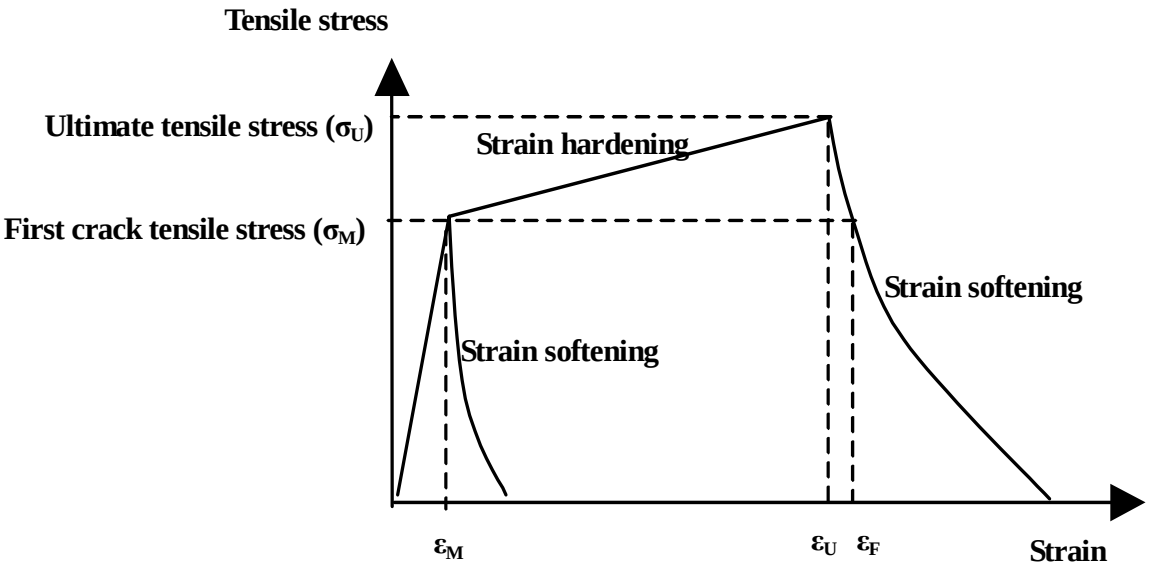

Figure 2.1 Definition of first cracking stress σ_M & strain ε_M, ultimate stress σ_U & strain ε_U, stress capacity ε_F, strain softening, and strain hardening.

Multiple cracks: Cracks are consecutively formed after first cracking under direct tension, and ultimately become evenly spaced in parallel. Deformation is often named in terms of strain instead of crack opening displacement. Multiple cracking results in the improvement in composite properties such as "ductility, toughness, fracture energy, strain hardening, strain capacity, and deformation capacity under either tension, compression, or bending" (JCI-DFRCC Committee, 2003). Multiple cracking in direct tension is also used to distinguish HPFRCC and normal DFRCC. Normal DFRCC does not show multiple cracking in direct tension but in bending tests.

Crack spacing of saturated multiple cracks: Under direct tension, the spacing between multiple cracks continues to decrease until saturation occurs.

Crack width: Crack width is the width of a crack when the cracks open at a constant tempo as tensile strain keeps on increasing.

First cracking strength: First cracking strength σ_M is the stress stage where the first crack is formed, under direct tension, and first cracking strain ε_M is the corresponding strain.

Ultimate tensile strength: Ultimate tensile strength σ_U is the maximum stress achievable under direct tension after first crack, and tensile strain is the corresponding strain. The ultimate tensile strain ε_U is a direct measurement of material ductility. Relatively, tensile strain capacity ε_F is defined as the tensile strain when the corresponding tensile stress reaches the first crack stress again in the strain softening stage.

Tension toughness, compression toughness, and flexure toughness: Toughness portrays energy absorption of the composite, which is given by the area below the stress-strain curve or load displacement curve either in tension, compression, or flexure. In practice, toughness is calculated based on the area up to a prescribed strain or displacement.

Fibre bridging function: Fibre bridging function is a composite property, which describe that the load has transmitted by fibre across a crack. When a crack occurs, load carried by the matrix in the crack zone is carried by bridging fibre and the matrix at the end of the crack becomes stress free, which means composite stress is transmitted through matrix and/or fibres. The bridging function is a basic parameter that governs ECC strain hardening/softening behaviour in tension, compression, or flexure.

Critical fibre volume fraction: Critical fibre volume fraction is associated with fibre, matrix, and interfacial properties. Under the critical fibre volume fraction, composites cannot form multiple cracking and strain hardening in direct tension.

Snubbing factor: Snubbing factor (g) is a parameter to describe the fibre snubbing pitch. Snubbing means a phenomenon of enhancing the bond properties when a fibre is embedded in matrix with an angle to the crack.

This is normally given by equation $g = \frac{2}{4 + f^2}\left(1 + e^{\pi f/2}\right)$, (2.1)

where f is the snubbing coefficient (Li & Maalej,1996), which has to be established experimentally for a specific mix. The snubbing factor increases with the interfacial bond and fibre aspect ratio.

2.2 Performances driven design approach (PDDA)

In present research, PDDA (Performances Driven Design Approach) was employed to design these mixes. The idea of the performance driven design approach was first introduced by V. C. Li. This is basically an approach where the performance and functionalities of a given structure or structural component are specified, and a material has to be designed specially so that the properties can meet the expected structural demand. That is a method to ensure a direct link between the material structure, material composition and the structural performance, to optimise the materials resulting in tailoring of the fibre, matrix, and fibre matrix interface, and hence to obtain the targeted requirements.

The design approach is illustrated in Figure 2.2. To establish the balance between structure performance and material requirement, PDDA is employed to unify the relationship between microscopic properties to the necessary composite properties needed to reflect actual structural performance. Suggested by Li (1992), the performance of target structural component may be given as durability, seismic resistance, deflection control, light-weight, and reliability. The properties of the material may be ductility, toughness, notch sensitivity, density, and wear resistance. The material structure typically includes the microstructure of fibre, matrix, and fibre/matrix interface respectively. In subsequent sections, the concept and method of tailoring of material microstructure will be discussed.

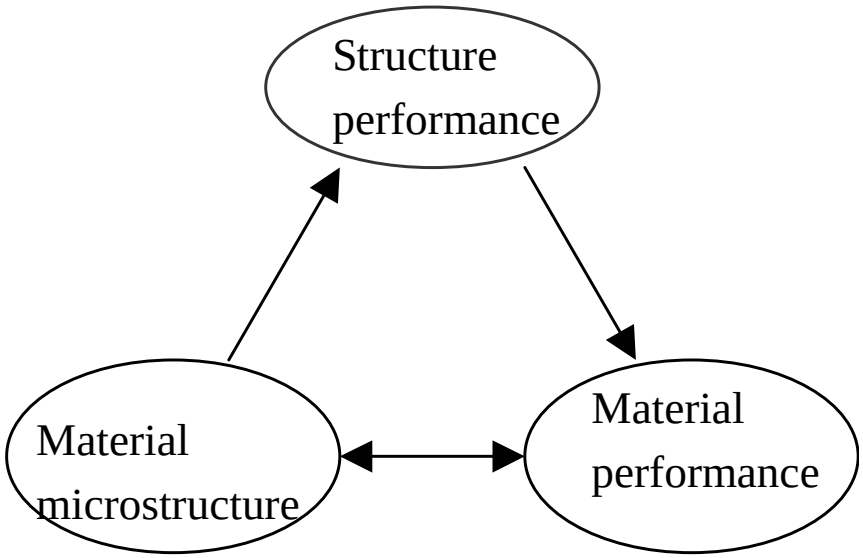

Figure 2.2 Performances driven design approach (Li, 1992)

2.3 Micromechanism theory of ECC

To relate material mix design to material properties based on PDDA, it is useful to establish the basic understanding of the Micromechanism theory of normal ECC and also the influences on composite properties. The micromechanisms of FA-ECC and Slag-ECC will be discussed in a subsequent chapter.

2.3.1 Griffith-type crack and steady state flat crack

The Griffith-type crack is a crack type in brittle material where, when the crack reaches the critical opening, the crack will continue growing, but with a decreased stress needed to propagate the crack, and the rate of the growth will be accelerated. Li suggests (2003) that if the complementary bridging energy J'_b is very small, it means that the interfacial bond is not strong enough, so that the ultimate strength is low, or too strong, resulting in fibre breaking and a small critical crack opening. The crack will form as a Griffith-type crack, resulting in a composite failure with reduced stress, or strain softening.

In other cases, if the J'_b is large enough, the opening of cracks keep a constant tempo and most fibres in the crack zone remain unbroken as the crack propagates under a constant, steady state stress. This means that tensile stress can be transferred to another weak zone, resulting in the multiple cracking (Li, 2003).

2.3.2 Theory requirement for strain hardening and multiple cracking

To achieve the composite performance of normal ECC materials, the high composite ductility and strain hardening stages need to be achieved. The requirements to attain strain hardening are multiple-cracks and steady state cracking. Kanda and Li (1998) suggested two important complementary requirements, which are a first cracking stress criterion and a steady state cracking criterion. Both are necessary for multiple cracking. If either cannot be satisfied, material failure will be localized. For first crack stress, if the first cracking exceeds the maximum tensile stress available from the fibre tensile stress of a matrix crack. The first crack will be created with bridging fibres being pulled out or broken and the stress will drop suddenly.

The first crack stress is highly correlated to the matrix flaw size and matrix toughness. If the flaw size is small and results in a Griffith crack, first crack stress is decreased approximately with a rate of the square root of the flaw size (Kanda & Li, 1998). This means that the FA-ECC has a lower first stress, which also has been proven by the experimental result in the present research.

In ECC, matrix cracks open with fibre bridging across the crack edges. During the cracking, the tensile stress increases when the fibre and matrix interface debond (fibre adhesive failure type) and crush of the transition zone with fibres stretching (the fibre cohesive failure type). The maximum fibre bridging stress σ_o is the stress at the peak in Figure 2.3. Maximum fibre bridging stress σ_o is equal to ultimate direct tensile stress σ_u in tensile stress-strain curve. Because the ultimate tensile stress occurs at the stage when the matrix is divided into several segments by parallel cracks, tensile load is all carried by bridging fibres at the ultimate crack zone. Thus, fibre in this zone will be supported by ultimate frictional force between fibre and matrix.

The first requirement can be expressed as the first matrix crack stress $\sigma_{fc} < \sigma_o$.

When the tensile stress increases, with the matrix cracking, due to the amount of applied load, the crack edges crush flatly to a state of cracking stress and then the steady cracking occurs. The second requirement for multiple cracking formation is steady state cracking. Li (1998), Marshall and Cox (1988) provide an inference of steady state stress σ_{ss} from the equation (2.2) to (2.6).

$$J_{tip} = \sigma_{ss}\delta_{ss} - \int_0^{\delta_{ss}} \sigma(\delta)d\delta \qquad (2.2)$$

where σ_{ss} = matrix steady state cracking stress, δ_{ss} = strain corresponding to σ_{ss} and J_{tip} is the composite crack tip toughness.

Certainly, σ_{ss} is less than σ_o. Then the composite crack tip toughness should also be smaller than the complementary bridging energy J'_b, which also can be named as complementary energy and can be defined with the following equation (2.3):

$$J_b^{'} = \sigma_0 \delta_0 - \int_0^{\delta_0} \sigma(\delta) d\delta \tag{2.3}$$

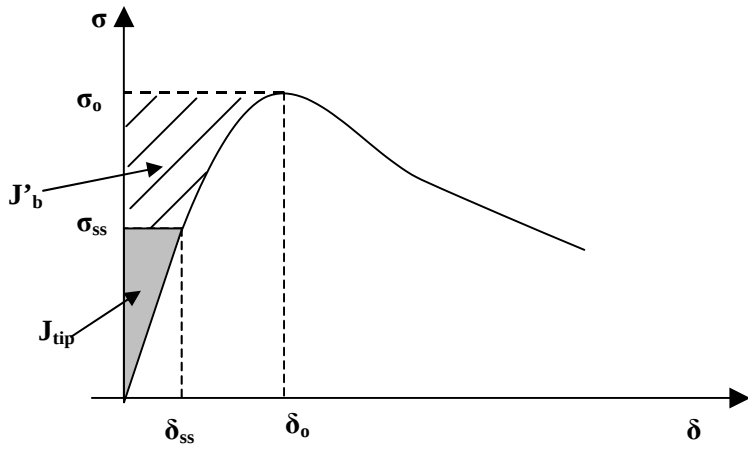

Figure 2.3 The single fibre pull-out bridging stress-displacement curve of ECC

Equation (2.3) interprets the external energy supply that is dissipated by the deformation of the inelastic processes of fibre deformation/rupture and interface debond and slippage of the bridging fibres across the crack (Li, 2002a). The relationship of J_{tip} and J'_b is illustrated in Figure 2.3. The second requirement can be described with the following equation (2.4)

$$J_{tip} < J_b^{'} \tag{2.4}$$

It is apparent that the method to achieve multiple cracking is to keep a sufficient margin between complementary energy J'_b and crack tip toughness J_{tip}. This can be achieved by reducing the crack tip toughness J_{tip} or increasing the complementary energy J'_b.

J_{tip} can be approximated as the matrix toughness when the fibre bulk is less than 5 % or 3%(Li, 1998 and 2002). That is

$$J_{tip} = K_m/E_m \tag{2.5}$$

where K_m is fracture toughness and E_m is elastic modulus. So the second requirement can also be expressed as equation (2.6), which indeed is based on energy balance.

$$\frac{K_m^2}{E_m} \le \sigma_0 \delta_0 - \int_0^{\delta_0} \sigma(\delta) d\delta \tag{2.6}$$

If the first crack stress is low, which means the matrix has a large flaw size, the first requirement can be achieved through matrix tailoring by adding an artificial flaw. However, if the energy balance is not satisfied, the crack may expand with increasingly large crack spacing so that the fibre will either rupture or pull-out.

The tailoring of material microstructure can be divided into three methods, which are matrix

tailoring, fibre tailoring, and interfacial tailoring. For example, Wang and Li attempted matrix tailoring by tailoring the pre-existing flaws in the matrix (Wang & Li, 2004). Li and his co-workers (1998 and 2002) used fibre oiling to tailor fibre. The Extrusion technique and some other techniques can be seen as interfacial tailoring through densification. In the present research, cement replacement used in the matrix tailored both matrix and interface, if one considers that the cement replacement modified the fibre failure type.

Furthermore, the relationship between the composite performance in terms of the ultimate tensile stress (σ_u) and the micro-mechanical parameters g, the snubbing factor, and τ, the ultimate shearing resistance between fibre and matrix, have been modelled as follows (1990 and Soroushian & Lee, 1990):

$$\sigma_u = 0.405\, V_f\, g\, \tau \frac{L_f}{d_f} \tag{2.7}$$

In equation (2.7), it is assumed that the snubbing factor is equal for the same fibre in the various matrices used in present research, produced by normal casting and vibration. The interface shearing resistance (also named interfacial bond strength) τ is solely responsible for variations in the composite ultimate bridging strength σ_u, found through direct tensile testing of the various specimens. However, the interfacial shearing resistance τ is only the ultimate frictional bond but not the only parameter to describe the fibre/matrix interfacial properties.

There are three main parameters to describe fibre/matrix properties, which are chemical bond Gd, interfacial bond τ, and slip-hardening coefficient β. Fibre/matrix interfacial properties will be presented next.

2.4 Interface properties

From the multiple cracking requirements introduced in section 2.3, matrix tailoring can satisfy the first requirement, but for the second requirement, interfacial tailoring needs to be used. Actually, the interfacial bond property is the most important parameter of ECC. Interfacial bond properties can be tailored by modifying the fibre surface and modifying the transition zone. Before introducing the interfacial-tailoring concept, the basic properties of fibre/matrix interface, mechanism and failure types will be introduced below.

2.4.1 Transition Zone and Fibre/matrix interaction type

The transition zone represents a weak zone between fibre and matrix, due to the higher porosity of the microstructure caused by the rapidly developed CH crystal layer of cement

hydration production. The transition zone has a higher porosity because of the “bleeding and inefficient packing of cement particles” (Chan & Li 1997) while it is fresh, resulting in a favoured growth of CH crystals in the zone close to the fibre surface. Certainly, the size of the transition zone can be diminished by tailoring the packing density and hydration product around the fibre. It is also expected that densification of the transition zone may improve the transition zone strength, resulting in higher interfacial bond. The transition zone is normally recognized to be largely responsible for bonding properties and is the explanation of bond strength development (Chan & Li, 1997). However, if the adhesive strength is satisfactorily lower than the strength of transition zone, then the slippage will occur at the fibre/matrix contact surface rather than the break down of transition zone structures. Therefore, adhesion may control the fibre interfacial failure. For such a failure type, transition zone strength may not be effective during the fibre debonding process.

It is worthwhile to introduce two basic fibre/matrix interaction types used to describe fibre interfacial failure, which are adhesion and cohesion. Adhesion is a model describing fibre debonding by frictional sliding between fibre surface and transition zone. Cohesion is used to describe the failure type that happens in a transition zone, which means break down of the transition zone itself, which is partly driven out by fibre pull-out.

Figure 2.5 (a) illustrates the fibre failure adhesive type. When a fibre bears a load beyond peak bridging stress (which is actually the Coulomb friction between fibre surface and transition), fibre will be pulled out and keep the equilibrium between tensile load and shear resistance at the transition zone. Certainly, interfacial adhesion (shear resistance) should be lower than the transition zone cohesion in this condition.

In the cohesive type featured in Figure 2.5 (b) a fibre pulls out by slippage along the outside perimeter of the transition zone.

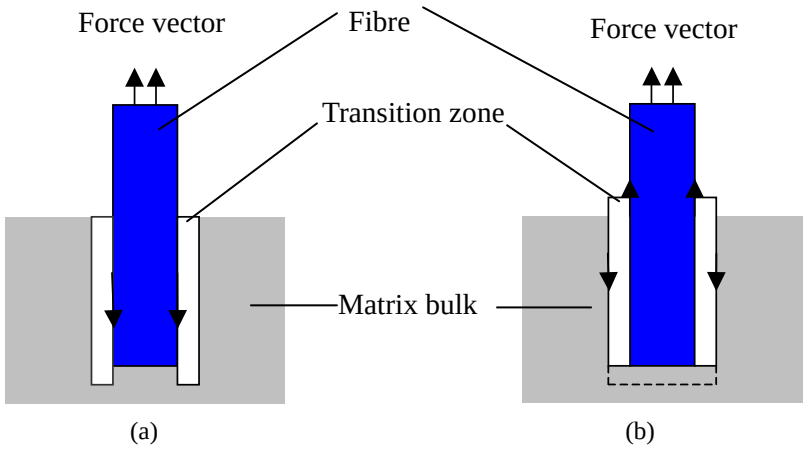

Figure 2.5 Schematic display of the realization of two interface failure types. (a) shows adhesive type and (b) shows cohesive type

Chan and Li (1997) verified that for brass fibre, bond failure is the cohesive type and for steel fibre and polyethylene fibre, bond failure is the adhesive type. However, bonding with PVA

fibre cannot be simply determined as adhesive type bonding, due to very strong chemical interface bonding.

It needs to be mentioned that both cohesion and adhesion latency exists in all fibre reinforced materials. Depending on fibre types and matrix constituents, either the adhesive or the cohesive type, or even both of bonding failure will occur. Figure 2.6 shows the section details of fibre, fibre/matrix interface.

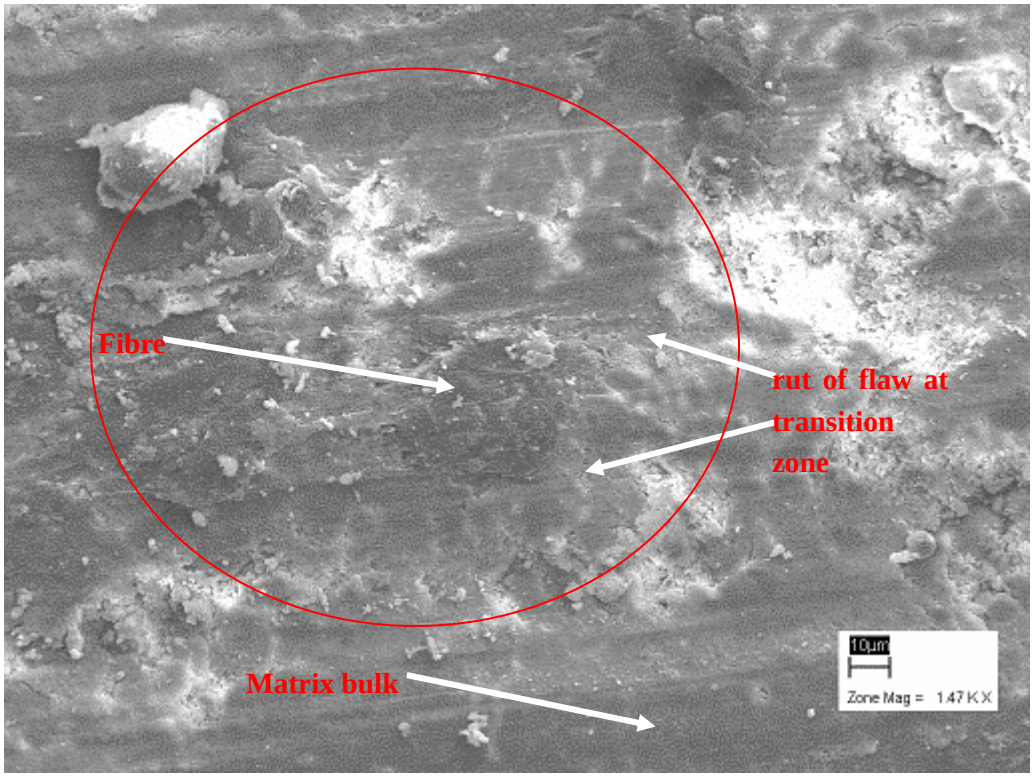

Figure 2.6 The SEM photo shows the fibre, transition zone, and matrix

2.4.2 Parameters to describe the interfacial properties

There are three main parameters controlling the fibre/matrix interfacial properties, which are: chemical debonding energy G_d, frictional bond strength at the beginning of fibre slippage τ_o, and fibre slip-hardening coefficient β.

The chemical bond can be determined via a single fibre pull-out test shown in Figure 2.7. Redon et al (2001). reported the determination of chemical bond G_d and pure frictional bond strength τ_0 in the case of nonchemical bond fibre by means of a single fibre pull-out load-displacement curve, as shown in Equation (2.8).

$$G_d = \frac{2(p_a - p_b)^2}{\pi^2 E_f d_f^3} \tag{2.8}$$

where (P_a-P_b) is the distance between two points where the fibre pull-out load drops suddenly through in a single fibre pull-out load-displacement curve (Figure 2.7), and E_f = fibre axial

Young's fibre; and d_f = fibre diameter (Redon et al., 2001).

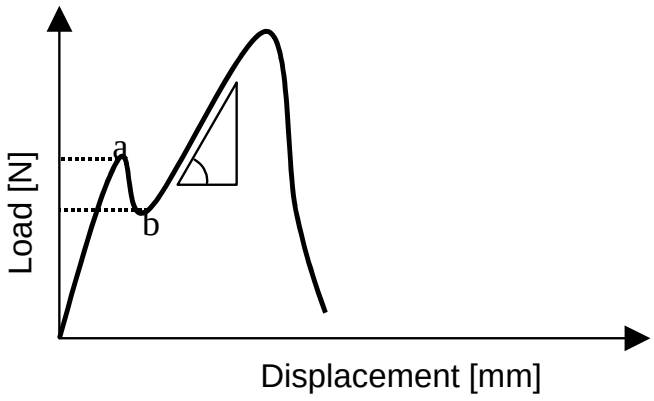

Figure 2.7 The single fibre pull-out test load-displacement curve (Redon et al., 2001)

In the case of nonchemical bond between fibre and matrix, such as steel fibre or polyethylene fibre, the frictional bond strength at the beginning of fibre slippage can be determined by $\tau_0 = P_b/\pi d_f l_e$ with P_b close or equal to P_a, d_f are fibre diameter, and l_e is the embedment length. That means point a closed or equal to point b in Figure 2.7(Redon et al., 2001).

Shah (2004) studied about fibre debonding processes and summarized these as follows: when fibre was impacted by tensile stress, adhesive bond which can be seen as kind of chemical bond for PVA fibre increased to a peak value and then the fibre debonds and pulls out in the certain frictional stress, which is lower than that peak adhesive bond. The frictional stress was generally assumed as a matrix-constant parameter. However, this parameter can be modified by a slip-hardening relationship with fibre pull-out by means of the damage process as fibre under slippage. The damage can be assumed as the damage on fibre surface and/or the transition zone. Li et al. (2001) described and defined a parameter β to characterize the slip-hardening behaviour during fibre pull-out. Redon et al. calculated β, which is a linear relationship to the grading of fibre pull-out load-displacement curve (Figure 2.7). Slip-hardening normally occurs with fibre, which is less hard than the surrounding normal matrix, such as polymer fibre. For PVA fibre, the slip-hardening behaviour often leads to incomplete pull-out of the fibre due to fibre rupture.

However, except these three parameters introduced above, there are certainly some other parameters, such as snubbing factor and fibre embedment length.

2.5 The role of materials in ECC

From the discussion in previous sections, it is clear that the development of ECC from FRC was made by tailoring the properties of fibre, matrix, and interface between fibre and matrix. The way to tailor matrix and interface is to optimise the materials used in the mix, such as fibre, cement replacement, graded sand content, and even mix additives like superplasticizer and viscous agents, resulting in development of matrix and fibre/matrix interface. Hence, the

composite failure type converts from brittle to ductile failure. The roles of the fibre, cement-replacement materials and sand in ECC are very important in ECC behaviour and will be presented below.

2.5.1 The role of fibre in ECC

The high cost of high performance fibre such as PE fibre limits commercial applications. The relatively higher strength and higher modulus of PVA fibre above those of other low cost fibres, such as Nylon and polypropylene fibre, showed PVA fibre to be most suitable for ECC in the present research.

The most important role of fibre mixed into brittle matrix is to enhance its toughness, which needs the fibre to carry tensile load after the matrix has cracked. The fibre chiefly enhances fracture toughness rather than tensile strength (Shah, 2004). For various HPFRCC materials, variation in fibre content and properties controls various performances. For instance, HPFRCC materials with large fibre content show extremely high tensile stress and strain capacity, steel fibre reinforced FRC (SFRC) shows high tensile stress but relatively lower strain capacity, and ECC with moderate fibre content shows relatively high tensile strain capacity but lower tensile stress than HPFRCC and SFRC.

How the fibre works in fibre reinforced materials needs to be investigated. In this section, the characteristics of fibre bridging function, fibre failure type, fibre critical content, and hybrid fibre properties will be introduced.

2.5.1.1 Bridging function

The fibre bridging function is the basic property of fibre-reinforced material. Fibre bridging provides traction to a crack and transfers tensile stresses across the crack. Coulomb-friction type behaviour with lower adhesion, or chemical bonding between fibre and matrix, is preferable. Thereby, the low chemical bond is overcome, but not all resistance lost, enabling fibre-matrix slippage accompanied by continued stress transfer to restore global equilibrium with external loads. Due to fibre bridging function ECC exhibits smaller crack widths and delayed cracking at the same stress level. This is beneficial to activate the aggregate interlock on a crack, and reduction in shear modulus after cracking can be avoided. Another benefit for ECC material mix with steel reinforced concrete is that ECC provides the transmission of stresses across a crack; thereby it shares the tensile stress with the steel reinforcement. This, for example, leads to the improved ultimate stress capacity and ductility of a structural member (JCI-DFRCC Committee, 2003).

2.5.1.2 PVA fibre pull-out or rupture

As a hydrophilic fibre, PVA fibres have a strong affinity to the hydroxy group existing in the matrix-hydrated product around the fibres. This creates a strong chemical bond between fibre and matrix, which is caused by strong chemical adhesion between fibre and matrix. The strong chemical bond of PVA fibres with cement-based material, as well as its filament microstructure, causes fibres have the additional possibility of rupturing rather than pull-out (Li et al., 2001 and 2002). When fibres break, stress re-distribution leads to progressive fibre breakage in a section, causing abrupt, brittle failure of the section in tension as a whole. Hence, too much fibre breakage reduces the transmission of tensile stress, resulting in a reduction of multiple cracking and therefore the reduction of tensile strain capacity. Hence, for PVA fibre, the critical fibre volume V_f^{crit} is also limited by interfacial properties.

2.5.1.3 Fibre dosage and properties

The critical fibre volume V_f^{crit} is the fibre volume below which a composite will not carry the load after a matrix cracks, and beyond which it is possible to achieve the multiple cracking and strain hardening. Critical fibre volume V_f^{crit} can be different in direct tension and flexural tension. So it is commonly assumed to refer to direct tensile properties.

Fibre properties determine the critical fibre volume, for instance, shorter length provides more opportunity to pull-out rather than rupture, hence the required stress for shorter fibre causing pull-out may be substantially less than for longer fibre. Thus the shorter fibre length may need a higher critical fibre volume. Similarly, for fibre diameter, thicker fibre causes more complexity of fibre distribution, thus resulting in equivalently lower fibre content and higher critical fibre volume.

$$V_f^{crit} \equiv \frac{12 J_{tip}}{g\tau\left(L_f / d_f\right)\delta_0} \tag{2.9}$$

Equation (2.9) indicates that V_f^{crit} depends on different values of $g\tau$ in the case of the same fibre length and diameter. For different types of ECC such there are different bond conditions in each mix. So the V_f^{crit} should be specific for a specific mix. Li (1998) suggests a normal relationship between V_f^{crit} and interface bond τ. From Equation (2.9) and Figure 2.8, it is clear that the V_f^{crit} reduces with interface bond increase, but the intensity also reduces when interface bond increases to a certain large value, which means that interface bonding need not be enhanced indefinitely.

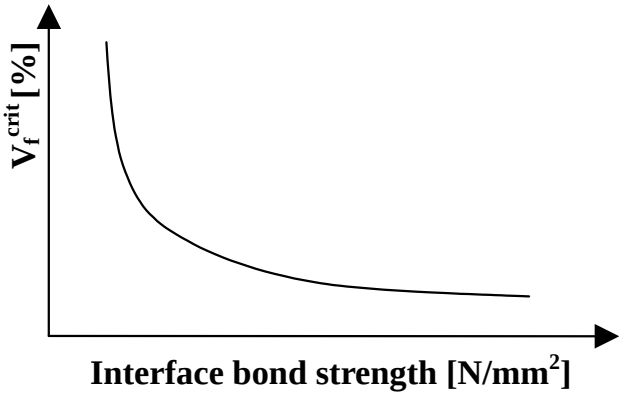

Figure 2.8 Illustration of interfacial bonding effect on critical fibre volume V_f^{crit} (Li 1997).

However, as discussed above, PVA fibre-ECC has a strong fibre/matrix interface bond, which may lead to fibre tending to rupture but not pull-out. Li (2002) also suggests another relationship between PVA fibre/matrix interface bonding and critical fibre volume V_f^{crit}, in this case, as shown in Figure 2.9.

From Figure 2.9, it is apparent that the critical fibre volume proportion V_f^{crit} first reduces but then increases because of fibre rupture at an increasingly high frictional bond τ_0. Fibre rupture of the hydrophilic PVA fibre is enhanced by strong chemical bonding G_d, due to the presence of the hydroxyl group in the PVA fibre (Li, 2002).

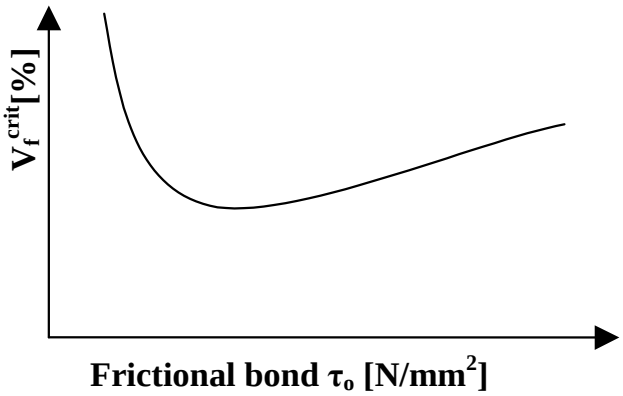

Figure 2.9 PVA fibre-ECC V_f^{crit} illustrated as interfacial friction τ_o all other parameters fixed (Li 2002).

Based on Li's definition, fibre content of ECC is 2%, or, typically, below 2.5% by volume (Wang & Li, 2004 and Li, 2002). Furthermore, consider V_f^{crit} as a function of interfacial friction τ_0 when all other parameters are fixed as shown in Figure 2.9. The frictional and chemical bond may be stronger than indicated by former experiments done by Li, due to fibre being used in present research without any treatment. In present research, a 2.5% PVA fibre bulk, by volume, was used.

2.5.1.4 Short cut fibre type and its quality influence in ECC

From the discussion and Equation (2.9) in the previous section, one may deduce that fibre physical and/or chemical properties and even geometrical properties affect ECC performance and therefore influence the critical fibre content. Fibre properties such as fibre tensile stress capacity, elasticity modulus, elongation, hydrophilic or hydrophobic properties, and aging can influence a composite significantly.

In one type fibre reinforced composite, the high modulus fibre tends to increase strength with slight improvement on toughness, while the low modulus fibres tend to a relatively improved high strain capacity with barely perceptible improvement on composite stress.

A method to develop both the tensile stress and strain of fibre reinforced materials is to use the combination of two types of different fibres, which has been studied by some previous investigations, such as investigation done by Kawamata et al. (2003).

For instance, Shah (2004) suggested that the hybrid-reinforcement involving fibres of varying size and modulus. He reported that usage of a micro-fibre and macro-fibre combination can successfully improve the composite strength and ductility of the matrix, and even reduce its permeability. Individual fibres work on the matrix materials, which they reinforce. Micro fibres improve composite strength by bridging micro cracks and resist the “coalescence” of these micro cracks into macro cracks, on the other hand, macro fibre can correspondingly improve the composite strain capacity by carry loading across macro cracks.

Kawamata et al. (2003) reported an investigation of a hybrid fibre reinforced system. Three-point bending and direct tensile tests show few mixes developing multiple cracks or pseudo strain hardening. Especially the mix with a combination of PVA fibre and steel cord shown slight pseudo strain hardening, but only until a strain of about 0.5-0.8 %.

2.5.2 FA role in ECC

As introduced in previous sections, stronger interface bond reduce the critical fibre volume fraction V_f^{crit}. However, PVA fibre has very strong chemical interface bond G_d, and therefore tends to break but not pull-out, resulting in an increase of critical fibre volume fraction V_f^{crit}. A increased chemical interface bond G_d will also lead to a decrease of complementary bridging energy J'_b, which is very important for the formation of multiple cracking and strain hardening.

The strong interface bond of PVA fibre is a big challenge for using it practically. The tailoring method to limit the interface chemical bond can be summarized as three aspects. They are tailoring of matrix toughness, tailoring of interfacial bond, and tailoring of fibre. As introduced in previous sections, there are many investigations dealing with these three aspects. For instance, Fibre oiling used to reduce the interfacial bond and then critical pre-flaw size (Li et al., 2001). However, fibre oiling is relatively expensive. In present research, an economical approach, which is FA used in matrix binder as cement-replacement, used in present research to provide a reduction of fibre/matrix interfacial bond as well as an increased

flaw size, and then result in reduction of crack tip toughness J_{tip}. Peled also reported that FA enhance fibre pull-out but reduce the composite strength, reported by Peled, the composite flexural stress may reduce 50% when 70% cement was replace by FA (Peled & Shah, 2003).

2.5.2.1 Reducing the chemical bond and enhancing the bridging function

High chemical bonding between PVA fibre and matrix can lead to an aggressive debonding process, with the transition zone having to carry an increasing shear force between fibre surface frictional debonding and the force caused by chemical debonding of transition zone microstructure decomposition from matrix bulk. Unlike other polymer fibres with low surface energy, for PVA fibre (which has strong surface chemical bonding properties), cohesive failure type may control the fibre/matrix debonding process. Experimental results will also confirm that in the present research in subsequent chapters.

FA enhances the bridging function of PVA fibre by decreasing the bond strength of the interface between fibre and matrix, resulting in a smoother fibre surface (Peled & Shah 2003). Either adhesive or cohesive type of bonding will occur for any mixes, depending on fibre type and matrix constituents.

2.5.2.2 Tailoring of pre-existing flaw and fracture energy

Multiple cracking and strain hardening are necessary for ductility development, which is generally observed in many ECC materials. However, density and spacing of cracks become important for many composite properties. Large cracking spacing implies that the potential of reinforcing fibres is not fully utilized (Wang & Li, 2004). This may perhaps be due to the lack of adequately sized flaws and too solid a matrix. Many ECC specimens exhibit large cracking space under direct tension. Wang also suggests that to achieve the desired saturated multiple cracking, flaws of sufficient size and frequency should exist in the matrix. Hence, crack tip toughness J_{tip} can be reduced and will result in a sufficient margin between J_b' and J_{tip}. FA starts hydration too slowly to contribute to the crystal form of the matrix in the early age, which leads to many pre-flaws existing in the matrix as weak points where matrix crack strength will be lower than peak bridging stress. As introduced in section 2.3.2, matrix crack strength lower than peak bridging stress is an important requirement for multiple cracking to occur.

2.5.2.3 Durability development

The durability of polymer fibre reinforced composite is very much dependent on its resistibility to an alkaline environment. PVA fibre shows excellent resistibility to an alkaline environment (Illston, 1994). Furthermore, since the crack width of the composite affects the water and alkalescent hydrate penetrability, clearly the control of crack width is also important for material durability. As introduced in the previous section, FA works in a matrix to reduce the chemical bond of the matrix/fibre interface, and adds to the pre-existing volume of flaws, hence limiting the crack width, and therefore contributes to the durability of the

composite. Some important influences by FA on crack and void control have been investigated before. For instance, Wang & Li (2004) verified that in the case of ECC with FA, the spread of multiple cracks was distinguished over a large area on the specimen surface, and the first crack stress was smaller than in a specimen without FA and ultimate strain was larger. The size and amount of voids are smaller than in those mixes without FA. The cracks seem to pass through air voids.

Another benefit of FA addition in the matrix for durability is to decrease and delay the peak heat of concrete hydration and thence to decrease the possibility of cracks caused by temperature grading. Figure 2.10 shows the heat of hydrated with age differences between FA and normal cement.

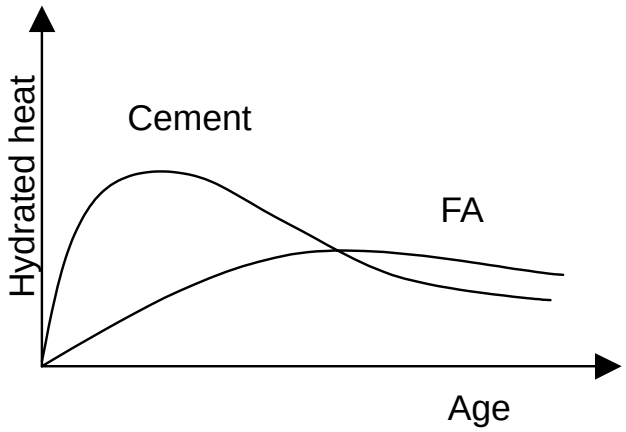

Figure 2.10 Comparison of the heat of hydrated for FA and normal cement

2.5.3 Role of slag in ECC

2.5.3.1 Influence on tensile and compressive strength

The studies of compressive strength by Loedolff and van Zijl (2003) show that specimens, which contained Corex slag, as blended in Surebuild (CEM II/B (L-S) 42.5) consistently developed a higher strength than specimens of identical mix proportions, but with OPC (CEM I 42.5) at ages beyond 14 days. Strength development of GGCS concrete shows slower initial strength development for up to about 3 days, but will increase noticeably more than normal concrete after seven days. The rapid strength development of GGCS concrete makes it advantageous for structural applications (Alexander et al., 2003).

Because of the small particle size, slag is able to fill the capillary pores and entrapped air voids in the matrix paste, resulting in effectively improving the matrix properties and fibre bonding conditions.

2.5.3.2 Influence on fresh and hardening properties

The workability of Corex slag concrete is not notably different from normal concrete of

similar composition. Due to fineness of slag particles, slag concrete is more cohesive than similar normal concrete (Alexander et al., 2003). This is very important for investigation of ECC tensile behaviour, and also of its properties at a high age.

The use of Corex slag in concrete will provide an increase in setting time, but a lower bleeding rate and capacity than usual concrete. In contrast with FA concrete, slag concrete creates a similar heat of hydration as usual concrete (Alexander et al., 2003).

For some other structural properties, such as elastic modulus, drying shrinkage and creep, the influence of sand is generally more significant than the effect of binder type. According to Alexander, the drying shrinkage of GGCS concrete is approximately 25% lower than normal concrete with W/B = 0.5 (drying environment 23^0C and 60% R.H). Specific creep (total and basic) of GGCS concrete is also lower than with normal concrete.

2.5.4 Influence of sand on ECC

It is known that sand grading and content influence matrix toughness, frictional bond and matrix strength. Wu (2004) suggests this fact, since low matrix toughness is critical in attaining pseudo strain-hardening behaviour. For the sake of the shrinkage control and constraint, high amounts of fine sand (50-150 um) should be used.

Another research by Li et al (1995) showed that for a given W/B, high content fine sand acts to increase fracture toughness and tensile strength. However, for higher aggregate-binder ratio (A/B), W/B will have a slighter influence on strength and crack toughness. For instance, when the A/B is 2, both composites with a W/B of 0.35 and 0.45 show approximately the same tensile stress and a low A/B leads to a smaller margin of fracture toughness than with a different W/B.

Van Zijl (2005) investigated the influence of different grading sand content on ECC behaviour. When sand grading is kept equal at F95, increased aggregate-binder ratio (S/B) leads to an increased first crack strength but decreases both ultimate strength and ultimate strain. In the same A/B, first crack stress keeps almost the same level, whereas, the ultimate stress and ultimate strain increases when sand grading varies from natural dune sand to sieved American standard (ASTM) F95- F110 sand (ASTM C 95 – 110), which was used by the research group at Michigan University (Li et al. 1995).

2.6 Bending MOR and Direct Tensile Stress

The need for a theoretical treatment of the comparison between flexure and bending arises from the large difference between the experimental MOR (modulus of rupture) and the direct tensile stress (Hannant, 1978). The MOR can amount to three times the direct tensile stress. Certainly, the unique behaviour of ECC will provide a different ratio of bending between MOR and tensile stress. Analysis made by Li and Maalej (1994) suggested that the three-point

bending strength of ECC material can be five times its tensile (first crack) strength, both in measurement and predicted result. Because they differ from normal Reinforced concrete beams, ECC materials have an advantage.

2.6.1 The modelling of flexural behaviour

One method of modelling flexural behaviour is the rectangle stress block analysis introduced by Hannant (Hannant, 1978). The ratio of three between bending MOR and direct tensile stress was predicted theoretically by using rectangular stress block analysis. The upper limit was 3.

Figure 2.11 (a) illustrates such rectangle analysis. When a beam carries the bending load, brittle materials show a linear stress and strain distribution, and the neutral axis is approximately at the middle of the beam thickness at failure. The same levels of compression and tension are put on the beam, therefore bending MOR is equal to the compression σ_{comp}. Figure 2.11(b) shows a linear strain distribution and a neutral axis moving upward to the compression surface, due to the extremely large tensile strain capacity of ECC materials. Figure 2.11(c) shows the associated, get simplified stress distribution. The tensile stress block shape shows merely the tensile behaviour of ECC under direct tensile test, which depends on fibre content, interface bonding and matrix properties.

For moment equilibrium, the resistance moment of MOR has to be equal to the resistance moment of the true stress distrubution, hence the relationship between bending MOR and tensile stress can be calculated through these two types of equilibriums.

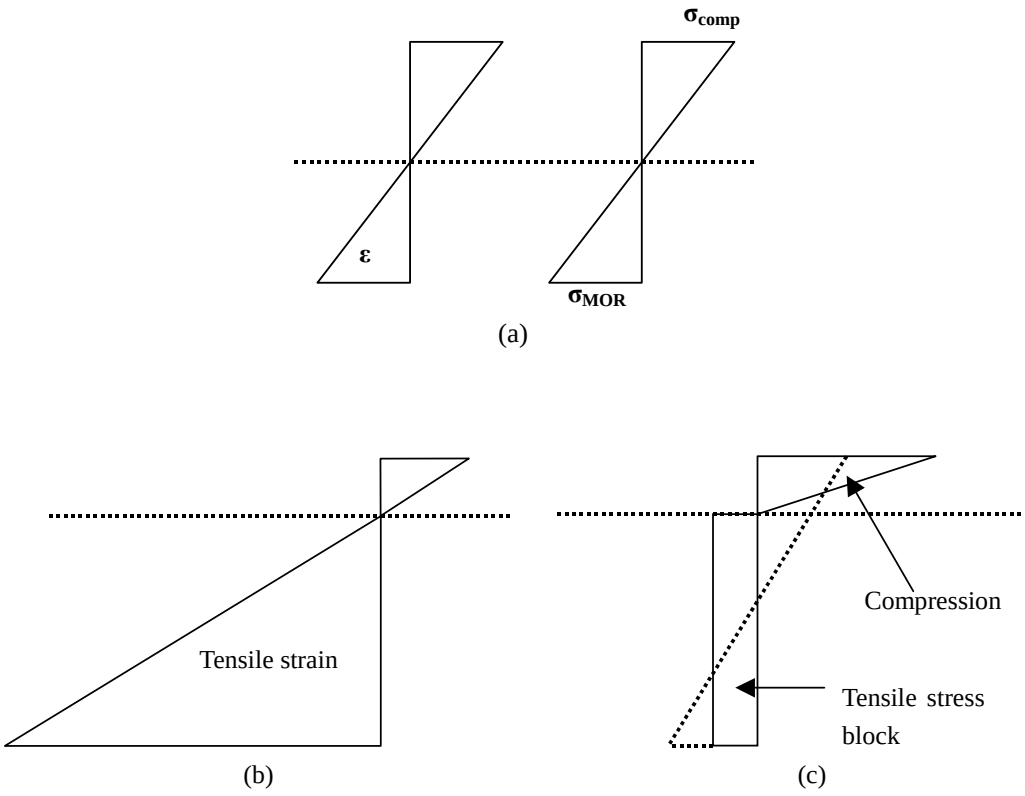

Figure 2.11 Schematic representation of rectangle stress block analysis.

The bending test shows the neutral axis moving toward the compression surface due to the quasi-plastic behaviour in tension of fibre reinforced materials.

The analysis assumed that a small change in the shape would not affect the calculation significantly.

2.6.2 Theoretical prediction of the ratio of bending MOR and direct tensile stress

Figure 2.12 shows the principle of rectangular analysis theory. Figure 2.12 (a) is for elastic material with neutral axis in the middle. The direct tensile stress, because it equals the bending MOR in the case of pure elastic material, can be named as σ_{MOR} and compression (σ_c) equals to MOR. In Figure 2.12(b) ultimate tensile stress of the composite (σ_{tu}) and compressive stress on the outer face of the beam (σ_{cu}) are shown.

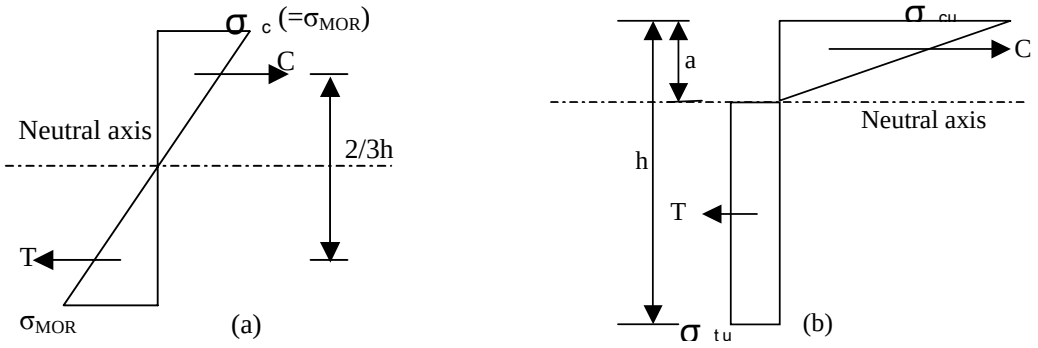

Figure 2.12 Stress block in flexure (a) Elastic material. Moment of resistance = $\sigma_c h^2/6$ (b) Elastic in compression; plastic in tension. Moment of resistance = σ_{tu} (h – a) (2a/3 + 1/2(h – a)).

In Figure 2.12(a):

For force equilibrium, stress block has same area, force T = C

$$T = \frac{\sigma_{MOR}}{2} \times \frac{h}{2} = \frac{\sigma_{MOR} h}{4} \tag{2.10}$$

Lever arm $l_a = \frac{2h}{3}$ (2.11)

Therefore moment of resistance $M^* = \frac{\sigma_{MOR} h}{4} \times \frac{2h}{3} = \frac{\sigma_{MOR} h^2}{6}$ (2.12)

In Figure 2.12 (b):

$$C = \frac{\sigma_{cu} \times a}{2} \tag{2.13}$$

$$T = \sigma_{tu} \times (h - a) \tag{2.14}$$

For force equilibrium, stress block has same area, force T = C

$$a \times (\frac{\sigma_{cu}}{2} + \sigma_{tu}) = \sigma_{tu} \times h \tag{2.15}$$

then $$a = \frac{h}{\frac{\sigma_{cu}}{2\sigma_{tu}} + 1} \tag{2.16}$$

Therefore moment of resistance $$M = \sigma_{tu}(h - a) \times \left(\frac{2a}{3} + \frac{(h - a)}{2} \right) \tag{2.17}$$

$M = M^*$, equate (2.12) and (2.17)

$$\sigma_{tu}(h - a) \times \left(\frac{2a}{3} + \frac{(h - a)}{2} \right) = \frac{\sigma_{MOR} h^2}{6} \tag{2.18}$$

$$\frac{\sigma_{MOR}}{\sigma_{tu}} = 3 - \frac{2a}{h} - \frac{a^2}{h^2} \tag{2.19}$$

It is clear that the maximum ratio value is 3.

However, for ECC materials, such ductile behaviour also works in the compression zone. Therefore, pseudo-rectangles can be assumed in the compression zone of a bending beam as shown in Figure 2.13 (b). To simplify the demonstration, a rectangular compression block will be used in the following demonstration.

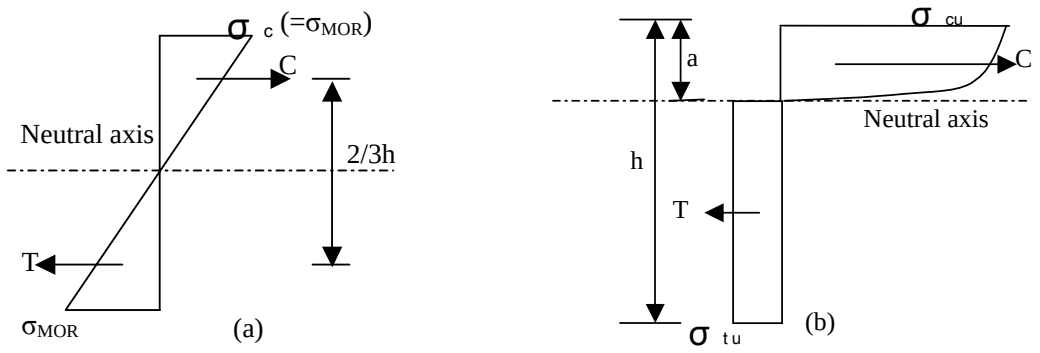

Figure 2.13 Stress block in flexure: (a) elastic bending; (b) rectangular block to simulate the compression zone of ECC materials bending.

Similarly, with the demonstration above,

In Figure 2.13(a):

For force equilibrium, the stress block has same area, force T = C

$$T = \frac{\sigma_{MOR}}{2} \times \frac{h}{2} = \frac{\sigma_{MOR} h}{4} \tag{2.20}$$

Lever arm $l_a = \frac{2h}{3}$ (2.21)

Therefore moment of resistance $M^* = \frac{\sigma_{MOR} h}{4} \times \frac{2h}{3} = \frac{\sigma_{MOR} h^2}{6}$ (2.22)

In Figure 2.13 (b)

$$C = \sigma_{cu} \times a \tag{2.23}$$

$$T = \sigma_{tu} \times (h - a) \tag{2.24}$$

For force equilibrium, the stress block has same area, force T = C. To simplify the equation, assume the compression stress block is rectangular.

Then:

$$a \times (\sigma_{cu} + \sigma_{tu}) = \sigma_{tu} \times h \tag{2.25}$$

then $a = \frac{h}{\frac{\sigma_{cu}}{\sigma_{tu}} + 1}$ (2.26)

Moment of resistance $M = T \times (\frac{a}{2} + \frac{h-a}{2}) = \sigma_{tu}(h-a)(\frac{h}{2})$ (2.27)

In order to keep force equilibrium, their moments of resistance should be equal.

Then M = M* replace (2.22) and (2.27)

$$\sigma_{tu}(h-a)\frac{h}{2} = \frac{\sigma_{MOR}h^2}{6} \tag{2.28}$$

$$\frac{\sigma_{MOR}}{\sigma_{tu}} = \frac{(h-a)\times\frac{h}{2}}{\frac{h^2}{6}} = 3 - \frac{a}{h} \tag{2.29}$$

The ratio of three point bending MOR over direct tensile stress of ECC in rectangle analysis is larger than triangle analysis but still keeps the maximum value of 3. Maalej and Li (1994) also observed and predict a high MOR to tensile strength ratio of ECC materials.

2.7 Influences on ECC performance

As shown in the introduction in Chapter 2.3, the dominant properties of a composite are the balance between the transmitted loading and composite crack tip toughness J_{tip}. The composite crack tip toughness J_{tip} can be simplified by the division of matrix fracture toughness K_m and the matrix elastic modulus E_m. Effects such as W/B, A/B on K_m and E_m, and consequent tensile properties of ECC materials require analysis.

2.7.1 The influence of the aging of composites

There are some investigations about the performance change of fibre reinforced materials with curing age. For example, Chan and Li (1997) investigated the single fibre pull-out test of a composite at an early age and reported that the interface bonding achieved a constant state magnitude at about two days without any considerable increase thereafter. The ECC strain achieved ultimate value at the age of about 10 days, of approximately 1.4 times the strain capacity at the age of 28 days (Lepech and Li, 2004). Another investigation done by Kanda and Li (1998) set the ratio of ultimate strain between the ages of one week and four weeks at about 1.8. One week's ultimate stress is 0.93 times that of four weeks. Van Zijl (2005) reported an increased trend of both first crack strength and strength during 7 to 28 days, keeping constant at 28 days and also a sharp increase of ultimate tensile stress during the aging process from 7 to 14 days, keeping approximately flat after 14 days.

However, ECC behaviour at high age has not yet been sufficiently studied. Aging may affect critical fibre volume bulk V_f^{crit}, Hannant (1994) figured out that a composite, which has just

sufficient fibre content for V_f^{crit} at an early stage, may have less fibre than V_f^{crit} at high age. This indicates that aging influence increase the fibre content required to achieve the same performance as at early age.

Unlike normal concrete, ECC is supposed to carry a tensile load across the cracks. Therefore, for ECC, the tensile behaviours are more important than only the matrix strength. From equation (2.7), the ultimate tensile strength of a composite is proportional to interfacial bonding properties. Aging can therefore influence tensile stress via its effect on the interfacial bond. There is a high porosity structure of transition zone around fibre surface as introduced in section 2.4.1. The different time-dependency due to the distinctions in microstructure between transition zone and matrix bulk lead to a different ratio of development between fibre/matrix interfacial properties and matrix bulk. Therefore, the aging influence on ECC performance is much more complicated than normal concrete and is worthy to be investigated.

FA and GGCS, as cement replacements, influence on fibre/matrix interface properties. Hence they certainly influence on composite aging behaviour.

PVA fibre aging that loses elastic modulus and tensile strength can significantly affect the high age properties of composites.

2.7.2 W/B influence

W/B influences matrix toughness, matrix structure, and interface bonding, and therefore influences the strength and strain capacity of composites. Consequently, the problem of W/B influence can be an important and complex issue. Kamada and Li reported a repair system using ECC with different W/B and also compared a higher bending load in the overlay area of a system with lower W/B ECC, but both result in similar level bending deflection (Kamada & Li, 2000). Other investigation has shown that HFRCC mixed with PVA fibre of length 12 mm was hardly influenced by the W/B (Kawamata et al., 2003).

An investigation by Li et al. (1995) has shown that a decrease in the W/B resulted in an increase in both tensile strength and fracture toughness in cases of matrix with A/B range from 0.5 to 2.0. For the matrix with A/B = 1.0, there is an increase of approximately 29% in tensile strength and 73% in toughness. However, for high S/B ratio, lower W/B has an influence on strength and crack toughness. For instance, when the A/B is 2, both a composite with W/B = 0.35 and one with 0.45 have shown approximately the same tensile stress. A low A/B leads to a smaller range of fracture toughness between different W/B when A/B = 0.5. The composite fracture toughness of a mix with W/B = 0.35 approached the value of the mix with W/B =0.45.

2.7.3 Workability and fibre distribution influence

Composite workability can be controlled and influenced by matrix properties, such as W/B,

the size and shape of particles of material, sand grading, superplasticizer and viscous agent, as well as fibre content and properties. Shah et al (2004) discovered that fibre could affect the fresh state properties of cementitious materials and therefore affect fibre distribution. A condition where the fibres occur in clumps in the matrix has a significantly negative influence on composite ductility.

Torigoe et al (2003) consider that fibre distribution strongly influences composite performance, provided that a relationship between the degree of distribution and the ultimate strain of the composite is maintained by adjusting the preferable unit size.

Stahli and van Mier (2004) investigated the rheological properties of FRC materials and suggest two important issues about composite rheological properties, the fact that they are composite “self-venting” and fibre segregation. Self-venting is an important behaviour of self-compacting concrete, which means that little air-bubbles can be released automatically from the fresh composite after casting. Fibre segregation is another important issue that influences workability. If a matrix is too liquid and fibre cannot drift in it, then the fibre will not be homogenously dispersed, due to fibre clumping and segregating. A high density of matrix, less water content, and longer mixing-time can prevent such problems.

2.8 ECC Application issues

Theoretical surveys in this chapter reveal the mechanisms of the behaviour of ECC materials and the tailoring approach to attain these behaviours. The aim in developing ECC materials is its commercial application.

2.8.1 The concept of ECC applications

In recent years, numbers of applications exploiting the unique characteristics of ECC were investigated. Li (2002) suggests that these characteristics include damage tolerance, shear resistance, energy absorption, delamination and spall resistance, high deformability and water infiltration, crack distribution, and crack-width repression control.

Damage tolerance of a structure, that is, the ability for the structure to sustain a load-carrying capacity (even when overloaded into the inelastic phase) can be enormous.

Shear failures in short columns in bridging piers or walls between stories in buildings were observed under strong seismic loading. Shear damage is similar to ductile tensile damage with diagonal micro-cracks.

Energy absorption in hinge zones is used to dissolve the significance of earthquake energy. In normal R/C structures, the concept of plastic hinges is introduced by ductile soft of steel reinforcement in seismic detailing.

DFRCC can form fine, well-distributed multiple cracks under tension or bending, as

compared to normal concrete and FRC. As may be expected, this results in the reduction of the infiltration of water-soluble aggressive substances, which cause steel reinforcement corrosion in steel bar reinforced concrete structures, and therefore in improved durability.

Concrete slab and bulk components may crack and undermine durability under restrained drying shrinkage and/or temperature loading. Such problems have typically been handled by introducing joints. However, the joints often cause damage and are costly to maintain. By relying on its large strain capacity, ECC can be utilized to accommodate imposed deformation by replacing standard joints with a strip of ECC material.

In a normal reinforced concrete structure, serious durability problems may occur due to cracking of the concrete in the tensile zone, migration of aggressive agents through the concrete cover, corrosion of the reinforcing steel, expansion of the corroded steel bar, spall-fracturing of the concrete cover, subsequent accelerated corrosion of the reinforcing bar, and loss of the load-carrying capacity of structure (Li et al., 2002). Unique properties of ECC limit cracking, thereby preventing corrosion, resulting in enhanced durability of the structure (Li, 2002).

The major property of ECC material is ductility. This is an important factor to consider. Compared with a high strength concrete strengthened beam, an ECC strengthened beam has better performance on both load capacity and ductility. One percent ductility of ECC materials might be enough for securing ductility of the flexural members.

There are numbers of applications of ECC materials, including reduction or elimination of shear reinforcement, sustaining of large imposed deformation, protection for reinforcement, high damage tolerance and reduction, and tight crack width (Li 2003).

2.8.2 The cost of ECC

As a commercial development of material is aimed at, the development of ECC has to take additional matters into consideration, such as processibility, availability of materials, standardization of the design of the mix and test methods, and, the most important issue, cost-benefit ratio.

The cost-benefit should be considered based on the whole structural life cycle cost. The life cycle cost includes the cost of materials, of the building, and maintenance costs. The use of ECC in construction members provides the possibility to eliminate shear reinforcement. Hence, reduction of construction cost is achieved. The durability of construction, particularly for infrastructure, which are supposed to use large volume ECC materials, is improved as it is supported by the ductility of ECC materials. Thereby, the cost of maintainance is reduced significantly.

Furthermore, the higher cost of ECC materials than normal concrete is caused by the use of fibre and higher cement content. Partial substitution of cement by an industrial by-product, such as FA and slag, can reduce the cost of ECC in comparison with other HPFRCC.

2.9 Summary

In this chapter, the normal terminology and characteristics of ECC were introduced for discussion in subsequent chapters. The basic micro-mechanisms of ECC were demonstrated in this chapter.

Predictions for the ratio of the bending MOR and direct tensile ultimate stress were demonstrated and will be compared with experimental data in Chapter 9.

The theory of roles of materials and influence of the matrix, such as W/B and workability, aging, and aggregate size and content, were also introduced in this chapter.

The concept of a transition zone as well as the fibre/matrix properties were also presented herein, which are very important for the explanation of experimental results and further discussing of cement replacement influence and aging influence.

The concept of application of ECC was briefly introduced here as well.

Chapter 3
Experimental programs

In the previous chapter the theoretical research already indicated that matrix properties such as interfacial properties, matrix flaws, would play the decisive role in EEC performance. To study and identify particular matrix factors, which influence the ECC performance, two series of tests have been designed and carried out.

Based on these two series, a further experimental design framework was made to investigate other influences on ECC properties. The whole experimental work mainly focuses on PVA-ECC, but with some exceptions. The influences that are investigated in the present study include matrix effects such as curing age, material particle size grading, W/B ratio, fibre type and combination, and procedure effects, such as mixing procedure, setting procedure, and processing (i.e. casting, or extrusion).

3.1 The experimental programme and postulation for the obtaining of engineering parameters

The engineering parameters σ_M, σ_u, $\varepsilon_{M,}$ ε_U, and ε_F of FRC are dependent on several variables. In this study the most important 9 variables were considered namely superplasticizer type (Sp-type), superplasticizer-Binder ratio (Sp/B), water-Binder ratio (W/B), FA- cement ratio (FA/B), GGCS-cement ratio (GGCS/B), VA- binder ratio (VA/B), workability, fibre volume (V_f), and fibre-type. This can be formulated as:

$$\sigma_M = \sigma_M(\frac{Sp}{B}, Sp-type, \frac{W}{B}, \frac{FA}{B}, \frac{GGCS}{B}, \frac{VA}{B}, workability, Fibre-type, V_f)$$

$$\sigma_U = \sigma_U(\frac{Sp}{B}, Sp-type, \frac{W}{B}, \frac{FA}{B}, \frac{GGCS}{B}, \frac{VA}{B}, workability, Fibre-type, V_f)$$

$$\varepsilon_M = \varepsilon_M(\frac{Sp}{B}, Sp-type, \frac{W}{B}, \frac{FA}{B}, \frac{GGCS}{B}, \frac{VA}{B}, workability, Fibre-type, V_f)$$

$$\varepsilon_U = \varepsilon_U(\frac{Sp}{B}, Sp-type, \frac{W}{B}, \frac{FA}{B}, \frac{GGCS}{B}, \frac{VA}{B}, workability, Fibre-type, V_f)$$

$$\varepsilon_F = \varepsilon_F(\frac{Sp}{B}, Sp-type, \frac{W}{B}, \frac{FA}{B}, \frac{GGCS}{B}, \frac{VA}{B}, workability, Fibre-type, V_f) \quad (3.1)$$

In all mixes of both series I and series II, VA/B was kept constant. The main influences on workability are the W/B and Sp/B ratio. This can be expressed as:

$$workability = workability(\frac{W}{B}, \frac{Sp}{B}) \quad (3.2)$$

It is postulated that workability dominant the fibre dispersion, thereby, higher workability provides more even fibre dispersion (Stahli & van Mier. 2004). In this work, for steel fibre-ECC materials mixing, the practical experiments require extremely strict workability, very high workability brings the fibre sedimentation problem, and too poor workability makes the composite hard to be set into the module and may lead to the extremely poor hardened state tensile properties.

Hereby, an important postulation is made to reduce the total number of the experiments required. It is assumed that the workability dominates the engineering parameter, especially σ_u, ε_U, and ε_F by its influence on fibre dispersion. This then means that equation (3.1) may be re-written as

$$\sigma_U = \sigma_U(workability(\frac{Sp}{B}, \frac{W}{B}), Fibre-type, V_f, \frac{FA}{B}, \frac{GGCS}{B}, Sp-type)$$

$$\varepsilon_U = \varepsilon_U(workability(\frac{Sp}{B}, \frac{W}{B}), Fibre-type, V_f, \frac{FA}{B}, \frac{GGCS}{B}, Sp-type)$$

$$\varepsilon_F = \varepsilon_F(workability(\frac{Sp}{B}, \frac{W}{B}), Fibre-type, V_f, \frac{FA}{B}, \frac{GGCS}{B}, Sp-type) \quad (3.3)$$

Subsequently, 2 series of tests were designed, in which all of the variables were keep constant at a time, accept one, to study its role. The mixes are listed in Table 3.1 and 3.2.

For series I, varying the FA/B and GGCS/B,

1) Varying FA/B: $\sigma_U = \sigma_U(\frac{FA}{B})$

$$\varepsilon_U = \varepsilon_U(\frac{FA}{B})$$

$$\varepsilon_F = \varepsilon_F(\frac{FA}{B}) \quad (3.4)$$

where PVA fibre, V_f = 2.5%, Zero GGCS/B, and ChrySo optima 200 Sp were used. Workability was maintained constant throughout all the mix in series I, by slightly adjusting W/B and Sp/B.

2) Varying GGCS/B: $\sigma_U = \sigma_U(\frac{GGCS}{B})$

$$\varepsilon_U = \varepsilon_U(\frac{GGCS}{B})$$

$$\varepsilon_F = \varepsilon_F(\frac{GGCS}{B}) \quad (3.5)$$

with PVA fibre at V_f = 2.5%, zero FA/B, and ChrySo optima 200 Sp. Workability was maintained constant throughout all GGCS influence test of series I.

Series II focuses on the steel fibre ECC matrix research.

3) Varying FA/B: $\sigma_U = \sigma_U(\frac{FA}{B})$

$$\varepsilon_U = \varepsilon_U(\frac{FA}{B})$$

$$\varepsilon_F = \varepsilon_F(\frac{FA}{B}) \quad (3.6)$$

where Steel fibre, V_f = 3%, zero GGCS/B, and ChrySo premia 100 Sp. Workability was maintained constant throughout all the series II tests.

Subsequently, a number of wide ranging experiments were made to investigate respectively individual properties, and then a complete framework will be built to list all influences and show how they control the matrix properties and subsequently the ECC performance. The mixes designed for these tests are listed in Table 3.3.

We need to mention here that the admixtures such as Superplasticizer and viscous agent were added by mass proportion of total binder. Fibre content is expressed as the volume of fibre as percentage of the volume of the whole mix. For all the PVA fibre ECC, PVA fibre content is 2.5% and for steel fibre ECC the fibre content is 3%. The A/B is 0.5 in all the mixes. The Viscous agent dosage is 0.3% for all casting mixes except mix SF15 and SF 18 because they are prepared also for extrusion process.

Table 3.1 Series I mix designs

Nr	Portland cement 42.5	Silica fume	Fly ash	Ground Granulated Corex Slag	Superplasticizer	Sand type & content	W/B
S1	0.50		0.50		1.0%	F110	0.45
S2	0.50			0.50	1.0%	F110	0.45
S4	0.30			0.70	1.0%	F110	0.40
S5	0.45		0.55		1.5%	F110	0.40
S6	0.45			0.55	1.5%	F110	0.45
S7	0.30		0.70		1.5%	F110	0.40
S8	0.46		0.27	0.27	1.5%	F110	0.45
S9	0.46		0.36	0.18	2.0%	F110	0.45
S10	0.30		0.70		2.0%	F100**	0.30
S11	0.30		0.50	0.20	1.5%	F110	0.45
S12	0.30	0.20	0.50		1.5%	F110	0.45
S13	0.30		0.60	0.10	1.5%	F110	0.45
S14	0.30		0.40	0.30	2.0%	F110	0.45
SF8	0.60		0.40		2.0%	F110	0.40
M34***	0.70		0.30		1.4%	F110	0.45

*****The sand types are discussed in section 3.1.5.

** ASTM F100 sand was used in mix S10.

*** Mix M34 was designed by W.P.Boshoff.

*** Superplasticizer used in Table3.1 is Optima 200.

Table 3.2 Series II mix designs

Nr	Portland cement 42.5	Silica fume	Fly-ash	Ground Granulated Corex Slag	Superplasticizer ***	Sand type & content	W/B
SF2	0.60		0.40		1.5%	Sieved sand	0.20
SF4	0.50		0.50		1.5%	Sieved sand	0.24
SF6	0.40		0.60		1.5%	Sieved sand	0.22
SF7	0.30		0.70		1.5%	Sieved sand	0.22

*****The sand types are discussed in section 3.1.5.

** W/B of each mix were slightly modified to obtain the workability requirements.

******* Superplasticizer used in Table3.2 is Premia 100.

Table 3.3 Mixes for Sensitivity Influences investigations

Nr	Portland cement 42.5	Fly-ash	Ground Granulated Corex Slag	Super-plasticizer	Superplasticizer type	V/B	Fibre type & content	W/B
SF9A	0.3	0.7		2.5%	Premia 100	0.3%	2.5%PVA	0.30
SF9B	0.3	0.7		1.5%	Premia 100	0.3%	2.5%PVA	0.45
SF10	0.4	0.3	0.3	2.0%	Premia 100	0.3%	1%PVA, 1%Steel	0.34
SF11	0.4	0.3	0.3	2.0%	Premia 100	0.3%	1.5%PVA, 1%Steel	0.36
SF12	0.4	0.3	0.3	2.0%	Premia 100	0.3%	2%PVA, 1%Steel	0.40
SF13	0.3	0.5	0.2	2.0%	Optima 200	0.3%	2.5% PVA	0.45
SF14	0.3	0.2	0.5	2.0%	Optima 200	0.3%	2.5% PVA	0.45
SF15	0.3	0.7		2.0%	Premia 100	1.0%	2.5%PVA	0.20
SF17A	0.3	0.7		1.5%	Optima 200	0.3%	2.5%PVA	0.40
SF17B	0.3	0.7		1.5%	Optima 200	0.3%	2.5%PVA	0.40
SF18	0.4	0.3	0.3	1.0%	Premia 100	1.0%	2.5%PVA	0.25
SF19	0.3	0.7		3.00%	Premia 100	0.3%	2.5%PVA	0.30
SF20	0.3	0.7		1.50%	Premia 100	0.3%	2.5%PVA	0.40
SF21	0.3	0.7		0.50%	Premia 100	0.3%	2.5%PVA	0.46

* All the sand used in Table 3.3 is F110.The sand types are discussed in section 3.1.5

3.2 Materials

3.2.1 CEMI 42.5

Ordinary Portland cement is hydraulic cement consisting essentially of hydraulic calcium silicates. Since the cement is composed of a heterogeneous mixture of several compounds, the hydration process consists of reactions of the anhydrous compounds with water occurring simultaneously. The hydrations of some components are immediate, while others follow later, producing a family of calcium silicate hydrates. This is currently named CEM in accordance with international practice, specifically CEMI 42.5. The density of CEMI 42.5 is approximately 3.14 kg /l.

3.2.2 Ground Granulated Corex Slag (GGCS) and Ground Granulated Blast furnace Slag (GGBS)

Slag is a potential hydraulic material with slow hydration speed. The reactivity of slag in a cementitious system depends not only on the chemical components, but also on its fineness. Both two types of slagment are by-products of steel manufacturing. GGBS is alternated from grounding Blast furnace slag, while GGCS is the ground product of slag from the Corex process of steel manufacturing. One particular source of GGCS is the Saldanha steel manufacturing company in the Western Cape. GGBS is usually cheap, as comparative with the price of CEM 42.5, making it a sensible cost reducing constituent material for cement-based material composites. However, GGCS from Saldanha is very expensive at 80% of the CEMI 42.5 price because of the beneficial influence of the latter on concrete strength and ductility (Alexander et al., 2004). Oxide analysis results on GGBS and GGCS by X-Ray Fluorescence Spectrometry (XRF) technique are listed in Table 3.4. Both GGBS and GGCS are finer than cement powder, but GGCS is finer than GGBS when measured by Blaine fineness tests (see Table 3.5). A SEM photo image of Saldanha GGCS is shown in Figure 3.1. In this research, only GGCS was used. The density of the GGCS used in present research is approximately 2.9 kg/l.

Table 3.4 Oxide analyses of GGBS and GGCS (XRF analysis) (Alexander et al., 2004)

Oxides	GGCS	GGBS
CaO	37.2	34.0
SiO_2	30.8	35.5
Al_2O_3	16.0	15.4
MgO	13.7	9.4
TiO_2	0.51	1.2
Fe_2O_3	0.87	0.98
MnO	0.09	0.88
K_2O	0.35	0.87
Na_2O	0.12	0.16
SO_3	3.19	2.49

Table 3.5 Powder fineness of GGCS & GGBS (Alexander et al., 2004)

Method	GGCS	GGBS
BET fineness (m^2/kg)	1145	991
Blaine fineness (m^2/kg)	467	390
% Passing 1 micron	7	6
%Passing 10 micron	51	45

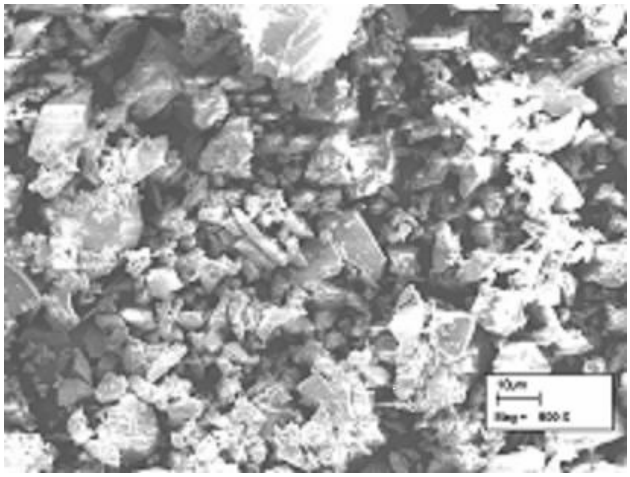

Figure 3.1 SEM photo of the particles of Ground Granulated Corex Slag (GGCS)

3.2.3 Fly ash (FA)

FA is one of the important cost reducing cementitious materials. It is the fine particle residue, resulting from the combustion of ground or powdered coal, usually in electricity generation plants. The FA used in this research is Pozz-Fill from sourced from Lethabo. It has the typical particles size about 74% below 100um and 52% less than 45um. Most FA particles are of perfect spherical shape. Usually, the main constituents or elements of fly ash are heterogeneous glassy and crystalline phases of aluminium, silicon, iron, calcium and magnesium, depending on the component ions in the parent coal. Oxides of Elements of current FA are shown in Table 3.6 as obtained by XRF analysis. The major phases of Lethabo FA were found to be glass (45-48%), mullite ($Al_6Si_2O_{13}$) 41-43%, and the reactive silica is in the range of 30-35%. Further research discovered that the components of the glass phase consisted of mainly SiO_2 (21-100%) and Al_2O_3 (0.1-49%). With the FA used in current research, the chemical content of SiO_2 and Al_2O_3 amounted to 85% (Johns, 1990). The SEM photo image of FA particles revealing the spherical shape is shown in Figure 3.2. The density of the FA used in present research is approximately 2.9 kg/l.

Table 3.6 Chemical components of FA used in current research

LOI*	Sum	Al_2O_3	CaO	Cr_2O_3	Fe_2O_3	K_2O	MgO	MnO	Na_2O	NiO	P_2O_5	SiO_2	TiO_2
1.77	100.74	28.10	4.93	0.003	3.97	0.71	1.36	0.09	0.70	0.02	0.38	57.22	1.49

*Note, the LOI is the loss on ignition.

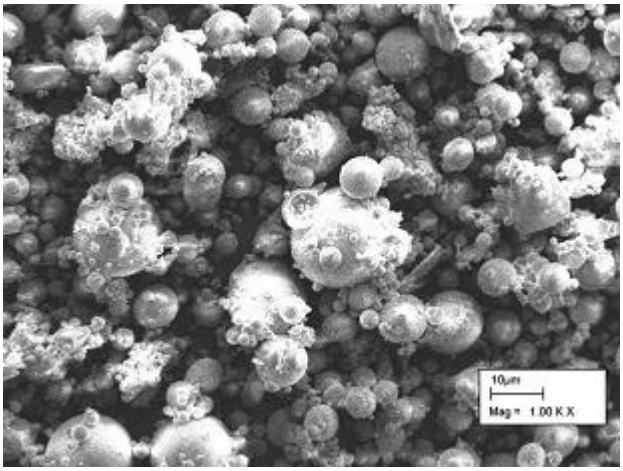

Figure 3.2 SEM photo of fly ash particles showing the very fine perfect spherical shape

3.2.4 Silica fume (CSF)

Silica fume, also called micro-silica, are very fine particles of silica condensed from the waste gases exhaled in the silica metal production process. In this research, Silica fume was used only in a few specific mixes. The role that Silica fume plays in ECC still requires further research. The density of CSF is 2.8 kg /l.

3.2.5 Aggregate

Aggregate used in the research is mostly natural dune sands (Philippi) originating from the Western Cape Province. Sand was sieved in the grading according to American standard F110 and F70 (ASTM) for series I PVA-ECC mixes. A unique grading was sieved for the series II Steel -ECC series. Figure 3.3 shows the gradings of various sands used in the present research, compared with normal Philippi sand in the Figure 3.3, No.1 is Dolomite sand, No.2 is natural dune sand of West Cape, No.3 is currently sieved sand used in steel fibre ECC mixes, No.4 is F70 sand, and No.5 is F110 sand which used in most PVA fibre ECC mixes. The density of the natural dune sands is 2.7 kg/l.

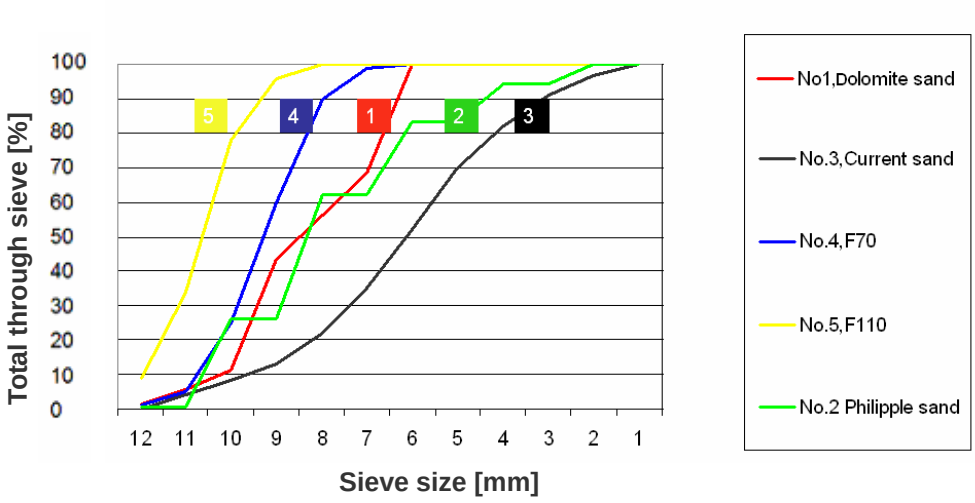

Figure 3.3 Grading of different sands used in this research

3.2.6 Superplasticizer (SP)

Two types of superplasticizer (SP) supplied from ChrySo were used in this research. They are Premia 100 and Optima 200.

SP improves the mix workability significantly and, subsequently affects the matrix flaw number, flaw size and flaw spatial distribution, as well as fibre distribution. Matrix flaw and fibre distribution both control tensile strain and stress. Data analyses from the Series I & II results provide information on how workability affects tensile and bending results.

Fibre distribution is an extremely important factor to determine ECC performance, because materials will always fail at fibre disconnections. Poor workability provides a weak matrix and affects fibre distribution; however, good workability does not automatically introduce good fibre distribution, although it seems to do so. The density of Superplasticizer is 1.2 kg/l.

3.2.7 Viscous agent (VA)

Another admixture in this research, namely the viscous agent methylcellulose, was added into the fresh mortar to provide good rheology and also even fibre distribution. The former is necessary for extruded material to be placed into the moulds and vibrated without the fibre settling on the bottom of the specimen. Also, for less heavy fibre, such as PVA fibre, MC enhances good fibre distribution in the matrix, an essential feature for good strain-hardening ECC.

3.2.8 Polyvinyl alcohol (PVA) fibre and steel fibre

Polyvinyl alcohol fibre is produced by Kuraray Co., Ltd., Japan. PVA fibre is hydrophilic, therefore, the strong bond between the matrix and fibre tends to break the fibre rather than pull it out of the matrix. This bounds the multiple cracking and leads to less or no strain hardening. To overcome this, PVA fibre is currently oil coated whereby fibres slip in the matrix, rather than break, following research by Li et al. (1997). The physical properties of

PVA fibre are listed in Table 3.7. Figure 3.4 shows the SEM photo image of the surface of PVA fibre and steel fibre. The straight high carbon steel fiber used in the investigation is produced by Bekaert. , Co., Ltd. The geometry and tensile strength of steel fibre is also listed in Table 3.7. The density of PVA fibre is 1.3 kg/L and of steel fibre is 7.85 kg/l.

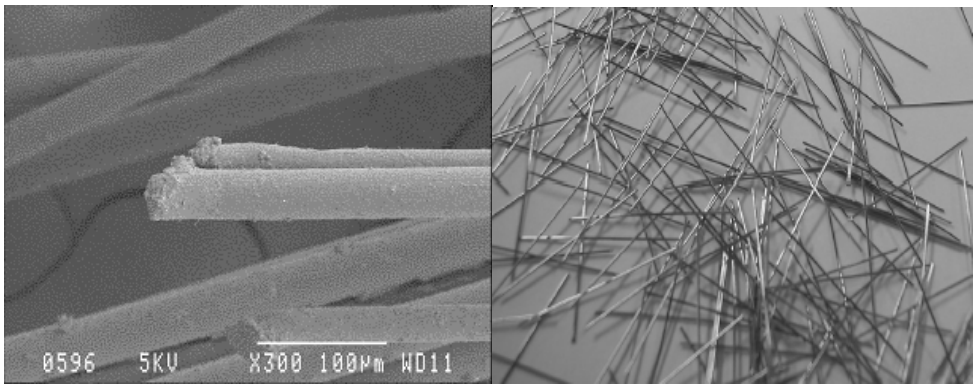

Figure 3.4 The surfaces of PVA fibre and steel fibre

Table 3.7 Geometry and physical properties of PVA fibre and steel fibre

Fibre type	Length (mm)	Diameter (um)	Elasticity modulus	Ultimate strain	Tensile strength	Coating
PVA	12	40	40KN/mm	6%	1600N/mm^2	Oil coated
Steel	13	160	200GPa		2000N/mm^2	Brass coating

3.3 Specimen preparation

The experimental programmes comprised direct tensile testing of dog-bone (generally four dog-bones/mix) and three-point bending of plates. The manufacturing procedure was either casting or extrusion. Most experiments were on cast examples, while a few plates produced by extrusion were also tested. The comparison between cast and extruded examples of the same mix is discussed in Chapter 4.

3.3.1 Dog-bone specimen preparation

The dog-bone specimen and the tensile clamp are showed in Figure 3.5. The size was 230 mm (length) x 60 mm (width) x 15 mm (thickness). The neck section was 30 mm wide.

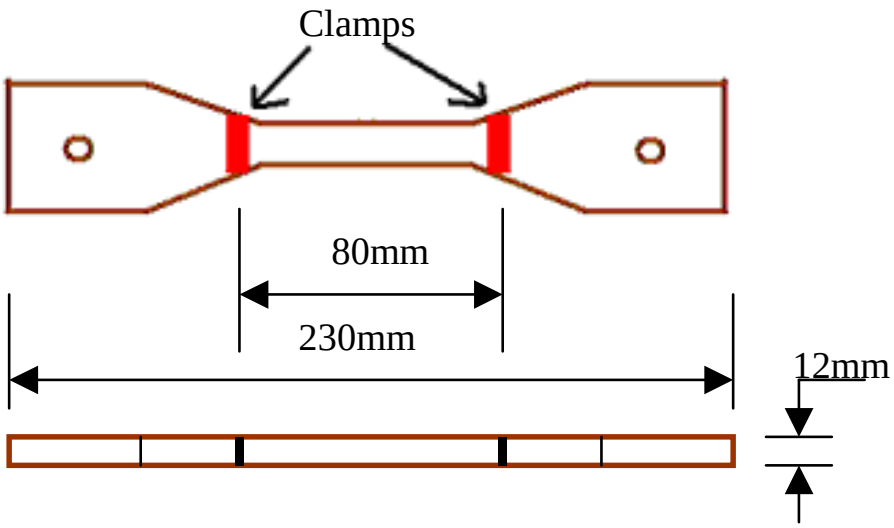

Figure 3.5 Dog-bone specimen showing LVDT fixing clamp positions

3.3.2 Bending beam specimen

The bending beam has the size of 500mm x 70mm x 15mm,as shown in Figure 3.6.

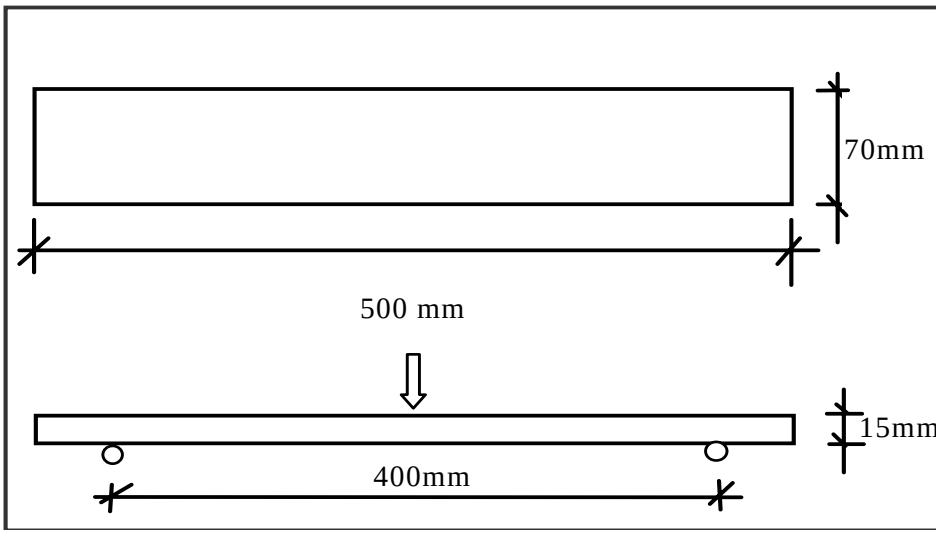

Figure 3.6 Three-point bending plate

3.4 Curing

All dog-bone specimens and plates were prepared, cured in constant temperature water (23^{o}C) for 14 days and then kept in a controlled climate of 23$\pm$2^{o} and RH 60$\pm$5% constant temperature for 7 days, and subsequently tested in direct tensile tests in the setup as shown by Figure 3.7 and 3.8.

3.5 Test methods

The tests used in the present research are direct tensile test and three point bending test.

3.5.1 The test equipments

The major equipments were used in this work are shown in Figures 3.7 to 3.9. They are the Zwick Z250 materials test machine, data collection equipment spider8 system, and the displacement measurement devices LVDT.

Figure 3.7 The Zwick Z250 Materials Testing Machine

Figure 3.8 The experimental data collection spider8 system

Figure 3.8 The displacement measurement devices LVDT set with sepcimen

3.5.2 Direct tensile test

A standard, constant displacement rate of 0.15 mm per minute for series I was set in a mechanical testing apparatus. After a comparison between the tensile displacement rate of 0.15 mm per minute and 1.5 mm per minute, series II and subsequent tensile tests were carried out at the constant displacement rate of 1.5 mm per minute.

LVDT measurement of deformation was made over a gauge length of approximately 80 mm, on both sides of each specimen and subsequently averaged. The cross section of the dog-bone in the gauge area was approximately 30mm x 15mm. All measurements were automatically maintained and collected. Figure 3.10 shows the set-up of direct tensile test.

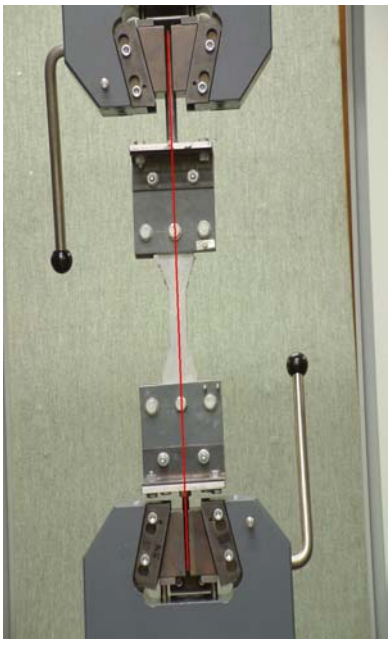

Figure 3.10 The direct tensile test set-up

3.5.3 Three-point bending test

The three-point bending tests were also performed at an age of 21 days. The crosshead speed was 1.5 mm per minute and the support span was 400 mm. All measurement were automatically maintained and collected.

Chapter 4

Experimental procedures

4.1 Mixing procedure

Chapter 3 introduced the materials and equipment used in this research. The manufacturing processes used were either casting of dogbones, and plates or extrusion of plates. All cast mixes were mixed by ‘cake’-mixer, and extruded mixes were mixed by ‘pan’-mixer in the Concrete laboratory of Structural Engineering Department, Stellenbosch University. Direct tensile tests and three point bending tests were employed to investigate the performance of FA-ECC, Slag-ECC and other influences on ECC properties. Some highly refined techniques were engaged to investigate the interface between fibre and matrix, micro-scale components of the matrix and the hydration product of ECC composites.

4.1.1 ECC mixing procedure and cast procedure

The mixing procedure for all PVA-ECC specimens is depicted in Figure 4.1. First, all materials of current mixes such as fibre, CEM I 42.5, or anything else, were weighed separately before starting the mix, the PVA fibre was blown by 4 bar air pressure in a specially prepared bin to separate the fibre. Subsequently, before mixing, the fibre was pre-wetted with 10 percent of the total water. All solid materials except PVA fibre were thrown into the ‘mixer’ for the dry mix. After 30 seconds dry mix, the remaining 90% water was added into the mixer. The mixer speed was then increased. SP was added into 1 minute after the water was added. The final step of mixing procedure was to add the damp PVA fibre into the mixer. The mixing was stirred at a high speed for another minute. Steel fibre did not need wetting.

After mixing was completed, workability and fibre distribution were judged and recorded. Workability was judged at 3 different levels uniformly, ranging between “self-compacting”, “moderated workability”, and “hard to compact”. Subsequently, the workability was measured by flow table tests (Stander & Li 2004). Also the fibre distribution was determined in a subjective way due to lack of an objective method. It was graded on a scale 1-3 by feeling (by hand) whether there were clumped (rated 1) or whether the fresh mix was smooth (rated 3).

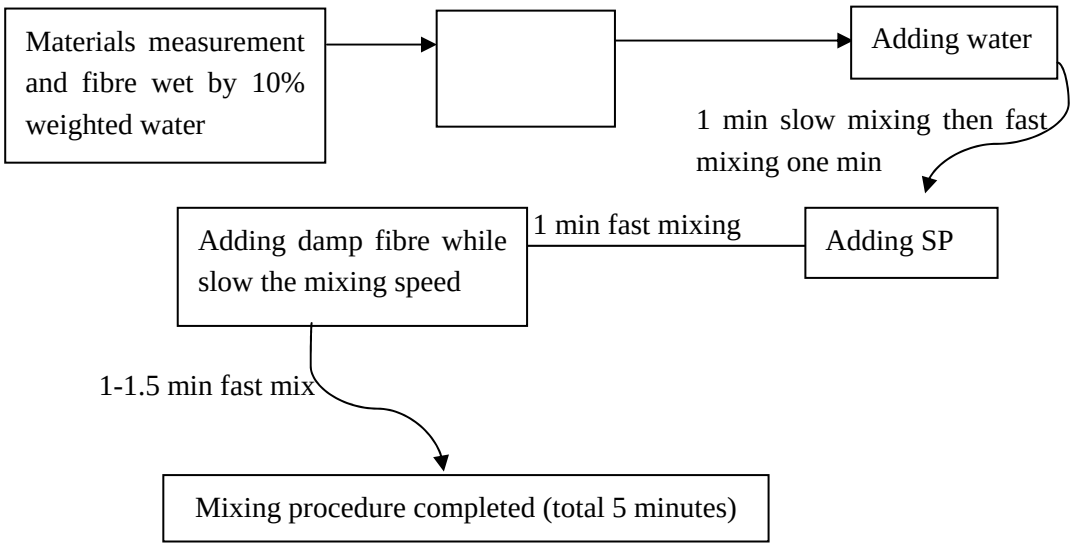

Figure 4.1 Flow chart of PVA fibre-ECC mixing procedure

After mixing was completed, the fresh mix was cast into four dogbone moulds. A heavy steel plate was put on the mould. Three 100 mm cube moulds were also cast. The fresh mix was also set into 13mm x 70mm x 500mm beam moulds for specimen preparing the bending test Then all specimens, with their moulds, were taken through an approximately one minute vibration. Some self-compactable material did not need to be vibrated, but poor workability materials (hard to compact) needed more than two minutes on the vibration table.

4.1.2 Extrusion mixing procedure

A piston extrusion machine used in the present research needs at least eight litres altogether. Thus, in all extrusion experiments, fresh materials were mixed in a 15-liter ‘pan’-mixer. Extrusion needs a much larger quantity of dry fresh material than normal cast processing. To save working time, the mixing procedure was approximately the same as the procedure of mixes for casting, but all water and SP were mixed and added into the pan together and fibre had to be mixed with the other solids at the dry mix stage. The final mixing step was extended to 3-4 minutes, to impose the workability influence. Thereby, the total mixing time was approximate 7-8 minutes.

The extrusion machine and processing were developed in a parallel research, conducted by Don De Koker & van Zijl (2004) at the University of Stellenbosch.

Only plates were extruded for bending tests, the cross section was also 70mm x 15mm as for

the cast specimen. All extrusion specimens were cut to a length of approximately 500 mm and made ready for curing.

4.2 Curing procedure

Most specimens were cured for 21 days for testing purposes. Certain variations in curing age will be specially mentioned at the appropriate junctures.

4.2.1 Cast specimen curing procedure

All dog-bone specimens and bending plates were stripped at the age of two days and then promptly taken into constant temperature (23^{o}C) water, after 12 days in water, the specimens were taken out and kept for 7 days in a controlled climate of 23$\pm$2^{0}C temperature and RH 60$\pm$5%.

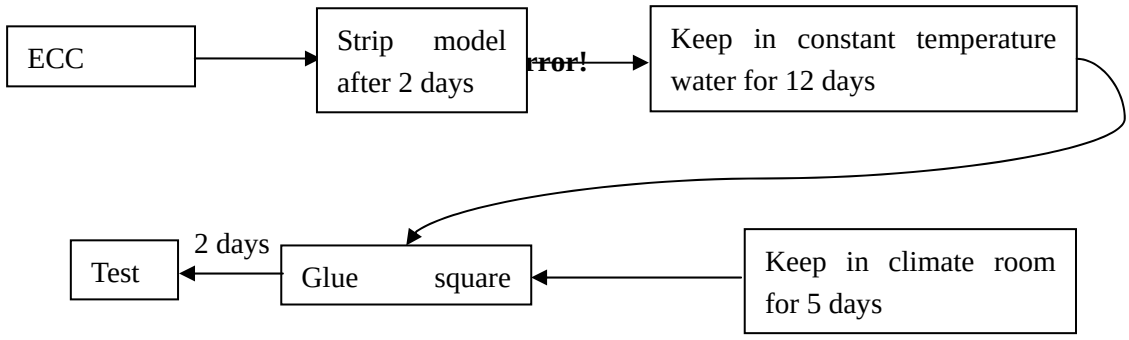

Figure 4.2 Curing procedures

4.2.2 Extrusion specimen curing procedure

Only bending plates were made by the extrusion process; all plates were kept in a curing room at RH = 100% for 14 days, subsequently moved and kept in controlled climate of 23$\pm$2^{0}C constant temperature and RH 60$\pm$5% for 7 days.

4.3. Direct tensile test

4.3.1 Specimen preparation

The preparation process started from two days before the test. First of all, all the dust on the surface of a specimen was carefully cleared away, and then two squares plastic plates were glued onto one side of the specimen. The position is shown in Figure 3.5. One square plate has a hole in the middle, so that LVDT could be clamped. On the second day, another two square plates were glued on the other side of the specimen. Before starting the test, the LVDT were calibrated.

4.3.2 Specimen setting up and test

The thickness of the specimen neck, its width and the distance between two square plates on same side of a specimen were measured. Afterwards, the specimen was encased in the upper clamping on the test frame and was tightened in it. Subsequently, the bottom clamping was raised till the hole through the clamping was equal to the hole in the specimen. The next step was to tighten clamping with six twist drills, first the bottom three were tightened; meanwhile the reading of the load cell was checked; if the reading was too large, then loose the handle on the bottom to release the supererogatory load on specimen. Subsequently, two LVDTs were set in the square plates. Before testing, the last step was to zero measurement readings, and then to start the measurements. A digital camera was used to record the cracks growing during the test.

4.4 Three point bending test

The preparation process of three point bending test is similar with that of direct tensile test. The only difference is that the specimen does not need glued on square plates for LVDTs.

Before starting the bending test, the bending equipment was set on the test frame. A digital camera was used to record the crack pattern during the test.

4.5 Micro-scale analyses

The next step was to investigate the interface between matrix and fibre and also composite hydration product influence. Micro-scale analyses were employed in this research, including Scanning Electron microscopy (SEM) photo image analysis and x-ray Spectrometry etc.

4.5.1 Scanning Electron Microscopy (SEM)

The SEM analysis was done at the University of Stellenbosch. The Leo 1430VP Scanning Electron Microscope is fitted with Secondary electron, Backscatter, Cathodoluminescence, Variable pressure, Cryo stage and Energy Dispersive detectors and a Link EDS system and software. The system is designed to do high-resolution imaging, quantitative analyses with errors ranging from 0.5 to 0.2wt% on the major elements and imaging of soft biological samples under variable pressure conditions. Quantitative analyses are performed with an accelerating voltage of 20 kV, beam current of 1.5 nA, spotsize of 473 and a working distance of 13mm. The ZAF procedure is applied for inter-element effects.

Approximately 1 cm cubes, sawn from tensile dog-bone specimens, were dried at 60^0C and gold-coated for observation by an SEM analysis. This was done to characterize the interface between fibre and matrix, fibre distribution and to identify the element component and shape of the cement replacement particles and composite hydrated products respectively. The hydration product crystal was also identified by X-Ray Fluorescence Spectrometry analysis.

4.5.2 X-Ray Fluorescence Spectrometry (XRF)

Whole specimen chemical analyses were done by XRFS on a Philips 1404 Wavelength Dispersive spectrometer, at the University of Stellenbosch. Major elements were analysed on a fused glass bead at 50 kV and 50 mA tube operating conditions and trace elements were analysed on a powder briquette at 60 kV and 40 mA tube operating conditions. Matrix effects in the samples were corrected for by applying theoretical apha factors and measured line overlap factors to the raw intensities measured with the SuperQ Philips software.

4.6 Remarks

4.6.1 Cast of series I, workability and W/B

To identity the influence of cement replacement content in matrix, some indices should be set uniformly, such as fibre content. Series I stick to PVA fibre 2.5% proportion by volume. For workability, it is very difficult to control the exact W/B ratio. Practically on a building site, workers would normally control the workability. Therefore the philosophy of this research was to ensure equal workability. The W/B ratios were modified slightly for this research. The main motivation for this choice is that good workability is essential for proper fibre distribution, an essential feature for multiple cracking, accompanied by strain hardening. Chapter 8 investigates W/B influence.

4.6.2 Cast of series II, workability and viscous agent

Series II is a series of mixes of steel fibre-ECC. There are obviously different rheological properties relating to steel fibre-ECC as opposed to PVA fibre-ECC. Steel fibre-ECC seems not as sensitive for the SP dosage as PVA fibre-ECC. Workability does not only depend on SP and W/B, but also VA content. VA addition in PVA-ECC is meant to handle the fibre-clumping problem, but in steel-ECC it works to prevent fibre separation. A clear phenomenon was observed from steel-ECC mixing, as follows: When no VA was added, the mix looks very fluid, even liquid. But as VA addition is stepped up per 0.1%, the mix becomes significantly tougher. However, the influence on workability of VA becomes less apparent when VA addition is stepped up above 0.5 % by binder.

SP working time seems to be affected significantly by workability. So the whole mixing time should be ruled by workability, as it appears and one should not stick to a fixed mixing time, which normally is based on SP work time.

Chapter 5

Experimental results

In previous chapters, a survey of theory and the experimental program involved in the present research were introduced. The present experimental program involves two kinds of investigations, i.e. strain & stress correlation and micro-scale exploration. The whole experimental program was carried out by performing tests on three series of mixes, which are PVA fibre-ECC, steel fibre-ECC and, thirdly, sensitivity studies to investigate various influences on ECC.

In many major applications, ECC materials are likely to be subjected to stress gradients, e.g. by flexural action rather than direct tensile constraint. However, flexural testing is not suitable for determining the material characterization of ECC, this is because the flexural strength measurement includes the fracture energy, whereby these individual mechanical properties cannot be distinguished. The direct tensile stress - strain relation is the most appropriate method used in the present research to analyse ECC performance. From these results, the first crack tensile strain ε_M [%], first crack tensile stress σ_M [N/mm^2], ultimate tensile strain ε_U [%], ultimate tensile stress σ_U [N/mm^2], as well as tensile strain capacity ε_F [%] can be determined. Note that the first point of significant gradient change in the zoomed in stress-strain response curve is recognized as the first crack. This gradient change indicates that the E modulus of the matrix changed. The corresponding stress and stain values are collected as the first crack stress σ_M and strain ε_M respectively. This point can be observed usually in three conditions; the gradient becomes negative after this point, the gradient reduces but is still positive after this point and the unusual situation that the stress-strain response grows up perfect smoothly in a nonlinear fashion, which means there is a continuous gradient change in the ascending stress-strain branch. In this chapter there is also reference to $g\tau$, which is a multiple of the snubbing factor g and the interfacial bond or the ultimate shearing resistance τ as introduced in Chapter 2. They work together for the creation of multiple cracking and strain hardening. To study how, uniaxial tensile behaviour translates to flexural behaviour, three point bending test were also performed in this study. Resistance and deflection in three-point bending testing also contribute to the sensitivity studies examining various influences on ECC investigations.

Section 5.1 presents the results of PVA fibre-ECC, including FA-ECC and Slag-ECC series, as well as the trend of these parameters with cement replacement content. Section 5.2 presents the results of a series of mixes of steel fibre-ECC. The different tensile strain trend of PVA fibre ECC and steel fibre ECC with binder portion of FA is also discussed here. Section 5.3 presents the results of a series of sensitivity study programmes.

5.1 Series I. PVA fibre-ECC

Tests were performed at a curing age of 21 days, during which the specimens were cured as described in section 4.2. The tests were performed at a standard displacement rate of 0.15 mm per minute in a mechanical material testing apparatus. All direct tensile parameters, as determined from the resulting stress - strain data, are listed in Table 5.1. The graph to illustrate these parameters was shown in section 2.1.2.

Table 5.1 (1) Direct tensile results for series I PVA fibre-ECC part I

	ε_M [%]	σ_M [N/mm^2]	ε_U [%]	σ_U [N/mm^2]	ε_F [%]	gτ [N/mm^2]
S1	0.018	1.48	0.29	3.32	2.42	0.42
	0.017	3.17	0.30	3.68	2.15	0.46
	0.025	2.75	0.83	3.05	0.99	0.38
AVG	0.020	2.47	0.47	3.35	1.85	0.42
STDEV	0.004	0.88	0.31	0.32	0.76	0.04
CoV	21.8%	35.6%	66.6%	9.5%	41.0%	9.5%
S2	0.023	3.39	1.02	5.34	1.63	0.67
	0.027	3.42	0.50	5.29	2.36	0.66
	0.025	3.42	0.55	4.50	1.12	0.56
	0.032	3.81	1.12	4.57	1.51	0.57
AVG	0.027	3.51	0.80	4.92	1.66	0.62
STDEV	0.004	0.20	0.32	0.45	0.52	0.06
CoV	14.4%	5.7%	40.0%	9.2%	31.3%	9.4%
S4	0.019	2.68	0.82	3.77	1.30	0.47
	0.021	3.48	1.60	6.19	1.96	0.77
	0.035	3.86	3.24	5.83	3.40	0.73
AVG	0.025	3.34	1.89	5.27	2.22	0.66
STDEV	0.009	0.60	1.24	1.31	1.07	0.16
CoV	35.6%	18.0%	65.6%	24.8%	48.4%	24.7%

Table 5.1 (2) Direct tensile results for series I PVA fibre-ECC part II

	ε_M [%]	σ_M [N/mm^2]	ε_U [%]	σ_U [N/mm^2]	ε_F [%]	gτ[N/mm^2]
S5	0.032	3.55	0.13	3.63	1.29	0.45
	0.034	2.95	5.48	6.03	5.13	0.75
	0.026	2.95	0.52	3.84	1.21	0.48
	0.024	2.56	4.17	5.09	5.70	0.64
AVG	0.029	3.00	2.58	4.65	3.33	0.58
STDEV	0.005	0.41	2.66	1.12	2.42	0.14
CoV	16.4%	13.5%	103.2%	24.2%	72.5%	24.2%
S6	0.017	3.23	0.13	6.26	1.29	0.78
	0.032	4.49	1.63	6.40	3.10	0.80
	0.031	5.02	0.11	5.04	0.11	0.63
	0.024	4.05	0.79	6.16	1.91	0.77
AVG	0.026	4.20	0.67	5.97	1.60	0.75
STDEV	0.007	0.75	0.72	0.62	1.25	0.08
CoV	26.8%	18.0%	107.7%	10.5%	77.9%	10.4%
S7	0.037	2.24	4.39	4.29	4.39	0.54
	0.040	1.70	4.86	3.17	5.97	0.40
	0.040	1.77	5.00	2.92	6.55	0.36
	0.031	2.15	5.76	4.14	6.38	0.52
AVG	0.037	1.96	5.00	3.63	5.82	0.46
STDEV	0.004	0.27	0.57	0.69	0.99	0.09
CoV	11.5%	13.7%	11.4%	19.0%	16.9%	19.5%
S8	0.013	2.62	4.02	6.58	4.77	0.82
	0.028	3.61	0.19	4.86	0.93	0.61
	0.027	3.97	3.71	6.47	4.69	0.81
	0.032	3.36	1.63	5.29	1.90	0.66
AVG	0.025	3.39	2.39	5.80	3.07	0.73
STDEV	0.008	0.57	1.81	0.86	1.96	0.11
CoV	33.1%	16.9%	75.8%	14.8%	63.6%	14.6%

Table 5.1 (3) Direct tensile results for series I PVA fibre-ECC part III

	ε_M [%]	σ_M [N/mm^2]	ε_U [%]	σ_U [N/mm^2]	ε_F [%]	gτ[N/mm^2]
S9	0.013	2.37	0.55	3.10	1.14	0.39
	0.027	3.07	2.00	4.79	7.93	0.60
	0.022	2.56	1.51	3.91	2.81	0.49
	0.017	2.60	1.97	4.55	2.67	0.57
AVG	0.020	2.65	1.51	4.09	3.64	0.51
STDEV	0.006	0.30	0.68	0.75	2.96	0.09
CoV	30.8%	11.2%	45.1%	18.4%	81.4%	18.3%
S10	0.056	2.10	6.34	4.62	7.97	0.58
	0.029	2.56	4.85	4.37	6.34	0.55
	0.065	2.42	2.21	3.27	5.00	0.41
	0.030	2.24	2.11	3.09	3.79	0.39
AVG	0.045	2.33	3.88	3.84	5.77	0.48
STDEV	0.018	0.20	2.08	0.77	1.80	0.10
CoV	40.6%	8.7%	53.6%	20.1%	31.1%	20.0%
S11	0.029	3.34	2.17	3.92	2.92	0.49
	0.024	2.45	1.14	3.31	2.33	0.41
	0.028	3.49	1.56	4.10	2.07	0.51
	0.027	2.64	5.75	4.91	6.89	0.61
AVG	0.027	2.98	2.66	4.06	3.55	0.51
STDEV	0.002	0.51	2.11	0.66	2.25	0.08
CoV	8.0%	17.1%	79.2%	16.2%	63.4%	16.1%
S12	0.110	1.15	2.86	3.47	4.27	0.43
	0.020	2.18	1.50	3.97	3.94	0.50
	0.024	2.08	0.79	2.79	2.31	0.35
	0.017	2.99	1.14	4.15	2.61	0.52
AVG	0.043	2.10	1.57	3.60	3.28	0.41
STDEV	0.045	0.75	0.91	0.61	0.97	0.08
CoV	105.1%	35.9%	57.7%	17.0%	29.5%	18.8%

Table 5.1 (4) Direct tensile results for series I PVA fibre-ECC part IV

	ε_M [%]	σ_M [N/mm^2]	ε_U [%]	σ_U [N/mm^2]	ε_F [%]	gτ[N/mm^2]
S13	0.018	1.69	0.85	3.53	1.83	0.44
	0.029	3.29	2.33	3.68	2.96	0.46
	0.096	2.48	1.51	3.23	3.15	0.40
	0.06	2.41	1.81	3.83	4.65	0.48
AVG	0.051	2.47	1.62	3.57	3.15	0.45
STDEV	0.035	0.66	0.62	0.26	1.16	0.03
CoV	69.0%	27.0%	38.0%	7.2%	36.8%	7.7%
S14	0.033	1.52	2.94	3.96	5.17	0.50
	0.020	1.80	0.52	2.62	1.89	0.33
	0.018	1.89	3.06	3.88	4.94	0.49
	0.020	2.49	1.69	4.02	2.38	0.50
AVG	0.023	1.92	2.05	3.62	3.60	0.46
STDEV	0.007	0.41	1.19	0.67	1.70	0.08
CoV	29.4%	21.2%	58.2%	18.5%	47.3%	18.3%
M34	0.042	5.32	0.04	5.33	0.04	0.67
	0.039	3.76	0.99	4.31	1.24	0.54
	0.036	4.26	0.94	5.10	4.79	0.64
AVG	0.039	4.45	0.66	4.92	2.02	0.61
STDEV	0.003	0.80	0.53	0.53	2.47	0.07
CoV	7.1%	18.0%	81.2%	10.8%	122.1%	10.8%
SF8	0.022	2.77	0.57	3.44	1.63	0.43
	0.010	1.23	0.38	3.21	3.61	0.40
	0.021	2.23	1.03	3.41	2.39	0.43
	0.018	2.49	0.81	3.34	1.23	0.42
AVG	0.018	2.18	0.70	3.35	2.22	0.42
STDEV	0.005	0.67	0.29	0.10	1.05	0.01
CoV	30.6%	30.9%	41.0%	3.0%	47.2%	3.0%

From the experimental results shown in Table 5.1 (1 – 4), some trends were observed.

1. A significant amount of FA content leads to a relatively low strength at 21 days, first crack strength shifting in the range between 2 and 4.5 N/mm^2, and the ultimate strength range from 2.5 and 5 N/mm^2, ductile post-cracking tensile response in some cases and an increase in tensile resistance, so-called strain hardening, exceeding 6% strain.

2. The replacement of cement with a significant amount of Corex slag (GGCS) results in a notable increase in matrix strength ranging between 3.3 and 4.2 N/mm^2, and ultimate tensile stress ranging between 4 and 6 N/mm^2, but significantly less ductile, inelastic behaviour less than 3 N/mm^2.

3. The replacement of cement with significant amounts of the combination of FA and slag, as was done in S 8, creates a cement-based material with a strong matrix, strain-hardening, tough post initial crack tensile response.

4. Considering the M 34, SF8, S1, S5, and S7, they are FA-ECC with FA content fraction range from 30% to 70%. The average ultimate tensile strains, which indicate the ultimate crack occurring, of are 0.66, 0.70, 0.47, 3.58, and 5.00, respectively. This indicates that if FA content exceeds 50%, the FA content significantly delays the ultimate crack occuring. The high volume FA content enhances the multiple-cracking formation, resulting in a delayed cracks amalgamation and localization. For Slag-ECC mix S2 (50% GGCS content), S6 (55% GGCS content), and S4 (70% GGCS content), the ultimate tensile strains are 0.8, 0.67, and 1.89. Only 70% content Slag-ECC shows significantly increased ultimate tensile strain.

5. The $g\tau$ can be considered as a parameter to indicate the ultimate frictional bond and slip hardening level. As the same workability was set for all mixes, it is assumed that they have the same fibre distribution and inclined angle. Therefore the same snubbing effect for the same fibre type and matrix workability is assumed. The $g\tau$ value of FA-ECC series M34, S1, S5, S7, and S10 are 0.61, 0.42, 0.58, 0.46, and 0.48 respectively. Distinct values can be found from Slag-ECC of S2, S4, and S6. They are 0.62, 0.66, and 0.75 respectively. The $g\tau$ value of Slag-ECC is approximately one and half times that of FA-ECC, which indicates that ultimately Slag-ECC has a much higher frictional force than FA-ECC, when considering $g\tau$ values of S7 and S10, which were mixed with ASTM F110 and F100 sand.

Furthermore, S7 and S10 have first crack strength of mixes with ASTM F110 and F100 sand with approximately the same $g\tau$, which indicates that the grading of sand does not affect the interfacial frictional bond of 70%FA content FA-ECC.

5.1.1 FA dominated binder replacement

The trend of first crack strength and strain, ultimate stress and strain, and failure strain with cement replacement levels are shown below in this section and the following sections. They are important indictors of ECC behaviour. First crack strength indicates matrix tensile strength; ultimate tensile stress indicates composite stress capacity. Ultimate tensile strain indicates the ability to delay the crack localization process. Failure strain indicates composite

tensile strain capacity. Figures 5.1 to 5.4 show the trend of first crack stress and strain, ultimate stress and strain, and failure strain with the binder portion of FA and the W/B. Note, the red line is the first crack stress of the composite at the W/B of 0.45, And the block points shows the first crack stress of the composite with W/B of 0.40. They are Mixes Mix34 (30%FA), SF8 (40%FA), S1 (50%FA), S5 (55%) and S7 (70% FA) respectively. This examines the influence of FA as cement replacement on ECC behaviour and aims at finding a constant matrix design for the investigation of other matrix influences. In Figure 5.2and subsequent parallel Figures, black dots show the average of values of various specimens of the same mix and lines through black dots show the scatter of values of different specimens of one mix.

There is a reduction trend of first crack stress and ultimate stress when the binder portion of FA varies from 30% to 40% but an approximately same level of binder portion of FA in the range between 40 and 70% in despite of W/B ratio changed. This is in agreement with the widely acknowledged fact that FA content beyond 30-40% does not participate in the hydration process, but should be seen as mere filler material, or aggregate.

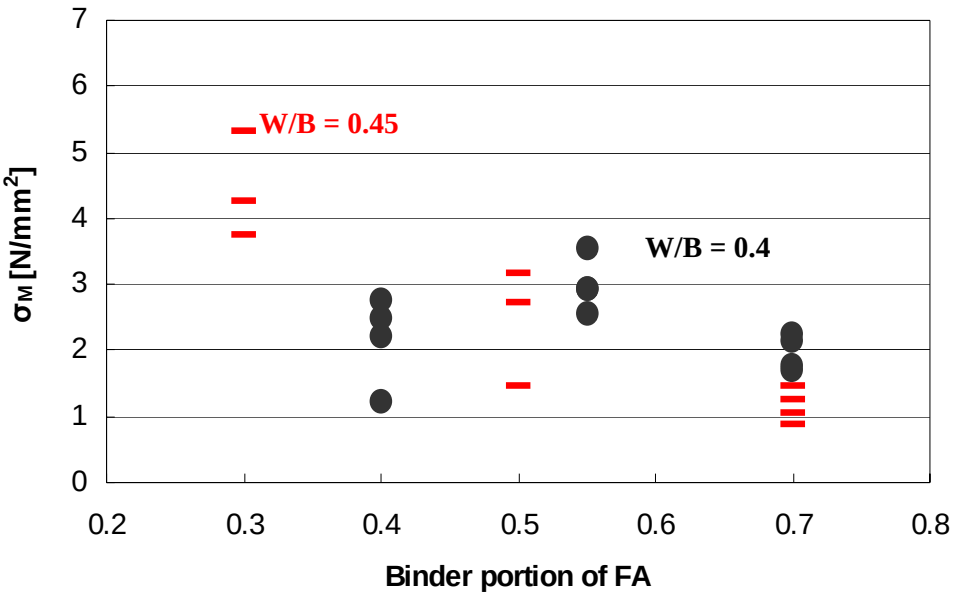

Figure 5.1 Trend of first crack strength with binder portion of FA

Figure 5.2 shows the ultimate tensile stress trend with the binder portion of FA range from 30% to 70%. Mix with 30% FA content has higher tensile stress and there is no significantly trend for the FA content range from 40 to 70%.

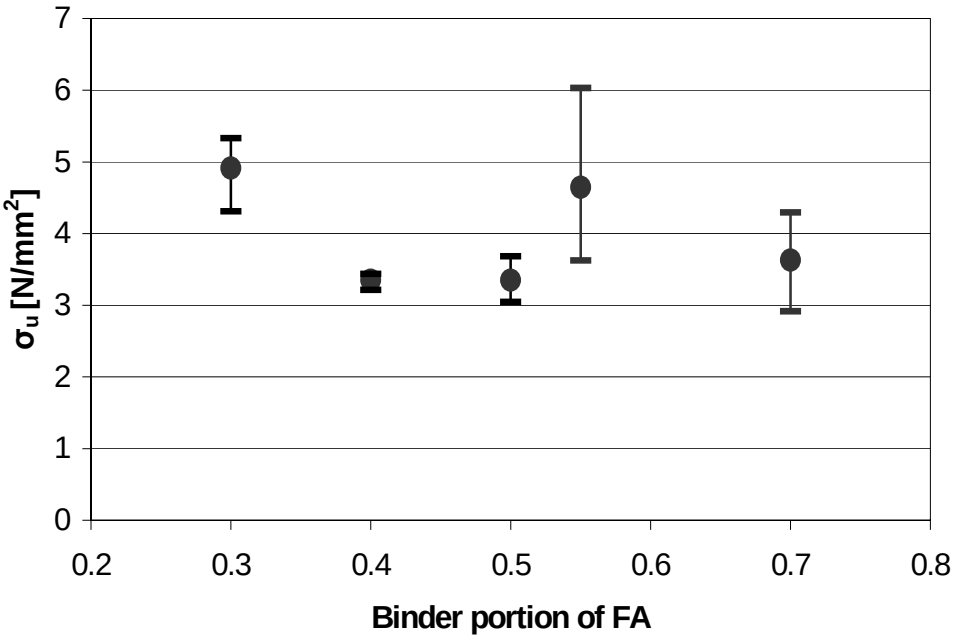

Figure 5.2 Trend of ultimate strength with binder portion of FA

Figures 5.3 and 5.4 show the tensile strain trend with binder portion of FA range from 30% to 70%. Ductility increases as binder portion of FA increases to more than 50%. Li also reports an ultimate tensile strain jumped from 0.38 to 1.86 when FA fraction of the binder ranged from 44% to 55% (Wang & Li 2004). The big change in tensile strain when the proportion of FA is about 50% might be because the FA may more effectively influence the interface properties when FA content is beyond 50%. In Chapter 6, the influence of FA on interfacial properties will be discussed. Nevertheless the high variability make clear calculation difficult, more experiments should be performed to shed light on this matter.

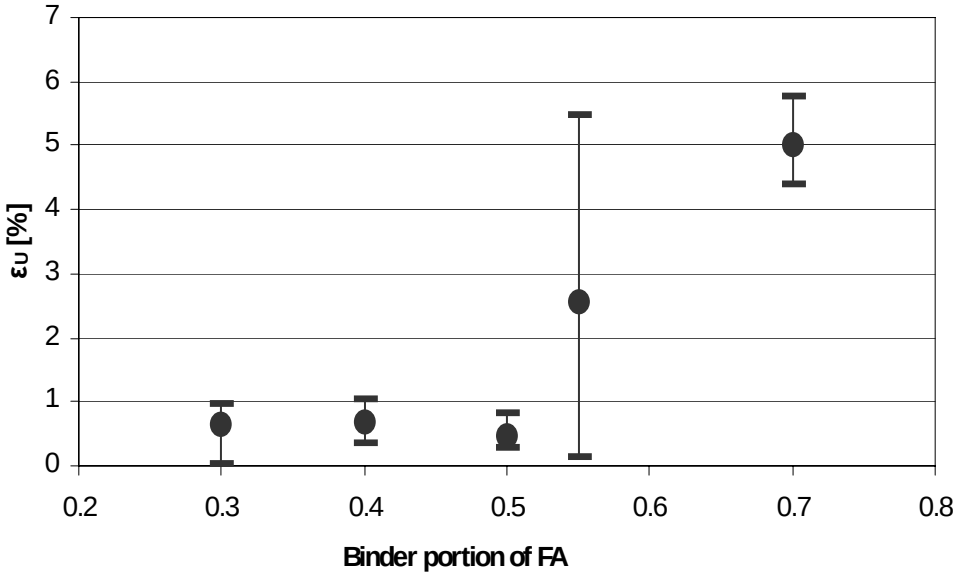

Figure 5.3 Trend of ultimate strain with binder portion of FA

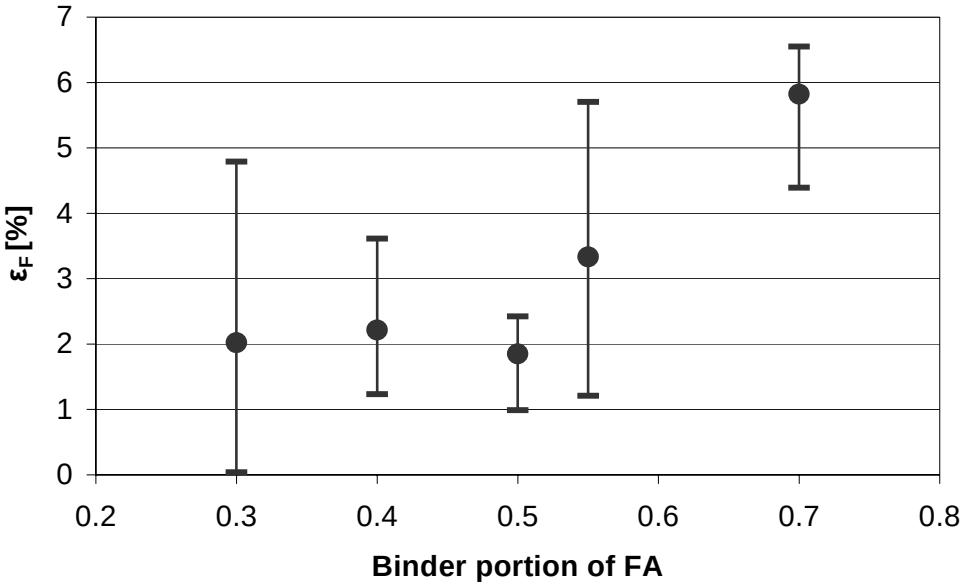

Figure 5.4 Trend of failure strain with binder portion of FA

There is a rough trend of ultimate tensile stress (σ_U) with first crack stress (σ_M) in the FA-ECC series, which indicates that high matrix crack strength leads to a high ultimate tensile stress for some mixes. However, also, some mixes have an ultimate tensile stress independent of matrix strength. It might possibly be because some mixes have a constant interfacial bond irrespective of matrix strength. The latter is in agreement with the prediction of the tensile strength by equation (2.7), where matrix strength does not appear.

5.1.2 GGCS dominated binder replacement

Figures 5.5 to 5.8 show the trend of first crack stress and strain, ultimate stress and strain, and failure strain with the binder portion of GGCS. This indicates the influence of GGCS as cement replacement on ECC behaviour. The mixes are S2 (50%GGCS), S6 (55%GGCS), and S4 (70% GGCS).

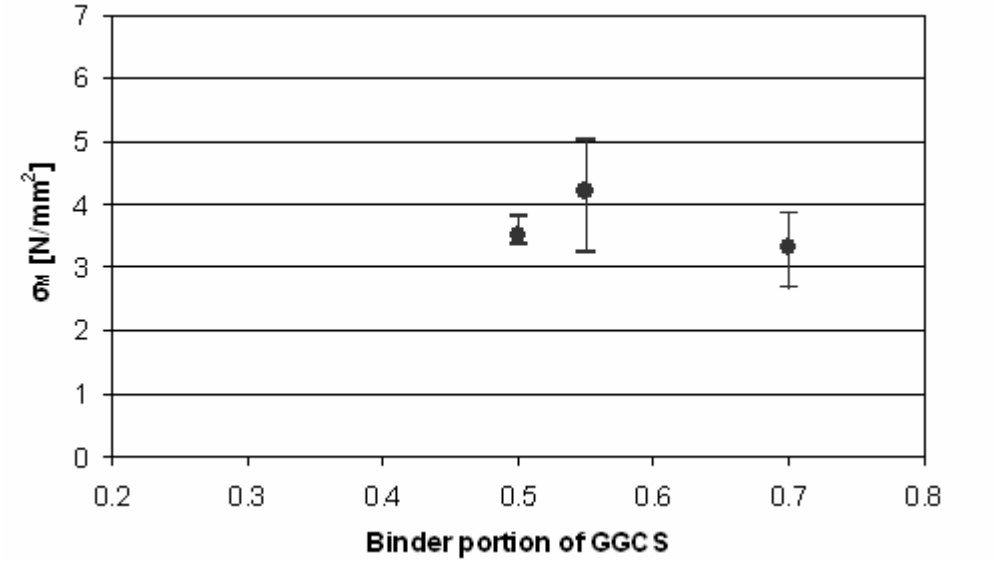

Figure 5.5 Trend of first crack strength with binder portion of Slag

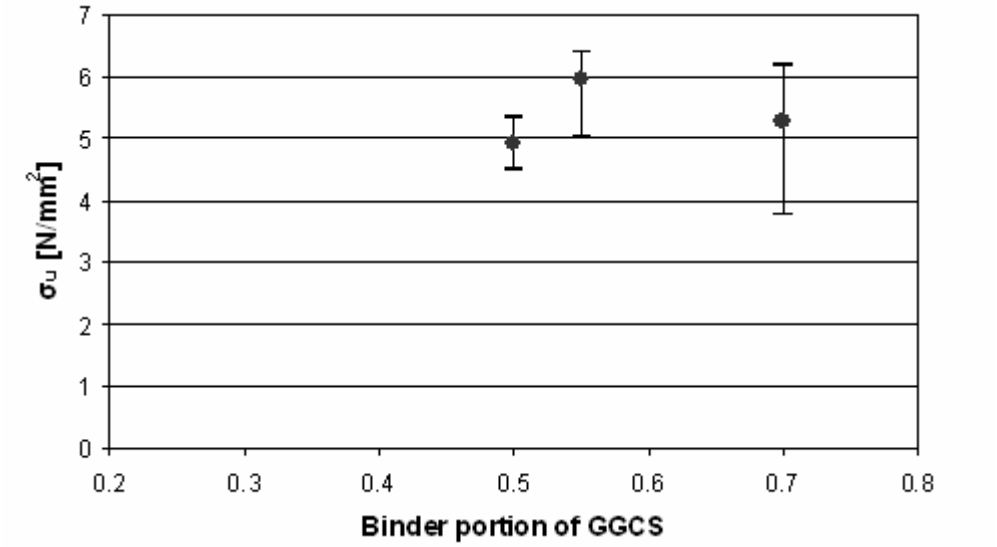

Figure 5.6 Trend of ultimate crack strength with binder portion of Slag

The results show a fairly equivalent trend in first crack strength σ_M and σ_U with the binder portion of GGCS. However, increased slag content does not lead to a clear trend of increased matrix strength and ultimate strength. The 55% GGCS content reaches the highest matrix and ultimate tensile stress. A similar result was obtained by Alexander (2003), namely that 50% GGCS proportion of binder has a higher compressive strength with a W/B ratio of 0.4 than cement concrete, at the age of 28 days. This may be an indication that binder portion of 50% GGCS has a negative effect on matrix strength. The reason may be that the rapid hydration speed leads to swift hydrated crystal growth, resulting in an extremely large crystal build-up, hence the matrix might have higher porosity after a relatively long curing age. In addition, high volume GGCS content also prolongs the cement hydration process and partially hydrated C-S-H gels build-up.

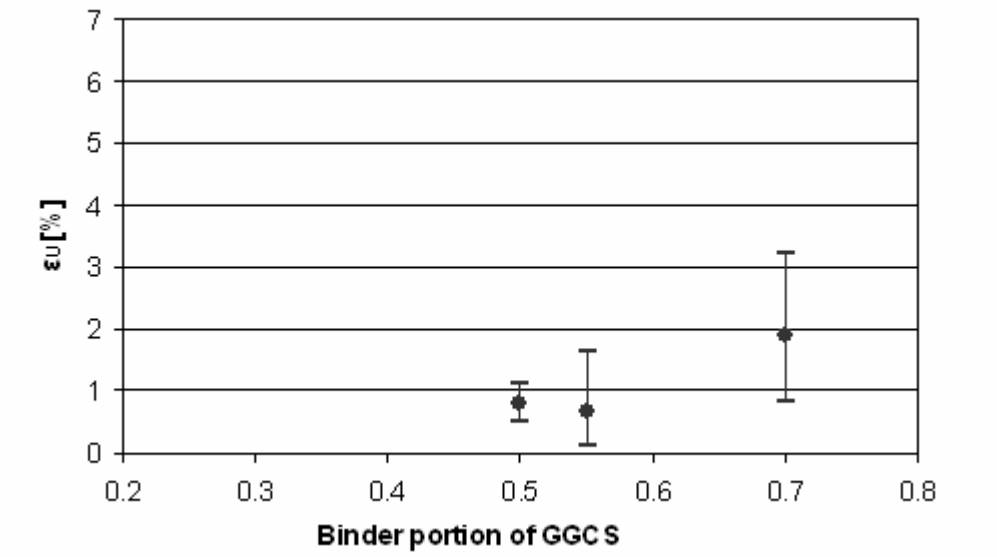

Figure 5.7 Trend of ultimate strain with binder portion of Slag

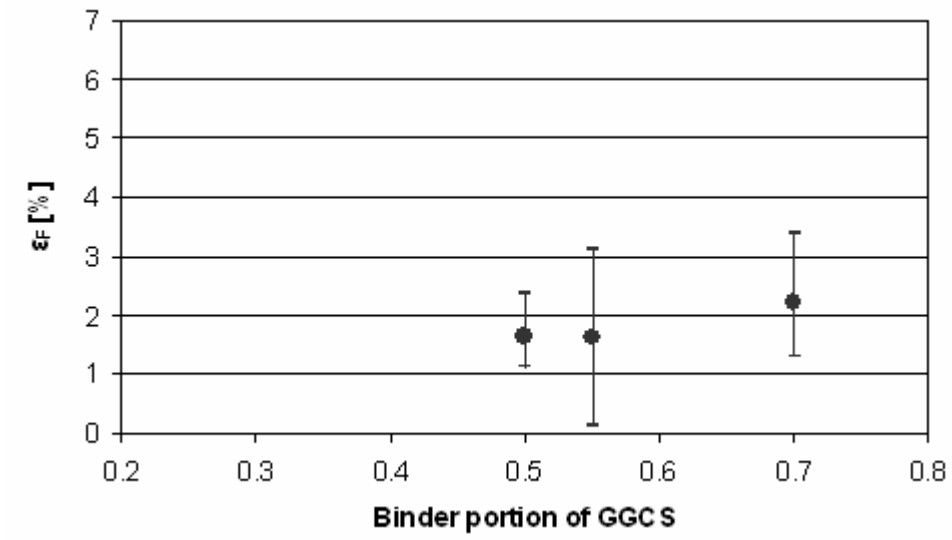

Figure 5.8 Trend of strain capacity with binder portion of Slag

The ultimate tensile strain and tensile strain capacity showed an opposite trend to that observed with tensile strength. Higher tensile strength leads to a lower strain capacity. Higher tensile strength means a higher interface bond for Slag-ECC, resulting in more fibre rupture, rather than fibre pull-out. Hence the fibre bridging functions were reduced, resulting in a much too small transmitted load to create multiple cracks. Tensile strain capacity was therefore reduced significantly from those for FA-ECC.

Due to the limited experimental period, there are only 3 mixes to show the trend of the GGCS content influence. It is actually not enough and can only be an indication. The more mixes and results will be reported in the next section.

5.1.3 Direct tensile behaviour trend with cement replacements of FA & GGCS

This programme of mix series led to the investigation of the combination of slag (GGCS) and FA as cement replacement, which showed very important behaviour at both early curing age and curing after a long time. The aim is to keep the large strain capacity of FA-ECC, but increase its lower tensile strength. Furthermore, we need to consider the situation of a lack of FA in Cape Province. The useful investigation of slag resulted in awareness of its potential. The investigation of the combination comprised a programme that replaced 70% or 55% of the cement with a FA and GGCS combination, and modified the FA and slag ratio of the combination.

The trends of tensile behaviour with the combination of FA and GGCS are shown in Figure 5.9 to Figure 5.12. The FA and GGCS content marked at the x-axis of these curves indicate the binder proportion of FA and GGCS respectively. The mixes are S8, S9, S14, S11, and S13 from left to the right respectively.

From Figure 5.9 and Figure 5.10 it can be observed that there is a slightly decreased trend in ultimate stress with the binder portion consisting of FA, but a flat trend of first crack stress with a binder portion of FA. Compared with FA-ECC tensile stress results, the matrix has slightly higher matrix crack strength than the same FA content FA-ECC, all ranging around approximate 2.5 N/mm^2 and 4.5 N/mm^2. Dissimilarly, the first crack strength of Slag-ECC is ranged between approximate 3.3 N/mm^2 and 4.2 N/mm^2. However, the ultimate tensile stress increased more than with FA-ECC. Mix S8 has a high ultimate stress of even up to 6 N/mm^{2}in spite of relatively low matrix crack strength.

Accordingly, Figures 5.11 and 5.12 show the trends of ultimate tensile strain and strain capacity with the binder portion consisting of FA and GGCS. In contrast with the tensile stress trend, both the ultimate tensile strain and strain capacities have nearly constant trends on average. Those values are clearly higher with than those for pure Slag-ECC.

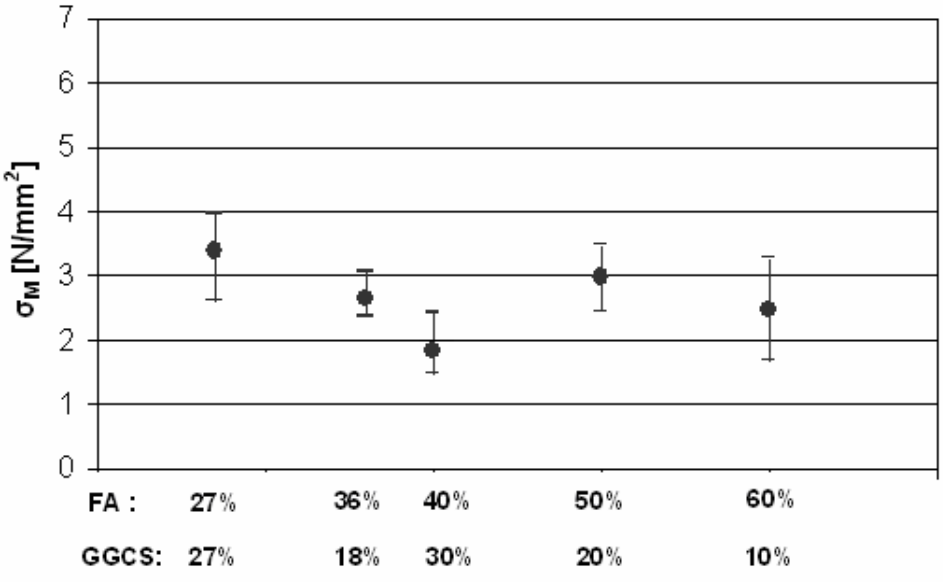

Figure 5.9 First crack stress with the combination of FA & GGCS

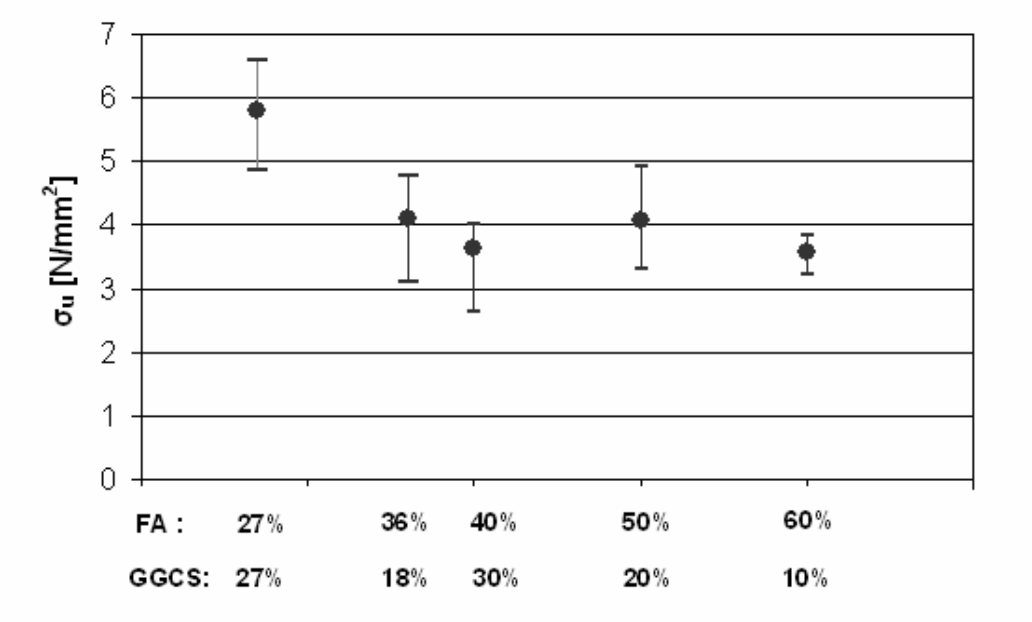

Figure 5.10 Ultimate tensile stress with the combination of FA & GGCS

The increase of tensile strain capacity can be due to the tailoring of matrix flaw size and distribution by FA content. Relatively stronger fibre/matrix interface bond is also achieved due to the enclosure of fibre by GGCS hydrated product. Thus, the larger transmitted force can reach the matrix crack strength in a shorter length and therefore enhance the multiple cracks.

Nevertheless, there is still some room for further study. That the tensile stress of combined FA & Slag-ECC has reasonable repeatability can be observed from the smaller scatter of strength. The strain trends, however, show a very large scatter with a coefficient of variation up to 80% (S9 Table 5.1). It indicates that the mechanisms of combined FA & Slag-ECC can be very complex and unpredictable.

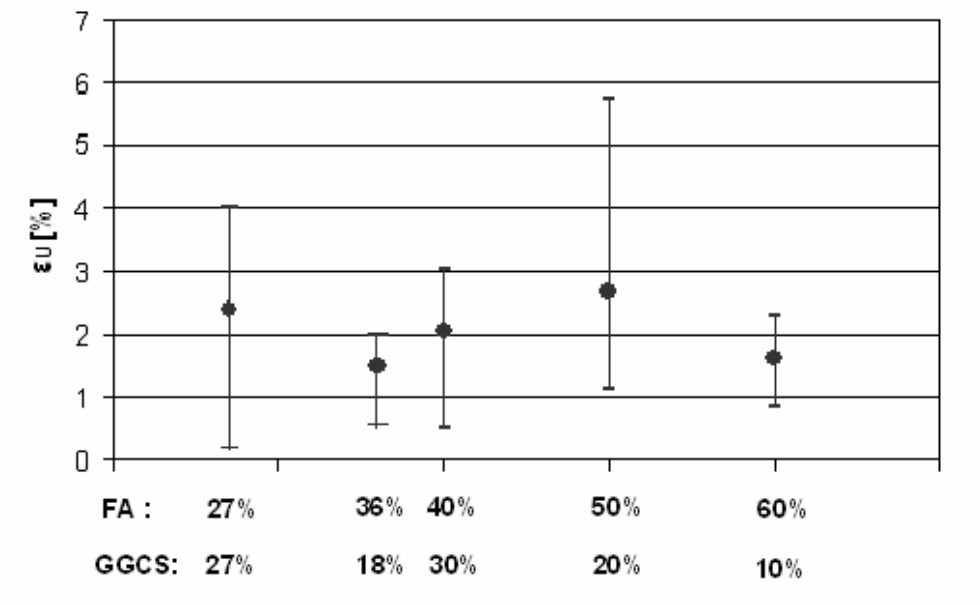

Figure 5.11 Ultimate strain with the combination of FA & GGCS

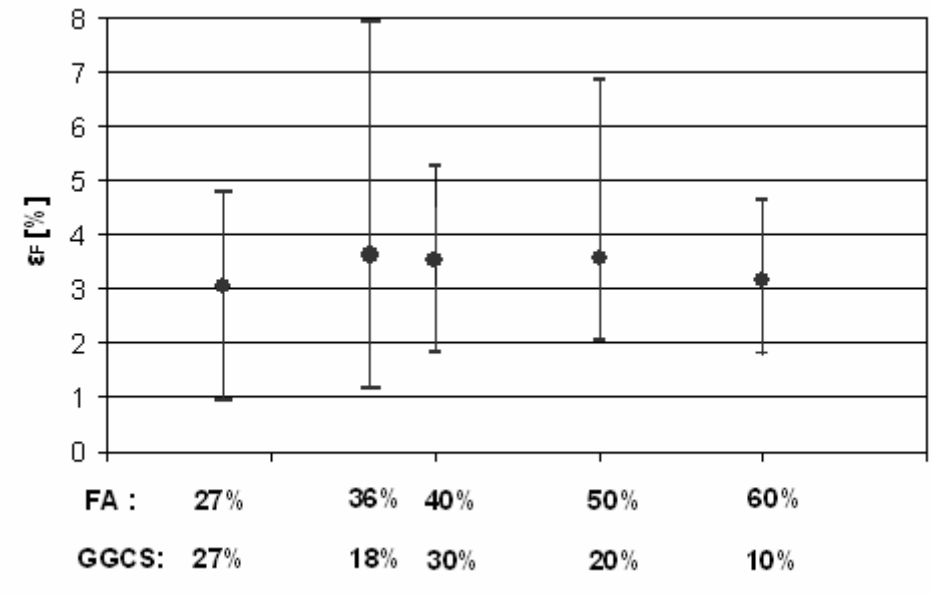

Figure 5.12 Failure strain with the combination of FA & GGCS

5.2 Steel fibre-ECC

As with PVA fibre-ECC system, the programme of tests of steel fibre-ECC was performed at an age of 21 days, during which time the specimens had been wet cured. The tests were performed at a standard displacement rate of 1.5 mm per minute in a mechanical -materials testing apparatus. All direct tensile parameters, as determined from the resultant stress- strain data, are listed in Table 5.2. The scheme to illustrate these parameters was shown in section

2.1.2. The mixes SF 1 to SF 7 are a steel fibre-ECC series with FA content ranging from 30% and 70%. Mix details can be found in Table 3.2. The trend of tensile behaviour with FA content and the difference in tensile behaviour between steel fibre-ECC and PVA fibre ECC are presented and discussed in subsequent sections.

Table 5.2(1) Direct tensile results for series II Steel fibre-ECC part I

	ε_M [%]	σ_M [N/mm^2]	ε_U [%]	σ_U [N/mm^2]	ε_F [%]	gτ[N/mm^2]
SF2	0.023	6.84	0.05	8.00	0.05	1.00
	0.023	7.07	0.03	7.98	0.57	1.00
	0.022	6.64	0.21	7.83	0.59	0.98
	0.020	6.93	0.27	9.98	0.42	1.25
AVG	0.022	6.87	0.14	8.45	0.41	1.06
STDEV	0.001	0.18	0.12	1.02	0.25	0.13
CoV	6.1%	2.6%	84.6%	12.1%	61.5%	12.1%
SF3	0.024	5.63	0.14	7.11	0.39	0.89
	0.022	3.41	0.06	6.21	0.59	0.78
	0.021	5.87	0.36	10.03	1.44	1.25
AVG	0.022	4.97	0.18	7.78	0.81	0.97
STDEV	0.002	1.36	0.16	2.00	0.56	0.25
CoV	6.7%	26.8%	16.4%	6.4%	10.1%	6.4%
SF4	0.025	7.33	0.14	8.71	0.41	1.09
	0.014	4.07	0.37	9.83	1.93	1.23
	0.026	6.75	0.17	9.26	0.76	1.16
	0.026	7.00	0.38	10.04	0.76	1.25
AVG	0.023	6.29	0.27	9.46	0.97	1.18
STDEV	0.006	1.50	0.13	0.60	0.67	0.07
CoV	25.7%	23.8%	47.3%	6.3%	69.0%	6.3%

Table 5.2(2) Direct tensile results for series II Steel fibre-ECC part II

	ε_M [%]	σ_M [N/mm^2]	ε_U [%]	σ_U [N/mm^2]	ε_F [%]	gτ[N/mm^2]
SF5	0.015	6.17	0.45	6.83	0.59	0.85
	0.016	5.77	0.02	5.88	0.02	0.74
	0.021	6.98	0.02	6.98	0.02	0.87
	0.025	6.21	0.03	6.21	0.03	0.78
AVG	0.019	6.28	0.13	6.47	0.17	0.81
STDEV	0.005	0.50	0.21	0.51	0.28	0.06
CoV	24.1%	8.0%	162.9%	7.9%	170.0%	7.9%
SF6	0.018	5.10	0.28	9.36	1.23	1.17
	0.016	4.17	0.21	8.66	0.67	1.08
	0.016	3.41	0.37	8.12	1.88	1.02
	0.021	5.51	0.39	8.06	0.95	1.01
AVG	0.018	4.55	0.31	8.55	1.18	1.07
STDEV	0.002	0.94	0.08	0.60	0.52	0.08
CoV	14.2%	20.7%	25.6%	7.1%	44.1%	7.1%
SF7	0.028	5.59	0.25	6.17	0.42	0.77
	0.018	4.24	0.19	7.17	0.22	0.90
	0.020	4.76	0.17	7.40	0.42	0.93
	0.022	4.71	0.15	7.05	0.37	0.88
AVG	0.022	4.82	0.19	6.95	0.36	0.87
STDEV	0.004	0.56	0.04	0.54	0.09	0.07
CoV	19.6%	11.7%	22.5%	7.8%	26.5%	7.8%

5.2.1 FA dominated binder replacement on steel-ECC

It can be seen from Figures 5.13 and 5.14, that there are slightly decreasing trends for both first crack strength and ultimate tensile stress with FA content ranging from 40% to 70%. They are SF2 (40%), SF4 (50%), SF6 (60%), and SF7 (70%). It is known that FA content reduces matrix strength due to the relative reduction of cement content and the delay of FA

hydration.

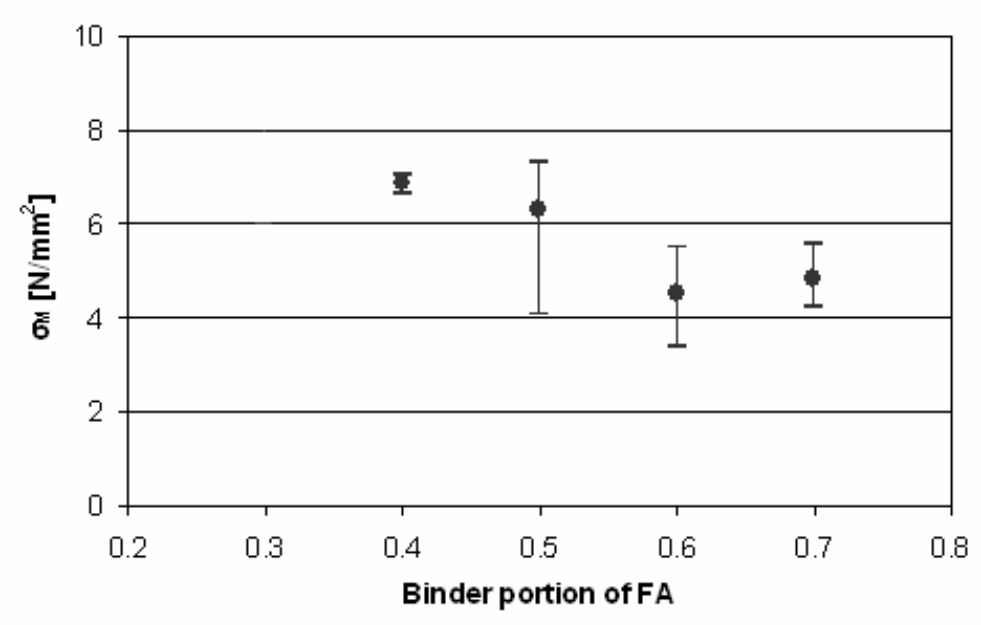

Figure 5.14 Trend of first crack strength with binder portion of FA

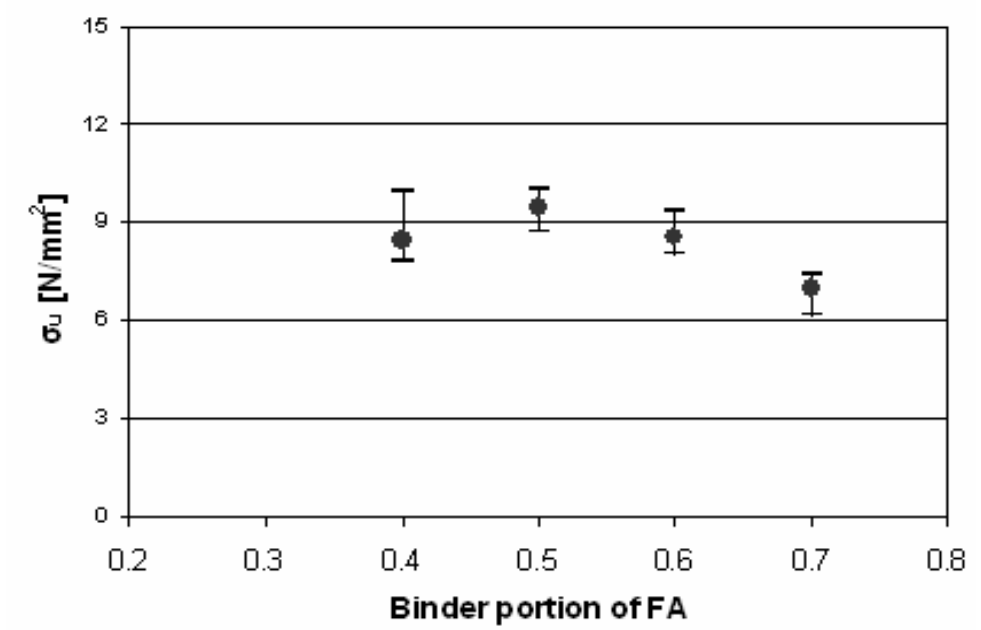

Figure 5.15 Trend of ultimate strength with binder portion of FA

But, unlike for PVA fibre ECC, there is no clear trend of tensile strain with FA content, as shown in Figures 5.15 and 5.16.

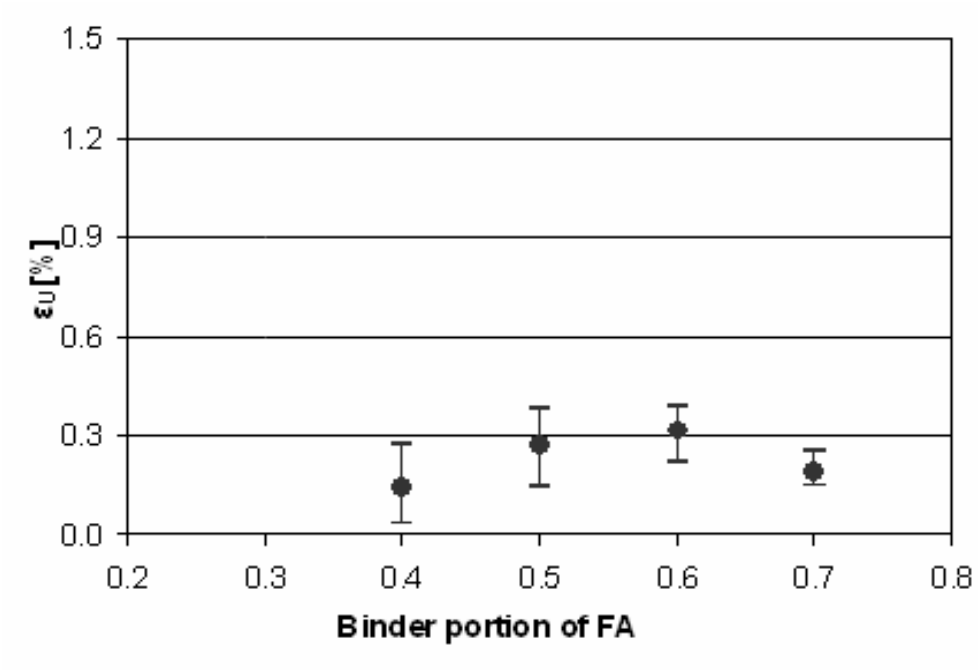

Figure 5.16 Trend of ultimate strain with binder portion of FA

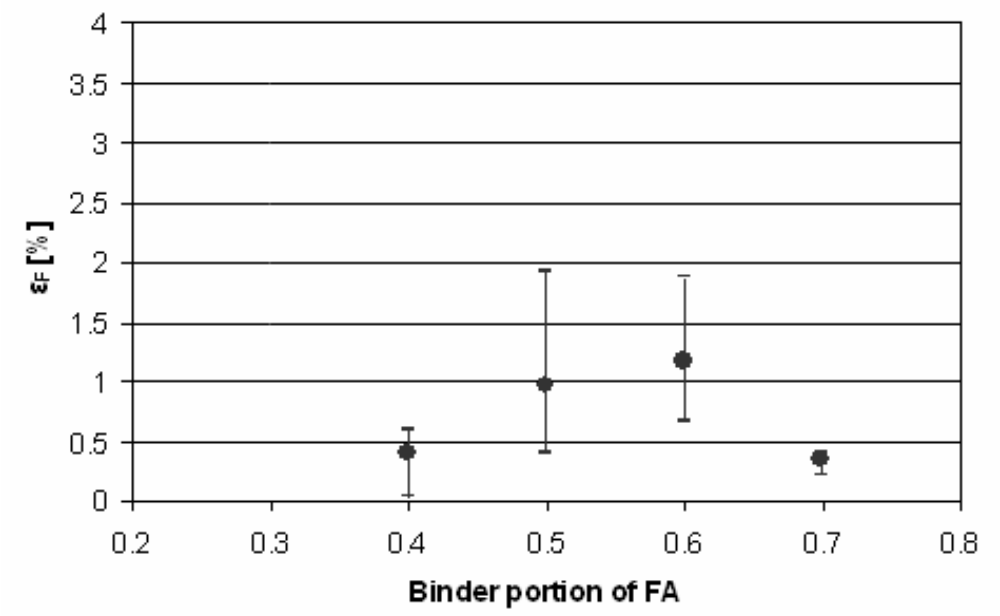

Figure 5.17 Trend of failure strain with binder portion of FA

Different with PVA-ECC, steel fibre-ECC shows an abridged trend on tensile stress as the binder portion of FA increases. As FA content increases, the bond strength reduces and the

toughness of PVA-ECC increases, whereas the toughness of steel fibre-ECC would reduce as bond strength is reduced.

It is clear that the ultimate value for both ultimate strain and first crack strain of PVA-ECC is the mix with the highest binder portion of FA. Contrarily, for steel fibre ECC, the ultimate value occurs at the moderate binder proportion of FA, which can be explained as resulting from a different fibre failure type for PVA Fibre and steel fibre.

The adhesion between steel and cement or mortar has been measured by Chan and Li (Chan & Li, 1997). For a steel fibre adhesive fibre/matrix bond, there is less chemical bond and slip-hardening occurring. Bridging fibre may transfer an approximately constant interfacial frictional force. Thus, if the first crack strength of the matrix is low, the transmitted force will also be low and remain constant at that low level until the fibre pulls out completely. Hence, unlike PVA fibre ECC, the tensile stress of steel fibre ECC can be determined by matrix strength rather than by interfacial properties like cohesion fibre/matrix reaction type. The theory of the relationship between ECC toughness and fibre bond strength is shown in Figure 5.21 (Shah, 2004). The steel fibre bond strength decrease cannot increase the composite toughness as PVA fibre-ECC.

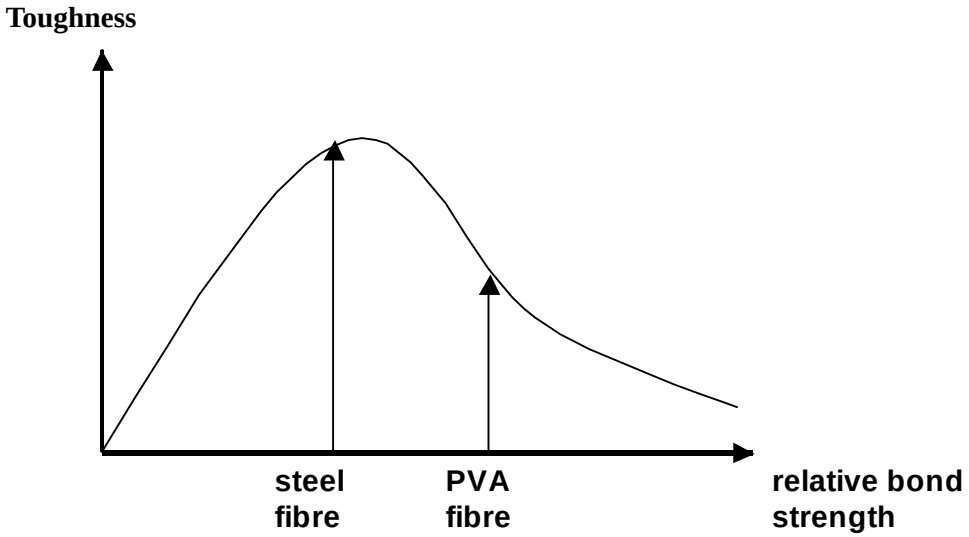

Figure 5.18 The relationship between toughness and bond strength of ECC

5.3 Results of sensitivity investigations

To identify various influences, it is extremely important to have a stable matrix of properties. The influence investigation is based on two types of such steady matrices. Especially, high FA volume content matrix provided good performance repeatability. The results of tensile testing or these mixes (Table 3.3) are listed in Table 5.3.

Table 5.3(1) Direct tensile results for influence investigation mixes part I

	ε_M [%]	σ_M [N/mm^2]	ε_U [%]	σ_U [N/mm^2]	ε_F [%]	gτ[N/mm^2]
SF9A	0.027	1.99	0.55	2.33	0.55	0.29
	0.032	2.50	3.29	2.90	4.10	0.36
	0.028	2.43	3.42	3.07	5.40	0.38
	0.022	1.63	0.54	2.47	3.28	0.31
AVG	0.027	2.14	1.95	2.69	3.34	0.34
STDEV	0.004	0.41	1.62	0.35	2.05	0.04
CoV	15.1%	19.0%	83.1%	13.0%	61.4%	13.0%
SF9B	0.021	1.26	4.11	2.65	5.34	0.33
	0.018	0.89	3.23	2.10	4.94	0.26
	0.030	1.48	2.02	1.98	3.40	0.25
	0.025	1.07	2.97	1.92	5.52	0.24
AVG	0.024	1.18	3.08	2.16	4.80	0.27
STDEV	0.005	0.25	0.86	0.33	0.96	0.04
CoV	22.1%	21.7%	27.9%	15.4%	20.1%	15.4%
SF10	0.034	3.18	0.28	5.59	0.95	0.70
	0.012	1.32	0.35	5.18	2.66	0.65
	0.015	1.46	0.37	5.16	2.20	0.64
	0.029	2.74	0.45	5.53	2.03	0.69
AVG	0.023	2.17	0.36	5.36	1.96	0.67
STDEV	0.011	0.93	0.07	0.23	0.73	0.03
CoV	47.4%	42.7%	19.2%	4.3%	37.0%	4.3%
SF11	0.028	5.67	0.51	6.23	0.75	0.78
	0.034	2.13	0.40	5.50	1.34	0.69
	0.022	4.97	0.78	6.95	1.38	0.87
	0.033	2.74	0.52	6.20	1.48	0.77
AVG	0.029	3.88	0.55	6.22	1.24	0.78
STDEV	0.006	5.67	0.51	6.23	0.75	0.78
CoV	18.8%	44.0%	28.8%	9.5%	26.5%	9.5%

Table 5.3(2) Direct tensile results for influence investigation mixes part II

	ε_M [%]	σ_M [N/mm^2]	ε_U [%]	σ_U [N/mm^2]	ε_F [%]	gτ[N/mm^2]
SF12	0.007	1.72	0.33	4.74	2.14	0.59
	0.018	1.91	0.61	4.34	1.88	0.54
	0.024	1.57	1.36	4.77	2.61	0.60
	0.030	2.00	1.10	6.09	2.75	0.76
AVG	0.020	1.80	0.85	4.99	2.35	0.62
STDEV	0.010	0.20	0.47	0.76	0.41	0.10
CoV	49.7%	10.9%	54.9%	15.3%	17.3%	15.3%
SF13	0.359	2.75	5.13	3.79	5.63	0.47
	0.269	2.43	0.62	2.91	1.71	0.36
	0.349	3.17	4.12	3.97	4.29	0.50
AVG	0.326	2.78	3.29	3.56	3.88	0.44
STDEV	0.049	0.37	2.37	0.56	1.99	0.07
CoV	15.1%	13.3%	72.0%	15.8%	51.4%	15.8%
SF14	0.036	4.76	5.18	6.18	5.99	0.77
	0.470	3.84	3.92	5.87	4.30	0.73
*	0.610	4.07	3.21	5.72	3.96	0.72
*	0.430	4.20	3.26	5.00	3.94	0.63
AVG	0.387	4.22	3.89	5.69	4.55	0.71
STDEV	0.246	0.39	0.92	0.50	0.97	0.06
CoV	63.6%	9.3%	23.5%	8.8%	21.4%	8.8%
SF15**	0.058	1.33	1.17	1.63	2.46	0.20
	0.023	0.94	0.34	1.37	0.96	0.17
AVG	0.041	1.13	0.75	1.50	1.71	0.19

***** 2 specimens of SF14 were tested without LVDT's installed, with only the cross-head displacement measurement of the Zwick Z250 Materials Testing Machine. The deformations and strains for these cases are, therefore, not accurate.

** The Mix SF15 was made for an extrusion test. Therefore, this workability was so poor that two of four specimens were broken before the test due to the matrix disconnection.

Table 5.3(3) Direct tensile results for influence investigation mixes part III

	ε_M [%]	σ_M [N/mm^2]	ε_U [%]	σ_U [N/mm^2]	ε_F [%]	gτ[N/mm^2]
SF17A	0.013	2.17	0.08	2.60	1.20	0.33
	0.019	1.76	0.82	3.35	4.30	0.42
	0.027	1.86	0.16	3.19	3.01	0.40
	0.017	1.49	0.15	2.79	2.59	0.35
AVG	0.020	1.82	0.30	2.98	2.78	0.37
STDEV	0.006	0.28	0.34	0.35	1.28	0.04
CoV	35.4%	14.3%	1.8%	9.6%	10.6%	9.6%
SF17B	0.020	2.90	0.20	3.86	0.93	0.48
	0.021	1.97	1.53	2.79	3.30	0.35
	0.027	2.24	0.69	2.37	0.95	0.30
AVG	0.023	2.37	0.81	3.01	1.73	0.38
STDEV	0.004	0.48	0.67	0.77	1.36	0.10
CoV	18.2%	8.1%	73.9%	10.0%	96.2%	10.0%
SF18	0.021	3.57	0.10	5.37	0.34	0.67
	0.012	1.87	0.22	4.95	0.94	0.62
	0.030	4.56	0.43	6.56	0.93	0.82
	0.025	5.66	0.03	5.73	0.37	0.72
AVG	0.022	3.92	0.19	5.65	0.65	0.71
STDEV	0.008	1.61	0.18	0.68	0.34	0.09
CoV	40.9%	34.7%	86.7%	14.7%	53.9%	14.7%

Table 5.3(4) Direct tensile results for influence investigation mixes part IV

	ε_M [%]	σ_M [N/mm^2]	ε_U [%]	σ_U [N/mm^2]	ε_F [%]	gτ[N/mm^2]
SF19***	0.090	2.41	5.07	4.09	4.75	0.51
	0.140	1.56	2.67	2.50	5.11	0.31
	0.110	2.00	1.68	2.23	2.76	0.28
	0.120	2.01	5.25	3.53	5.75	0.44
AVG	0.115	1.99	3.67	3.09	4.59	0.39
STDEV	0.021	0.35	1.77	0.87	1.29	0.11
CoV	18.1%	17.4%	48.3%	28.1%	28.1%	28.1%
SF20***	0.06	1.81	3.00	2.45	4.10	0.31
	0.06	1.85	4.50	2.92	4.02	0.36
	0.07	1.50	1.88	1.73	2.94	0.22
	0.06	1.70	4.22	2.58	5.49	0.32
AVG	0.063	1.72	3.40	2.42	4.14	0.30
STDEV	0.005	0.16	1.20	0.50	1.05	0.06
CoV	0.0%	1.8%	56.2%	19.2%	1.8%	19.2%
SF21***	0.080	1.64	4.33	3.28	4.79	0.41
	0.060	1.97	3.63	2.78	4.51	0.35
	0.050	1.61	3.58	2.81	4.08	0.35
	0.060	1.92	4.39	2.86	4.87	0.36
AVG	0.063	1.78	3.98	2.93	4.56	0.37
STDEV	0.013	0.19	0.44	0.23	0.36	0.03
CoV	24.4%	11.2%	10.5%	9.5%	7.8%	9.5%

******* For these specimens a smooth nonlinear ascending stress-strain response is found, followed by a plateau (zero E-modulus). For these specimens, the average matrix strength, indicated by the plateau stress-level, is given in the $\sigma_{M,}$ column. The collection of these σ_M values is shown in Appendix (3) for SF19 – SF21. Appendix (3) presents the concept for obtaining the average σ_M value.

These investigations of sensitivity included influence of aging, which is presented in Chapter 7, W/B ratio and fresh state rheology influences, which will be presented in Chapter 8, they are important for practical applications.

Other varied issues contribute to understand the ECC properties including fibre type influence,

comparison of casting and extrusion, the relationship of compression results and tensile stress, and the relationship of bending MOR and tensile stress will be presented in Chapter 9.

Chapter 6

ECC behaviour tailoring by cement replacement

The development of ECC from FRC results in high performance, including strain hardening and high strain capacity.

As introduced and discussed in Chapter 2, the approach to achieve ECC high performance is to either increase the complementary energy J_b' or reduce the composite crack tip toughness J_{tip} (Li et al., 2001). Practically, the first approach is to work on tailoring of matrix properties such as matrix strength and toughness, flaw size and distribution, as well as fracture toughness. The second approach is to modify the interface interaction and bond between fibre and matrix. There are many ways to achieve these aims, for example, oiling agent and plasma treatment for the fibre surface to tailor the interface properties (Li et al 2001, 2002), indirectly through specific fabrication techniques such as extrusion (Peled & Shah, 2003) and also by using cement replacement to modify both the matrix and interface properties.

Fibre oiling and plasma treatment are very effective methods; however they are extremely expensive. Extrusion is limited by mix processibility. It needs a very specific matrix, with dough-like fresh properties (de Koker & Van Zijl G, 2004), which has implications for fibre distribution and orientation. In addition an extrusion facility customised to the particular product, is required, making it a specialised method. It is a difficult task to find a cheap and easy way to tailor ECC behaviour. However, this chapter discusses a cheap approach, namely replacement of the cement used in the matrix to tailor the properties of both the matrix and the interface between fibre and matrix.

There were various kinds of fibre used in FRC materials during last 40 years, such as steel, brass, asbestos, polyethylene, glass, and polypropylene. The application of PVA fibre arose in recent years in order to reduce the cost. A particular challenge for the usage of PVA fibre is the high chemical bond between fibre and matrix, due to the fact that it is a product falling under the hydroxyl group, which results in cement hydration. So, the interface tailoring of PVA fibre ECC might mostly consist of reducing the chemical interface bond between fibre and matrix.

In the present chapter, the cement replacement tailoring function will be introduced and discussed under two different aspects, the tailoring of matrix properties and the tailoring of

interfacial properties. As introduced in previous chapters, the cement replacements used in this research are FA and GGCS.

6.1 FA and GGCS used for tailoring the matrix properties.

The primary aim to use FA in ECC is to reduce its high cost. However, as a product of coal-fire thermoelectric power stations, FA has a very specific spherical particle shape and extremely fine size, see Figure 6.1, which can be even less than 1μm. Both these qualities contribute to enhance ECC performance. The major phases of Lethabo FA were found to be glass (45-48%), mullite ($Al_6Si_2O_{13}$) 41-43%, and the reactive silica is in the range of 30-35%. Glass phases contain mainly a SiO_2 range from 21-100% and an Al_2O_3 range from 0.1-49% (Bosch 1990). The XRF analysis result shows that about a proportion of 60% of FA used in the present research is SiO_2. This indicates that the most frequent component of current FA is the glass phase. Both the glass phase and the spherical shape of the FA may result in sluggish hydration and indicates that FA-ECC may have many unhydrated binder particles with smooth surfaces, which will make FA particles difficult to connect with other cement product crystals, resulting in considerable interface between the matrix and the FA particle. Similarly, with its spherical shape working as an aggregate in the concrete, the presence of unhydrated FA particles contributes to the crack pattern and eventual tortuous crack path of the localised, failing crack, shown in Figure 6.2. Because of randomly distributed unhydrated FA particles in the matrix, spatially random areas of weakness arise. These weak points are closely spaced. By shear transfer along fibre-matrix interfaces, the low limiting stress of such weak spots is achieved over short shear transfer lengths. This causes the small crack spacing in FA-ECC, ranging between 1 and 3 mm for the specimen seen in Figure 6.3 (a).

Further evidence of the presence of unhydrated FA particles in the matrix is presented by dust from the fracture surface of FA-ECC specimens. It is apparent that FA-ECC specimens subject to tensile testing produce more dust. Some of this dust was gathered by breaking the remaining parts of a specimen by hand over a container. SEM studies shown in Figure 6.1 revealed that it contained mostly FA particles, in their original, spherical form.

The hydrated product of FA is a multi-component dependent on the components of FA. However, whatever the FA hydration product is, the delayed, but continued crystal structure build-up may bulge and destroy the weak point of pre-existing matrix structure resulting in additional flaws. As Li suggested (2001), for achieving saturated multiple cracking, a sufficient number of large flaws is necessary. Enough large flaws reduce the matrix cracking strength, as well as the matrix crack tip toughness J_{tip}. Consequently, for FA-ECC, a high volume of FA can be used also to create artificial flaws.

Contrary to the sluggish hydration of FA, GGCS contains a high proportion of CaO, Al_2O_3 and MgO, which are quite close to normal Portland cement components, and fine, irregular particles. All three cause GGCS to hydrate rapidly. Alexander et al. (2003) verified that compression strength of concrete systems with GGCS replacement level of 25%, 50% and 75% are equal or slightly higher than concrete without GGCS, at the age of 28 days (Alexander et al 2003). High-speed hydration leads to a more compact matrix and a higher

matrix strength at an early age. Compared with FA-ECC, Slag-ECC has a much more compact fracture surface. Cracks tend to occur along the flaw edge, if the matrix contains many large flaws. However, if the matrix is too compact to keep the desired flaw size, cracks should occur perpendicularly to the principal tensile direction. The straight, well spaced, crack pattern, which is shown in Figure 6.3 (b), confirms the high compactness of Slag-ECC. A larger crack spacing in Slag-ECC, ranging between 3 and 10 mm, can also be observed in Figure 63 (b). This can possibly be related to the higher matrix strength of Slag-ECC compared with FA-ECC. Longer shear transfer lengths are required to reach high matrix strength. Cracks arise at these positions where the limiting stress is exceeded, which are at a larger spacing than for a weaker matrix.

As presented in Chapter 5, both the Slag-ECC first crack strength and ultimate tensile strain of the mix with 70% GGCS were lower than in the 55% GGCS mix. This can be due to the too much GGCS hydrated crystal produced to maintain the ordinary hydrated crystal structure size and distribution. The large crystal is more brittle and affects the cement hydrated C-S-H gel build-up.

Finally, if we compare FA and GGCS working in the matrix, some facts become apparent. FA as cement replacement reduces the composite first crack strength and ultimate cracking stress, whereas GGCS retains these and even improves them in some cases. FA content increases the pre-existing flaw number and size, but GGCS reduces or eliminates them. Therefore, FA-ECC has a reducing matrix crack tip toughness J_{tip} with binder portion of FA and Slag-ECC has a much larger J_{tip} than FA-ECC.

The hydration condition of the ECC composite with a combination of FA and GGCS is quite complex. Whatever hydration process, both finer particle size and irregular shape make GGCS hydrate earlier than FA, which might indicate that a matrix containing both FA and GGCS will exhibit characteristics resembling those of Slag-ECC, rather than those of FA-ECC. However, approximately 30%-40% of the FA remains in the matrix in its role as aggregate. The spherical particle will lead to disconnected points between cement hydration crystals. This causes flaws or micro-cracks in the matrix bulk after a long maturing time, resulting in the development of composite ductility. This effect is not so clear at the very early stages of composite hydration because not all the crystals have yet completely grown and the matrix is still weak at an early stage.

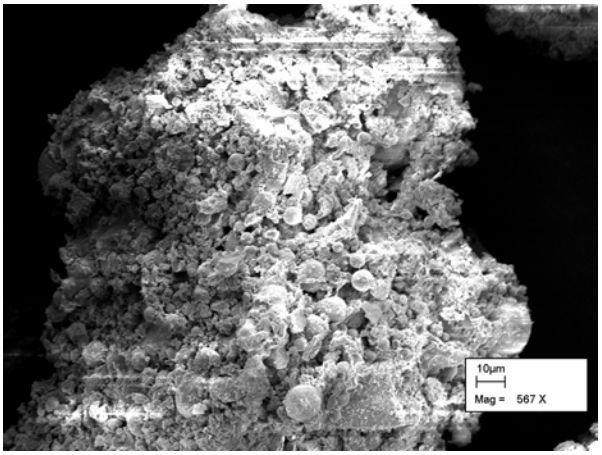

Figure 6.1 The dust from rupture surface mainly containing fly ash particles.

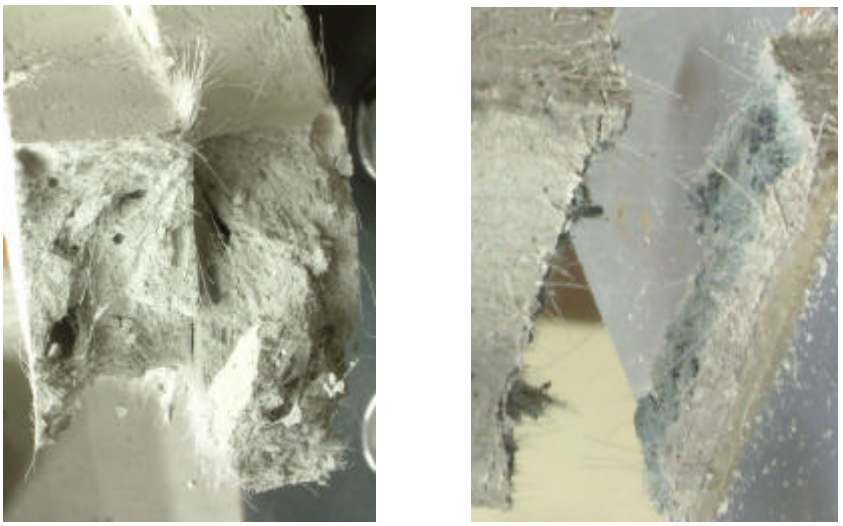

Figure 6.2 Tortuous failure path for FA-ECC (left), in contrast to plane failure in Slag-ECC (right).

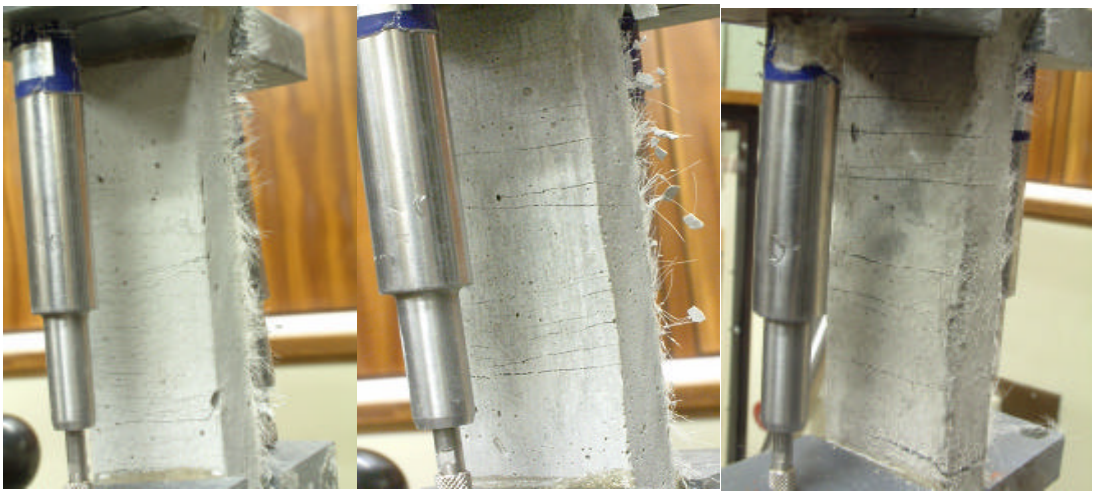

Figure 6.3 Varied crack of ECC with varied cement replacement (a): FA-ECC (S 5), (b): Slag-ECC (S6), (c): FA & Slag-ECC (S 8).

6.2 Interfacial tailoring by cement replacement

There are three important parameters controlling the fibre/matrix interfacial properties, which are: chemical debonding energy G_d, frictional bond strength at the beginning of fibre slippage t_o, and fibre slip-hardening coefficient ß (Redon et al., 2001). As introduced in Chapter 2, a big challenge of PVA fibre usage in ECC materials is to reduce the interface bond, including all these three aspects. Previous attempts comprised fibre coating by oiling agent (Li et al., 1997). In this section, cement replacement of FA and GGCS is used to tailor the fibre/matrix interface properties.

As presented in Chapter 2, the chemical bond G_d can be obtained via single fibre pull-out stress-strain response curve. To generalize this parameter to include all fibres in a cross-sectional area of the specimen (the chemical bond of the specific crack), an extended equation can be formulated through multiplying G_d by the number of fibres per unit cross-sectional area, which can be obtained by the equation

$$N_1 = 0.405\ V_f/A_f \tag{6.1}$$

where V_f is the fibre volume fraction of fibre and A_f is cross-section area of fibre (Soroushian & Lee, 1991). Thus, the average chemical bond per crack can be formulated as

$$G_{dm} = 0.405\frac{V_f 2(p_a - p_b)^2}{p^2 E_f d_f^3 A_f} \tag{6.2}$$

It can reasonably be assumed that the drop of tensile stress-strain curve can indicate the chemical bond of certain crack.

6.2.1 Different direct tensile behaviour of FA-ECC and Slag-ECC

The typical direct tensile stress-strain curves of FA-ECC, including the cracking evolution and pattern are shown in Figure 6.4. As discussed above, the load drop level indicates the chemical bond level. If the load drop is significant in fibre pull-out curve, it implies that the strong chemical bond between fibre and matrix is broken. In the case of PVA fibre, the load drop is normally distinct and occurs suddenly (Redon et al., 2001), which means that with PVA fibre there normally is a strong interface chemical bond between fibre and matrix. However, the crack fluctuation of FA-ECC is much finer than that of Slag-ECC. This indicates that the FA-ECC has a lower chemical bond than Slag-ECC. Because for given fibre strength complementary energy J_b' has an approximate negative linear relationship with chemical bond (Li et al 2003). Therefore, the lower interfacial bond of FA-ECC provided higher complementary energy J_b'.

Kanda and Li (1998) suggested that larger cracks might be initiated first and smaller cracks

would occur as tensile stress levels increased during strain-hardening stage. FA-ECC significantly improved this behaviour. During the FA-ECC multiple cracking stage, cracks spread evenly, seen Figure 6.4.

It is apparent that a smooth tensile stress-strain relation, indicating a stable de-bonding process, and less chemical bond can be achieved in FA-ECC.

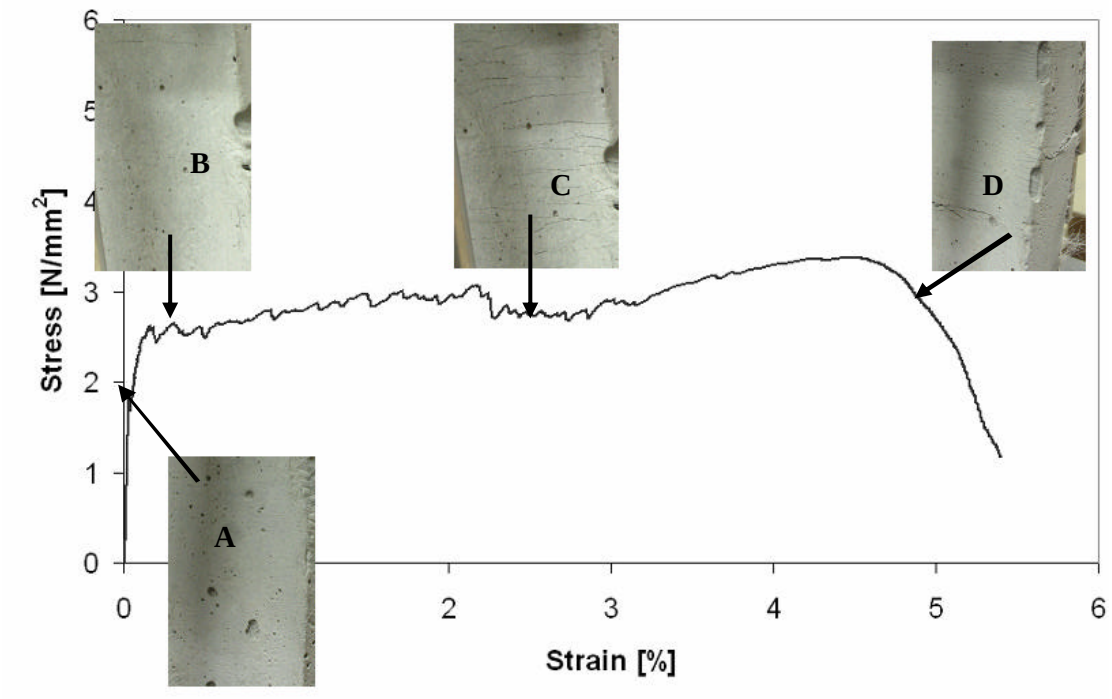

Figure 6.4 Direct tensile behaviour model of FA-ECC

Figure 6.5 shows the typical direct tensile stress-strain curves of Slag-ECC with the cracking pattern. Other than with FA-ECC, high first crack strength and ultimate tensile strength, large crack spacing, and acute fluctuation in the tensile stress-strain relation can be observed. Acute fluctuation implies a strong interface chemical bond existing between fibre and matrix, therefore leading to more fibres rupturing rather than pulling out. This means a high transferred force and energy release occurs in Slag-ECC composite.

Furthermore, the first crack was supposed to be the lowest one of all crack peak points in the stress - strain curve, so that it can satisfy the requirement that the matrix crack stress should be less than the fibre bridging stress. Yet, there are fibre crack onset points lower than the first crack in many cases, as shown in Figure 6.5. This irregular relation between tensile stress and strain may be due to both the random collapse of the transition zone as the fibre pulls out and energy release as the fibres rupture randomly. Thus, this kind of irregular relationship occurs in cohesion type fibre failure rather than in adhesion type failure. That can also explain why the FA-ECC curve shows a more flat stress-strain curve during the multiple-cracking stage.

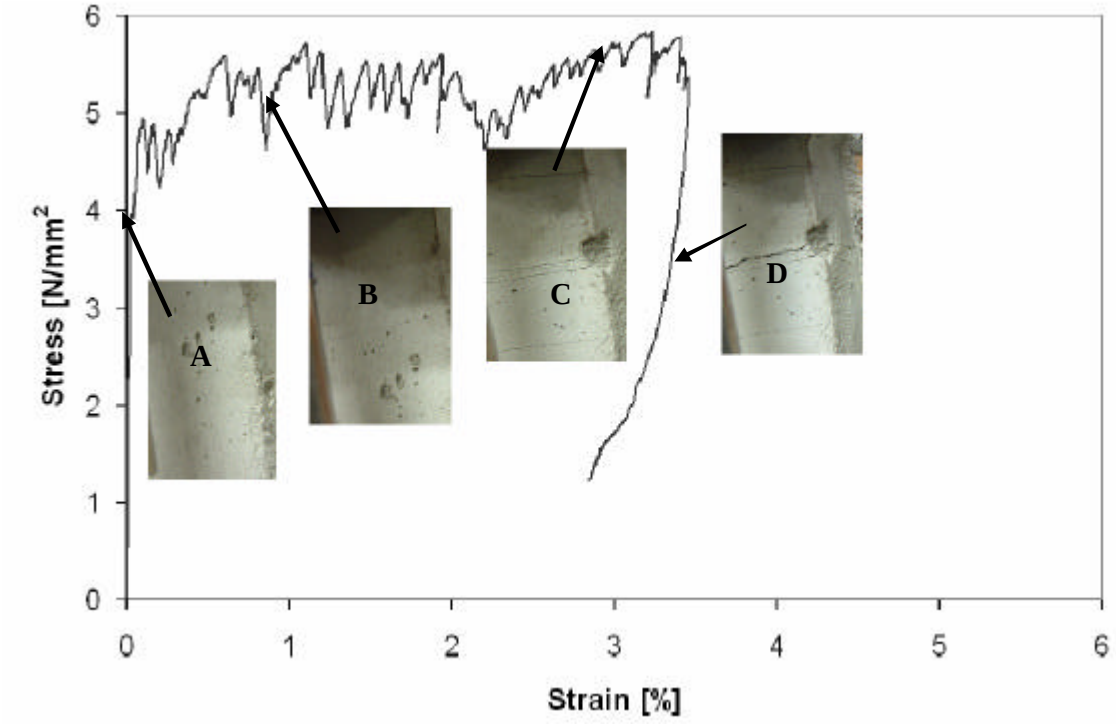

Figure 6.5 Direct tensile behaviour model of Slag-ECC

6.2.2 Different interface properties between FA-ECC and Slag-ECC

FA hydrates sluggishly at room temperature due to its glass phase and perfect spherical shape, resulting in high structure porosity in both matrix and transition zone. Furthermore, a weaker interface bond between PVA fibre and the transition zone around it occurs. Compared with the strong swathe around the fibre and stronger interlock with the matrix of Slag-ECC, FA-ECC impairs the fibre/matrix bond and transition zone structure significantly. Peled and Shah (2003) also reported an observation of the FA role in ECC behaviour, namely that a high content of FA reduced the bonding strength and resulted in a relatively smooth surface of fibre. As presented by Redon et al. (2001), the damage of the fibre surface is the main reason for fibre slip hardening as fibres pull-out. Thus, high FA content also contributes toward reducing fibre slip hardening. However, there is still uncertainty in this regard. The FA hydration crystal products can be varied, depending on FA component and cement component, therefore the structure of the transition zone can be varied. Hence, it is hard to determine whether the fibre surface was damaged by the matrix. Actually, both a strain hardening curve and flat stress-strain curve were observed in the same mix design, whatever the hydrated product is. The FA particles filling in the transition zone around the fibre surface reduce the contact area between fibre and matrix at the early stage, hence reducing frictional bonding. Moreover, FA-delayed influence on cement hydration limited a large crystal build-up and therefore reduces the crystal attachment on fibre surface, as well as reducing porosity. Both influences

might convert the fibre debonding type from cohesion to adhesion. Further discussion will be presented in a subsequent section.

GGCS has irregular and extremely fine particle size (7% less than 1 micron and 51% less than 10 micron) causing exceptionally rapid hydration of Slag-ECC. It has a high compressive strength comparable to that of Portland cement (Alexander et al., 2003) and a much more compact matrix than FA-ECC. These high-speed hydration products enclose the fibre surface fully and strongly. Which will cause more effective shear transfer than in a slip/fibre pull-out scenario, as suggested to be the case in FA-ECC. This fact seems to contradict the argument above for larger crack spacing in Slag-ECC, because the more effective shear transfer will cause limiting stress to be reached over a shorter shear transfer length. However, the matrix strength is also increased, causing a larger shear transfer length required to cause cracking, whereby crack spacing is increased.

The tensile stress and strain results of the composites with the FA and GGCS content are presented in Table 5.1. The first crack strength of Slag-ECC with 50% GGCS content is 1.42 times that of the FA-ECC with 50% FA content, and 70% GGCS content has 1.58 times the first crack strength of a composite with 70% FA content. For the ultimate tensile strengths these ratios are 1.47 and 1.87 respectively. In the same cement replacement content, Slag-ECC has approximately 1.5 times the first crack strength of FA-ECC. However, the 70% slag has 1.87 times the ultimate strength of 70% content of FA. Boshoff did another parallel mix M5 with 2% PVA fibre and no cement replacement. The first crack stress is 3.79 MPa by average and the ultimate tensile stress is 6.11 by average. The content of both GGCS and FA reduced the tensile stress. This can only be because the matrix strength changed, and the cement replacement had an influence on interfacial properties, as has already been discussed. The question remains as to how its influence on changing these properties needs to be evaluated. Let us examine the direct tensile stress comparisons presented in Figures 6.6 and 6.7.

Figure 6.6 shows the first crack stress of a mix with the combination of 27% GGCS and 27% FA (S8), then 30% FA content (mix34), and finally, 70% FA (S7) content. It seems that the first crack strengths of 30%FA content composite and the 27% are both significantly higher than the specimens with 70% FA content. Note that if we consider the W/B influence on matrix crack stress (Mix S8 has higher W/B than S7), the s_M of specimen with the combination of 27% GGCS and 27% FA should even higher at the same W/B with S7. This indicates that the 27% GGCS took the place of 27% cement, which was in its turn replaced by 27% FA. At mix with 30% FA content, the FA did not partake in the cement hydration but remained as aggregate.

Other than with first crack strength, from Figure 6.7, the ultimate tensile strength of a mix with a combination replacement is approximately 1.2 times the ultimate tensile strength of a 30% FA content mix. The ultimate stress is proportionate to the frictional force and slip hardening of the fibre/matrix interface. The results indicate that 27% GGCS improves the interface bond more than 27% FA.

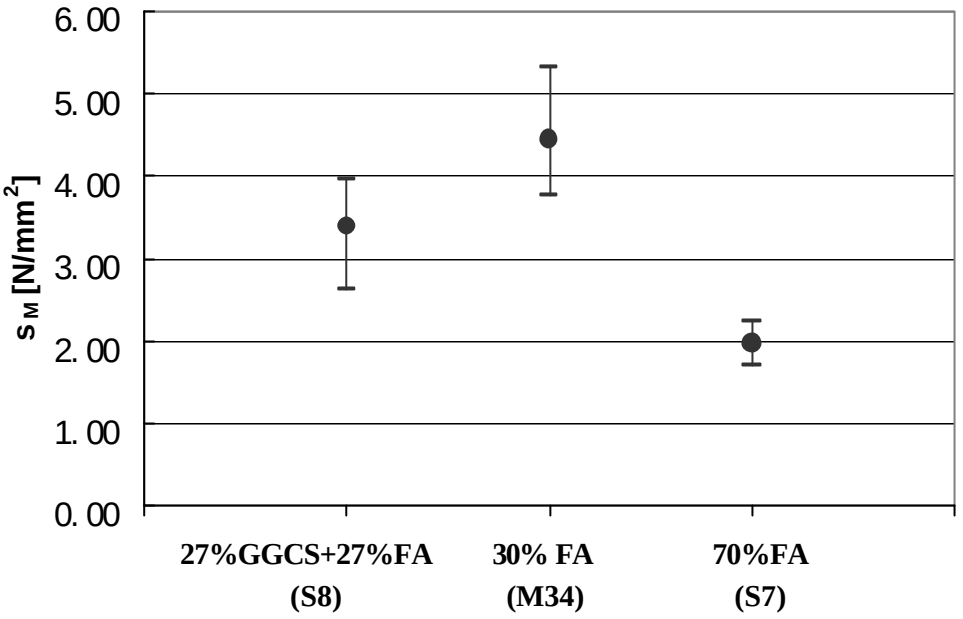

Figure 6.6 Comparison of the influence on first crack stress by FA and GGCS.

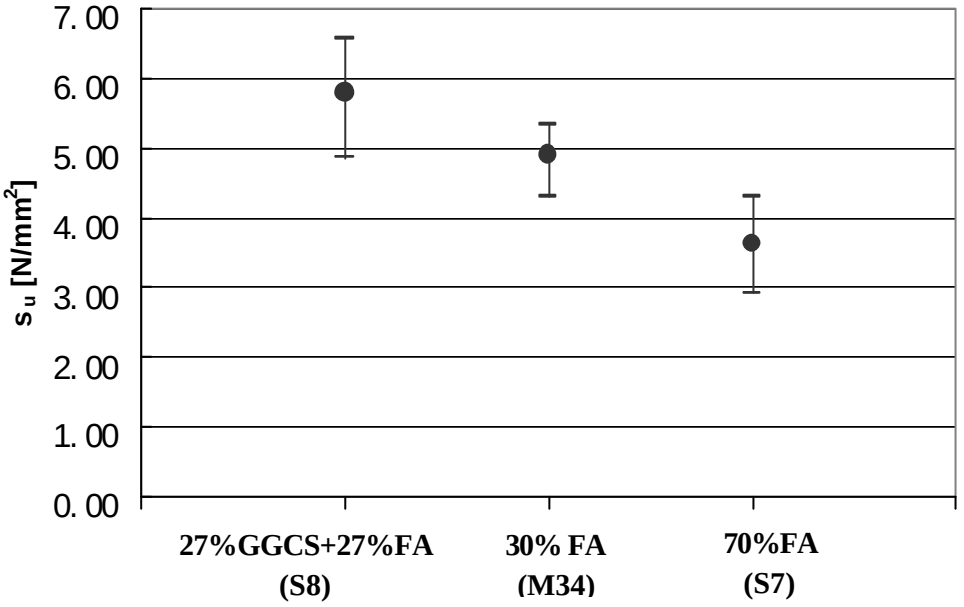

Figure 6.7 Comparison of the influence on ultimate tensile strength by FA and GGCS.

Because the typical transition zone thickness is approximately 50 micron away from the fibre surface and the weakest zone is about 30 micron from the fibre surface (Chan & Li, 1997), the very fine particle size (again: 7% less than 1 micron and 51% less than 10 micron) can effectively fill the transition zone, therefore reducing the highly porous structure of the transition zone and resulting in a stronger transition zone structure with cohesive strength. As

introduced in Chapter 2.4.2, both cohesion and adhesion fibre/matrix reactions exist in composites. Which type will take precedence depends on the properties of both fibre and matrix, because there is no visible evidence that 27% GGCS can provide stronger attachment between fibre and matrix than 27% cement. It is reasonable to assume that the cohesive bond leads to the fibre failure in the type of composite with 30% FA content. Therefore, the improvement of ultimate tensile stress is caused by additional densification of the transition zone filled by the GGCS fine hydrated product and unhydrated particles. Chan and Li (1997) suggested that the "densification of transition zone may serve to strengthen the transition and enhance the fibre-cement interfacial bond strength". Furthermore, they postulate that lower fibre/matrix adhesive bonding leads to more adhesive type fibre failure. Consequently, further assumptions that Slag-ECC has a stronger interface chemical and frictional bond, such cohesion could be responsible for the fibre/matrix reaction. The SEM analysis confirms that. Figure 6.8 (b) shows the slag-ECC fibre/matrix strongly interlocking when fibre failure occurs. Figure 6.9 (left) shows the fibre split by the crushed part of the transition zone. On the other hand, FA-ECC fibre failure with clearly gap (see the white arrow in Figures 6.8 (a) left and 6.9(right)) between the fibre surface and matrix bulk. Returning to Figures 6.6 and 6.7, the 70% FA-ECC has much lower matrix crack strength but closer ultimate tensile stress. The question remains as to how fibre failure behaves in high FA content ECC composites. Section 6.2.4 will discuss whether FA changes the fibre failure type.

6.2.3 SEM analysis of interfacial properties

In the present research, SEM and XRF analyses were used to recognize the composite and interface microstructure and distinguish the hydration product. In the current section, SEM photos of various kinds of interfaces of FA-ECC, Slag-ECC, and FA & Slag-ECC and accompanying analyses are presented.

Clear differences in the matrix surrounding a fibre are seen between specimens containing FA and Slag. In Figure 6.8 (a) left, the gap between fibre and transition zone around it can be clearly observed, as well as the small fluffy-like product enclose the fibre surface. Similar matter can also be seen in Figure 6.8 (c) that shows the fibre/matrix interface of FA & Slag-ECC, but it is not visible in Slag-ECC in Figure 6.8(b).

In the FA-ECC the spherical FA particles are visible in this area, Figure 6.8(a). These particles have not (yet) formed hydration products. In this setting, it is apparent from the photo that the fibre was pulled out from the matrix, leaving a smooth interfacial surface. Note that there should be more unhydrated particles than observed in the photo. It is believed that these particles are pulled from the matrix during tensile testing, as FA-ECC specimen testing was in all cases accompanied by dust formation in the testing apparatus. An SEM photo of the dust revealed that it contained mainly spherical FA particles (Figure 6.1).

In Figure 6.8(b) slag-ECC hydrate products of irregular form completely cover the fibre. For a fibre to be pulled out of the Slag-ECC matrix, de-bonding at the fibre-interface or fracture of the hydrate product is required to overcome interlocking of the hydrate product. Figure

6.8(c) shows the combined effects of FA particles and slag hydrates in the matrix-fibre interface. This case seems to be intermediate in the sense that unhydrated, spherical FA particles are present, which fact is benefic ial for fibre slip/pull-out, but so are slag hydrates, which will counteract the slippage mechanism.

In Figure 6.9, different fibre failure conditions of Slag-ECC (rupture) and FA-ECC (debonding with matrix bulk) can be seen. The fibre of FA-ECC may also be damaged by the matrix product, which leads to slip hardening less than with Slag-ECC.

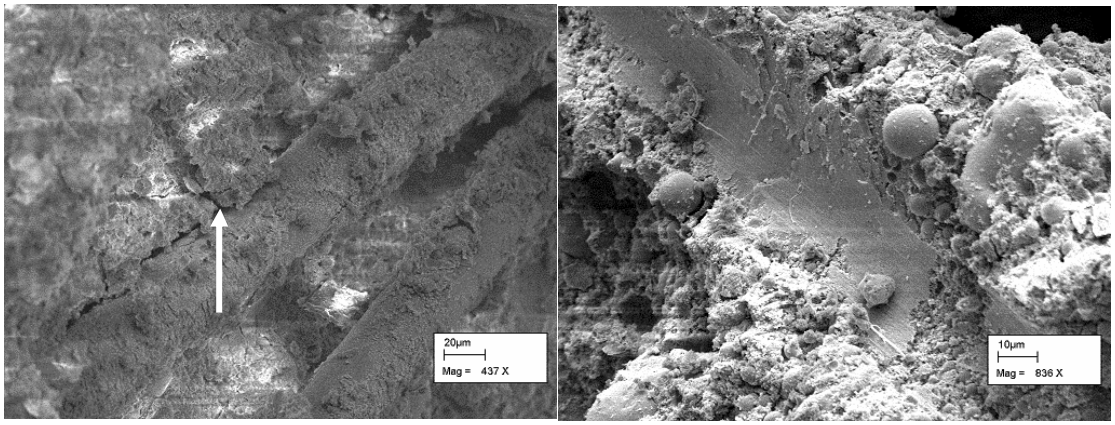

(a) FA-ECC (S7 70% FA content)

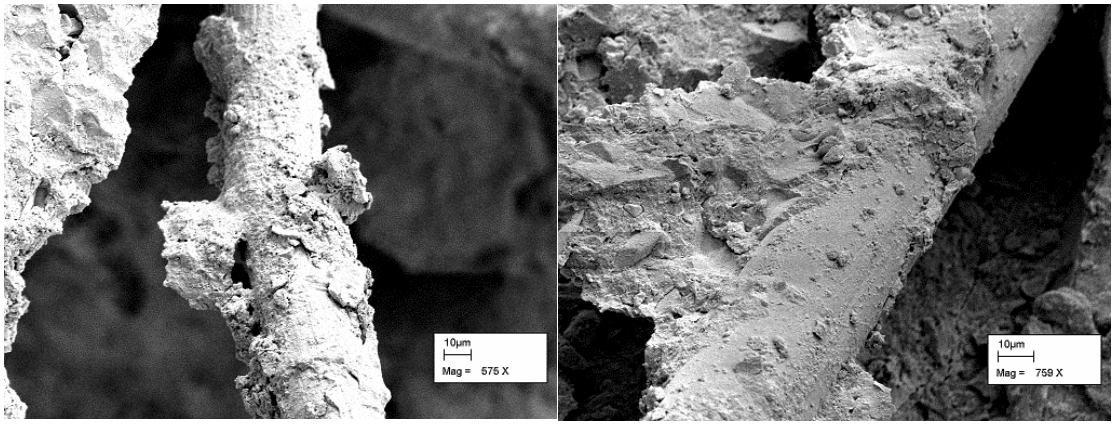

(b) Slag-ECC (S4 70% GGCS content)

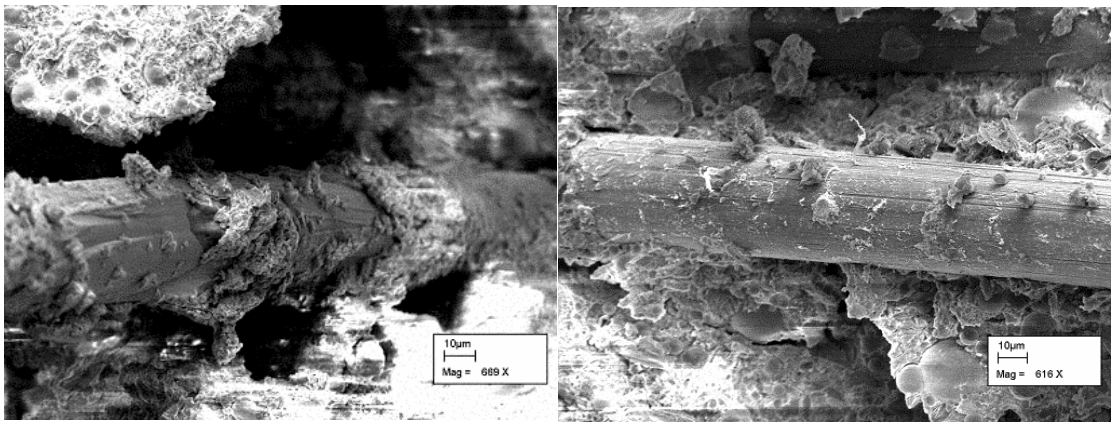

(c) FA & Slag –ECC (S8 27% FA & 27% GGCS content)

Figure 6.8 SEM analyses of FA-ECC (a), Slag-ECC (b), and FA & SLAG-ECC (c)

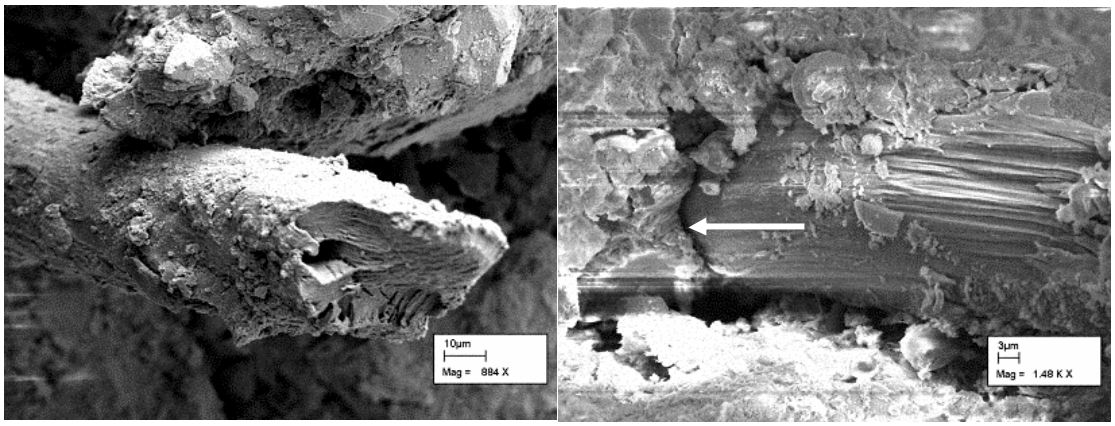

Figure 6.9 Different failure types of 70% Slag-ECC (left) and 70% content FA-ECC (right)

6.2.4 Changing of fibre failure type by FA tailoring

The intense alteration of direct tensile strain around a mix with FA proportion of 50% has been presented in Chapter 5. The tensile stress sharply drops at around 40% - 50% FA content. The ultimate strain suddenly has a significant increase when the FA content is more than 50%. We have compared the three series results of 30% FA content, 50% FA content and 70% FA content: first crack, ultimate tensile stress, and gt value. These are all shown in Table 5.1. The first crack stress of 30% FA content mix (M34) is about 1.35 to 1.76 times the value of 50% FA content mix (S1) and 70% FA content mix (S7). The ultimate tensile stress of 30% FA content mix is about 1.25 to 1.36 times the ultimate stress of 50% FA content mix and 70% FA content mix by percentage. The matrix crack strength reduces with FA content increase from 30% to 70%. This agrees with the fact that FA content reduces composite strength. However, the ultimate tensile stress is reduced when FA content ranges from 30% to 50%, but remains approximately constant when FA content ranges from 50% to 70%. There is a linear relation between ultimate tensile stress and interface frictional bond t if the matrix fibre/matrix snubbing factor remains constant, as assumed in Equation (2.7). This means that the interfacial frictional bond is reduced with FA content decrease, until about 50%, and remains at a constant value when FA content ranges from 50% to 70%, while matrix strength keeps reducing. Fibre failure type changing by FA tailoring may explain it. As presented in Chapter 2, there are two types of fibre/matrix reaction cohesion and adhesion, both latently exist in ECC materials, and either cohesion or adhesion occurs, depending on fibre type, and matrix constituents.

Figure 6.10 shows the typical tensile stress-strain response of mix with 30% FA and 70% FA content. The full curves of these mixes are shown in Appendix (1). In the subsequent chapters, the comparison of typical behaviours will also be presented, while the full curves of each mix are shown in Appendix (1)-(3).

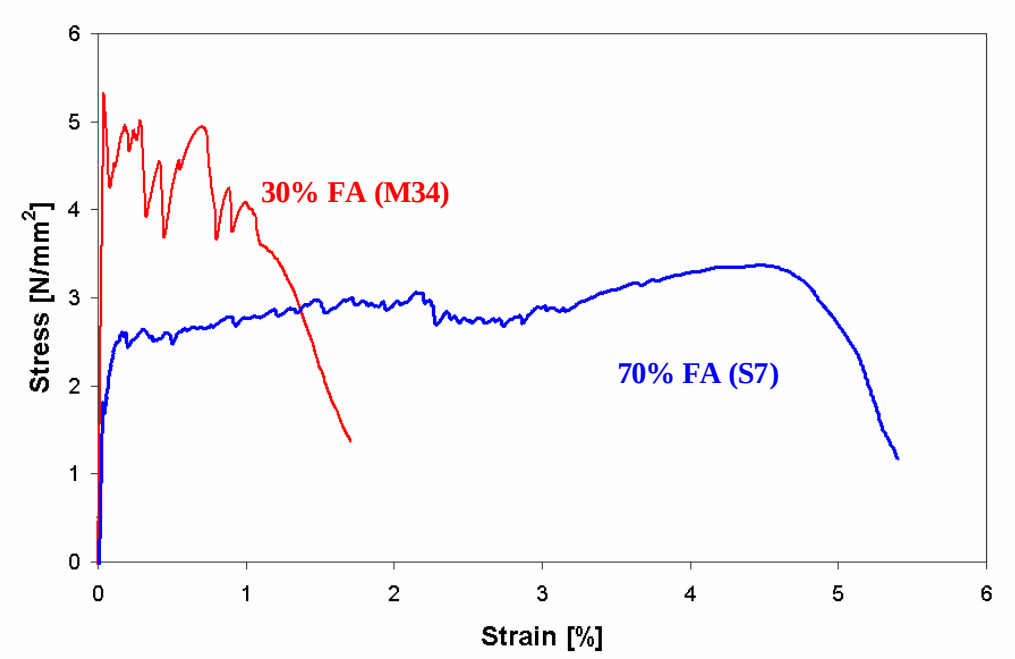

Figure 6.10 Typical direct tensile strain trends with FA content in matrix of FA-ECC

The sharp load drop can be observed from the tensile stress-strain curve of 30% FA content mix, whereas, the 70% FA content mix shows small fluctuations in the tensile stress-strain curve. See Figure 6.10, which indicates that a 30% FA content composite has much stronger chemical bonding between fibre and matrix around it than in the 70% FA content composite. Lower fibre/matrix surface energy and/or lower fibre/matrix adhesive bonding tend to result in an adhesive type reaction occurring (Chan & Li, 1997). Therefore, a rational assumption can be used to describe the fibre failure type in the composite with a high volume FA content. That is when FA content achieves approximate 50% of binder. The adhesion controls the fibre/matrix reaction instead of cohesion in normal PVA fibre ECC, because frictional stress t has usually been seen as a material constant if slip hardening can be ignored (Shah et al., 2004). For high FA-content ECC, although matrix strength can be reduced with FA content increase, interfacial bonding keeps approximately constant in spite of the eventual change of the transition zone structure. The relatively low interfacial adhesive bonding between fibre and matrix reduces fibre rupture and enhances fibre pull-out, resulting in the enhancement of the fibre bridging function. This might be the main FA role to enhance the fibre bridging function.

Further information comes by comparing the mix with the combination of SCF 20% and 50% FA and a mix with combination of 20% GGCS and 50% FA on stress, as shown in Figures 6.11 and 6.12. These are mixes S11, S12, and S1. There are indistinct variations of direct tensile results, especially the ultimate tensile stress, which can be used as criterion of interface frictional force. It is known that very fine silica fume particles filled the transition zone, and therefore densification of transition zone structure led to an increased strength of transition zone structure. Hence, the interface bond increased with the strengthening of the transition zone if the fibre failure type is cohesion (Chan & Li, 1997). However, the interface bonding

does not increase with strengthening of the transition zone. Therefore, the cohesive type fibre failure cannot be attributed to high FA content in the ECC.

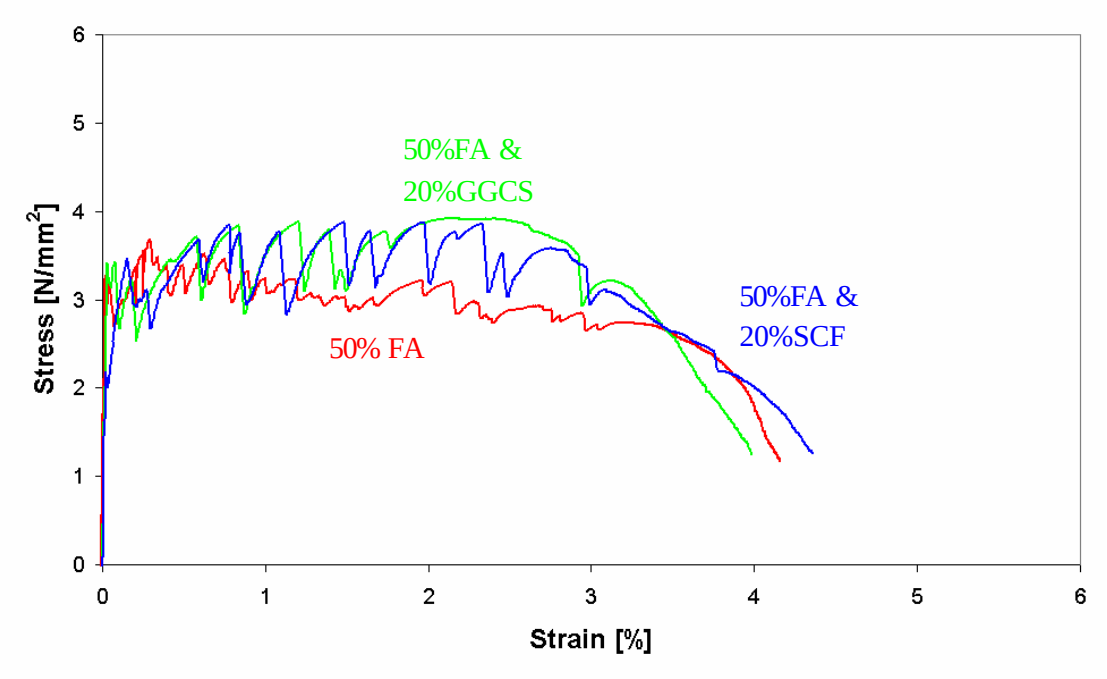

Figure 6.11 the tensile behaviour comparison of mixes with 50% FA, combination of 50%FA and 20% SCF, and combination of 50% FA and 20% GGCS

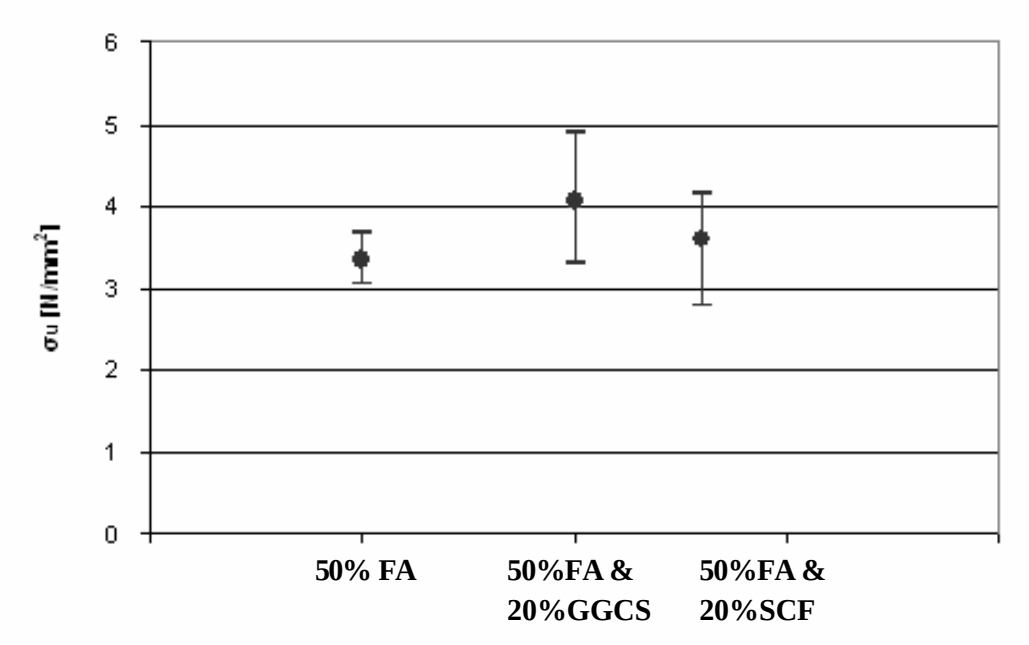

Figure 6.12 The ultimate tensile comparison of mixes with 50% FA, combination of 50%FA and 20% SCF, and combination of 50% FA and 20% GGCS

Because FA content diminishes the cement hydration and FA particles obstruct the structure of cement hydrated product crystals both in matrix bulk and transition zone, FA actually enhances both adhesive and cohesive fibre/matrix reactions. Nevertheless, adhesion is the main contributing factor in high volume FA content mixes and cohesion mainly controls the fibre failure type in low FA content mixes.

6.3 Summary

It is apparent that the method to achieve multiple cracking is to keep a sufficient margin between complementary energy J'_b and crack tip toughness J_{tip}. This can be achieved by reducing the crack tip toughness J_{tip} or increasing the complementary energy J'_b.

One method was used in the present research by mixing with cement replacement FA, which can sharply reduce the interface bond as well as optimise the flaw size and distribution.

The high FA content provided enough initial flaws, resulting in the reduction of matrix crack tip toughness $J_{tip.}$ It also reduced the interfacial bond, therefore lessening the PVA fibre rupture, leading to an increased complementary energy J_b'. Both increase the margin between J_{tip} and J_b'. Hence, a more ductile behaviour can be achieved.

There is an opinion that FA contributes only to extend matrix flaws, but not to the interfacial tailoring, which means the same grading as FA sands can be used instead of FA. However, the discussion in this chapter verified the usefulness of FA for tailoring interfacial properties. It also agrees with the suggestion by Shah that FA enhances the bridging function of fibre (Peled & Shah, 2003). Furthermore, Li (2004) reported that, for extensive artificial flaw purposes, with some similar particles mixed into the matrix, much larger tensile strain was obtained from the composite comprising spherical shaped particles than other mixes. This also indicates that the (cement replacement) particle shape is also very important for tensile behaviour.

For GGCS, the higher interface bonding compared with FA-ECC leads to a larger transferred force across the crack and a longer distance to bridge a more compact matrix. This results in a much higher tensile strength and relatively smaller ductility than FA-ECC. The higher matrix strength of Slag-ECC was compared with FA-ECC. Longer shear transfer lengths are required to reach the highest matrix strength, therefore resulting in larger crack spacing and wider crack width.

Chapter 7

Aging influence

Practical works require not only fresh and early stage properties, but also high age properties of ECC. Aging influence is a complicated challenge for ECC commercial application. It is known that normal concrete has an increased strength with curing age due to the matrix compactness caused by cement-hydrated product. However, for ECC materials, many unknown factors can influence the high age behaviour, such as crystal shape and size, C-S-H gel, microstructure fabric, the fibre/matrix interfacial bond and the transition zone structure. These parameters are usually time-dependent. The ECC behaviour does not only depend on these parameters separately, but also their combination and complex interaction. Therefore, the time-dependent behaviour of ECC materials can be very unpredictable.

As presented in Chapter 2, here are many previous studies about structural durability influenced by ECC materials, even about the fibre durability problem. Lepech & Li (2004) investigated the early age tensile behaviour via a single fibre pull-out test. They reported that the ultimate strain reduced with curing age, and Chan & Li, (1996) reported that ultimate strength remained approximately constant when the fibre failure type is adhesion. Shah et al. (2004) suggest that the aging influence distinctly affects the tensile strain, but does not significantly alter the tensile, or flexural strength.

In this chapter, the aging influence on FA-ECC is investigated and a similar result is reported, namely that aging influences the strain capacity significantly, but not the tensile strength. SEM and XRF studies are performed to explain this phenomenon. Subsequently, ECC's with superior high age behaviour are presented, based on combination of FA and GGCS cement replacement materials.

7.1 Aging influence on the behaviour of high volume FA-ECC

High fraction FA-ECC has been studied for the FA role at rather early age (21 days) in the previous chapters. However, time-dependent influence of a high volume FA on the matrix, the interface properties, and therefore the tensile response, hence the structural durability, has not been studied, specifically after long curing.

There is clearly different tensile stress-strain behaviours of 70% FA-ECC at the age of 21, 128, and 225 days, as can be observed from Figure 7.1. The comparison shows the approximately same level of ultimate tensile stress, but significantly different ultimate strain. The various peak positions indicate the onset of crack localization. More early tensile crack localization occurs in the specimens with higher curing age, accompanied by reduced multiple cracking. The tensile stress-strain curves shows similarity between specimens at 128 days and at 225 days, which indicates that high volume FA-ECC tensile behaviour seems to stabilise after some time.

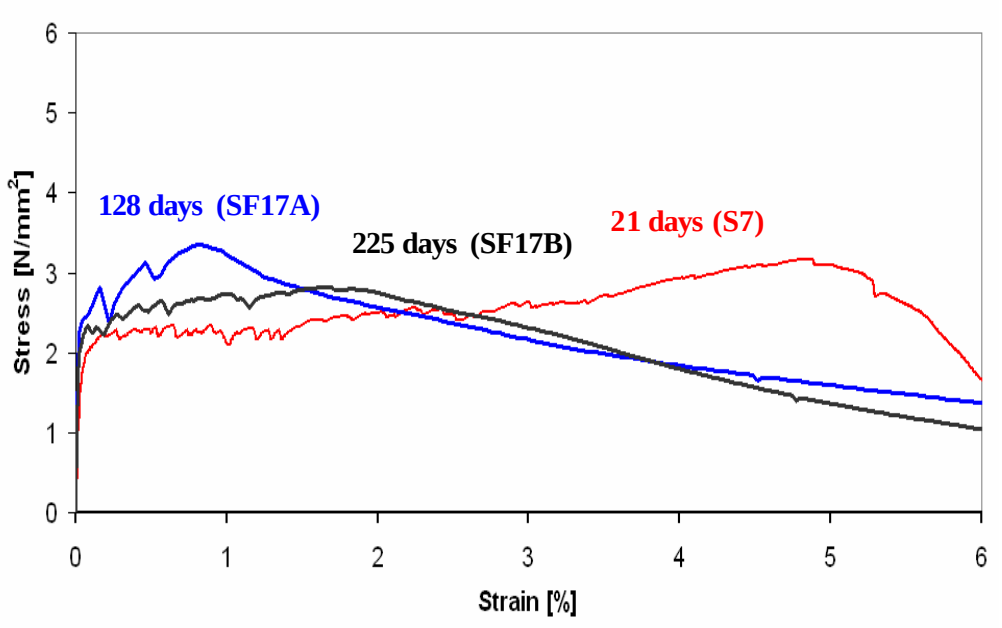

Figure 7.1 Direct tensile result comparison of FA-ECC at age of 21, 128 and 225 days

Figure 7.2 shows the photo obtained from the direct tensile test of the specimen at the age of 128 days. Large crack widths and fibre pull-out across the cracks can be observed clearly. That is also reflected in the stress-strain curve. Furthermore, the special crack pattern indicates that the FA continuous to enhance fibre bridging function, but the composite lost the multiple cracking feature. This phenomenon contradicts the argument above for PVA fibre that more fibre pull-out improves the multiple cracking. However, it is likely that the fibre/matrix frictional forces indeed remain low, causing pull-out, but that it is not accompanied by high enough stress transfer to cause new cracks, due to the more compactness of matrix at higher age.

Figure 7.2 The crack pattern of high fraction FA-ECC at the age of 128 days

The bending results comparison in Figure 7.3 shows that the aging influence on bending is significant on ultimate both bending resistance and deflection. The first crack strength is approximately at the same level for both 21days and 128 days. However, the ultimate strengths and deflections are evidently different, due to the better ductility of the specimen at 21 days, resulting in larger ratio of bending MOR to direct tensile strength. This demonstration was done in Chapter 2.

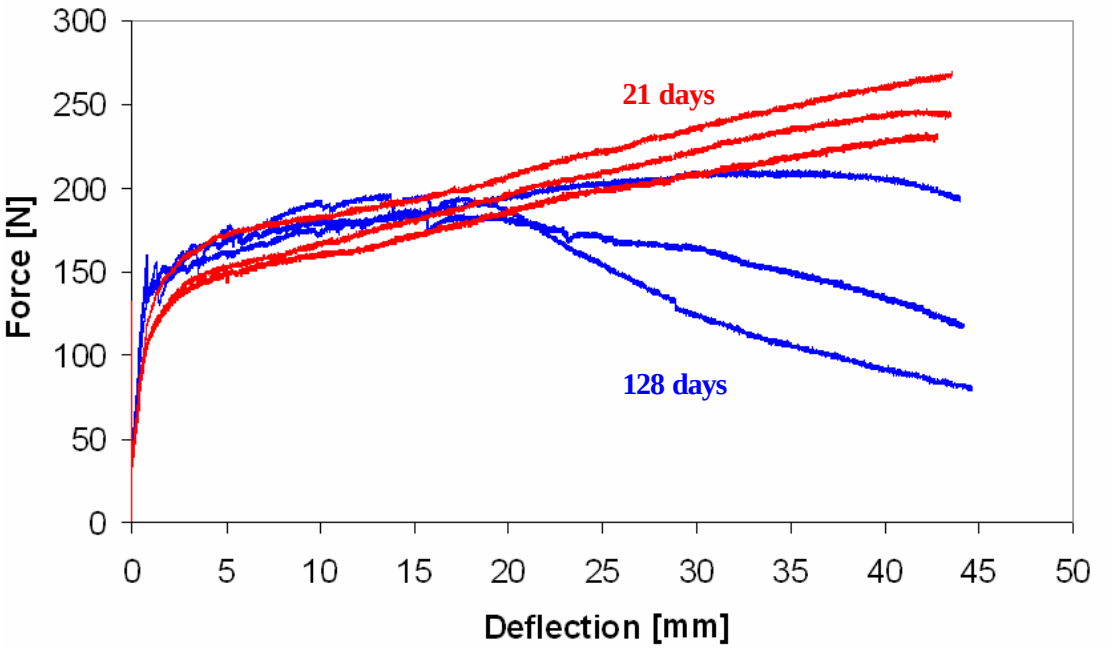

Figure 7.3 Aging influence on three point-bending result of FA-ECC

Figures 7.4 and 7.5 show the first crack stress and ultimate stress of FA-ECC specimens at the curing ages of 21 days (S7), 128 days (SF17A), and 225 days (SF17B). It is clear that the first crack tensile stresses range between approximate 2 and 2.4 by average and the matrix at the age of 225 days has a higher strength than more early age specimen. That is attributed to the

prolonged hydration process of cement and FA.

The ultimate tensile stresses for all specimens are at the same level, ranging between 3 and 3.6 by average. The specimens with the ages of 128 and 225 days have approximately the same ultimate tensile stress. Chan and Li (1996, 1997) investigated the interface properties influence on ECC materials performance at various curing ages and reported the densification of the transition zone between fibre and matrix as the age increased, therefore strengthening the transition zone structure. Hence, the fibre/matrix interface bond could increase if fibre/matrix reaction type is cohesion, otherwise, the interface bond should remain constant. The ultimate stress of the specimen at varied curing age has the approximate same level, which indicates that the interface frictional bond remains constant (see Chapter 2). Also refer to the adhesive type fibre/matrix reaction of high volume FA-ECC, which was presented in Chapter 6.

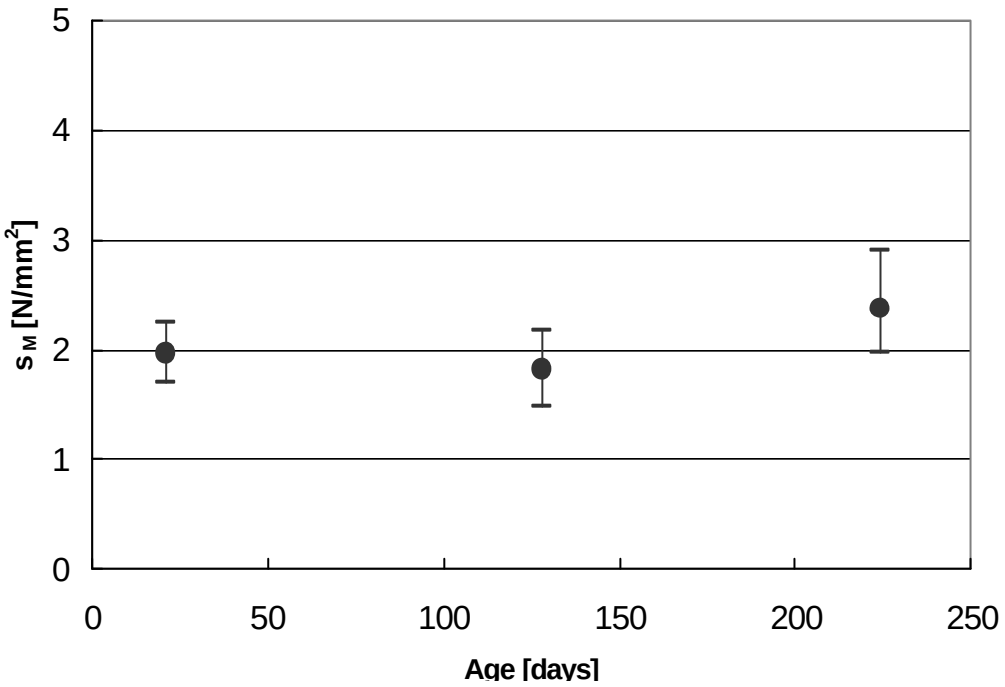

Figure 7.4 Aging influence on first crack stress in FA-ECC

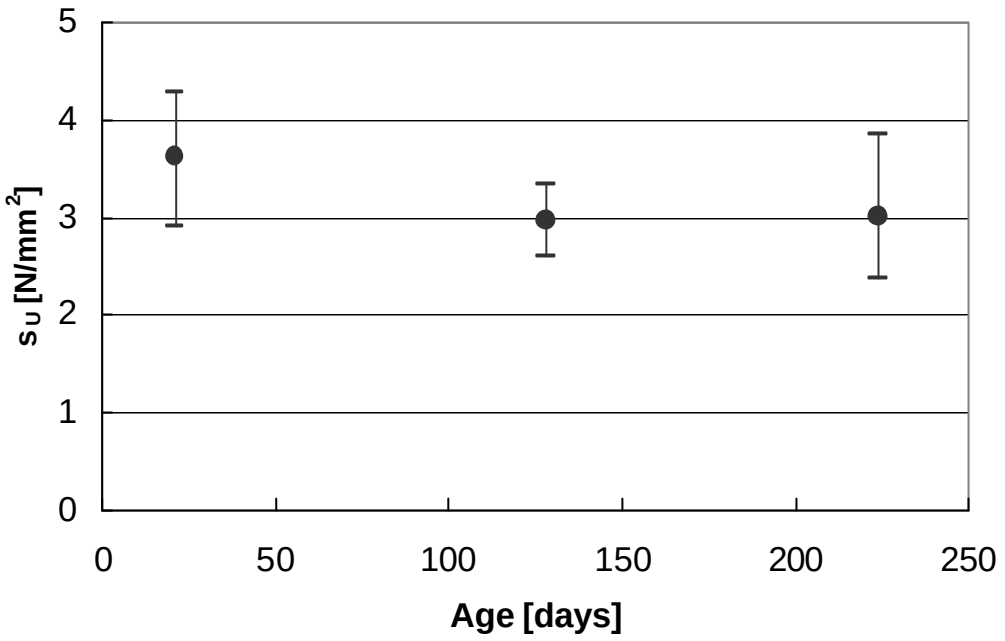

Figure 7.5 Aging influence on ultimate tensile stress in FA-ECC

Figure 7.6 shows the ultimate strain of FA-ECC at the age of 21, 128, and 225 days respectively. The ultimate stress occurs at a low strain in the high age specimen. This may indicate that, the flaws of FA-ECC have been reduced through continued hydration, in the high age. Thereby, the composite crack tip toughness J_{tip} is actually increased, while the fibre/matrix frictional force remains unaltered due to the adhesion between fibre and matrix remains unaltered. Then, the requirement that composite crack tip toughness J_{tip} must be less than the complementary bridging energy J_b' is difficult to satisfy. Therefore, the multiple cracking was hardly achieved, and the strain capacity was reduced with curing age increase, which can be seen in Figure 7.7.

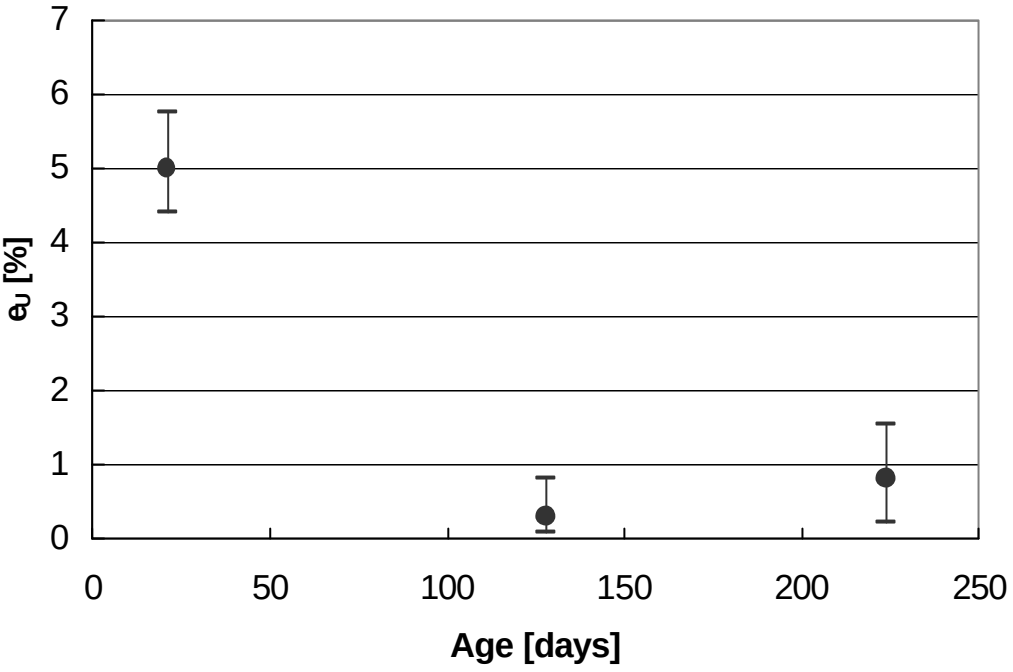

Figure 7.6 Aging influence on ultimate strain in FA-ECC

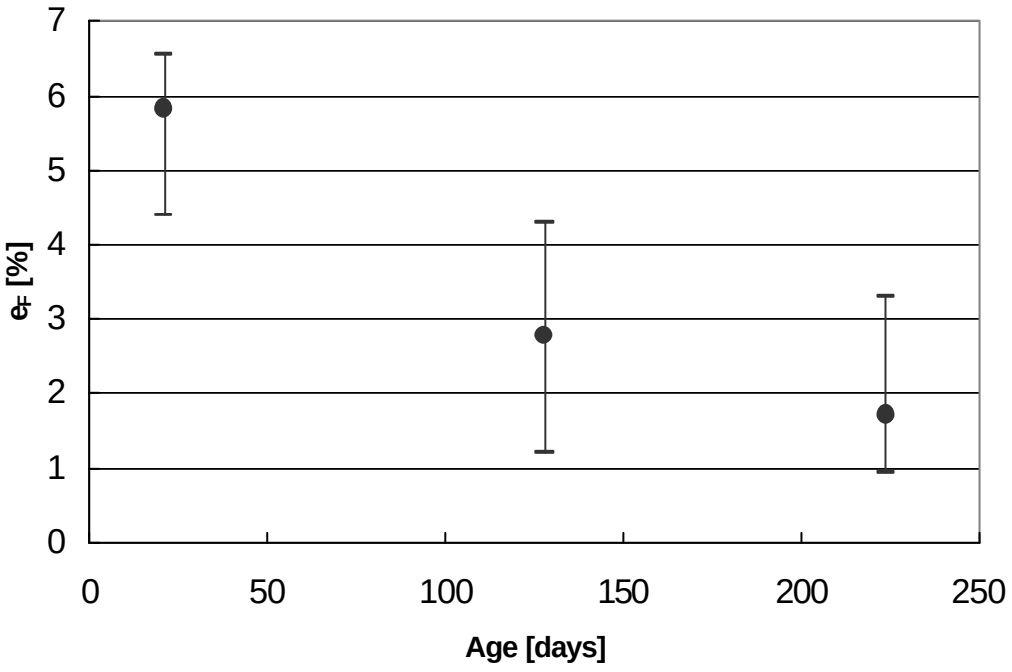

Figure 7.7 Aging influence on tensile strain capacity of FA-ECC

7.2 Micromechanism analysis

First of all, the aging influence on tensile stress and strain needs to be clarified herein. These are:

1. Both the first crack stress and ultimate tensile stress develops sharply from 1 to 7 days and reaches a steady state magnitude at very early age of 10 or 14 days with no significant increase thereafter (Van Zijl, 2005). In the present research, for 70% FA-ECC, the tensile stresses are approximately equally for the specimens with the age grown from 21 days to 225 days.

2. The ultimate tensile strain of the specimens at the age of 128 days and 225 days reduced to approximate 20% of the value at 21days. The strain capacity reduced approximate 50% and 70% when curing age increased from 21 days to 128 days and 25 days respectively.

3. For high volume FA-ECC, the crack width increased significantly. It is virtually impossible to obtain fine, multiple cracking at the age of more than 128 days.

The micromechanism studies associated with micro-scale analysis, such as XRF, EDS, and SEM contributed to the attempt to analyse the aging influence on ECC interfacial properties.

The mechanical properties of ECC materials are time-dependent, because of aging influence on matrix strength and compactness, stiffness, fracture toughness, and fibre/matrix interfacial micromechanical properties. As presented in Chapter 6, the transition zone has a higher porosity and weaker zone than matrix bulk. The densification of transition zone due to the aging influence strengthens the transition zone, and then might affect the interfacial bond between fibre and matrix. However, the matrix properties also affect the ECC tensile performance. The time-dependence of the transition zone seems to be different from that of the matrix bulk (Chan & Li, 1996). This difference in the microstructure development rate between transition zone and matrix bulk might lead to a complicated composite age-dependent behaviour. Figure 7.8 shows the fibre/matrix interface details of 70% FA-ECC at varied curing ages. It is clear that the transition zone grows with curing age. The interface at the age of 2 days, shown in Figure 7.8 (a), has only few hydration crystals attached on the fibre surface. The EDS analysis and XRF analysis results are shown in Tables 7.1 and 7.2. Note that the EDS analysis will automatically normalize data to 100wt% due to the uneven surface (Spicer, 2004). From the EDS analysis results shown in Table 7.1, crystals attached on the surface of the fibre have very high Ca content (25.2%) but low Si content (4.2%). Compared with the XDF result of the FA particle shown in Table 7.2, it has only small Ca content (CaO 4.93%), but huge Si content (57.22%), this indicates that crystal of transition zone at very early age is mainly composed of the cement-hydrated crystal. The binder potion of 70% FA does not hydrate at very early age of 2 days, therefore the composite might still remain retarded and the interface bone is very low.

Figure 7.8 (b) shows the 70% FA content ECC at the age of 56 days with more hydrated product covering the fibre surface than that at 2 days and still some unhydrated FA particle, if compared with specimens at the age of 128 days (Figure 7.8 (c)). There are very similar

fibre/matrix interfacial situations between the specimens at 56 and 128 days. Unhydrated FA particles lie on the surface of fracture rupture. It seems that fibre composite hydration has a stable stage after significant hydration at very early stage. The EDS analysis of the two different positions in the Figure 7.8 (c), shows the different element component of transition zone (position 1) and the matrix bulk (position 2) in the rupture section surface of the specimen at the age of 128 days. The transition zone has higher content element Ca and O but less Al and Si than the matrix bulk. It seems to indicate that the transition zone structure has more cement-hydrated crystal than matrix bulk, which agree with the argument in the previous chapters that transition zone has higher porosity and the rate of development of cement hydrated with age is faster than that of the matrix bulk (Chan & Li, 1996).

It is clear from the SEM photo shown in Figure 7.8(d) that the transition zone of high age specimen is much less compact, compared with matrix bulk. The EDS analysis shows that high age specimen has less Ca content but higher Si content than early age samples and some new element appears in the transition zone, probably due to the more FA glass phase corrosion and hydration (comparative with the mineral component of FA particle). Because the cement-hydrated crystal frame structure has already been formed, the FA hydrated product can only be filled into the voids of the transition, therefore, leading to the densification of the transition zone.

The interface area between fibre and matrix become more compact and FA hydrated product fill in the transition zone and therefore strengthen the transition zone structure with age increase. However, the composite tensile stress does not increase with transition zone strengthening. This indicates that the fibre/matrix interfacial bond is not controlled by transition strength. It can be reasonably explained by the fibre/matrix adhesive interaction, that for high volume FA-ECC system, the interfacial adhesive bond is so low that debonding occurs at the fibre surface. Strengthening of the transition zone cannot effectively improve the interfacial bond.

On the other hand, the matrix development of FA-ECC can be observed from the XRF analysis of FA-ECC hydration at varied ages (shown in Table 7.2). The trend is clear of a SiO_2 and Al_2O_3 decrease, while the CaO content increases with age. Because the SiO_2 and Al_2O_3 are the main content of FA glass phase (see Chapter 3), the SiO_2 and Al_2O_3 content can be seen as an indication of the degree of hydration. The major phases of Portland cement are: tricalcium silicate ($3CaO•SiO_2$), dicalcium silicate ($2CaO•SiO_2$), tricalcium aluminate ($3CaO•Al_2O_3$) and a ferrite phase of average composition $4CaO•Al2O_3•Fe2O_3$ (Mehta 1993). Therefore, the relative CaO content can be used to evaluate the cement hydration degree.

The reduction of SiO_2 and Al_2O_3 is an indication of the FA hydration level, due to the high SiO_2 and Al_2O_3 content in FA particle. The cement-hydrated crystal structure has been formed since the age of 21 days, the additional hydrated product will fill and entwine the cement-hydrated crystal structure, leading to the compactness and densification of the whole composite matrix. The densification of the matrix reduces the flaw number and size, therefore resulting in an increased composite crack tip toughness J_{tip}, whereas the fibre/matrix frictional force remained constant. As a result, FA-ECC hardly showed multiple cracking and, therefore, the crack width becomes large at high age.

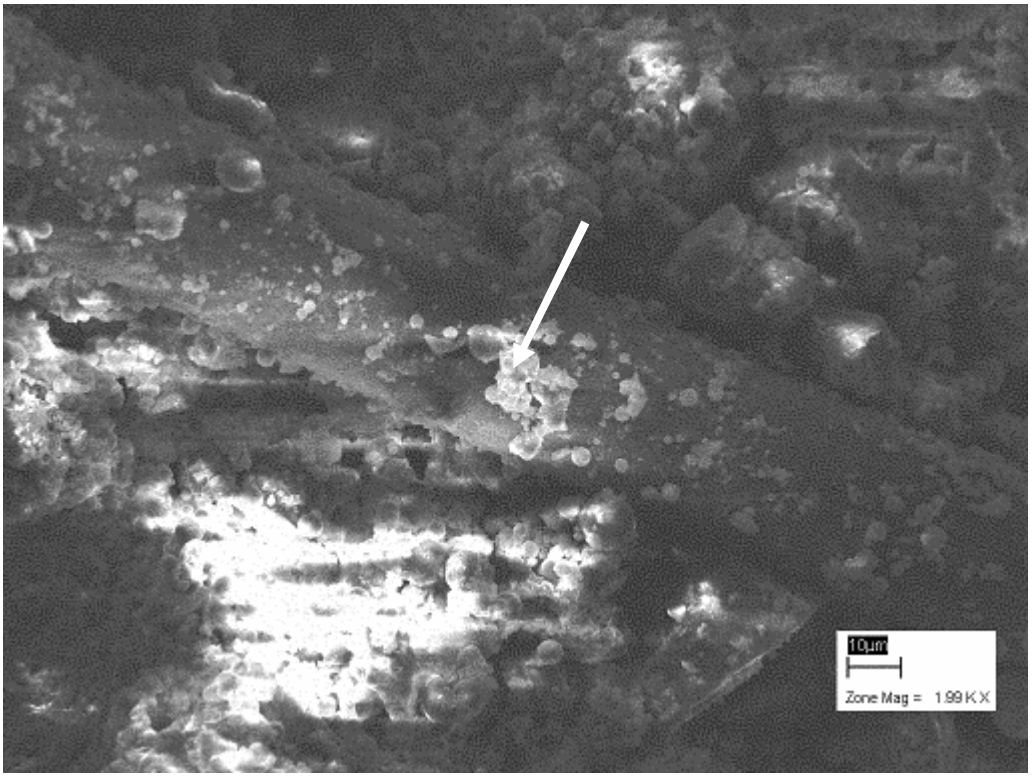

(a) 2 days

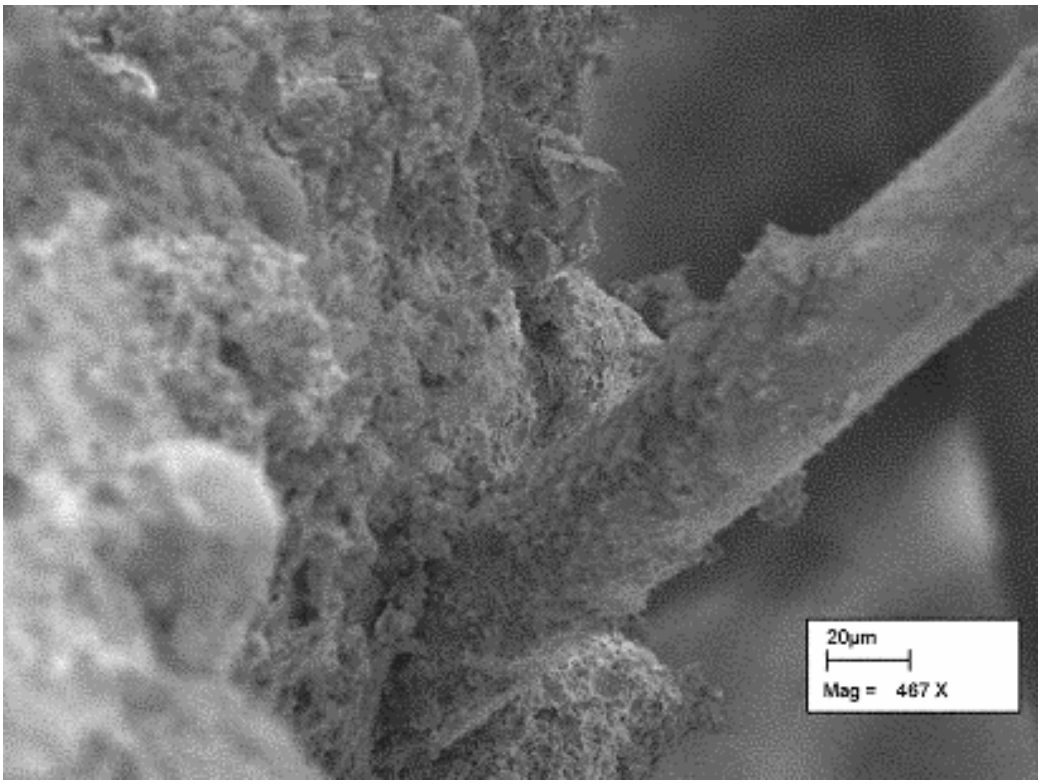

(b) 56 days

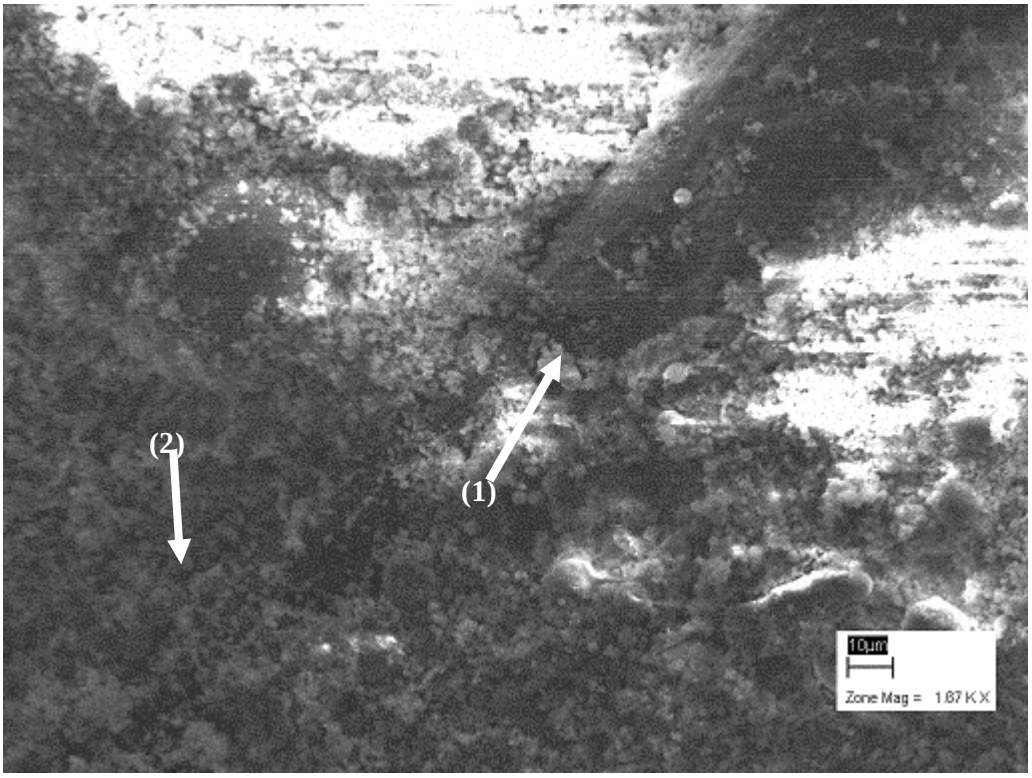

(c) 128 days

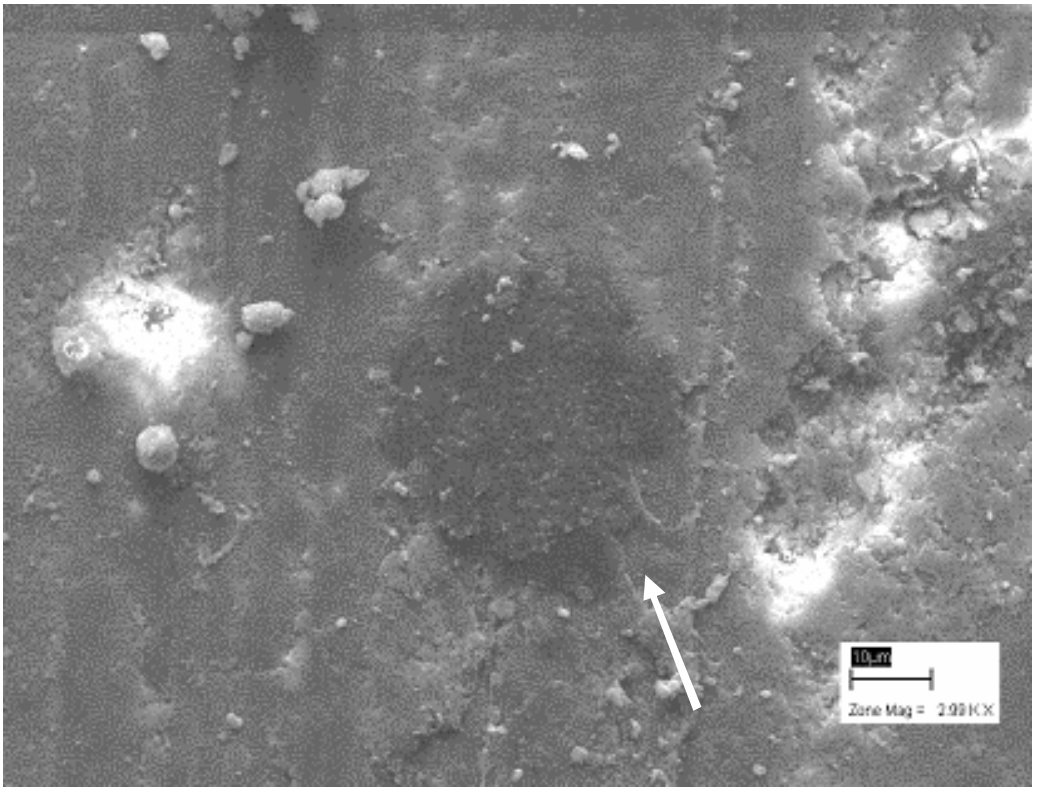

(d) 253 days

Figure 7.8 The interface details for 70% FA-ECC at varied ages

Table 7.1 The EDS analysis (Element abundance in wt%, data normalised to 100wt% due to uneven surfaces) corresponding to the SEM photos

Spectrum	C	O	Na	Mg	Al	Si	K	Ca	Ti	Fe	Nb	Total
2 days	23.8	45.5	0.0	0.0	0.5	4.2	0.0	25.2	0.0	0.0	0.8	100.0
128 days (1)	15.8	60.2	0.0	0.0	1.0	2.8	0.0	19.7	0.0	0.4	0.0	100.0
128 days (2)	32.6	40.9	1.6	0.0	8.5	14.1	0.0	2.2	0.0	0.0	0.0	100.0
252 days	44.4	5.9	0.0	0.7	11.7	21.6	1.5	6.8	3.7	3.7	0.0	100.0

Table 7.2 The chemical component of FA particle, 70% FA-ECC at the age of 130 days and 14 days

	LOI	Sum	Al_2O_3	CaO	Cr_2O_3	Fe_2O_3	K_2O	MgO	MnO	Na_2O	NiO	P_2O_5	SiO_2	TiO_2
FA particle	1.77	100.74	28.10	4.93	0.00	3.97	0.71	1.36	0.09	0.70	0.02	0.38	57.22	1.49
70% FA-ECC 14 days	3.24	94.17*	15.35	20.49	0.00	3.30	0.77	0.98	0.08	0.81	0.02	0.23	48.05	0.87
70% FA-ECC230 days	4.18	88.35	13.32	24.19	0.00	2.43	0.49	1.35	0.08	1.05	0.02	0.46	39.97	0.83

*Low totals might be due to volatile elements, either not analysed for (C, N, S etc), or volatiles that did not burn off completely during LOI determination.

The problem of FA-ECC at high age is due to the reduced difference between complementary energy J_b' and composite crack tip toughness J_{tip} cannot satisfy the criterion for multiple cracks creation. This can be modified by either reducing the composite crack tip toughness J_{tip} or increasing the complementary energy J_b'. Normally, for PVA-ECC, due to the very high fibre/matrix interfacial bond, the method to increase the complementary energy J_b' is to smoothen the fibre surface, through for instance fibre oiling treatment, resulting in more fibre pull-out instead of rupture. Hence, the energy dissipation is increased, through the fibre pull-out mechanism.

For FA-ECC, the perfect fibre pull-out was observed in the direct tensile test at a long curing age (shown in Figure 7.2). This indicated that the fibre/matrix interfacial bond is much less than fibre rupture strength. Therefore, an increase in the fire/matrix bond should be attempted to cause multiple cracking, but without causing fibres to rupture. This is presented in the next section.

7.3 The modification for aging influence

The method followed here to increase the interfacial bond is to add fine, high hydration speed cement replacement material, such as GGCS and CSF. For economic motivation, GGCS was used in this attempt to improve the ECC high age properties. As discussed in the previous chapter, the usage of GGCS can significantly increase the interfacial bond. The combination of FA and GGCS can increase the tensile stress, but also maintain a relatively large strain capacity. Based on this ideal, two sets of modification mixes: one with the combination of 20% FA & 50% GGCS and another one with 50% FA & 20% GGCS were made and tested at the age of 340 days. To compare the high age behaviours of the mix with 50% FA & 20% GGCS, mixes with the 50% FA and the combination of 50% FA and 20% GGCS, 50% FA and 20% CSF were tested at 21 days. For the same purpose, mixes with 50% GGCS and 70% GGCS were tested at 21 days.

Differ from pure FA-ECC, combination FA and Slag ECC shows remarkable high age tensile ductility for 20% FA + 50% Slag and 50% FA + 20% Slag ECC specimens. However, the former has higher tensile stress and less strain capacity.

Figures 7.9, 7.10 show the comparison of varied influence on 50% FA-ECC, which are mix S1, S11, S12, and SF13. The usage of fine particle cement replacement such as silica fume (CSF) and GGCS can significantly densify the transition zone. The aging also has a densification influence on the transition zone (Chan & Li, 1997). However, as was discussed in the previous section, when the adhesive type fibre/matrix interaction controls the interfacial properties, the tensile stress does not increase clearly with the densification of the transition zone.

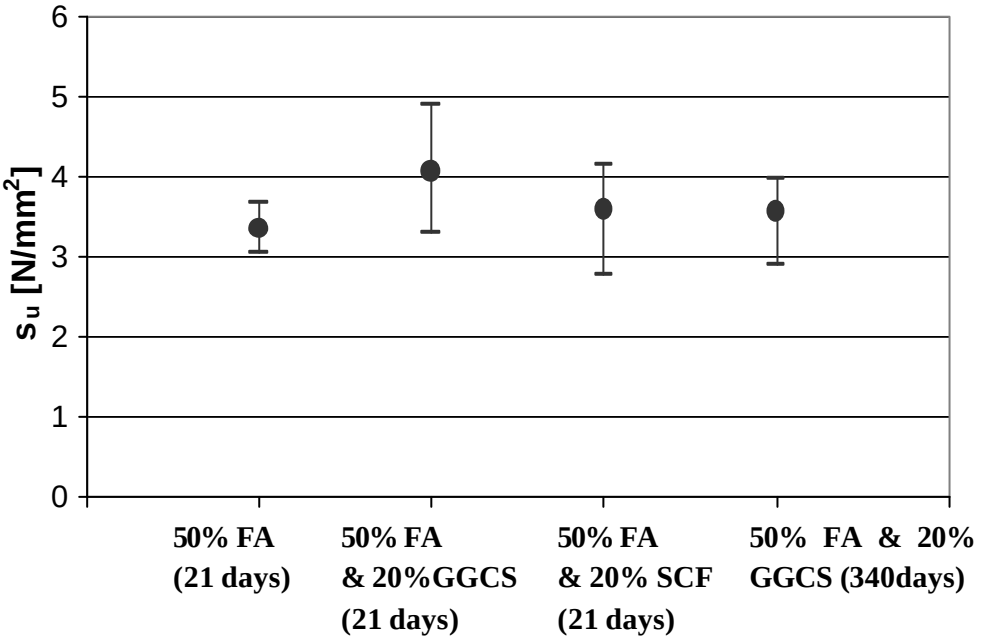

Figure 7. 9 The comparison of ultimate tensile stress with varied cement replacements

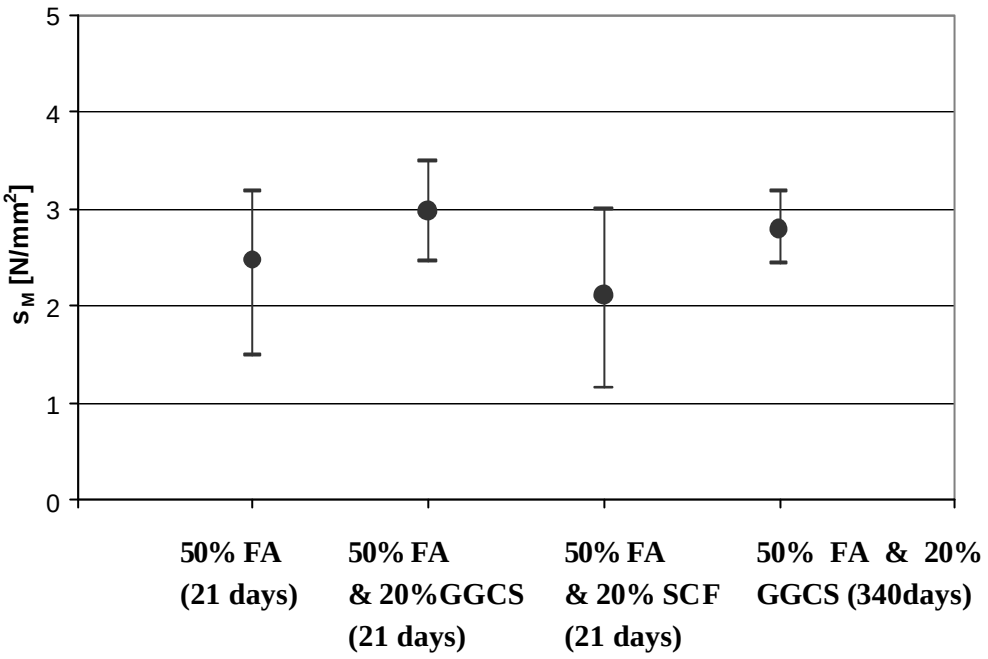

Figure 7. 10 The comparison of first crack tensile stress with varied cement replacements

The tensile strain capacities of ECC with varied cement replacement are shown in Figure 7.11. The ECC mix with the combination of 20% GGCS & 50% FA at the age of 340 days has a larger strain capacity than the mixes with 50% FA content, 50% FA & 20% SCF, and 50% & 20% GGCS at the age of 21 days by average. This may be attributed to a balance between transferred shear force and matrix crack strength.

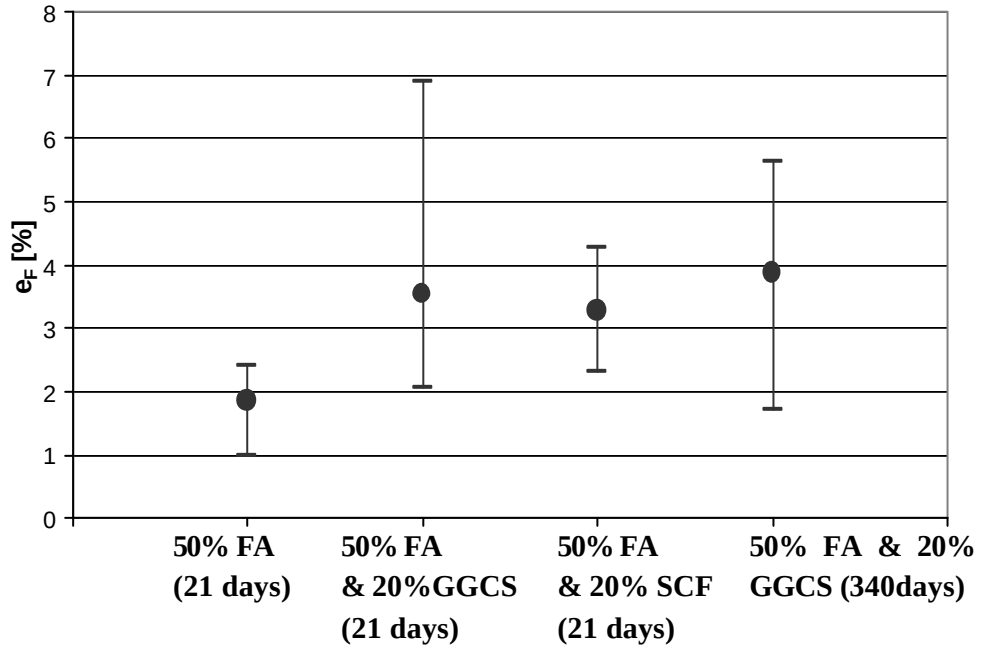

Figure 7. 11 The comparison of strain capacity with varied cement replacements

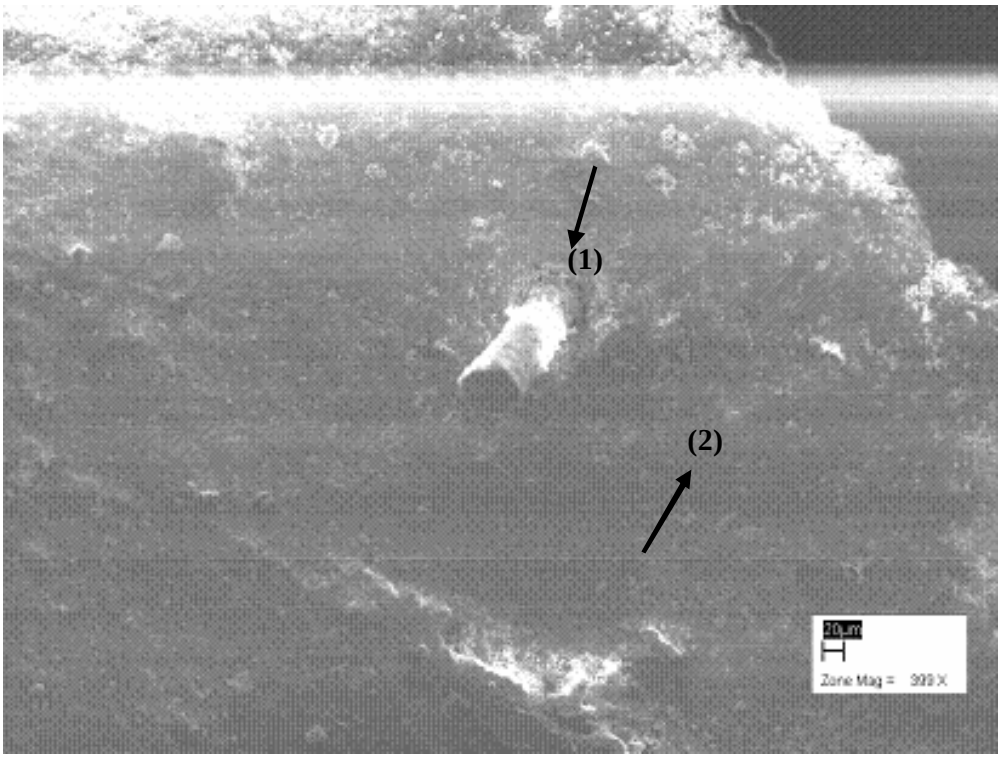

Figure 7.12 The details of the fibre/matrix interface

Table 7.3 shows the element component of the transition zone (Figure 7.12 position (1)) and matrix bulk (Figure 7.12 position (2)) respectively in the surface of composite rupture. The Ca, Al, and Si content of different positions indicate that the transition zone mainly composes of cement-hydrated product and the FA fills in the matrix bulk structure.

Table 7.3 The EDS analysis of specific position corresponding to SEM photo

Spectrum	C	O	Na	Mg	Al	Si	K	Ca	Ti	Fe	Nb	Total
50%FA (1)	22.9	61.7	0.0	0.3	1.1	2.5	0.0	11.6	0.0	0.0	0.0	100.0
50%FA (2)	0.0	65.4	0.0	0.0	16.1	16.4	0.5	1.0	0.0	0.6	0.0	100.0

Note, the (1) and (2) refer to the position (1) and (2) in Figure 7.12

Another type of combination replacement is the mix with the cement replacement of 50% GGCS & 20% FA. The higher fraction of GGCS content provided it the higher tensile stress than the former mix with 50% FA & 20% GGCS. The higher age behaviour of this mix has a comparable tensile stress with the mix with 70% GGCS content and better ductility, as shown in Figure 7.13.

It is apparent from Figures 7.13, 7.14, and 7.15 that mixes with 50% GGCS and 70% GGCS have approximate same level first crack tensile stress but mix with 50% GGCS & 20% FA has a higher first crack strength. It means that the matrix structure of the mixes with high volume GGCS content strengthening with age, which is different with FA-ECC.

The mix with the combination of 20% GGCS & 50% FA at later age has higher ultimate tensile stress than pure GGCS-ECC. The tests herein confirm postulation in the previous chapter that Slag-ECC has the cohesive interface bond failure type, which means the stronger transition zone provides higher interfacial bond strength. The higher interfacial shear transfer provide an increased complementary energy J_b'.

The significant improvement of strain capacity may probably be due to the 20% FA content, which provides sufficient flaws dispersed in the matrix. This leads to a reduced composite crack tip toughness J_{tip}. Both the increased complementary energy J_b' and reduced composite crack tip toughness J_{tip} contribute to provide a sufficient difference between J_b' and J_{tip}, resulting into a better high age performance.

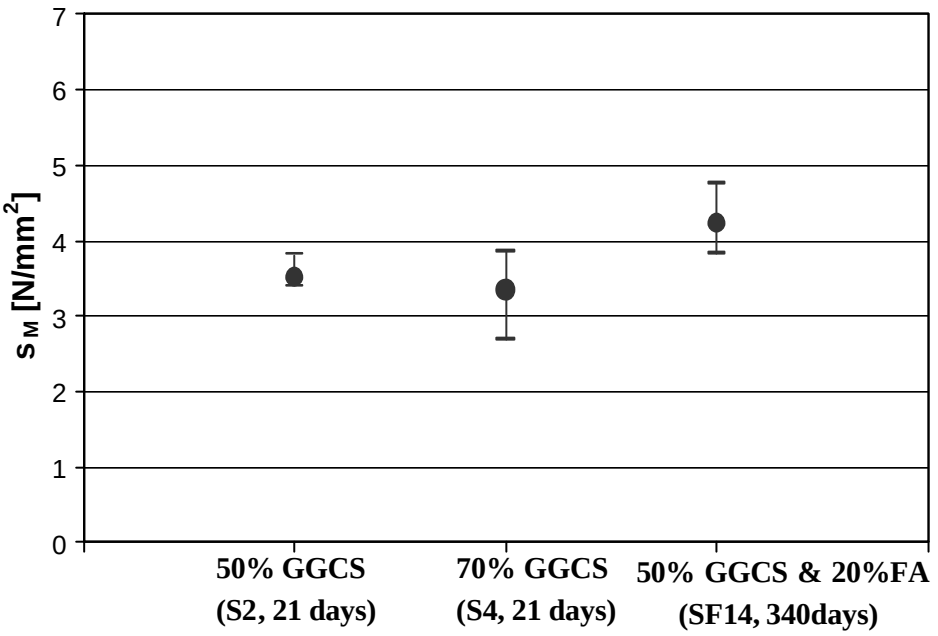

Figure 7.13The comparison of first crack tensile stress of mix with 50%, 70% GGCS, and 50% GGCS & 20% FA at the age of 340 days

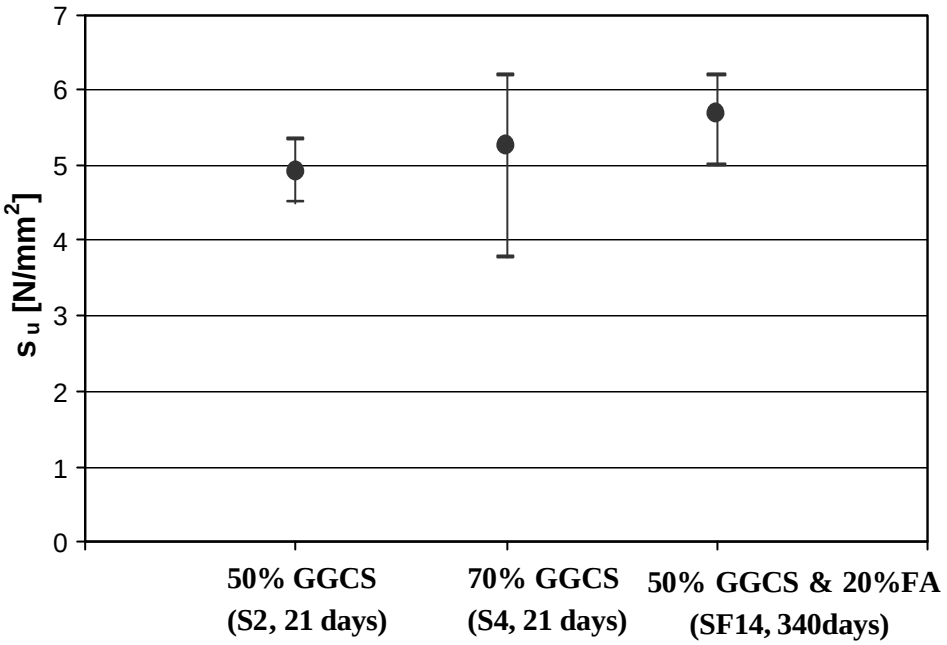

Figure 7.14 The comparison of ultimate tensile stress of mix with 50%, 70% GGCS, and 50% GGCS & 20% FA at the age of 340 days

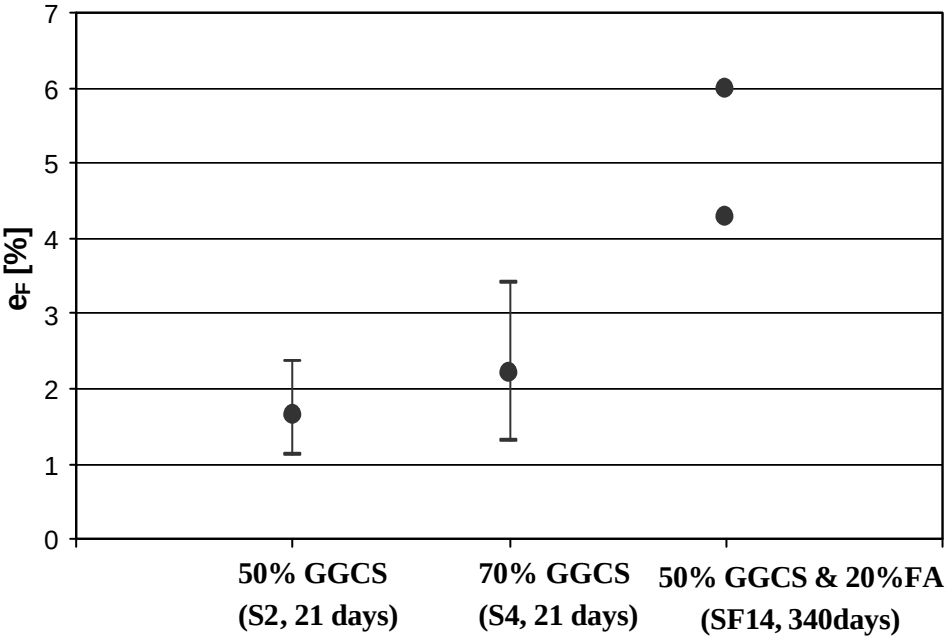

Figure 7.15 The comparison of tensile strain capacity of mix with 50%, 70% GGCS, and 50% GGCS & 20% FA at the age of 340 days

In Figure 7.15, the strain results of only two specimens of SF14 are shown, due to the inaccuracy in measurement of the other two, as stated in Table 5.3(2).

7.4 Remarks

Fibre aging problem can be extremely important, because it may affect the bridging function significantly, which is the fundamental character of ECC materials.

The transition zone size and structure can be studied by SEM, as well as EDS and XRF analysis of specimens. Transition zone structure of FA-ECC specimen at high age was different with that at early age. However, this difference did not affect the interfacial force. It was found that aging impairs FA-ECC ductility significantly. The good strain hardening, ductile tensile behaviour reported for FA-ECC at the age of 21 days in Chapter 5, is lost in time, due to the change of the flaws in the matrix bulk.

The combination of FA & GGCS was used to improve both tensile stress and strain capacity at higher age. The combination of 50% FA and 20% GGCS had superiour tensile properties at the age of approximate one year, showing multiple crack formation, high tensile strength and ultimate strain.

Furtherer work is needed to understand the shrinkage of ECC at high age. Some investigations showed that the concrete mixed with South African FA, with contents up to 30%, had similar drying shrinkage to the concrete made with pure Portland cement. However, FA is a complex ingredient, obtained from industrial by-products. The hydration can be varied for FA from different resources. Moreover, the shrinkage of FA-ECC with FA content as high as 70% needs to be investigated.

Chapter 8

W/B and workability influences

In the practical applications, the requirement of processibiliy of ECC materials may arise. Engineers want to obtain a quick and easy production process. To achieve it, the influences of W/B and workability on matrix properties and on ECC performance are worthy to be investigated.

It is known that W/B controls the matrix compactness. Through this effect it also enhances both the transition zone structure strength and the compactness of the fibre/matrix contact interface. Because a more compact fibre/matrix contact interface leads to stronger interface adhesion and the stronger transition zone structure leads to higher cohesion, it can be expected that the influence of influences of W/B the composite tensile strength. Therefore, the knowledge about the influence of W/B on tensile strain becomes useful. For instance, if engineers know how the W/B influences the ECC tensile strain, they can modify the W/B to obtain a targeted tensile behaviour. Based on this consideration, the influence of W/B on direct tensile behaviour, as well as three point bending were investigated and the results presented in this chapter.

W/B affects composite strength, but also influences the composite fresh state rheology. This manifests in the workability, but also fibre distribution. The ultimate tensile strain might be reduced by the clumping of fibre and/or by matrix disconnection. Low workability results in a poor fibre distribution. Light fibre, such as PVA, tends to clump together in a matrix of low workability. On the other hand, if the matrix is too fluid, heavy fibre, such as steel fibre, tend to drop down to the bottom of the specimen. Both mechanisms significantly influence ECC performance.

In the current chapter, the experimental results are reported of tests on specimens with W/B varying in the range 0.3 to 0.46. It was noted that ECC ultimate tensile strain could be maintained in this range of W/B, if the same level of the fresh state properties (workability) was maintained. Next, the fresh state rheology influence on ECC performance is presented. The workability influences the fibre distribution most strongly. Thereby, it affects the tensile strain capacity. In the case of extremely poor workability, at which the matrix can only be set into the mould by significant vibration, the matrix disconnection leads to extremely low tensile strength and ductility. For too high fluidity, sedimentation of steel fibre may influence behaviour, most clearly shown by bending tests. The experiments show that the specimen with fibres congregated at the bottom has approximately 4 times the bending resistance of the specimens with the fibres congregated at the top.

8.1 W/B influence on ECC behaviour

The W/B influence investigation is carried out by the series mixes SF9A (W/B = 0.3), SF9B (W/B = 0.45), SF19 (W/B = 0.3), SF20 (W/B = 0.4) and SF21 (W/B = 0.46). As indicated, W/B ranged between 0.3 and 0.46, but the workability of all these mixes were made approximately equal, namely moderate workability on the scale defined in Chapter 3. The tensile strengths of the mixes with varied W/B are shown in Figures 8.1 and 8.2. The first cracking stress of the mix with W/B of 0.3 is clearly the highest, whereas the first crack stress remains at lower level for the W/B ranging from 0.4 to 0.46. It agrees with the expectation that lower W/B causes a stronger matrix. The transition zone is also supposed to be denser at lower W/B. However, there are many unknowns, which can affect the interfacial properties when the W/B varies. The irregular ultimate tensile stress trend with varied W/B indicates the uncertain fibre/matrix interfacial properties.

Note that in this chapter, the s_M for mixes SF 19 – SF21 is not the first crack stress but the average matrix strength. Because of the smooth, nonlinear ascending stress-strain response of these mixes, there is no clear point where the gradient changes. Therefore, the first crack determination becomes subjective and may not indicate the matrix properties properly. The nonlinear ascending part is followed by a plateau in the stress-strain response, which indicates an average matrix strength. This stress value is recognized as the average matrix strength, as was also stated in Table 5.3(4). The zoomed in curves for SF 19 – SF 21 are shown in Appendix 3.

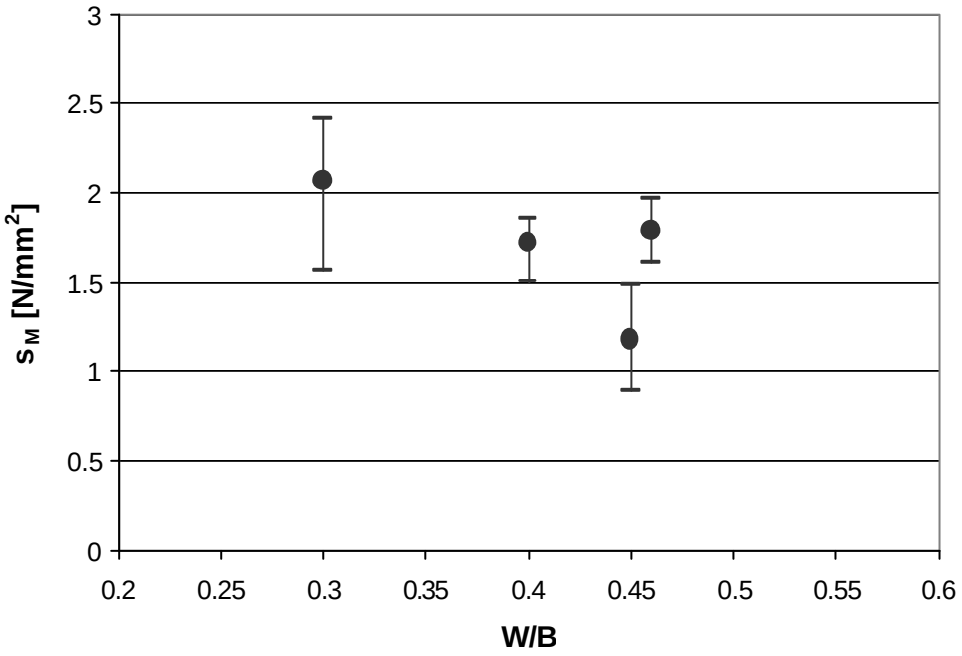

Figure 8.1 W/B influence on first cracking stress

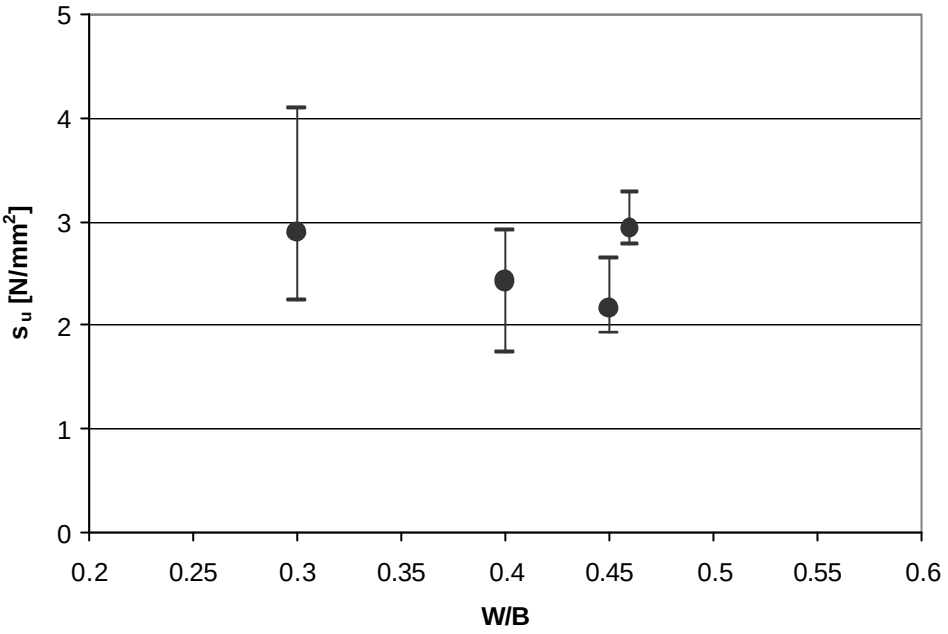

Figure 8.2 W/B influence on the ultimate tensile stress

It is apparent from the tensile strain results shown in Figures 8.3 and 8.4, that the tensile strain capacities are approximately at the same level in spite of the varied W/B. It can be ascribed to the very specific mix of the FA-ECC with a rich pre-existing flaw pattern in the matrix, leading to a low matrix toughness and, therefore, a low crack tip toughness J_{tip}. Also, the high FA content brings about a reduction of interfacial bond, which induces more fibre pull-out and an associated high complementary energy J_b'. Hence, for FA-ECC, moderate improvement on matrix strength and toughness may still keep a sufficient margin between J_b' and J_{tip}. Consequently, sufficient tensile strain capacity of the mix with high W/B can still remains

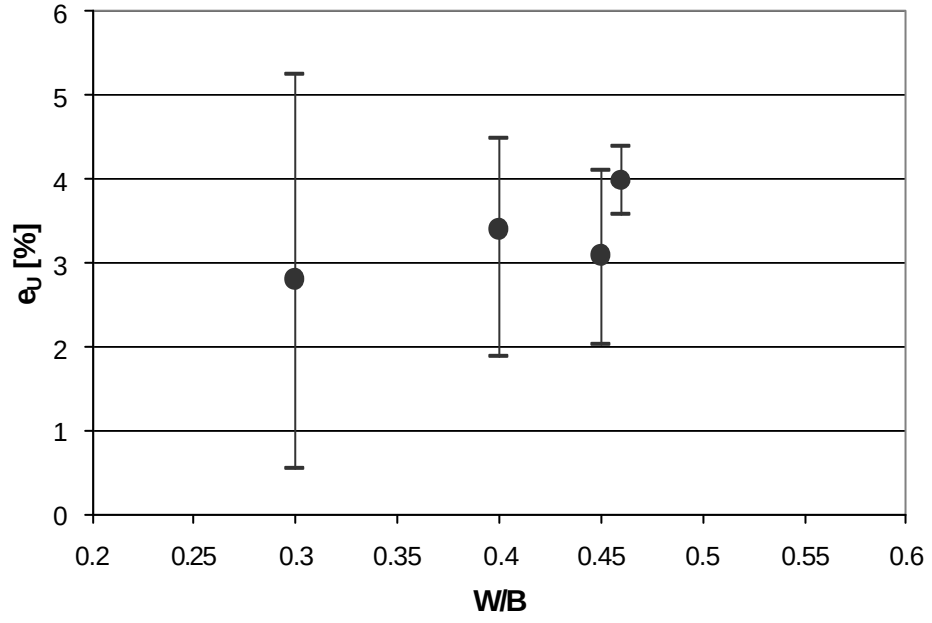

Figure 8.3 W/B influence on the ultimate tensile strain

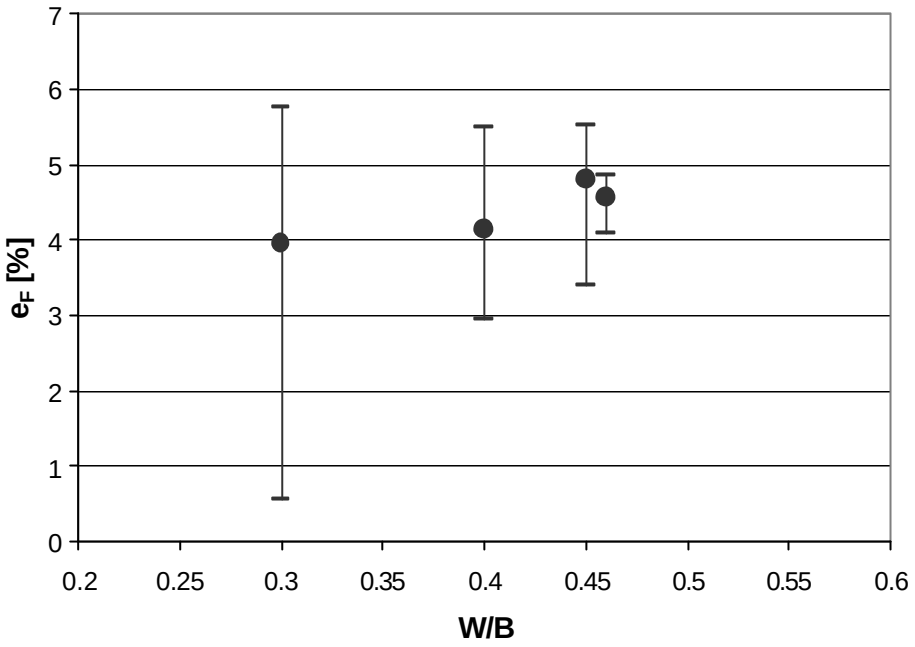

Figure 8.4 W/B influence on tensile strain capacity

Figure 8.5 shows the three point bending results of specimens with varied W/B in the range from 0.3 –0.46. It is clear that the specimen with lower W/B has a higher matrix bending resistance, but the entire range of specimens have a similar grading of bending resistance-deflection response. This indicates that the specimens with varied W/B, but the same workability, have a similar increase bending resistance. Furthermore, it seems from the bending resistance-deflection curve, that the lower W/B leads to a larger bending deflection at the price of repeatability; the mixes with higher W/B have better repeatability.

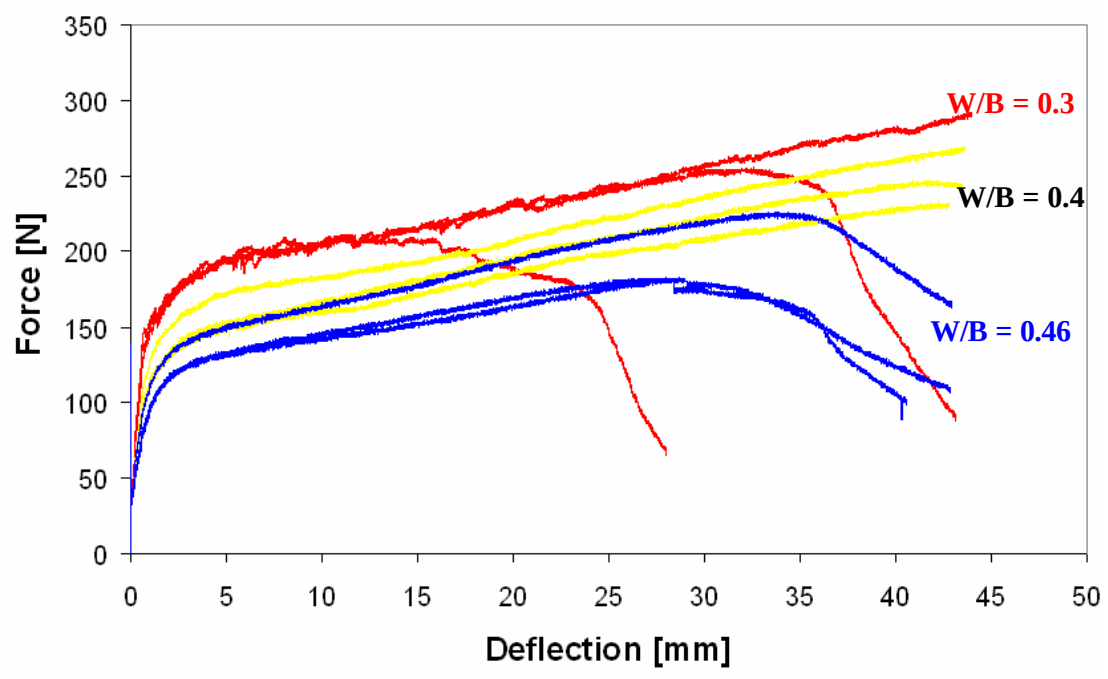

Figure 8.5 W/B influence on three point bending response

8.2 Workability and fibre distribution influence on ECC tensile behaviour

It is known that the use of fibre in cementitious materials can distinctly reduce the workability in the fresh state. In fibre-reinforced cementitious materials, it can cause fibre clumping. Thus, the workability affects the fibre distribution. The present research reports the experimental results of tensile behaviour of ECC, as influenced by workability.

Generally, the influence of workability on the ECC matrix structure alone can be ignored. As long as appropriate pre-flaw size and distribution are present, multiple cracking should occur (Wang & Li, 2004). However, it is known that matrix workability affects the fibre distribution. The failure of ECC indicates the position where less fibre sustained and transferred the load, leading to predominant matrix fracture. Therefore, the fibre distribution becomes an important parameter associated with tensile performance. The workability influence on fibre distribution therefore makes it an important role player in determining ECC tensile performance. In the present research, workability was evenly divided into three levels which are hard to cast/compact, moderate workability, and self-compacting. Figure 8.6 shows the tensile responses of specimens with identical 70% FA content, but at different workability levels, achieved by manipulating only the SP content. The three mixes are SF15 (hard to compact/cast), SF20 (moderate workability), and S7 (self-compacting). Note the mix SF20 and S7 are both the W/B of 0.4 and SF15 is W/B 0f 0.2, because it is hard to obtain an extremely poor workability with a higher W/B.

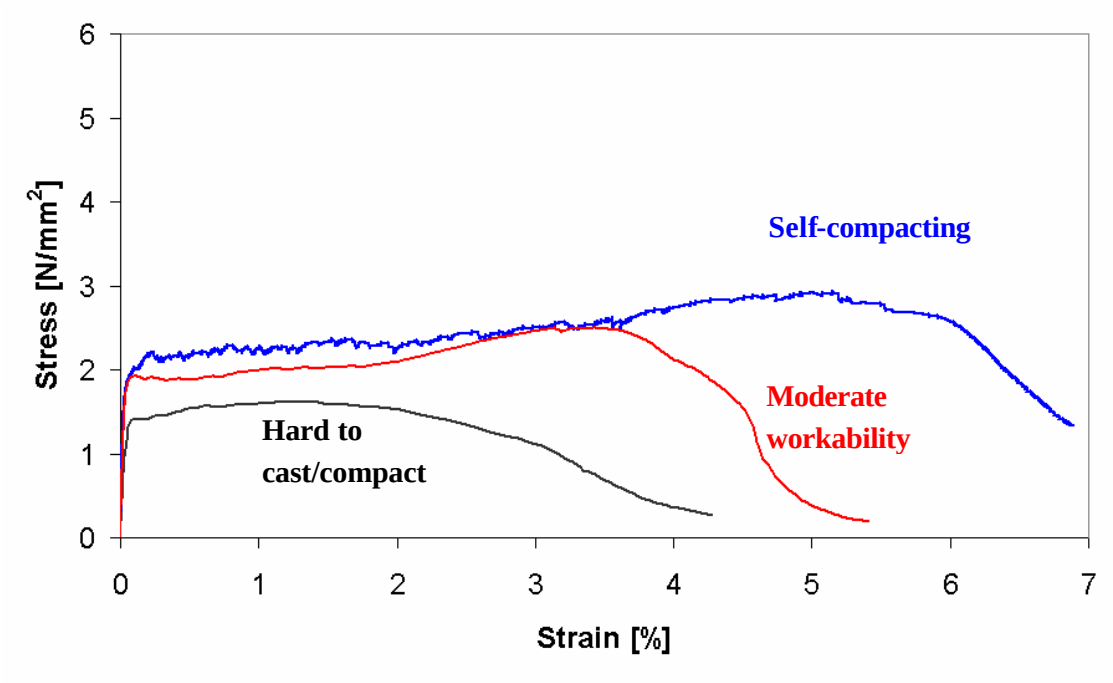

Figure 8.6 Workability influence on direct tensile behaviour

Figures 8.7 to Figure 8.10 show the workability influences on tensile stress and strain. It is apparent from these Figures that the workability influence is significantly on both tensile stress and strain in despite of it has a slightly influence of first crack stress. The mixes with self-compacting workability and moderate workability have significant discrepancy on their tensile behaviours. This phenomenon, which ECC behaviours are sensitive to the workability instead of W/B, occurs so many during all the experimental works that the experiments have to require the uniform workability for the comparative test sets.

As the postulation in Chapter3, the workability dominated the engineering parameter of ECC tensile performance, especially s_u, e_U, and e_T by its influence on fibre dispersion. From the comparison of the tensile response of specimens at different workability, the experimental results presented herein indicate the postulation.

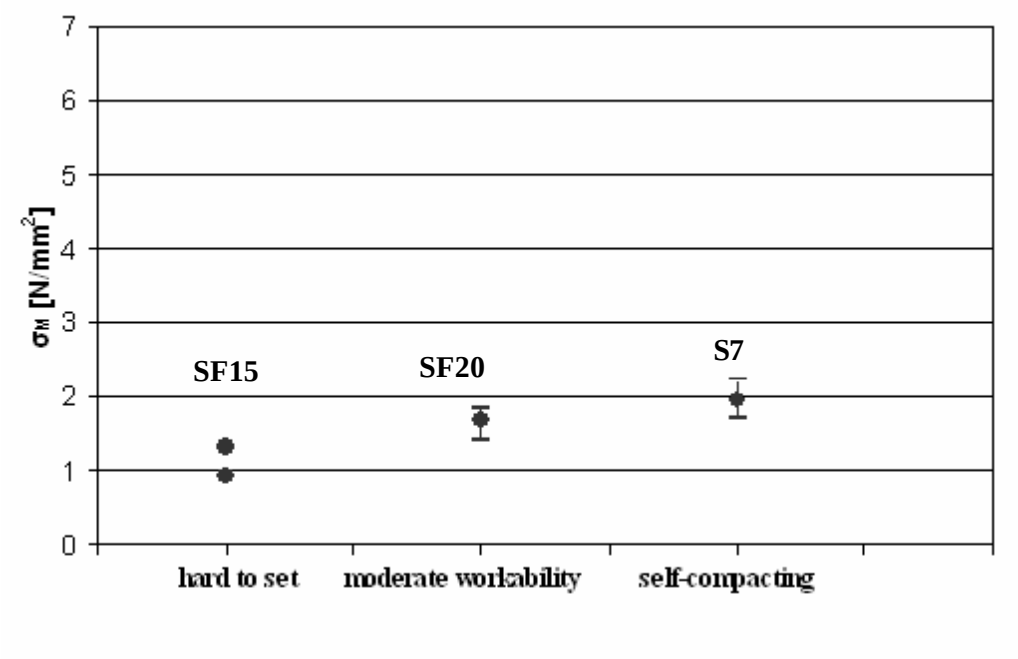

Figure 8.7 Workability influences on first crack tensile stress

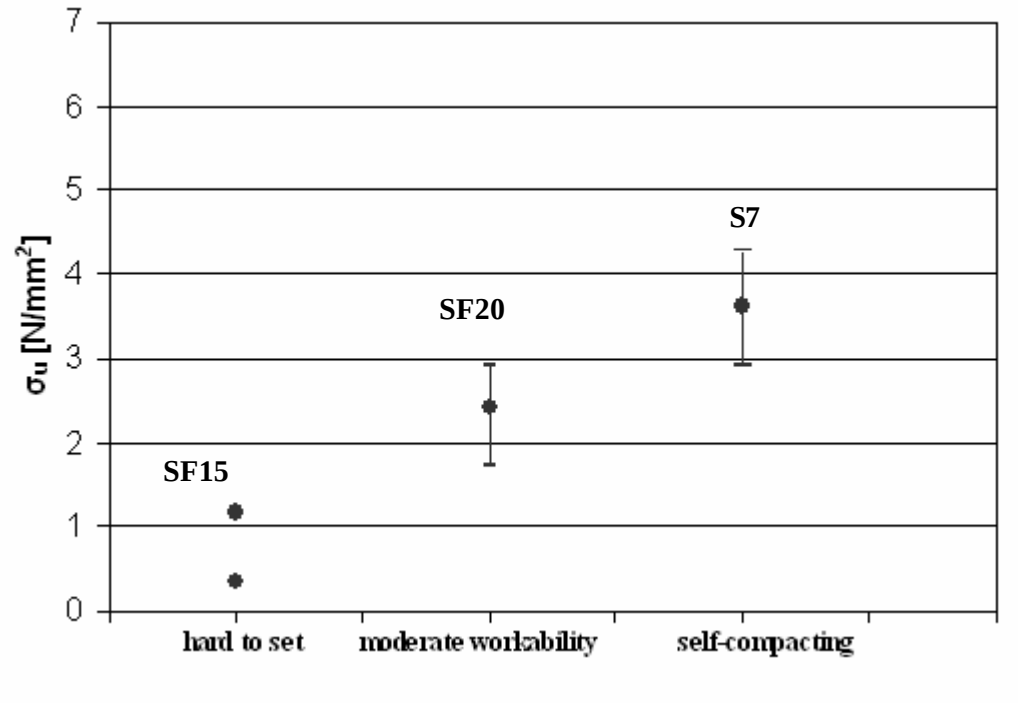

Figure 8.8 Workability influences on ultimate tensile stress

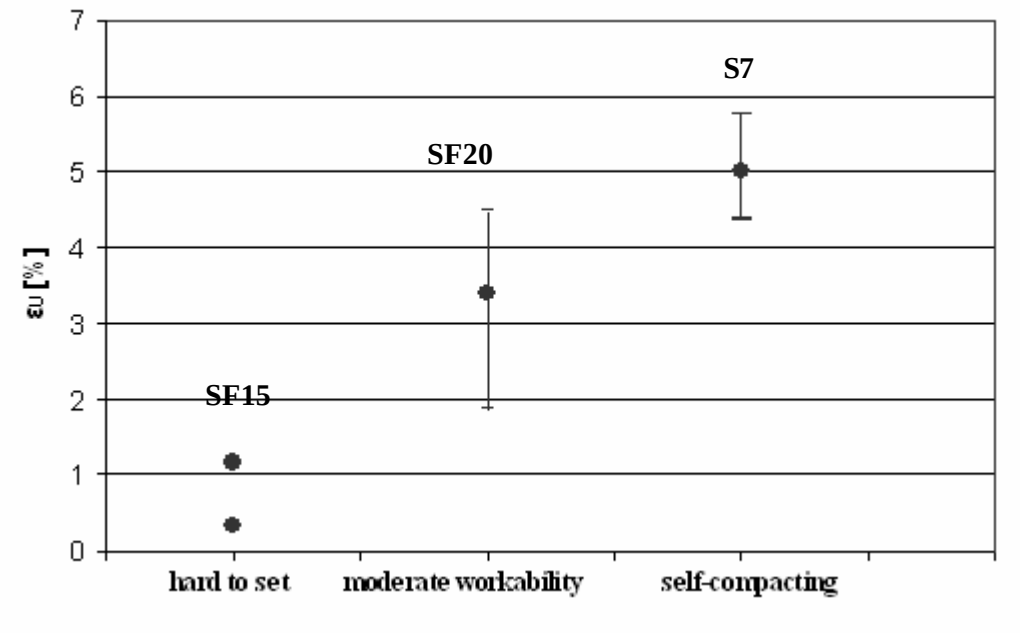

Figure 8.9 Workability influences on ultimate tensile strain

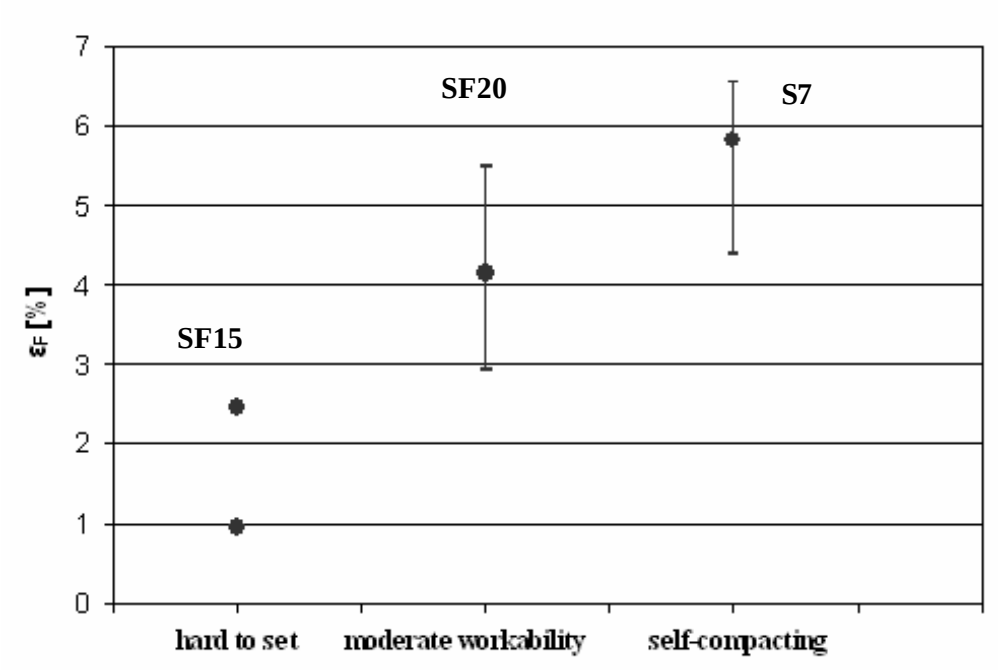

Figure 8.10 Workability influences on tensile strain capacity

The workability influence on fibre distribution is known, the poor fibre dispersion leads to poor fibre bridging and subsequent premature crack localising and composite failure. Good fibre distribution ensures good load bridging by fibres, enhancing multiple cracking and good composite strain capacity. In Figure 8.11 examples of good fibre dispersion (left) and clumping (right) are shown.

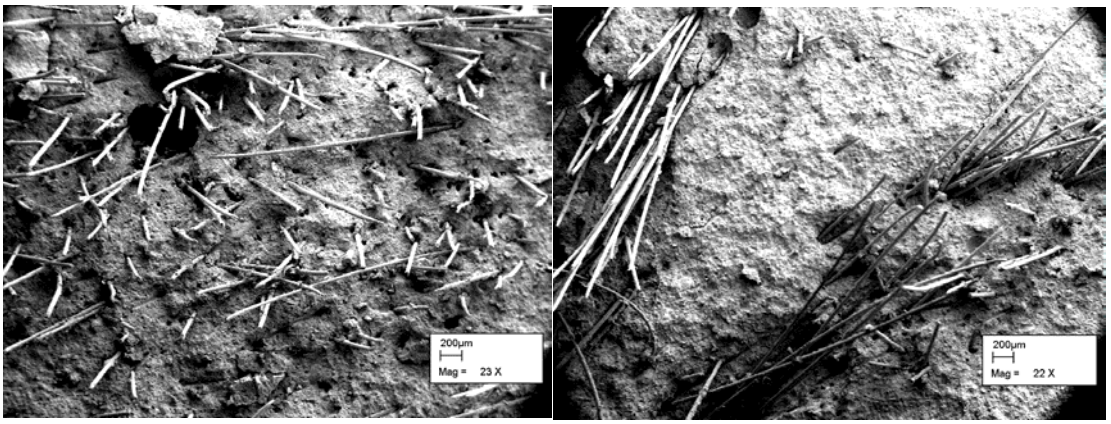

Figure 8.11 Good (left) and poor (right) fibre dispersion or clumping

Furthermore, poor fibre dispersion leads to less multiple cracks and large crack space because visible cracks tend to occur at the position of less fibre, despite the crack spacing increasing.

For the case of extremely poor workability, the matrix structure may have large initial flaws, which is actually a matrix disconnection the fresh state. In such case both the composite strength and ductility can be reduced significantly. The stress-strain curve of the hard to cast/compact setting mix in Figure 8.6 shows the extremely poor workability influence on both tensile stress and strain.

In some situations, after the composite was vibrated sufficiently, the surface of the specimen seemed in order. However, internally the structure might still have been segmented. When such a specimen is subjected to tension, it will break along the disjunction. Such a case of a specimen breaking along the matrix disconnection rut is shown in Figure 8.12.

(a) An apparently good surface, except for flaw on one side. (b) First crack under low tensile load. (c) Crack opens along the initial crack rut. (d) Eventual fracture at initial gap without substantial resistance increase beyond stage (c).

Figure 8.12 Illustration of fracture along the disjunction caused by poor workability

8.3 Steel fibre segregation influence

If the fresh state matrix is too liquid and fibre is too heavy to remain in suspension, such as steel fibre, to float in it, then there will be fibre segregation, as was the case in some steel fibre ECC specimens of this research project. Thus, for steel fibre, the fibre segregation occurs mostly in the form of fibre sedimentation.

Figure 8.13 shows the flexural behaviour of the steel fibre reinforced composites of mix SF5. If the specimens are tested with the steel fibres congregated at the bottom, or tension face of the beam, it has much higher bending resistance than when the beam is rotated so that the settled steel fibres are at the top, compression face.

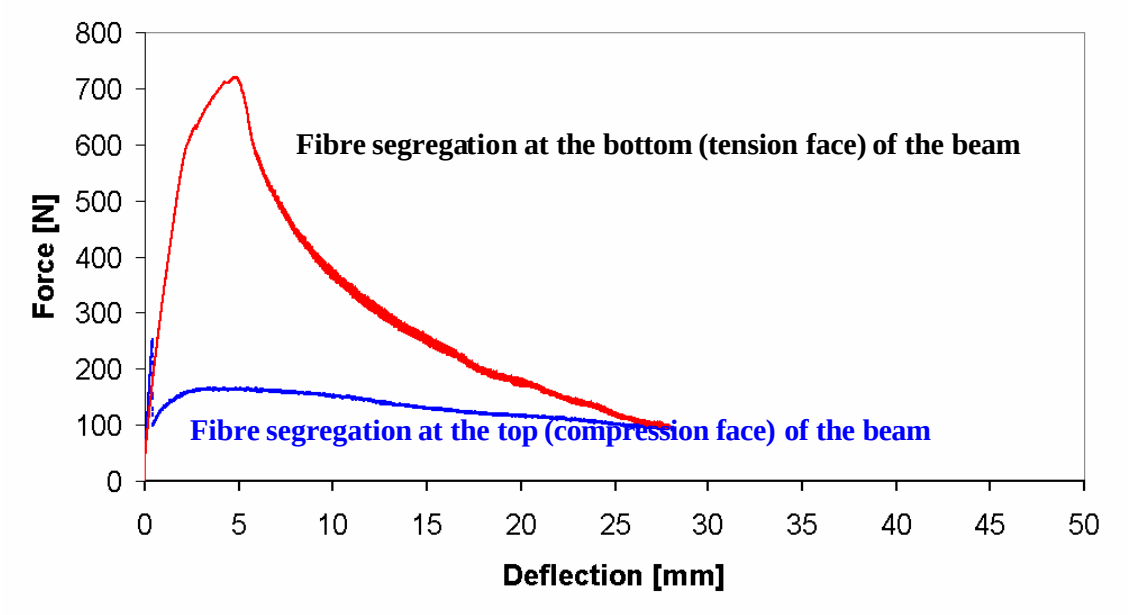

Figure 8.13 Fibre segregation influence on three point bending response

Furthermore, vibration can also enhance the fibre sedimentation. Photo images about the vibration influence on steel fibre sedimentation are shown in the photographs in Figure 8.14. It is clear that both specimens have fibre sedimentation. Particularly, specimens, which were subjected to vibration have worse fibre segregation, or downward settlement. This fact implies for practical application that engineers need to consider the processing effect on a structural member, which might be multi-directive loaded.

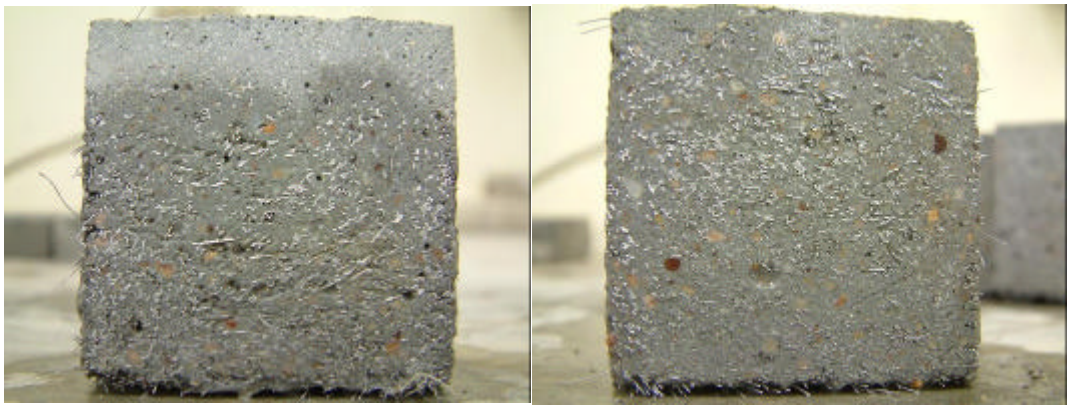

Figure 8.14 Comparison between mix SF6 specimens with vibration (left) and without vibration (right)

8.4 Summary

The W/B hardly influences ECC tensile behaviours, especially the strain capacity, if the same level of ECC fresh state workability is maintained. From the comparison presented in this chapter, the workability influences on all the engineering parameters of ECC tensile behaviours via influence fibre distribution. In the worse case of extremely poor workability, composite matrix structure disconnection may occur, which leads to an extremely low composite tensile strength.

Thus, the experimental results presented in this chapter implied that workability could be seen as a more important factor than W/B for engineering parameters of ECC.

The postulation made in Chapter 3 that the workability dominates the ECC tensile behaviour rather than W/B and thereby the judgement to maintain workability constant throughout series I and II respectively, is therefore also worthy and necessary.

Fibre distribution can affect ECC tensile behaviour significantly. Therefore, it is also an important parameter to evaluate ECC performance. It must be noted that in addition to fresh state workability, other influences, such as VA usage, aggregate content and grading, and mixing time also influence on the fibre distribution.

As mentioned in Chapter 5, the first crack was recognized at the point where a significant gradient change occurs in the zoomed in stress-strain response curve, which indicates a change in the E modulus of the matrix. This point can be observed usually in three conditions; the tensile stress reduces after this point, which probably indicates that fibre/matrix debonding occurs and leads to the load reduction. The second condition is a lower, but still positive gradient. For these cases, the tensile stress still increases after this point, due to the small crack occurrence, which reduces the specimen section equivalent area. The third, unusual situation is that the stress-strain response ascends nonlinearly, which means there is no

significant gradient change point at the early stage. This situation appears in mixes SF 19 – SF21 and was presented in this chapter. The instance is not fully understood yet. The mixes SF 19- 21 are 70% FA content, therefore, it seems FA content influences the matrix properties, resulting in a smoother tensile stress-strain response. However, the mix S7, SF 9A and 9B are also 70% FA content, but do exhibit a significant gradient change point, such as described for case 1 or 2. This also can be due to the weakness of the matrix, or the test process. The smoother stress-strain response indicates the weaker fibre/matrix debonding and less visible crack occurs. The one aim of ECC materials is to improve the toughness and reduce the matrix crack widths. Therefore, it is worthy to investigate the reason that smoother curve happens as well as to establish the criteria of first crack point and matrix properties in such smooth stress-strain response.

Chapter 9

Other influences on ECC behaviour

As a new class of fibre reinforced cementitious materials, ECC has many unknowns which influence on its performance. This chapter presents four important issues, which contribute to understand ECC performance.

Section 9.1 introduces the direct tensile and three point bending behaviour for hybrid fibre reinforced ECC.

Section 9.2 presents the ratio between the MOR, as determined from three point bending results, and direct tensile strength. Three FA-ECC mixes with different W/B are used for this discussion.

Section 9.3 investigates the comparison of three point bending behaviour of specimens fabricated by the cast process with those produced by the extrusion process.

Section 9.4 presents the relation between compression and tensile strength for FA-ECC and Slag-ECC.

9.1 Hybrid fibre influence

In recent years hybrid fibre reinforced ECC has been developed. Two or more types or lengths of fibre are combined to improve the performance of the composite. Typically, two major combinations are used, which are the combination of micro (short) fibres and large fibres, as well as the combination of varied fibre type and size. The combination of high modulus and low modulus fibre has been investigated to optimise the performance of ECC by various research groups. However the combination of two types of high modulus fibre has hardly been studied. Fibres used in this research are high strength, straight, steel fibre and Poly Vinyl Alcohol (PVA) fibres. Their characteristics were introduced in Chapter 3. The matrix used herein has the binder portion of 30% FA and 30% GGCS.

Figure 9.1 shows the tensile behaviour of the hybrid ECC, for specimens containing steel fibre and PVA fibre at three different ratios (mixes SF 10, 11, and 12). It is apparent that the mix with the combination of 1% steel fibre and 1% PVA fibre has the lowest tensile stress and strain. The mix with the combination of 1% steel fibre and 1.5% PVA fibre has the highest tensile strength and the one with 1% steel fibre and 2% PVA fibre has largest tensile strain capacity. It seems to indicate that the usage of PVA fibre contributes to the tensile strain capacity. It is in agreement with the results of Chapter 5, where it was showed that PVA fibre ECC has larger strain capacity then steel fibre. However, too much PVA fibre content might not contribute to improve the composite tensile stress.

A reasonable explanation is that, because PVA fibre has stronger fibre/matrix interfacial bond with the matrix than steel fibre, the moderately higher PVA fibre usage can correspondingly improve the composite tensile stress. The PVA fibre ECC failure is mainly controlled by cohesive type in this kind of matrix (which was presented in Chapter 6). That means that PVA fibres tend to destroy the transition zone structure, rather than merely slipping out of the matrix by overcoming the adhesion between the fibre and the matrix. At high PVA fibre content, fibres may interfere by, for instance, overlapping transition zones, and hence lead to the matrix break down under a lower tensile load.

Note, however, that this should be investigated further, extending the experimental work for more than the current four specimens per fibre combination.

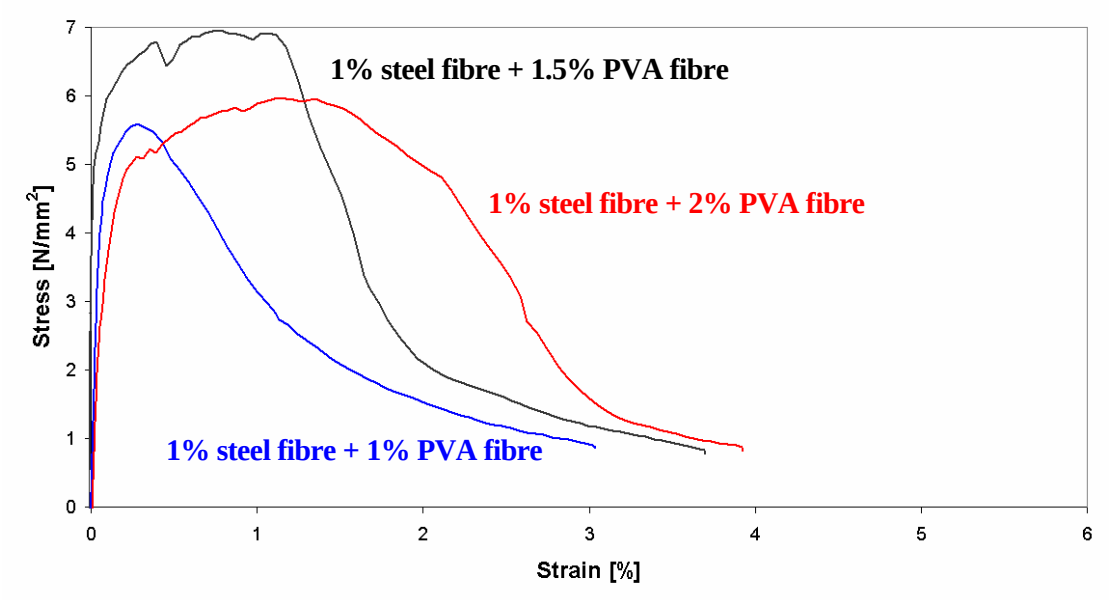

Figure 9.1 Comparisons of direct tensile response of hybrid ECC at various fibre type ratios

Figure 9.2 shows the three point bending result comparison of hybrid ECC mixes. This differs from the direct tensile behaviour. The bending resistance of 1% steel fibre and 1% PVA is highest, whereas it has the lowest tensile strength in direct tension. The postulation above that the cohesive fibre-matrix failure type and fibre interfacial zone interference may cause the reduction in ultimate resistance with increased PVA content applies for bending as well. Note, once again, that more tests are required to verify this trend.

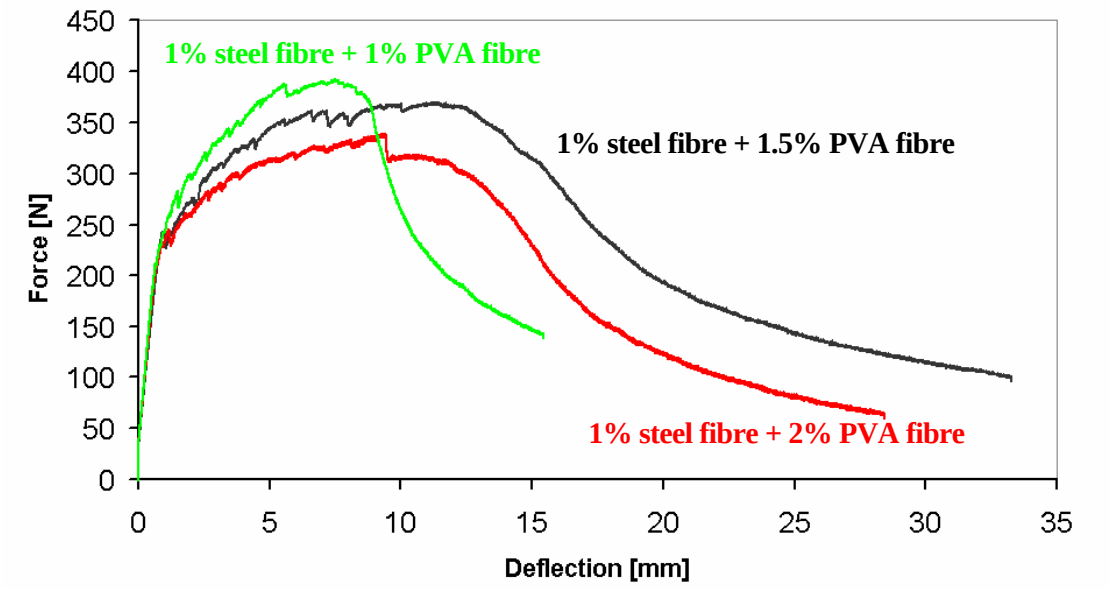

Figure 9.2 Comparison of three point bending response of hybrid ECC at various fibre type ratios

9.2 The ratio of bending MOR and direct tensile strength with varied W/B and different curing age of FA-ECC

The investigation of the comparison between Bending MOR and direct tensile results are important, for instance to establish objective test methods. Linear elastic bending theory cannot be applied to ECC. The theoretical analysis by Hannant (1978) found that the MOR could be up to three times the direct ultimate tensile strength for common fibre composites.

Furthermore, it is worthy to discuss the ratio of bending MOR and tensile strength for different W/B and different age, because the matrix fracture toughness K_m and Young's Modulus E_m are sensitive to these influences, as introduced in Chapter 2.

Table 9.1 presents the three point bending MOR, direct tensile strength, and the ratio of them. It can be seen that a moderate W/B gives the highest ratio. Aging reduces the ratio, because of the FA-ECC tensile strain softening phenomenon at high age, discussed in Chapter 7.

Table 9.1 Bending MOR and ultimate tensile stress in typical FA-ECC

	MOR	σ_U	MOR/σ_U	σ_M	MOR/σ_M
W/B= 0.3 (SF19)	13.71	3.09	4.44	1.91	7.18
W/B= 0.4 (SF20)	11.11	2.37	4.70	1.49	7.46
W/B= 0.46 (SF21)	9.94	2.96	3.36	1.52	6.54
W/B=0.4(SF 17A at 128days)	8.03	2.98	2.69	1.82	4.42

As presented in Chapter 2, the three point bending MOR can be predicted to be up to 3 times the direct tensile stress. The theoretical prediction was based on the assumption of using a rectangular tensile stress block. In the present research, ECC shows a strong strain hardening behaviour in tension. Therefore, the theoretical prediction of the MOR should be adapted. A modified stress distribution is shown schematically in Figure 9.3. The tensile stress block of FA-ECC at the age of 21 days can be simplified as a trapezium shown in Figure 9.3 (a). Thereby, a high ratio of MOR and tensile strength can be predicted, following similar steps as presented in Chapter 2. The tensile stress block of FA-ECC at high age is shown schematically in Figure 9.3 (b). The strain softening tensile behaviour is the major difference with the figure in (a) for low age response. The shorter leverage arm of the stress distribution in (b) indicates a lower bending moment, associated with a lower MOR.

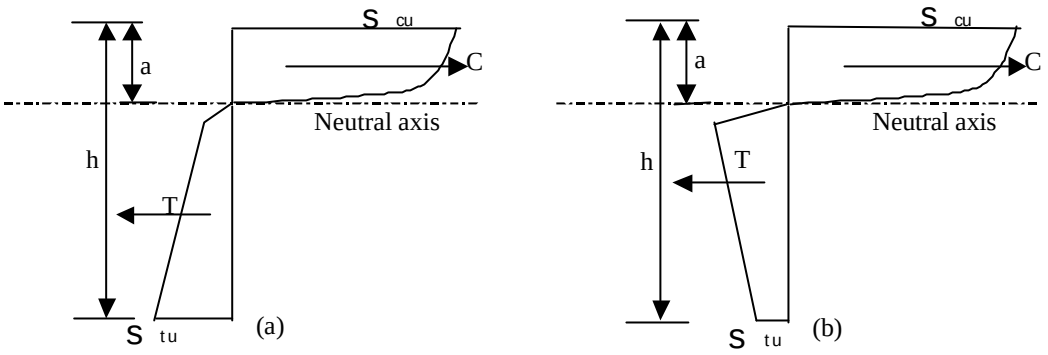

Figure 9.3 Schematic of rectangular stress block analyses to calculate the ratio of bending MOR and direct tensile stress of ECC materials FA-ECC (a) at 21 days and (b) at high age

9.3 Extrusion and casting process influence on ECC properties

It is known that extrusion and casting are very important processes employed for ECC or HPFRCC application. This justifies a study to compare the properties of products of extrusion and casting. In this research, three point bending results are compared. Dogbone specimens could not be prepared by extrusion for testing and comparison of direct tensile behaviour. The extrusion machine was made in a parallel research project (de Koker & van Zijl, 2004). Figure 9.4 shows the comparison of bending behaviour of extrusion and cast specimens, which are mix SF15 and the mix SF20. Note that the extrusion process needs much less water than the cast process so that water is not squeezed out from the fresh materials during extrusion. Hence, the fresh state workability for extruded materials was extremely poor. However, for comparison, the cast specimen was made with the same low water binder ratio (W/B=0.25), and the same poor workability. It is apparent that low workability presents a lower bending resistance and deflection for the cast specimen than for the extruded specimen. However, the essential role of workability to insure good fibre dispersion in ECC was discussed in detail in Chapter 8. The comparative bending behaviour of SF20, which has moderate workability, shows much high bending resistance and deflection in spite of higher W/B than SF15. The extruded specimen of SF 15 has much lower bending resistance and deflection than the specimens with good workability. This is due to the extremely poor workability for SF 15, resulting in a poor fibre distribution, despite the high pressure in the extrusion chamber, which improves fibre distribution and alignment for mixes containing stiff fibres, such as steel fibres (de Koker & van Zijl, 2004). This influence of the extrusion process explains the improved bending resistance of SF15.

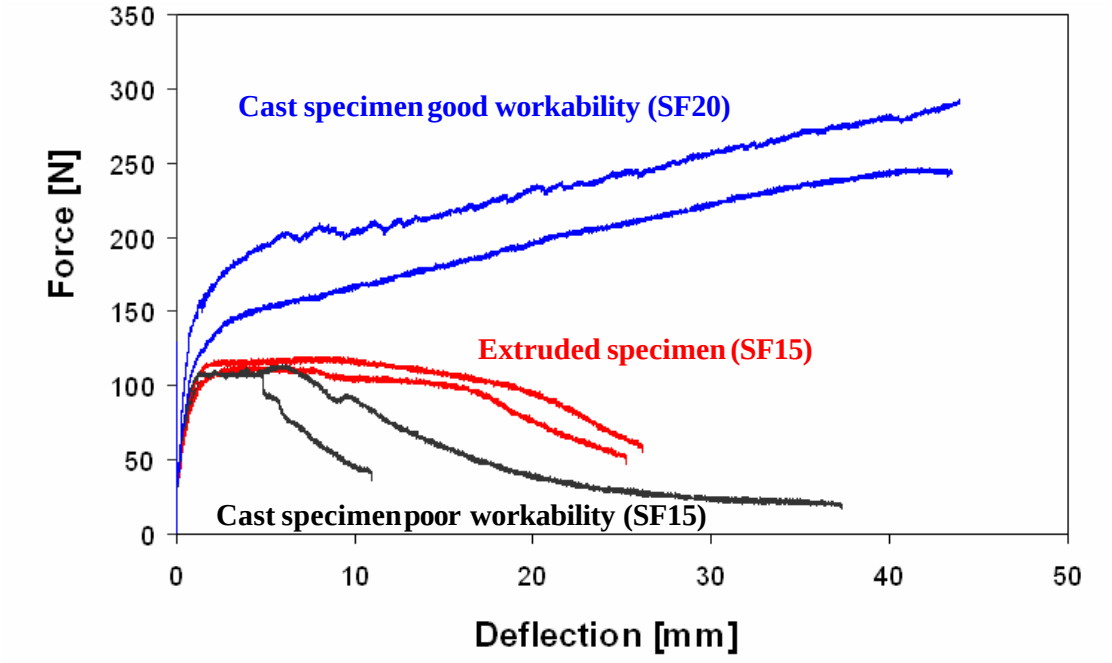

Figure 9.4 Three point bending comparison of different processes

Figure 9.5 shows the different crack patterns of a cast beam and an extruded beam. Instead of multiple cracks seen in the cast beam (with good fresh state workability), a shear-like diagonal major crack can be observed in the extruded beam. It is probably due to the combined effect of firstly tension at the outer face, and shear stress arising away from the surface.

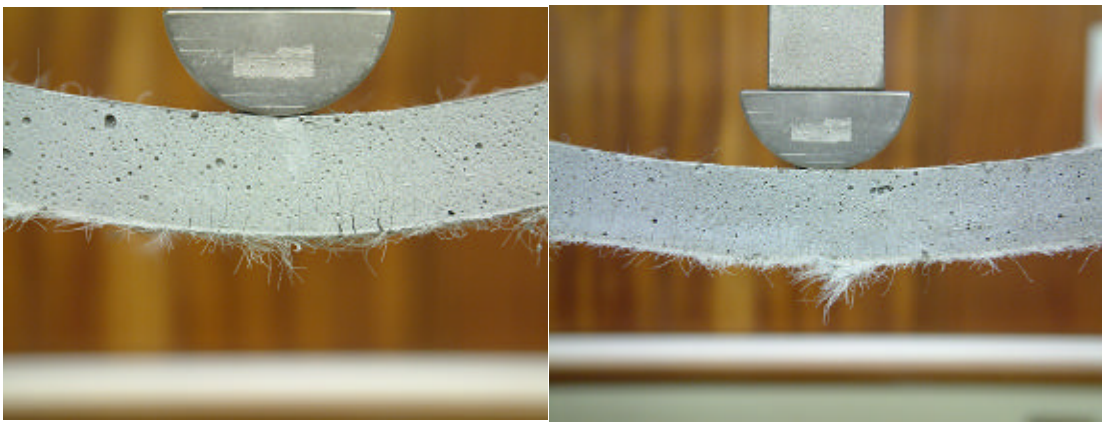

(a)

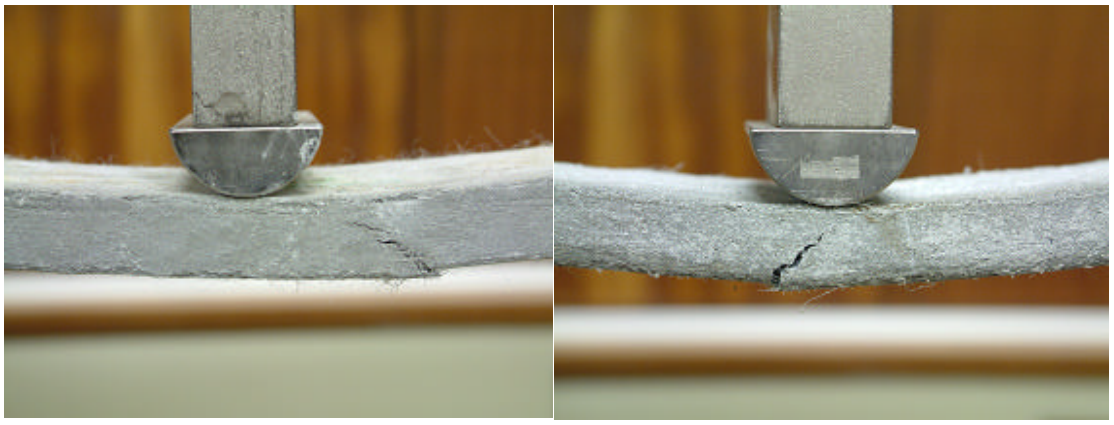

(b)

Figure 9.5 The different crack pattern details in three point bending specimens: (a) multiple cracking in a cast beam and (b) shear cracking pattern of an extruded beam

After some modifications of the matrix, an improved mix (SF18) was tested and an enhanced result was obtained, as shown in Figure 9.6. SF18 has the mix design of 30% FA, 30% GGCS, 40% Cement, and 2.5%PVA fibre with the W/B of 0.25. The bending responses show a similar trend as SF 15 shown in Figure 9.4, but a much stronger bending resistance, due to the 30% GGCS enhance the matrix strength as well as the better workability. There is insignificant difference in strength between extrusion and cast specimens, but the deformability of extruded specimen is larger than that of cast specimen.

From Equation (2.6), the ultimate tensile strength σ_U is directly proportional to the interfacial bond and the snubbing factor. For FA-ECC, the smooth, spherical shape of the FA particles reduce interfacial bond significantly and convert fibre failure type from the cohesion failure in normal PVA fibre ECC, to adhesive (bond-slip) failure. This reduces the fibre orientation affect on composite strength. Extrusion process directs the fibres from a random orientation, to a single orientation. That means snubbing may plays a role in cast specimens, but not in piston-extruded specimens, where the fibre angles lie approximately perpendicular to the cracks. Nevertheless, no significant difference in the MOR between cast specimen and piston-extruded specimen is found in the experiments. Therefore, snubbing does not appear to

influence PVA FA -ECC behaviours.

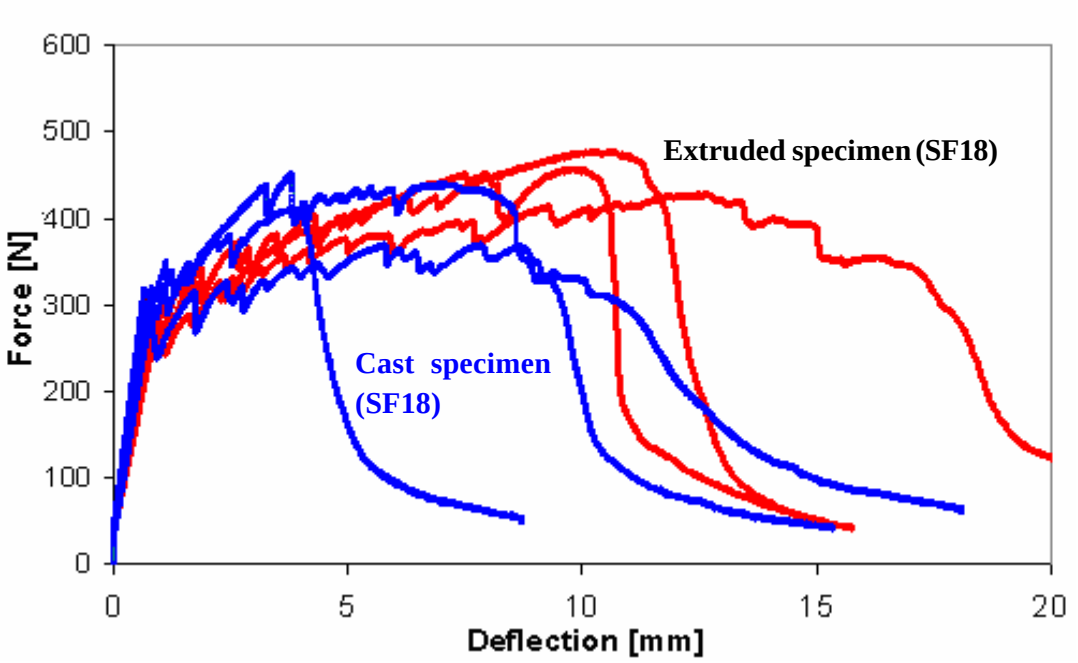

Figure 9.6 Three point bending comparison of different process

9.4 The relation between ECC compressive and tensile test or three point bending test result

From Chapter 2, it is known that the matrix properties influence the ECC tensile behaviour. The relation between compressive and tensile strength is investigated in this section.

Figures 9.7 and 9.8 show the relation between average compression strength and average ultimate tensile stress of steel fibre-ECC and PVA fibre-ECC respectively. The values of compression strengths for each mixe are shown in Appendix 3.

It can be observed from Figures 9.7 and 9.8 that, for steel fibre ECC, there is not a clear trend of ultimate tensile strength with the compressive strength. However, a trend of increased tensile strength with increased compressive strength is seen for PVA fibre ECC. This may be ascribed to the cohesive type failure of PVA fibre ECC, where a strong interfacial bond exists between PVA fibre and the matrix. This has the effect that a stronger matrix, indicated by a higher compressive strength, result in the cohesive failure at a higher stress level, leading to a higher tensile strength.

On the other hand, a steel fibre-matrix system is a kind of adhesive interaction (Chan & Li, 1997). The interface bond does not vary much with matrix strength increase, so an increase in tensile strength is not associated with a higher compressive strength.

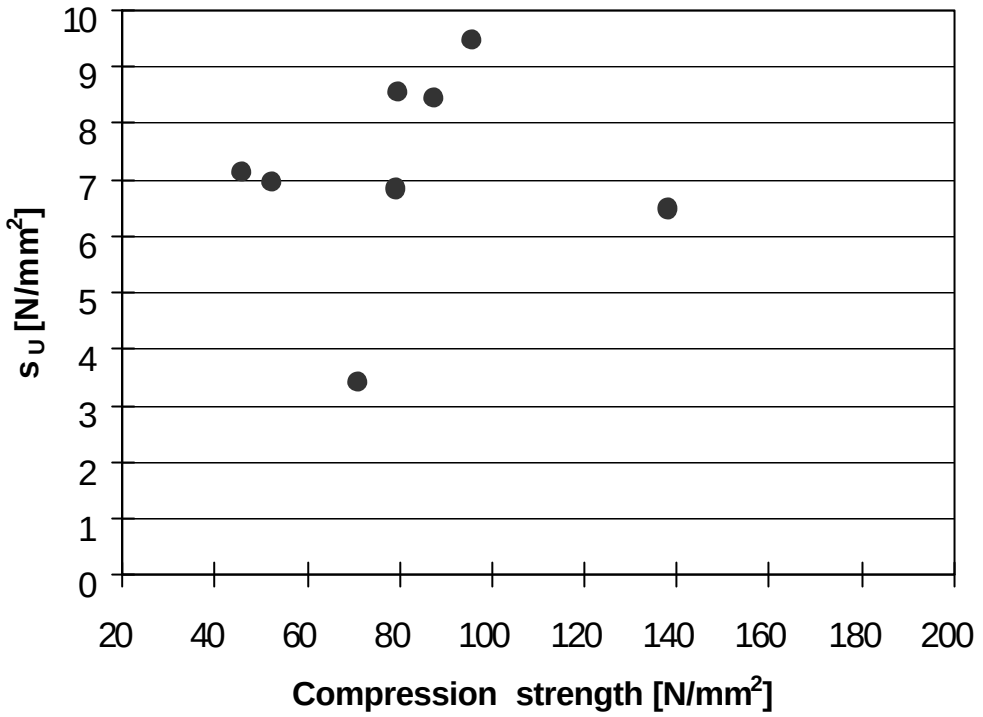

Figure 9.7 Average ultimate direct tensile strength and compressive strength of steel fibre ECC

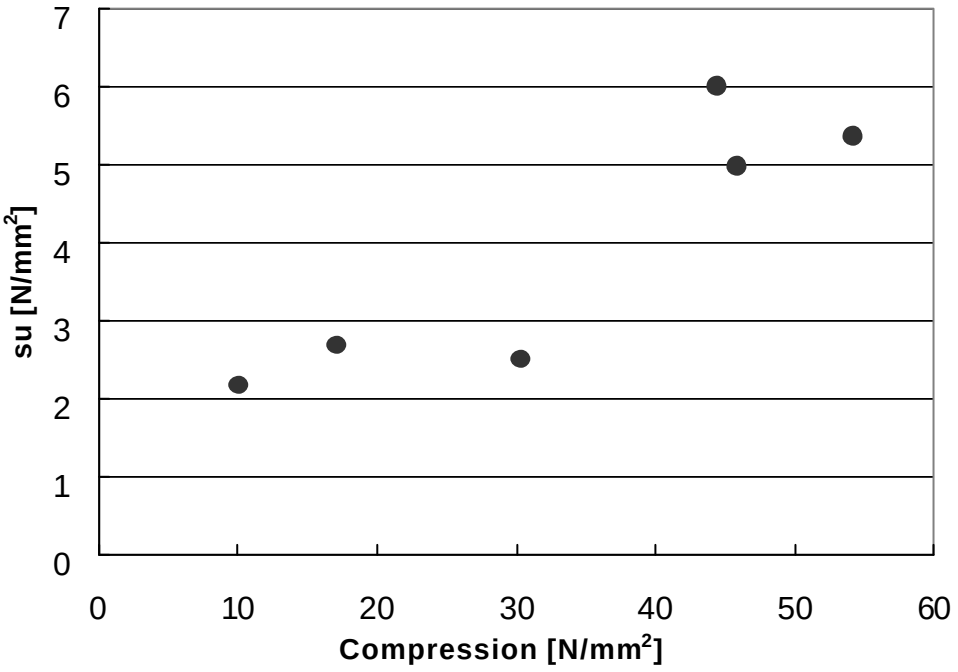

Figure 9.8 Average ultimate direct tensile strength and compressive strength of PVA fibre ECC

Chapter 10
Conclusions and remarks

In this study, various parameters playing a role in the mechanical response of ductile fibre reinforced cement-based composites have been studied. Three major aspects of the project are presented in Chapters 5 to 8. They are 1) the use of various types of cement replacement to improve the ECC performance as well as to save on costs; 2) the study of the influences of aging; 3) analysis of the influence of matrix W/B and fresh state rheology.

In each chapter conclusions were made pertaining to the corresponding work. The purpose of this chapter is to present the major conclusions drawn from the research as a whole. Some remarks will be presented based on these conclusions.

1) In the process two classes of ECC have been successfully developed to meet particular minimum requirements. One has the properties of low strength, but high toughness/ductility, which ensures a capacity for large energy dissipation. Another class exhibits high strength, while meeting a minimum requirement of 3% deformability before failure. Criteria in common for the two classes are low costs and high workability, which will enable viable application.

In the research described above, the fibre/matrix interfacial properties of ECC composites, with as cement replacements FA or/and GGCS, were investigated, with attention to their tensile behaviour, as well as micro-scale analyses, such as SEM analysis and XRF analysis. Two types of interaction between fibre and matrix occur in ECC composites, either adhesive or cohesive types, or even both. Interaction will occur depending on fibre types and matrix constituents. There are two balances involved in the mechanism of ECC properties. These are, firstly, the balance between fibre/matrix interfacial adhesion and the transitional structure cohesion, and secondly, the balance between transmitted shear force and the matrix crack strength. If the fibre/matrix interfacial adhesion is less than the strength of the transition zone structure, debonding between fibre surface and the transition zone will occur, otherwise a transition zone structure break-down will occur with fibre pull-out. Any tailoring of fibre/matrix interfacial properties has to consider the balance between fibre/matrix interfacial adhesion and cohesion. Therefore, the correct method can be used to modify the fibre/matrix interfacial adhesion or to optimise the material in order to modify the transition zone structure. The latter balance is between the transmitted forces and matrix crack strength. If the fibre transmitted forces are too small to achieve matrix crack strength, multiple cracking can not occur; on the other hand, if the matrix is too weak compared to the fibre transmitted forces, the transmitted forces will destroy the matrix microstructure before strain hardening happens and lead to a smaller strain capacity. The two balances form the relationship between

fibre/matrix interfacial and the ECC performance. The high interfacial bond of PVA fibre determines that the cohesive type is predominant in the fibre/matrix interaction in PVA fibre ECC. However, the high volume FA content contributes towards converting such cohesion to adhesive type interaction.

In contrast with the trend of increased toughness of PVA fibre ECC composite with increased FA content, the steel fibre ECC has a decreased trend with FA content. This is due to the adhesive type fibre failure in steel fibre ECC. To overcome such reduction in toughness, a stronger interfacial bonding matrix is desirable for steel fibre ECC. Furthermore, the reason for reducing the fibre/matrix interfacial bond is to reduce fibre breakage and thereby to improve shear transfer. If the fibre can hardly rupture, which is the case for steel fibre, the tailoring of fibre/matrix interface must focus on increasing the interfacial bond.

2) Next, the aging influence on ECC properties was investigated. The ECC composite mix with pure high volume fly ash has a beneficial effect on the properties of the composite at an early stage. However, for a high age, it has some difficulty to cause multiple cracking, due to the fact that shear transfer becomes less than the matrix crack tip toughness with aging, which leads to the reduction of strain capacity and the increase of crack width. The modified mix design with the combination of FA and GGCS successfully increased the interfacial bond and, thereby, improved the shear transfer to reach the matrix crack strength. Therefore, an improved late stage (high age) tensile behaviour can be achieved. Furthermore, whether the curing process can influence the high age properties in terms of the influence of shrinkage and degree of hydration, is worth investigation.

3) The matrix W/B and fresh state workability influences were also investigated, showing that the W/B has hardly any influence on tensile strain at early age. Further work focusing on the influence of aging on varied W/B mixes has already been started in parallel research carried out by Boshoff (2005). However, the fresh state workability significantly influences composite tensile strain capacity, due to fibre dispersion influenced by workability. Extremely poor workability will induce the reduction of both tensile stress and strain caused by extant matrix disconnection.

Four more issues regarding the comprehensive understanding of ECC performance were studied subsequently.

4) The proper combination of hybrid fibre reinforced ECC can achieve an increase in both tensile stress and strain.

5) The extrusion process has an enhancing influence on PVA ECC bending deflection comparative to the same mix made through the cast process. However, cast composites with the same mix, but higher workability, has better bending behaviour than extruded specimen. This is in contrast with the findings for steel fibre PVA (De Koker, 2004), which indicated a significantly improved flexural response induced by extrusion, even compared with cast specimens with good workability. This may be due to the higher rigidity of the steel fibres, which are thicker and of higher Elasticity than the PVA fibre, whereby the high extrusion pressure can successfully align steel fibres. Also, the densification of the matrix by extrusion

improves adhesive fibre bond, which was argued above to improve steel fibre ECC. Further research is required to enable PVA ECC to benefit from extrusion densification and fibre alignment, for instance by using shorter fibre, but mainly by improving the matrix rheology.

6) In many major applications, ECC materials are expected to be subjected to stress gradients, such as, flexural action. However, flexural testing is not suitable for determining the material characterization of ECC. The investigation of the relation between bending MOR and tensile stress attempt to create a prediction for material flexural resistance based on the tensile stress value.

7) The relationship between compressive strength and tensile strength were investigated to exploit the composite strength influence on ECC tensile behaviours. It is clearly relation between composite strength and tensile stress in PVA fibre-ECC but not in steel fibre-ECC, possibly due to the different interfacial properties.

It has to be mentioned herein that ECC is kind of new material and has unique properties, different from of normal concrete materials. Restricted by the insufficient understanding of this new material, the evaluation rule and criteria are still in making, and the society does not yet have an identical test standard method and the quantity evaluated criteria.

The presented work is attempted to study the properties of and influences on this material. Due to the short experimental period some studies are only at the beginning. Also, the variability of the results was high. This in addition to the small number of tests per set (3-4), cause the trends obtained in the study to be statistically flawed. However, it successfully provides the indication of trends. The micro scale analyses of the microstructure and its properties assist to discover the properties of this new material. The work in this thesis has been expanded. More experiments and results will be reported in future work to confirm this study.

References

Alexander, MG and Magee, BJ. (1999). Durability performance of concrete containing condensed silica fume. Cement and Concrete Research, 29,.pp.917-922.

Alexander, MG.,. Jaufeerally, H. and Mackechnie, JR. (2003). Structural and durability properties of concrete made by Corex slag. Research monograph No. 6, Departments of Civil engineering University of Cape Town, South Africa.

Bosch, G.L. (1990). The mineralogy and chemistry of pulverised fuel ash produced by three South African coal-burning power stations, MSc Thesis, University of Cape Town, South Africa.

Boshoff, W.P. (2005). Private discussions. University of Stellenbosch, South Africa

Chan, Y.W. and Li, V.C. (1997). Age effect on the characteristics of fibre/cement interfacial bond, J. Materials Science, Vol. 32, No. 19, pp. 5287-5292.

Chan, Y.W. and Li, V.C. (1997). Effects of transition zone densification on fibre/cement paste bond strength improvement, Advanced cement based materials 1997; 5, pp.8-17.

De Koker, D. and Van Zijl, GPAG.. (2004). Manufacturing Processes for Engineered Cement-based Composite Material (ECC), Department of Civil Engineering, University of Stellenbosch, South Africa, Corresponding paper in proceedings of BEFIB, pp. 1301-1310.

Gao, S. and Van Zijl, GPAG.. (2004). Tailoring ECC for commercial application, Department of Civil Engineering, University of Stellenbosch, South Africa, Corresponding paper in proceedings of BEFIB, pp 1391-1400.

Hannant, D.J. (1978). Fibre cement and fibre concrete, John Wiley & Sons, New York.

Illston. J.M. and Domone. P.L.J. (1994). Construction materials: Their nature and behaviours. E & SN Spon, an imprint of Chapman & Hall, 2-6 Boundary Row, London SE1 8 HN, UK.

Kamada, T. and Li, V.C. (2000). The Effects of Surface Preparation on the Fracture Behavior of ECC/Concrete Repair System, J. of Cement and Concrete Composites, Vol. 22, No. 6, pp.423-431.

JCI-DFRCC Committee. (2003). DFRCC Terminology and Application Concepts, Journal of Advanced Concrete Technology Vol. 1, No. 3, pp.335-340, November 2003 / Copyright © 2003 Japan Concrete Institute.

Kanda, T. and Li, V.C. (1998). Multiple Cracking Sequence and Saturation in Fiber Reinforced Cementitious Composites, Concrete Research and Technology, JCI, Vol. 9, No. 2, pp. 19-33.

Kawamata, A., Mihashi. H. and Fukuyama, H. (2003). Properties of Hybrid Fiber Reinforced Cement - based Composites, Journal of Advanced Concrete Technology Vol. 1, No. 3,

pp.283-290.

Kopescsk,Ó. K. (2004). Durability of Glass Fibres, Corresponding paper in proceedings of BEFIB, pp.583-592,

Kunieda, M., Kamada, T. and Rokugo, K. (2002). Size Effects on Flexural Failure Behavior of ECC Members," Proceedings of the JCI International Workshop on Ductile Fiber Reinforced Cementitious Composites (DFRCC) - Application and Evaluation (DRFCC-2002), Takayama, Japan, Oct. 2002, pp. 229-238.

Li, V.C. (1992). Performance driven design of fiber reinforced cementitious composites, in Proceedings of 4th RILEM International Symposium on Fiber Reinforced Concrete, Ed. R. N. Swamy, pp. 12 - 30, Chapman and Hall.

Li, V.C. (1998). Engineered cementitious composite (ECC)-tailored composites through micromechanical modelling, in Fiber Reinforced Concrete: Present and the Future edited by N. Banthia, A. Bentur, A. and A. Mufti, Canadian Society for Civil Engineering, Montreal, pp. 64-97.

Li, V.C. (2002). Advances in ECC research, ACI Special Publication on Concrete: Material Science to Applications, SP 206-23, pp. 373-400.

Li, V.C. (2002a). Reflections on the research and development of Engineered Cementitious Composites (ECC), Proceedings of the International Workshop on Ductile Fibre Reinforced Cementitious Composites (DFRCC), Japan Concrete Institute, Takayama, Japan, pp. 1-24.

Li, V.C. (2003). On Engineered Cementitious Composites (ECC) A Review of the Material and Its Applications, Journal of Advanced Concrete Technology Vol. 1, No. 3, pp.215-230.

Li, V.C. and Maalej, M. (1996). Toughening in cement based composites, Part II: Fiber Reinforced Cementitious Composites, J. of Cement and Concrete Composites. Vol. 18, No. 4, pp. 239 – 249.

Li, V.C., and Wang, S. (2003). On High Performance Fiber Reinforced Cementitious Composites, Proc. of the JCI Symposium on Ductile Fiber Reinforced Cementitious Composites (DFRCC), Tokyo, Japan, pp. 13-23.

Li, V.C. and Stang, H. (2004). Elevating FRC material ductility to infrastructure durability, Corresponding paper in proceedings of BEFIB, pp.171-186.

Li, V.C., Mishra, D.K. and Wu, C. (1995). Matrix Design for Pseudo Strain-Hardening Fiber Reinforced Cementitious Composites, RILEM J. Materials and Structures, Vol. 28, No. 183, pp. 586-595.

Li, V.C., Lepech, M., Wang, S., Weimann, M. and Keoleian. G. (2004). Development of Green ECC for Sustainable Infrastructure Systems. Proc., Int'l Workshop on Sustainable Development and Concrete Technology, Beijing, China, Ed. K. Wang, Published by Iowa State Univ., pp181-192.

Li, V.C., Wang. S. and Wu, C. (2001). Tensile strain hardening behaviour of Polyvinyl Alcohol Engineered Cementitious Composites (PVA-ECC), ACI Materials J., 98(6), pp. 483-492.

Li, V.C., Wu, C., Wang, S., Ogawa, A. and Saito, T. (2002). Interface Tailoring for Strain-hardening PVA-ECC," ACIACI Materials Journal, Vol. 99, No. 5, Sept.-Oct., 2002, pp. 463-472.

Loedolff. GF. and Van Zijl. GPAG.. (2003). Storage of cement, Submitted to The Journal of the South African Institute of Civil Engineers.

Maalej, M. and Li, V.C. (1994). Flexural/tensile-strength ratio in engineered cementitious composite, Journal of Materials in Civil Engineering, Vol. 6, No. 4, pp. 513-528.

Marshall, D.B. and Cox, B.N. (1988). A J-integral method for calculating steady-state matrix crack stress in composite, Mechanics of materials Vol. 7, pp. 127-133.

Peled, A. and Shah, P.S. (2003). Processing effect in cementitious composites: extrusion and casting, Journal of Materials in Civil Engineering. Vol. 15, No.2, pp. 192-199.

Redon, C., Li, V.C., Wu, C., Hoshiro, H., saito, T. and Ogawa, A. (2001). Measuring and modifying interface properties of PVA fibers in ECC matrix, Journal of Materials in Civil Engineering, Vol. 13, No. 6, pp. 399-406.

Shah. S. P. (2004). Private discussions. University of North West, U.S.A

Shah. SP., Kuder, K.G. and Mu, B. (2004). Fibre-reinforced cement-based composite: A forty year odyssey, corresponding paper in proceedings of BEFIB, pp3-30.

Soroushian., Parviz. and Lee, Cha-Don. (1990). Distribution and orientation of fibers in steel fiber reinforced concrete, ACI Materials Journal, V.87, No, 5,Sep-Oct 1990, pp.433-434.

Spicer. E. (2004). Private discussions. University of Stellenbosch, South Africa.

Stahli. P. and van Mier, J. G.M. (2004). Rheology Properties and Fracture Processes of HFC, Corresponding paper in proceedings of BEFIB, pp.299-308,

Stang, H. and Li, V.C. (2004). Classification of fiber reinforced cementitious materials for structural applications, Proceedings of BEFIB, Varenna, Lake Como, Italy, pp197-218.

Torigoe, S,. Horikoshi, T,. Ogdashi, T. and Hamada, T. (2003). Study on evaluation method for PVA fibre distribution in engineered cementitious composite, Journal of Advanced Concrete Technology, Vol.1, No. 3, pp. 265-268.

Van Zijl, G.PAG.. (2005). The role of aggregate in high performance fibre reinforced cement-based composites, in publishing.

Wang, S. and Li, V.C. (2004). Tailoring of Pre-existing Flaws in ECC Matrix for Saturated Strain Hardening, Proceedings of FRAMCOS-5, Vail, Colorado, U S A, pp. 1005-1012.

Wu.C. http://ace-mrl.engin.umich.edu/NewFiles/publications/cyndythesis.html. (30/01/2005)

Appendix 1

Experimental result

Series I

S1

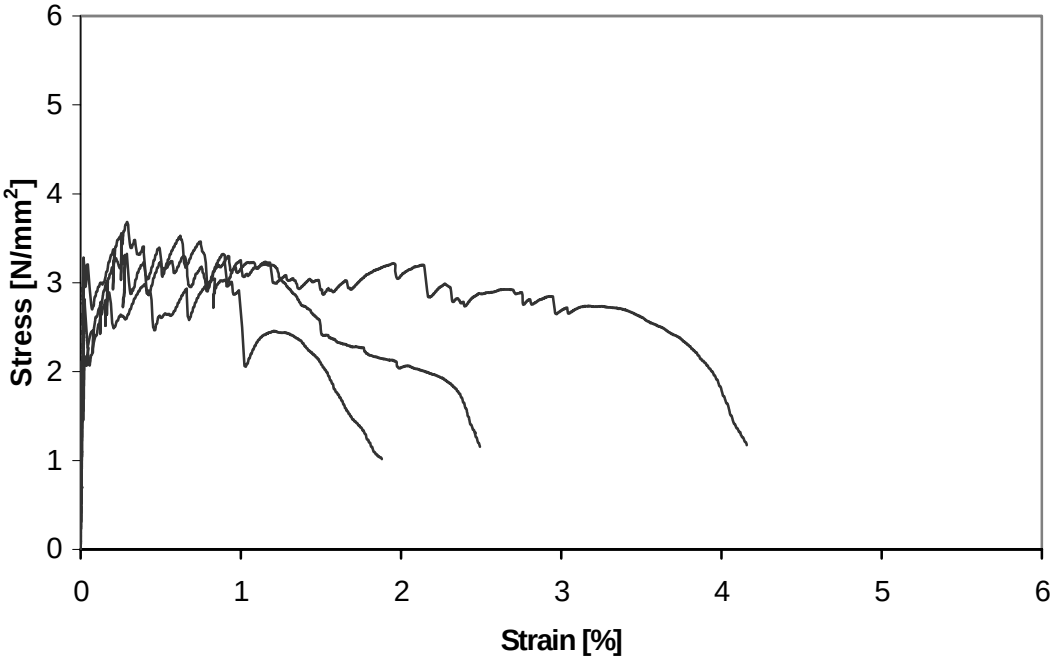

		Tensile strength					Age on test
		ε_M	σ_M	ε_U	σ_U	ε_F	
S1	1	0.018	1.48	0.29	3.32	2.42	21
	2	0.017	3.17	0.30	3.68	2.15	
	3	0.025	2.75	0.83	3.05	0.99	

S2

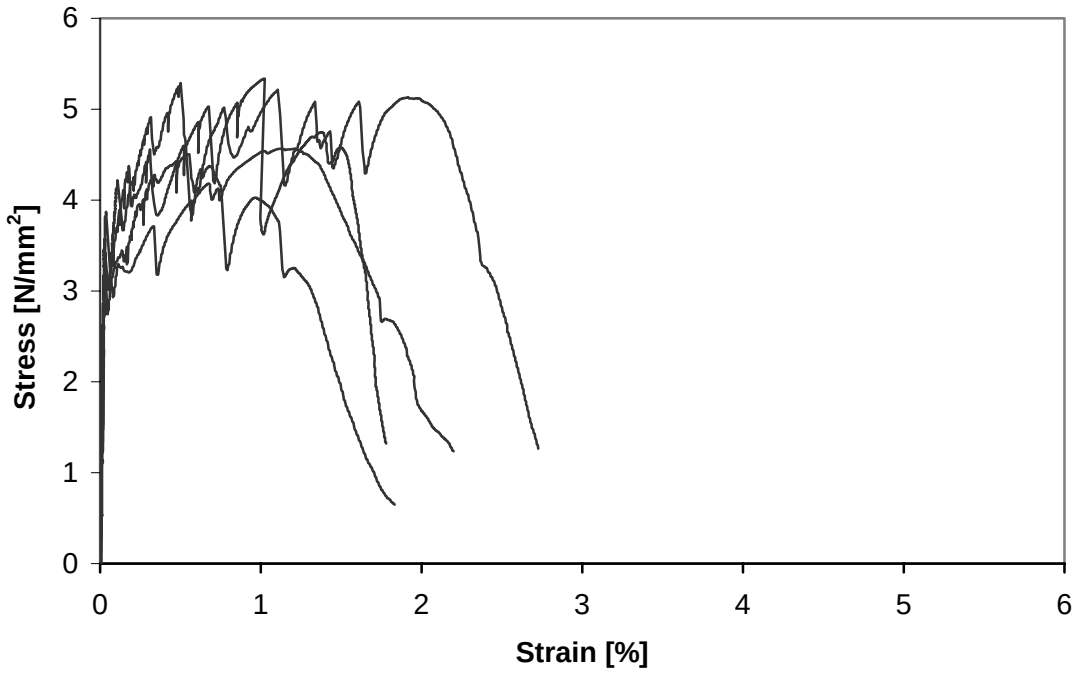

		Tensile strength					Age on test
		ε_M	σ_M	ε_U	σ_U	ε_F	
S2	1	0.023	3.39	1.02	5.34	1.63	21
	2	0.027	3.42	0.50	5.29	2.36	
	3	0.025	3.42	0.55	4.50	1.12	
	4	0.032	3.81	1.12	4.57	1.51	

S4

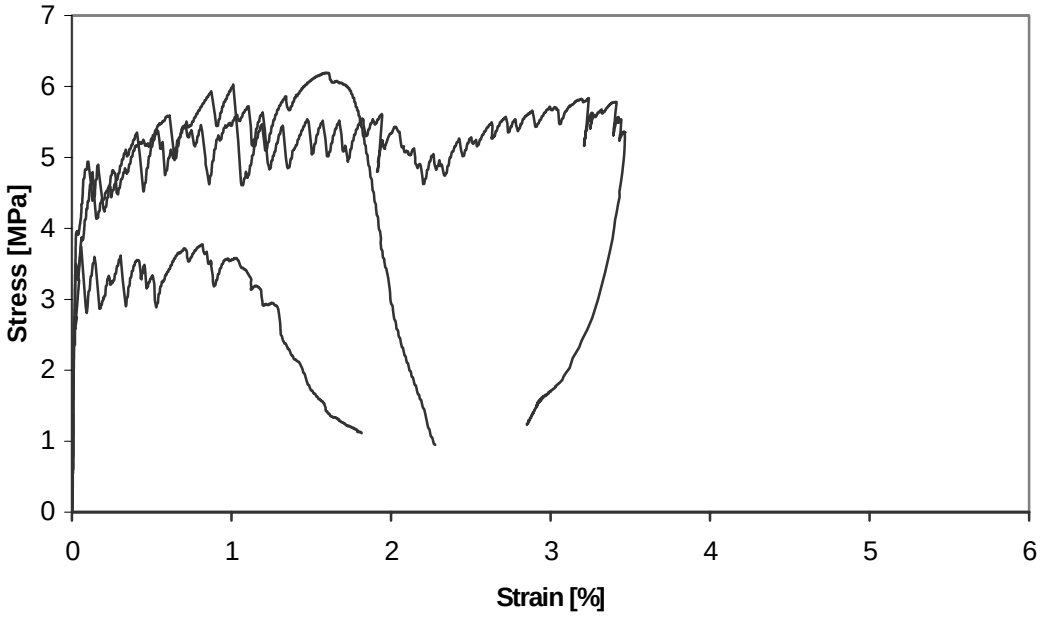

		Tensile strength					Age on test
		ε_M	σ_M	ε_U	σ_U	ε_F	
S4	1	0.019	2.68	0.82	3.77	1.30	21
	2	0.021	3.48	1.60	6.19	1.96	
	3	0.035	3.86	3.24	5.83	3.40	

S5

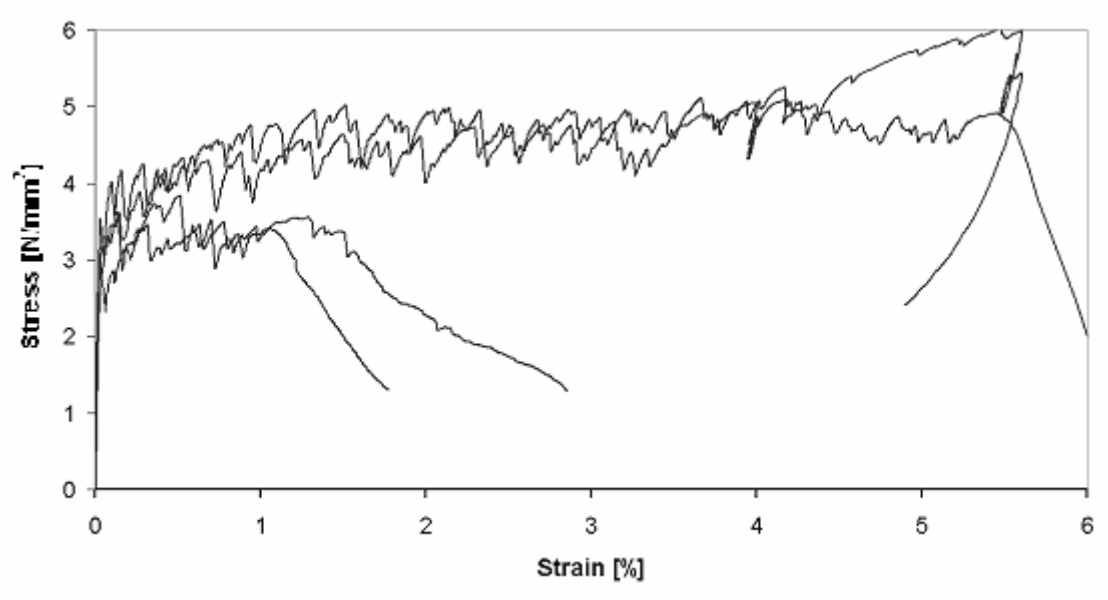

		Tensile strength					Age on test
		ε_M	σ_M	ε_U	σ_U	ε_F	
S5	1	0.032	3.55	0.13	3.63	1.29	21
	2	0.034	2.95	5.48	6.03	5.13	
	3	0.026	2.95	0.52	3.84	1.21	
	4	0.024	2.56	4.17	5.09	5.70	

S6

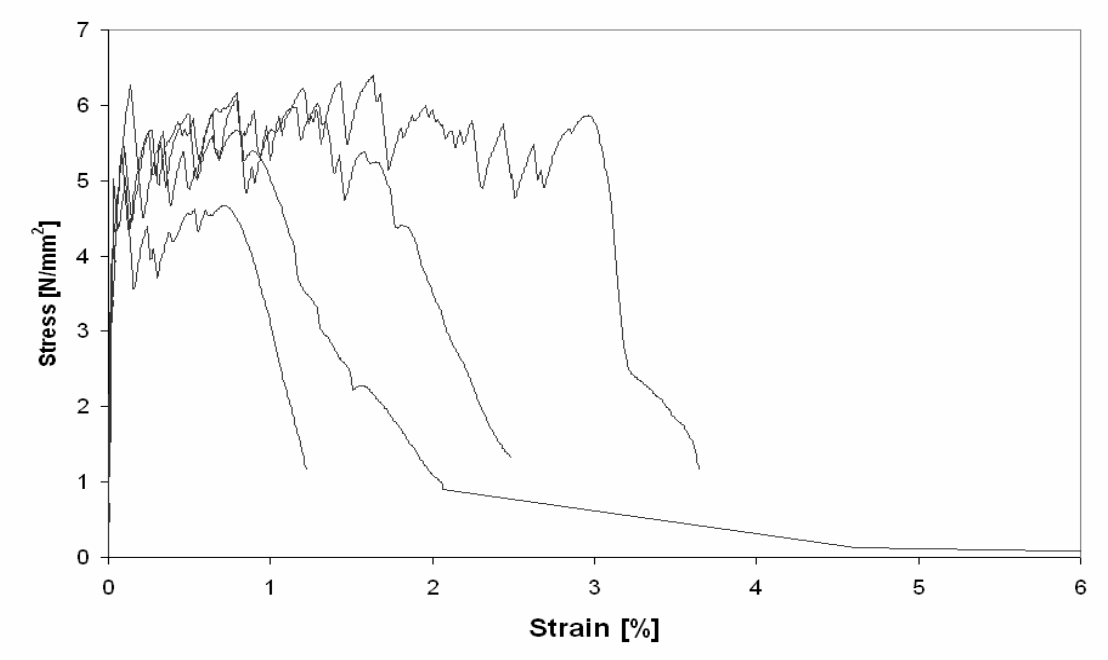

		Tensile strength					Age on test
		ε_M	σ_M	ε_U	σ_U	ε_F	
S6	1	0.017	3.23	0.13	6.26	1.29	21
	2	0.032	4.49	1.63	6.40	3.10	
	3	0.031	5.02	0.11	5.04	0.11	
	4	0.024	4.05	0.79	6.16	1.91	

S7

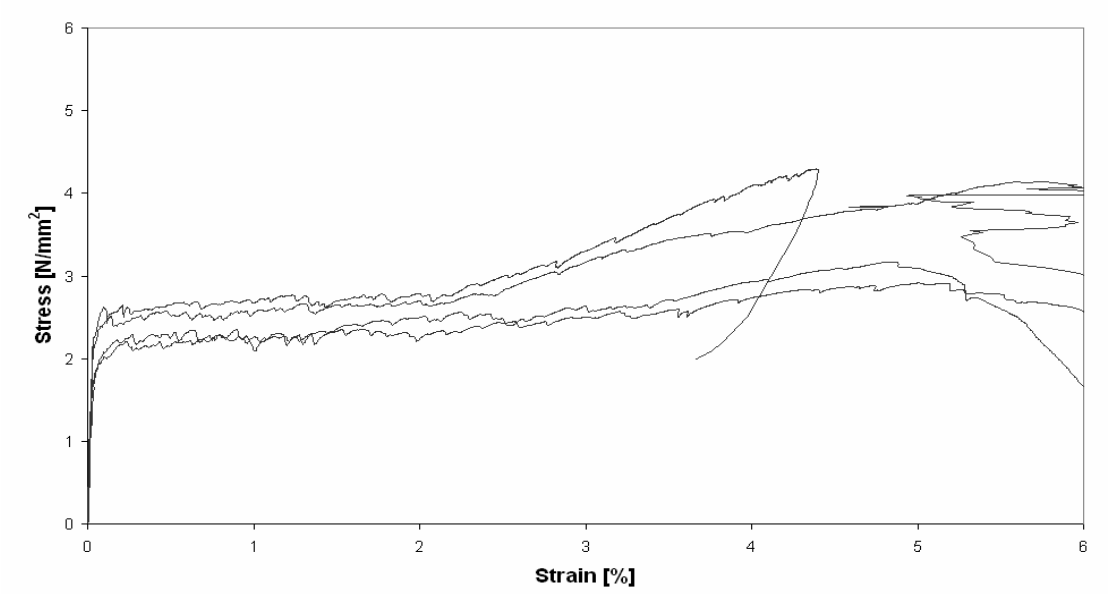

		Tensile strength					Age on test
		ε_M	σ_M	ε_U	σ_U	ε_F	
S7	1	0.037	2.24	4.39	4.29	4.39	21
	2	0.040	1.70	4.86	3.17	5.97	
	3	0.040	1.77	5.00	2.92	6.55	
	4	0.031	2.15	5.76	4.14	6.38	

S8

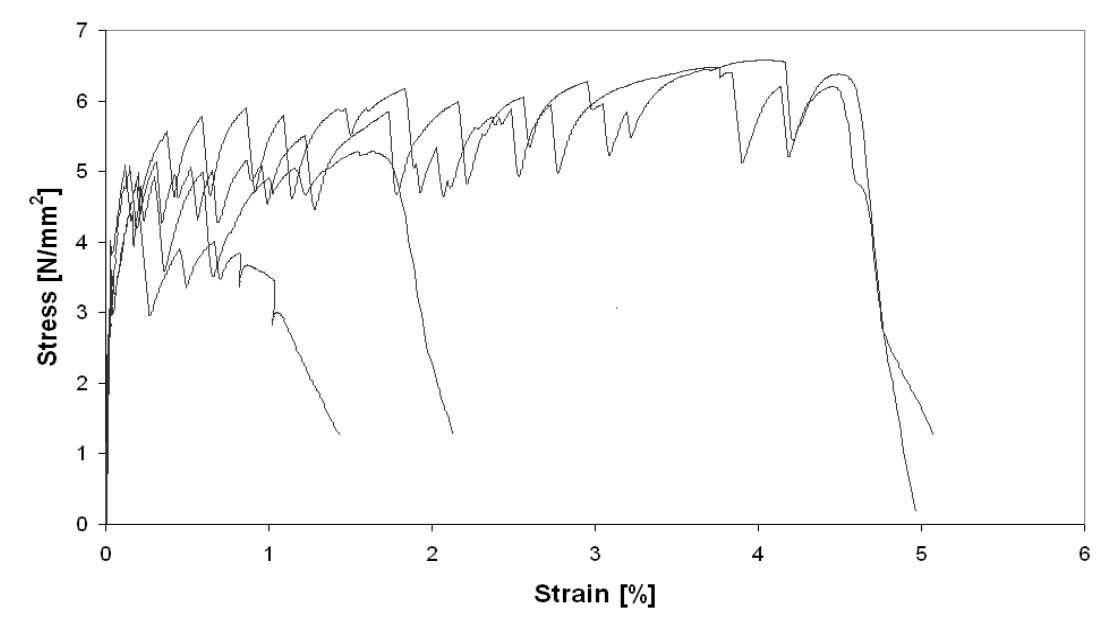

		Tensile strength					Age on test
		ε_M	σ_M	ε_U	σ_U	ε_F	
S8	1	0.013	2.62	4.02	6.58	4.77	21
	2	0.028	3.61	0.19	4.86	0.93	
	3	0.027	3.97	3.71	6.47	4.69	
	4	0.032	3.36	1.63	5.29	1.90	

S9

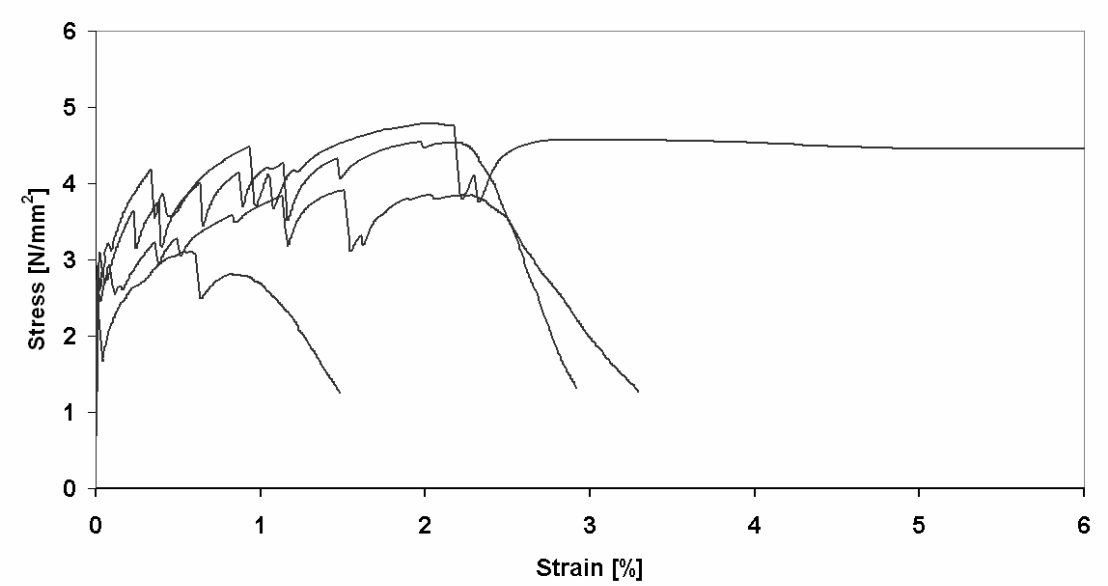

		Tensile strength					Age on test
		ε_M	σ_M	ε_U	σ_U	ε_F	
S9	1	0.013	2.37	0.55	3.10	1.14	21
	2	0.027	3.07	2.00	4.79	7.93	
	3	0.022	2.56	1.51	3.91	2.81	
	4	0.017	2.60	1.97	4.55	2.67	

S10

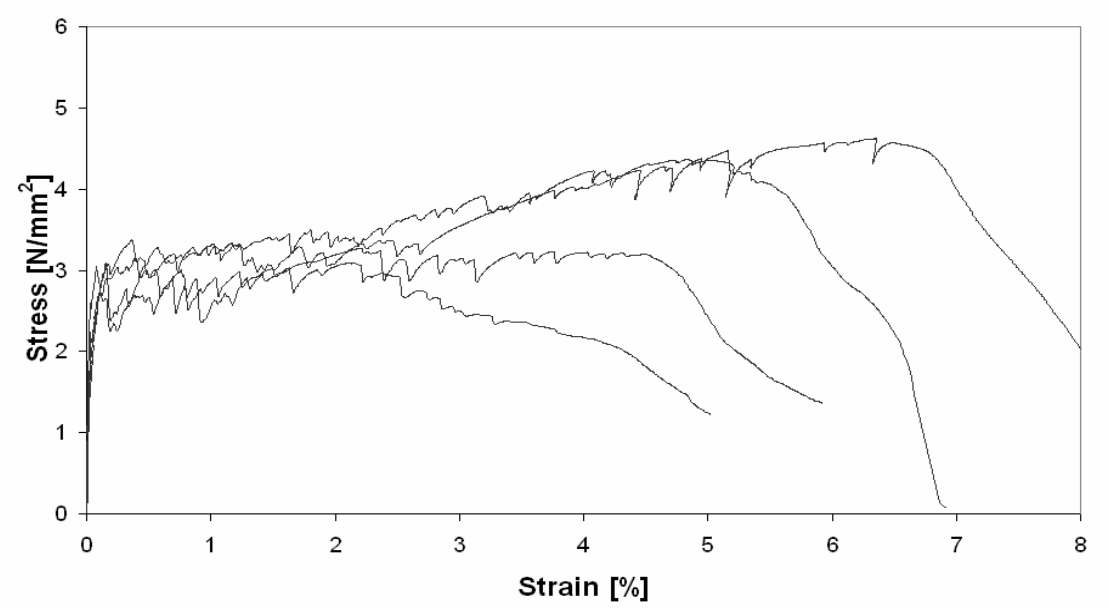

		Tensile strength					Age on test
		ε_M	σ_M	ε_U	σ_U	ε_F	
S10	1	0.056	2.10	6.34	4.62	7.97	21
	2	0.029	2.56	4.85	4.37	6.34	
	3	0.065	2.42	2.21	3.27	5.00	
	4	0.030	2.24	2.11	3.09	3.79	

S11

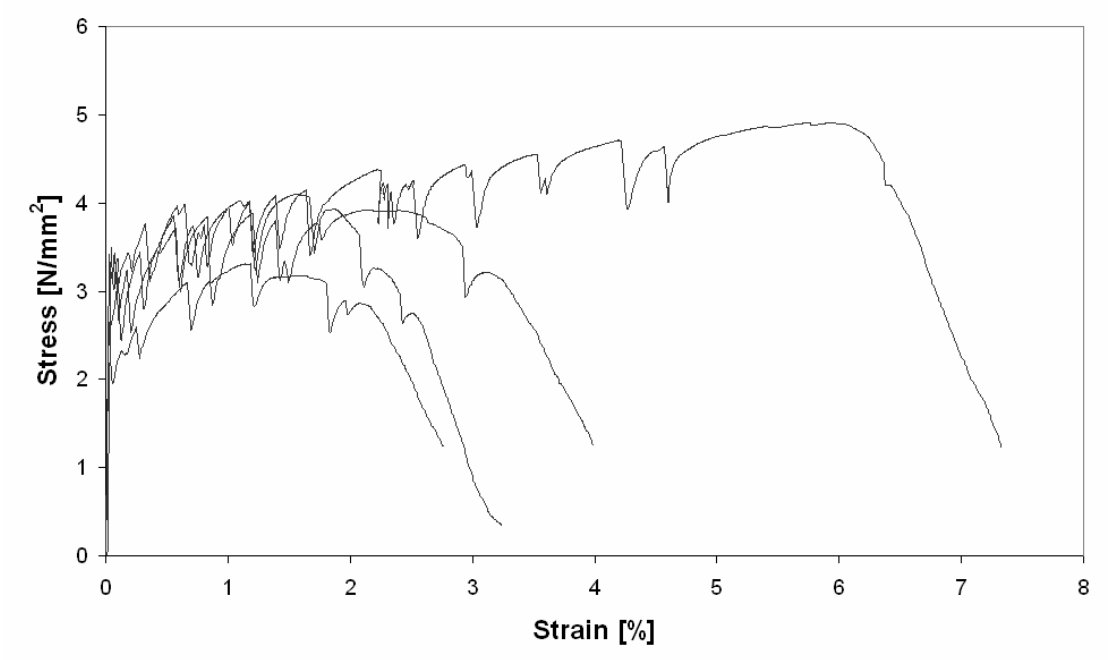

		Tensile strength					Age on test
		ε_M	σ_M	ε_U	σ_U	ε_F	
S11	1	0.029	3.34	2.17	3.92	2.92	21
	2	0.024	2.45	1.14	3.31	2.33	
	3	0.028	3.49	1.56	4.10	2.07	
	4	0.027	2.64	5.75	4.91	6.89	

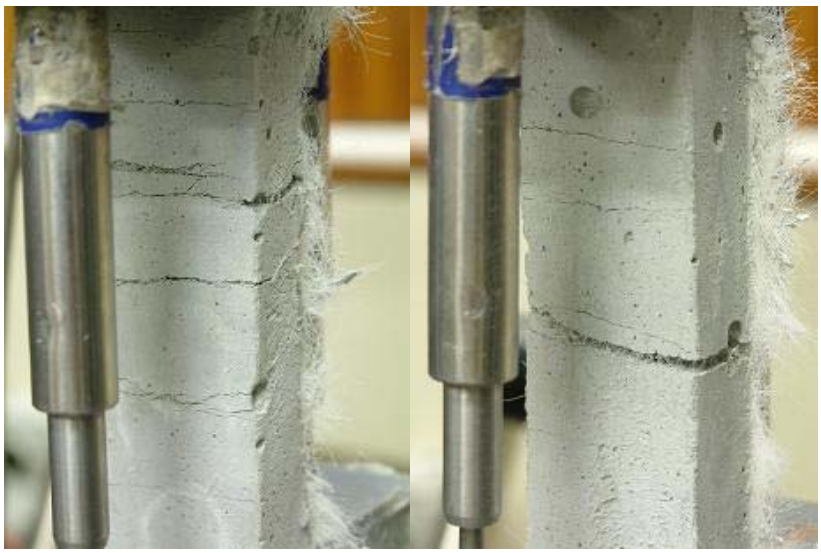

S12

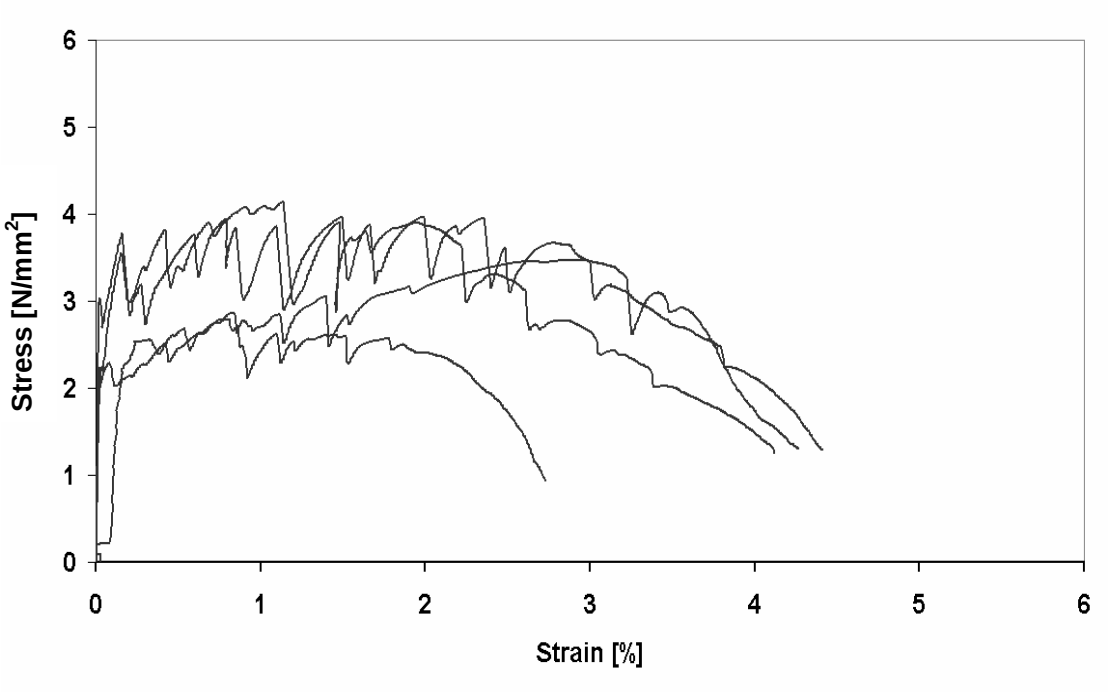

		Tensile strength					Age on test
		ε_M	σ_M	ε_U	σ_U	ε_F	
S12	1	0.110	1.15	2.86	3.47	4.27	21
	2	0.020	2.18	1.50	3.97	3.94	
	3	0.024	2.08	0.79	2.79	2.31	
	4	0.017	2.99	1.14	4.15	2.61	

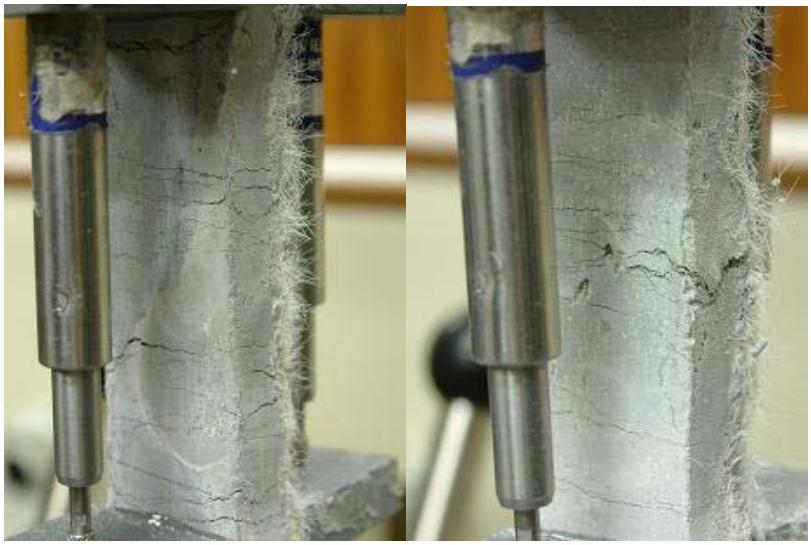

S13

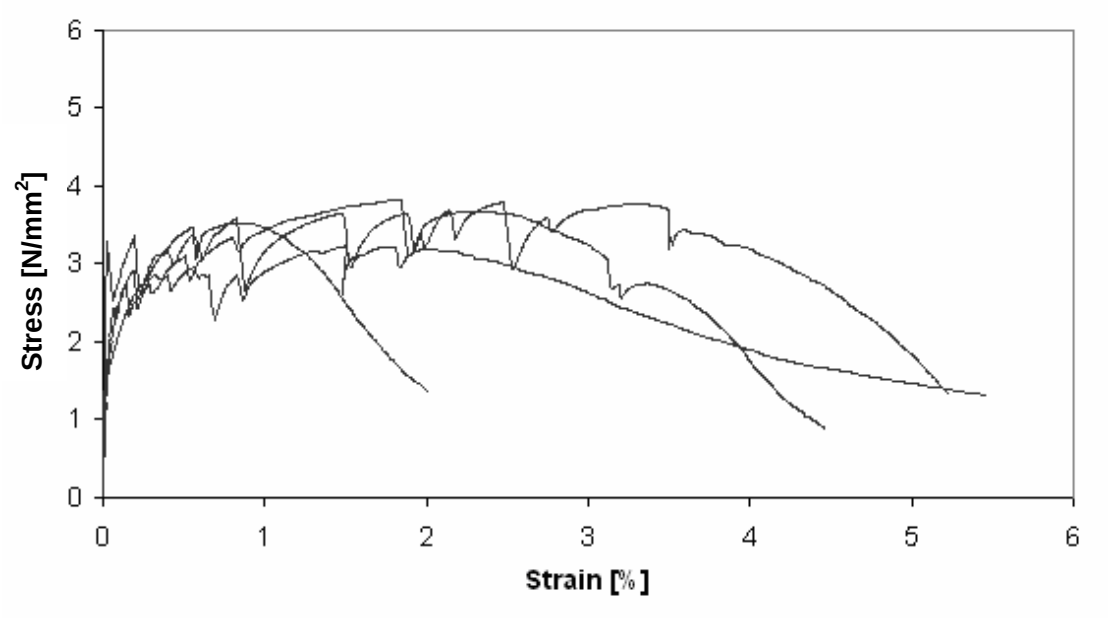

		Tensile strength					Age on test
		ε_M	σ_M	ε_U	σ_U	ε_F	
S13	1	0.018	1.69	0.85	3.53	1.83	21
	2	0.029	3.29	2.33	3.68	2.96	
	3	0.096	2.48	1.51	3.23	3.15	
	4	0.06	2.41	1.81	3.83	4.65	

S14

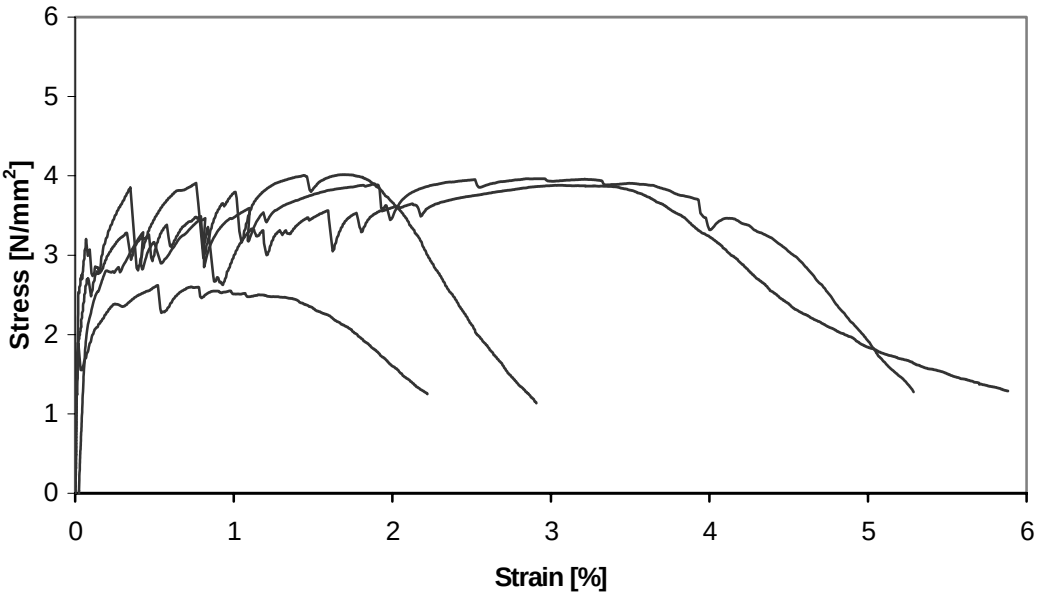

		Tensile strength					Age on test
		ε_M	σ_M	ε_U	σ_U	ε_F	
S14	1	0.033	1.52	2.94	3.96	5.17	21
	2	0.020	1.80	0.52	2.62	1.89	
	3	0.018	1.89	3.06	3.88	4.94	
	4	0.020	2.49	1.69	4.02	2.38	

Mix34

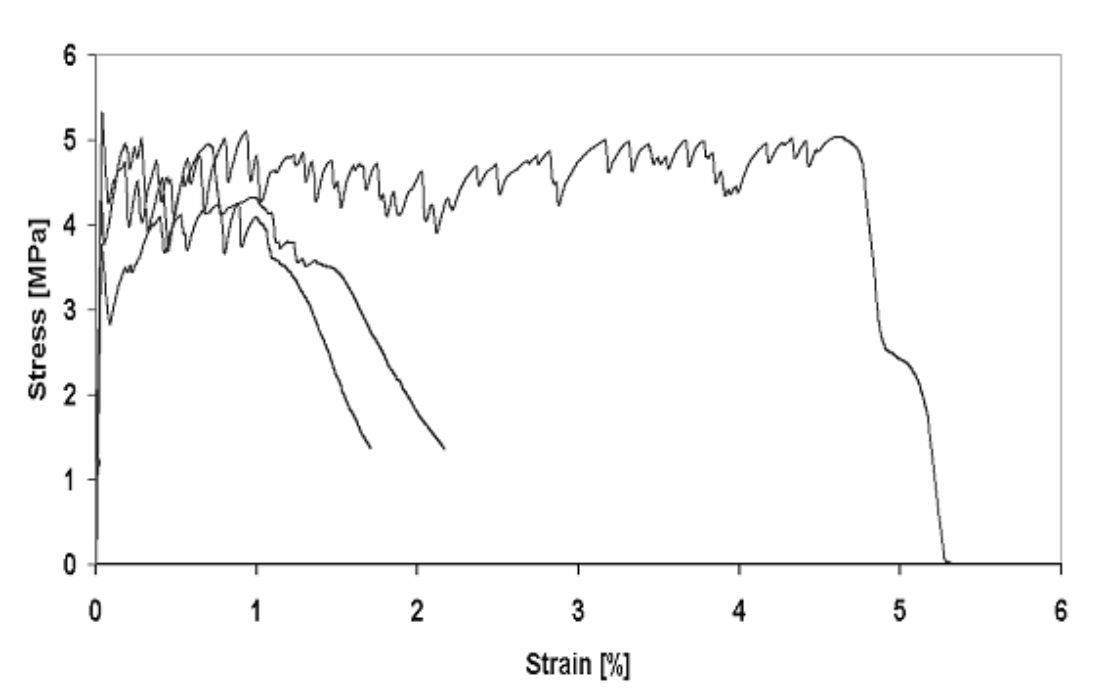

		Tensile strength					Age on test
		ε_M	σ_M	ε_U	σ_U	ε_F	
Mix34	1	0.0415	5.32	0.04	5.33	0.04	21
	2	0.039	3.76	0.99	4.31	1.24	
	3	0.036	4.26	0.94	5.10	4.79	
	4						

Appendix 2

The test details of series II mixes

SF2

		Tensile strength					Age on test
		ε_M [%]	σ_M [N/mm^2]	ε_U [%]	σ_U [N/mm^2]	ε_F [%]	
SF2	1	0.023	6.84	0.05	8.00	0.05	30
	2	0.023	7.07	0.03	7.98	0.57	
	3	0.022	6.64	0.21	7.83	0.59	
	4	0.020	6.93	0.27	9.98	0.42	
	AVG	0.022	6.87	0.14	8.45	0.41	

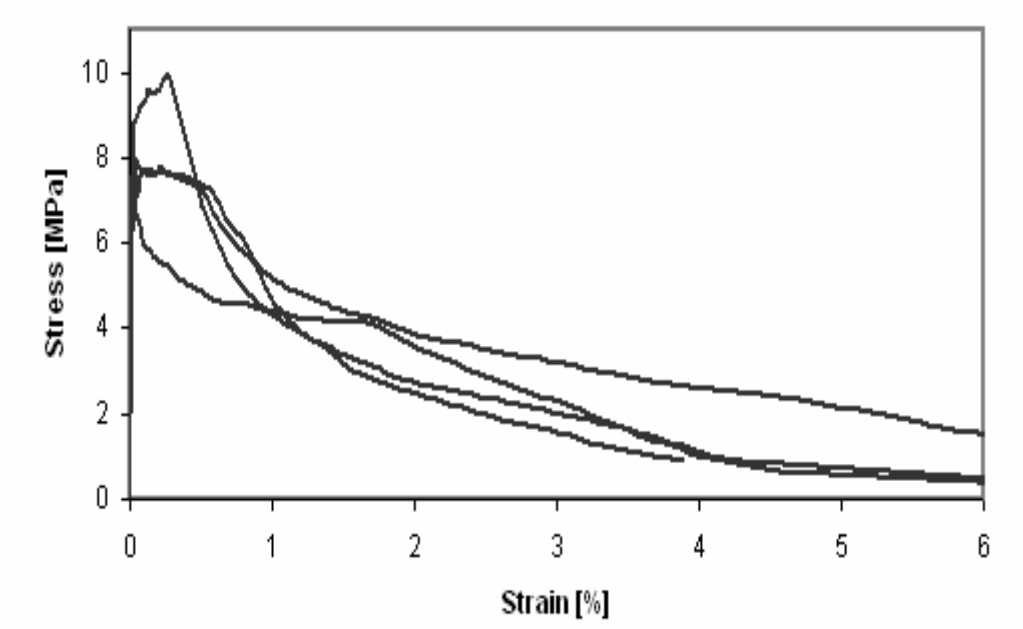

SF3

		Tensile strength					Age on test
		ε_M [%]	σ_M [N/mm^2]	ε_U [%]	σ_U [N/mm^2]	ε_F [%]	
SF3	1	0.024	5.63	0.14	7.11	0.39	21
	2	0.022	3.41	0.06	6.21	0.59	
	3	0.021	5.87	0.36	10.03	1.44	
	AVG	0.022	4.97	0.18	7.78	0.81	

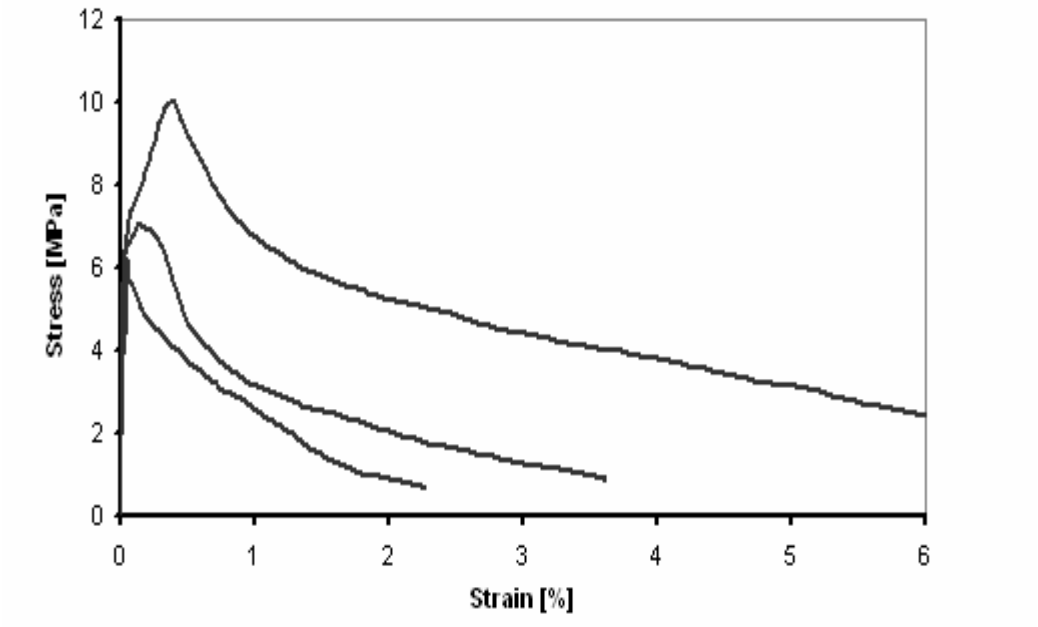

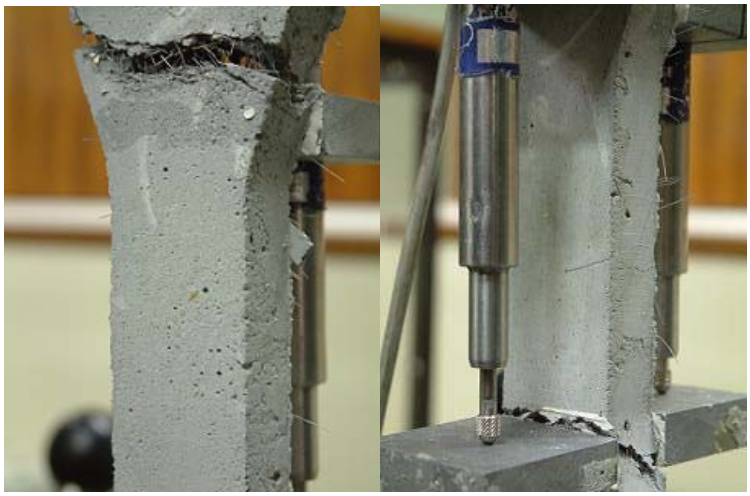

SF4

Table A2.4 direct tension test result for SF4

		Tensile strength					Age on test
		ε_M [%]	σ_M [N/mm^2]	ε_U [%]	σ_U [N/mm^2]	ε_F [%]	
SF4	1	0.025	7.33	0.14	8.71	0.41	23
	2	0.014	4.07	0.37	9.83	1.93	
	3	0.026	6.75	0.17	9.26	0.76	
	4	0.026	7.00	0.38	10.04	0.76	
	AVG	0.023	6.29	0.27	9.46	0.97	

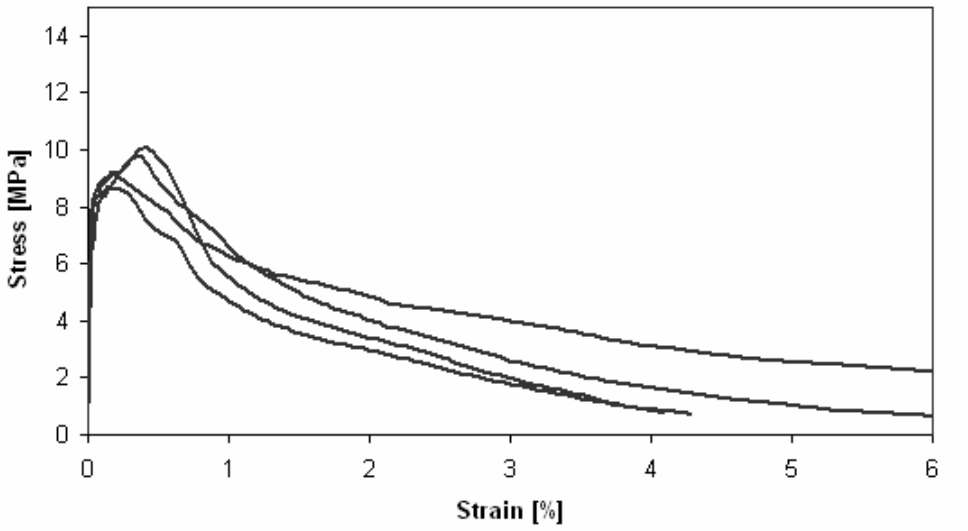

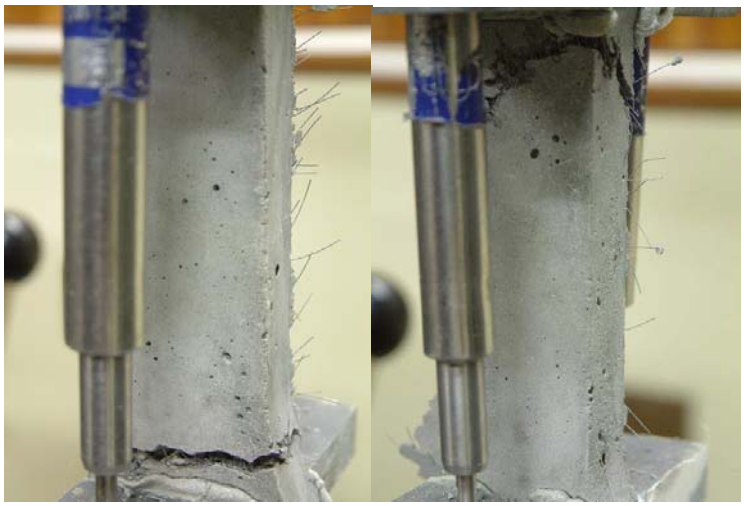

SF5

		Tensile strength					Age on test
		ε_M [%]	σ_M [N/mm^2]	ε_U [%]	σ_U [N/mm^2]	ε_F [%]	
SF5	1	0.015	6.17	0.45	6.83	0.59	25
	2	0.016	5.77	0.02	5.88	0.02	
	3	0.021	6.98	0.02	6.98	0.02	
	4	0.025	6.21	0.03	6.21	0.03	
	AVG	0.019	6.28	0.13	6.47	0.17	

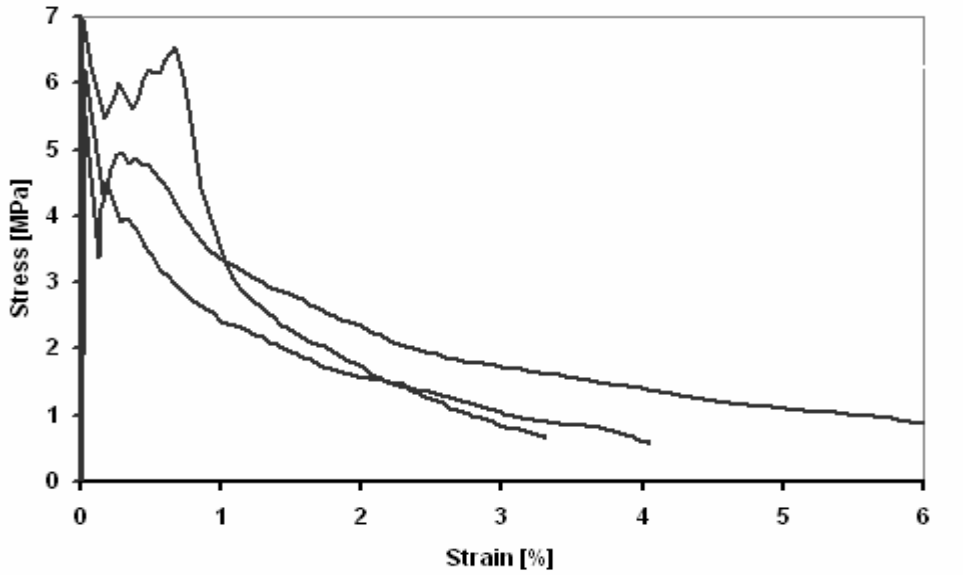

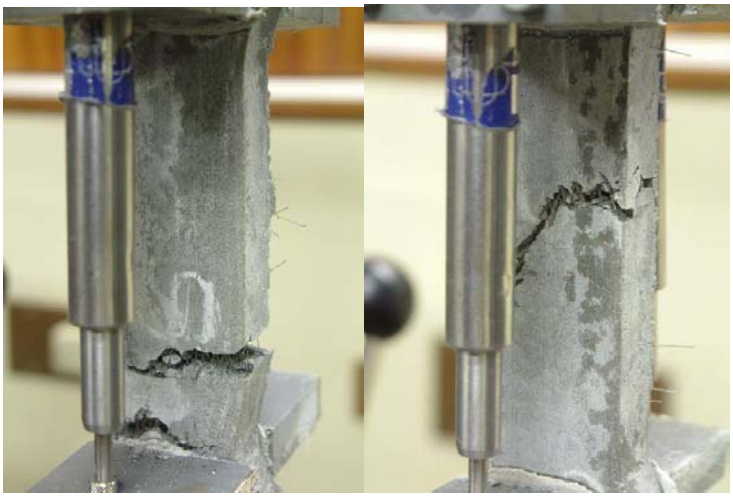

There's been a steel fibre segregation occurring in GSF5. This mix also use for investigate the workability effect to the air bubbles and the fibre displacement, also the comparison of bending and directly tension.

SF6

		Tensile strength					Age on test
		ε_M [%]	σ_M [N/mm^2]	ε_U [%]	σ_U [N/mm^2]	ε_F [%]	
SF6	1	0.018	5.10	0.28	9.36	1.23	21
	2	0.016	4.17	0.21	8.66	0.67	
	3	0.016	3.41	0.37	8.12	1.88	
	4	0.021	5.51	0.39	8.06	0.95	
	AVG	0.018	4.55	0.31	8.55	1.18	

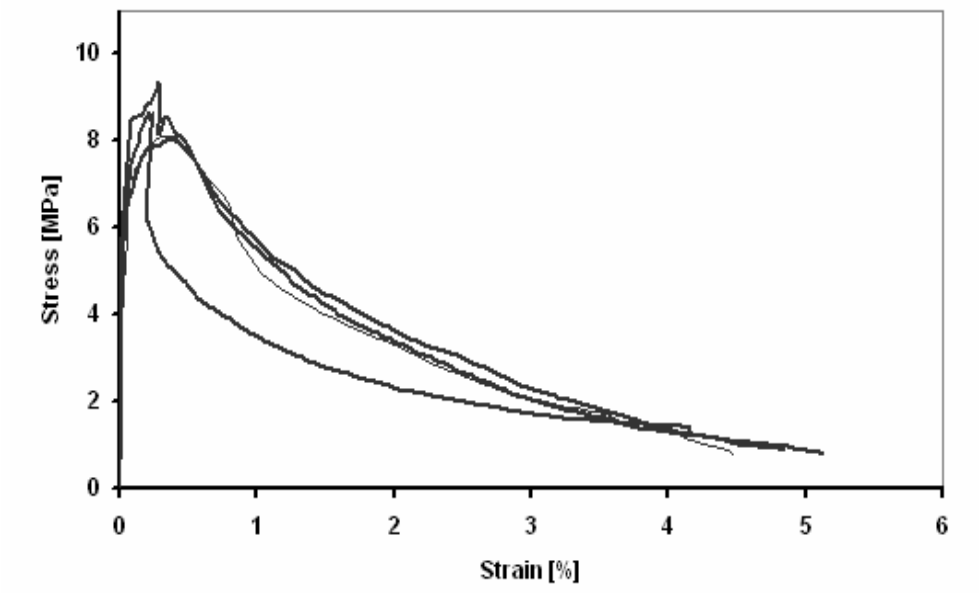

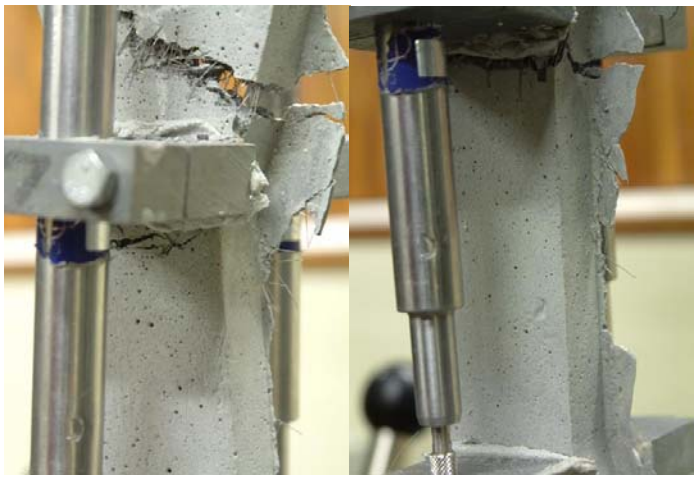

SF7

		Tensile strength					Age on test
		ε_M [%]	σ_M [N/mm^2]	ε_U [%]	σ_U [N/mm^2]	ε_F [%]	
SF7	1	0.028	5.59	0.25	6.17	0.42	21
	2	0.018	4.24	0.19	7.17	0.22	
	3	0.020	4.76	0.17	7.40	0.42	
	4	0.022	4.71	0.15	7.05	0.37	
	AVG	0.022	4.82	0.19	6.95	0.36	

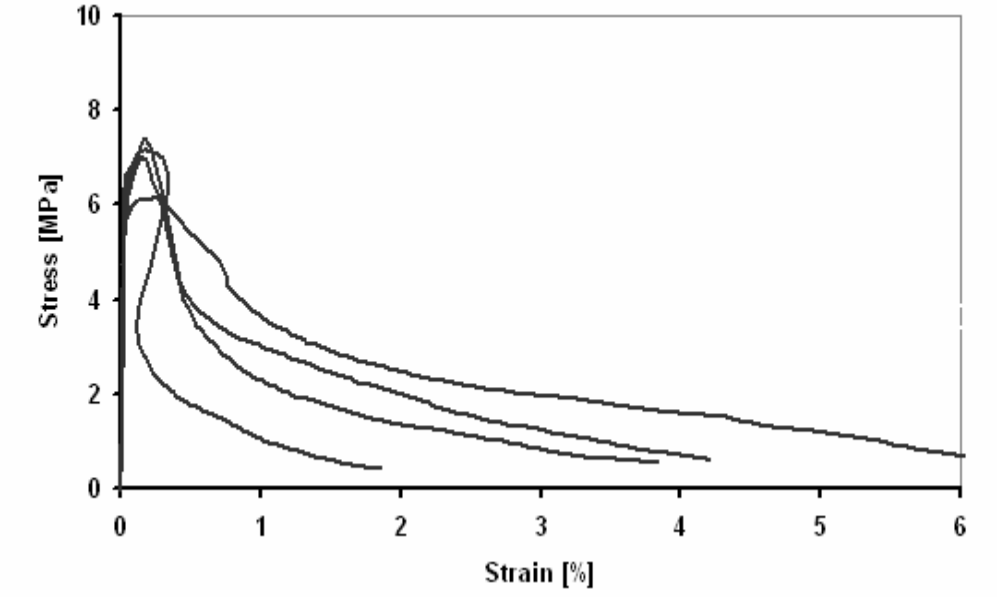

Appendix 3

The test details of series III mixes

SF8

		Tensile strength					Age on test
		ε_M [%]	σ_M [N/mm^2]	ε_U [%]	σ_U [N/mm^2]	ε_F [%]	
SF8	1	0.022	2.77	0.57	3.44	1.63	21
	2	0.010	1.23	0.38	3.21	3.61	
	3	0.021	2.23	1.03	3.41	2.39	
	4	0.018	2.49	0.81	3.34	1.23	
	AVG	0.018	2.18	0.70	3.35	2.22	

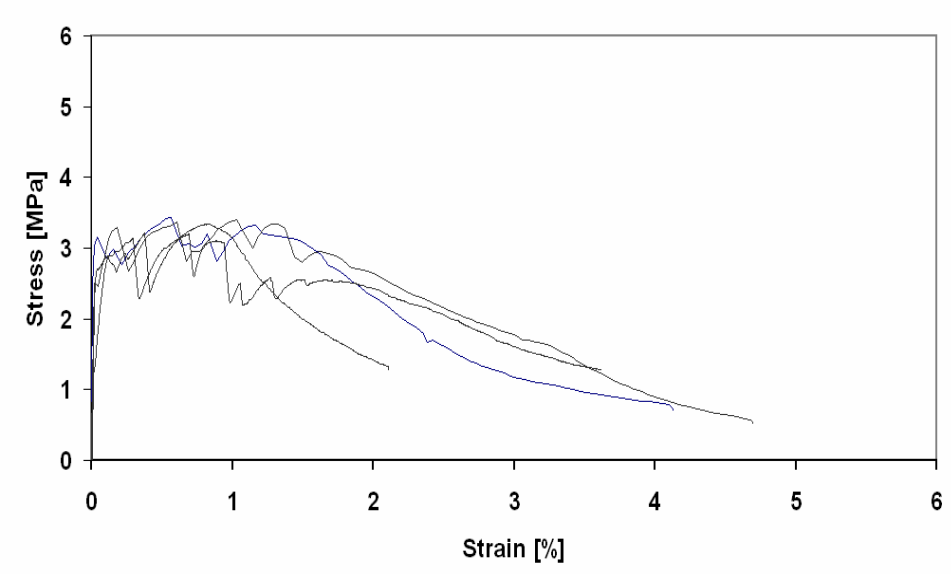

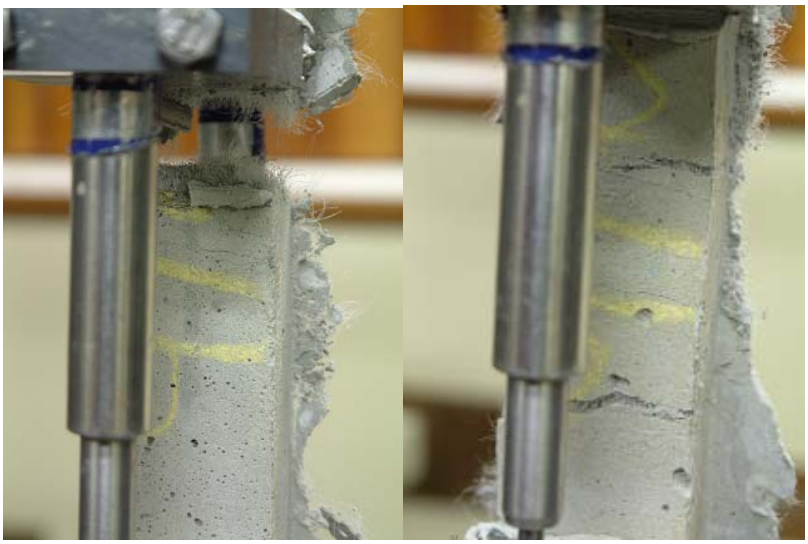

SF9A

		Tensile strength					Age on test
		ε_M [%]	σ_M [N/mm^2]	ε_U [%]	σ_U [N/mm^2]	ε_F [%]	
SF9A	1	0.027	1.99	0.55	2.33	0.55	21
	2	0.032	2.50	3.29	2.90	4.10	
	3	0.028	2.43	3.42	3.07	5.40	
	4	0.022	1.63	0.54	2.47	3.28	
	AVG	0.027	2.14	1.95	2.69	3.34	

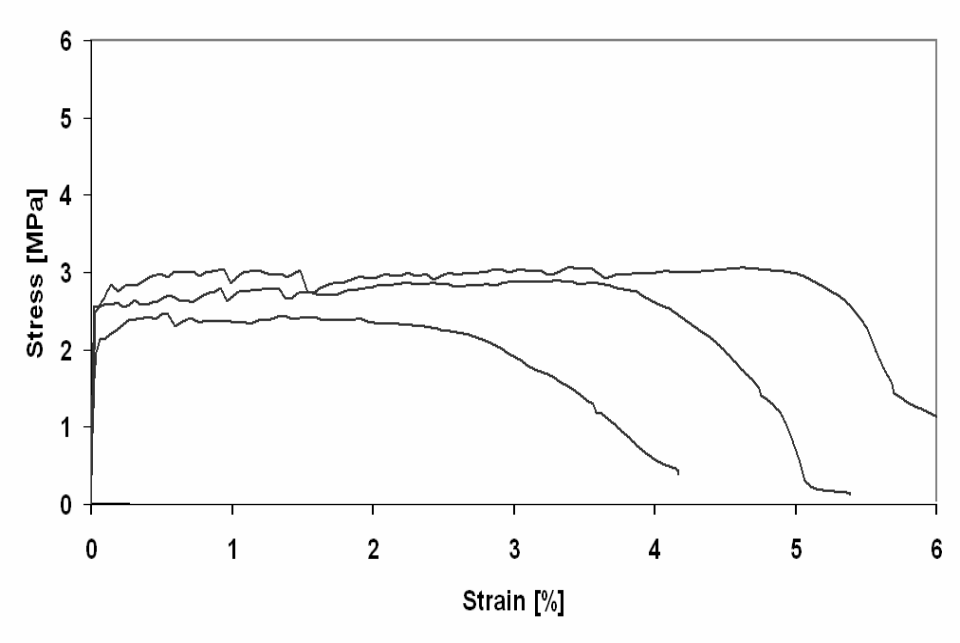

SF9B

		Tensile strength					Age on test
		ε_M [%]	σ_M [N/mm^2]	ε_U [%]	σ_U [N/mm^2]	ε_F [%]	
SF9B	1	0.021	1.26	4.11	2.65	5.34	21
	2	0.018	0.89	3.23	2.10	4.94	
	3	0.030	1.48	2.02	1.98	3.40	
	4	0.025	1.07	2.97	1.92	5.52	
	AVG	0.024	1.18	3.08	2.16	4.80	

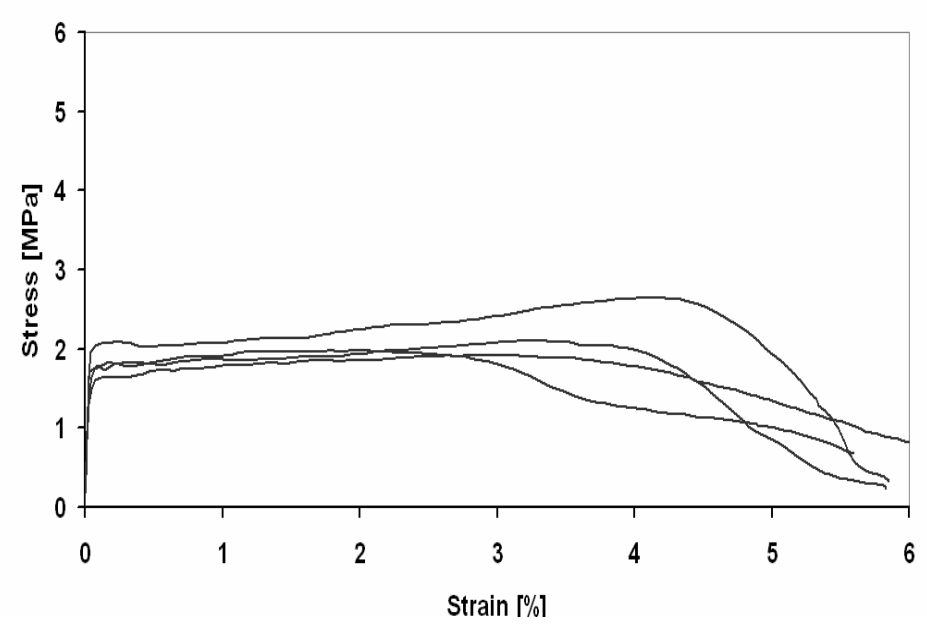

SF10

		Tensile strength					Age on test
		ε_M [%]	σ_M [N/mm^2]	ε_U [%]	σ_U [N/mm^2]	ε_F [%]	
SF10	1	0.034	3.18	0.28	5.59	0.95	21
	2	0.012	1.32	0.35	5.18	2.66	
	3	0.015	1.46	0.37	5.16	2.20	
	4	0.029	2.74	0.45	5.53	2.03	
	AVG	0.023	2.17	0.36	5.36	1.96	

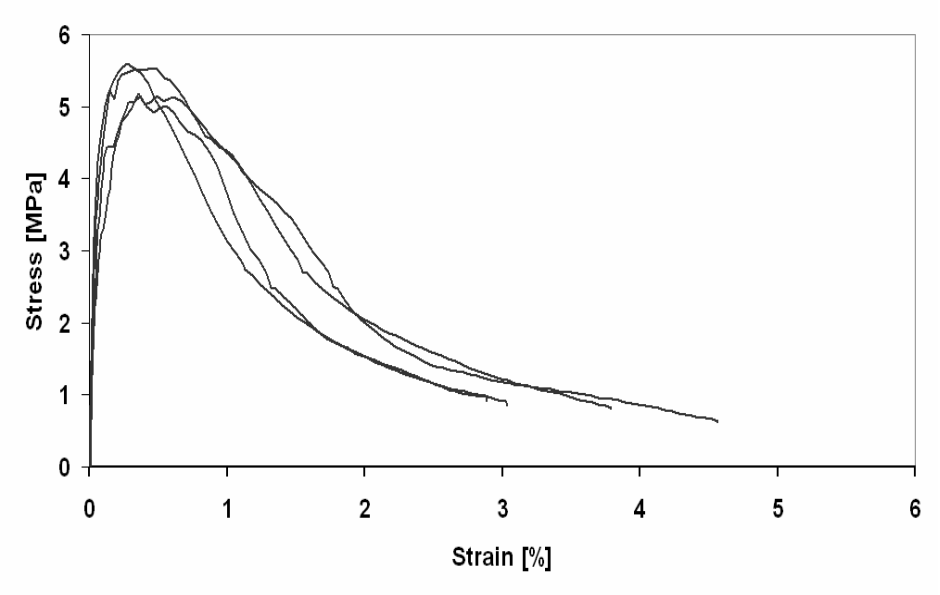

SF11

		Tensile strength					Age on test
		ε_M [%]	σ_M [N/mm^2]	ε_U [%]	σ_U [N/mm^2]	ε_F [%]	
SF11	1	0.028	5.67	0.51	6.23	0.75	21
	2	0.034	2.13	0.40	5.50	1.34	
	3	0.022	4.97	0.78	6.95	1.38	
	4	0.033	2.74	0.52	6.20	1.48	
	AVG	0.029	3.88	0.55	6.22	1.24	

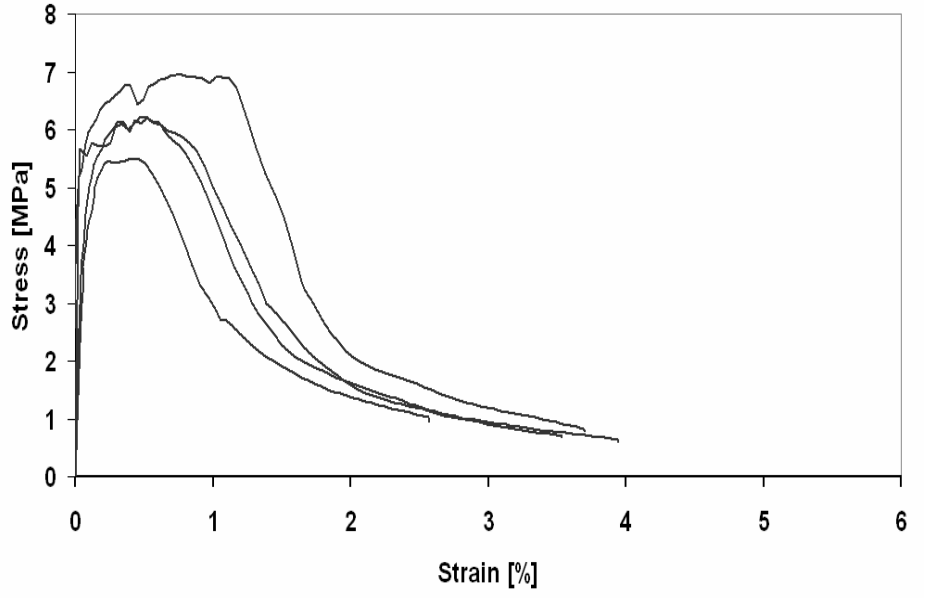

SF12

		Tensile strength					Age on test
		ε_M [%]	σ_M [N/mm^2]	ε_U [%]	σ_U [N/mm^2]	ε_F [%]	
SF12	1	0.007	1.72	0.33	4.74	2.14	21
	2	0.018	1.91	0.61	4.34	1.88	
	3	0.024	1.57	1.36	4.77	2.61	
	4	0.030	2.00	1.10	6.09	2.75	
	AVG	0.020	1.80	0.85	4.99	2.35	

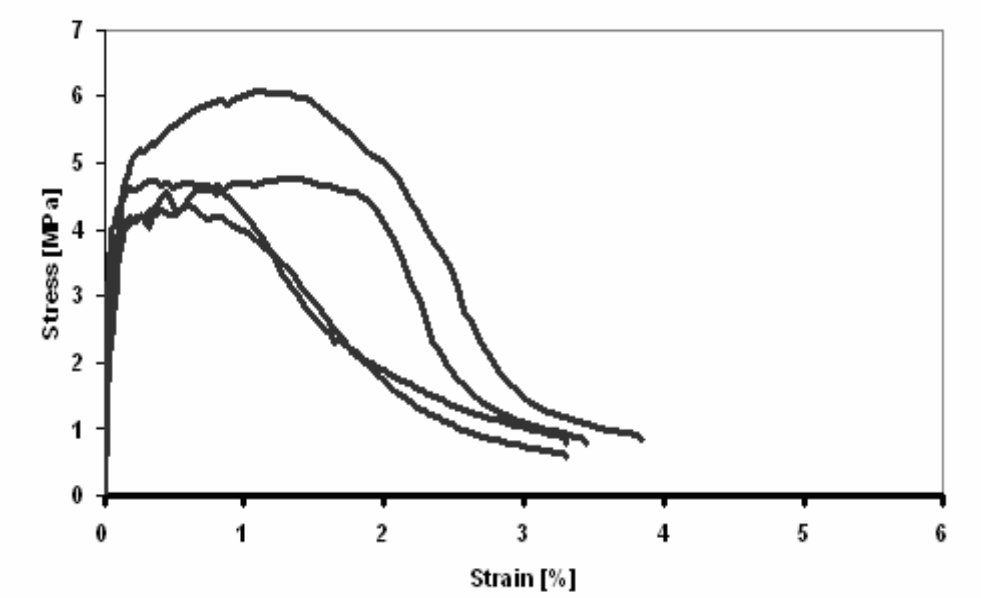

SF13

		Tensile strength					Age on test
		ε_M [%]	σ_M [N/mm^2]	ε_U [%]	σ_U [N/mm^2]	ε_F [%]	
SF13	1	0.359	2.75	5.13	3.79	5.63	340
	2	0.269	2.43	0.62	2.91	1.71	
	3	0.349	3.17	4.12	3.97	4.29	
	4						
	AVG	0.326	2.78	3.29	3.56	3.88	

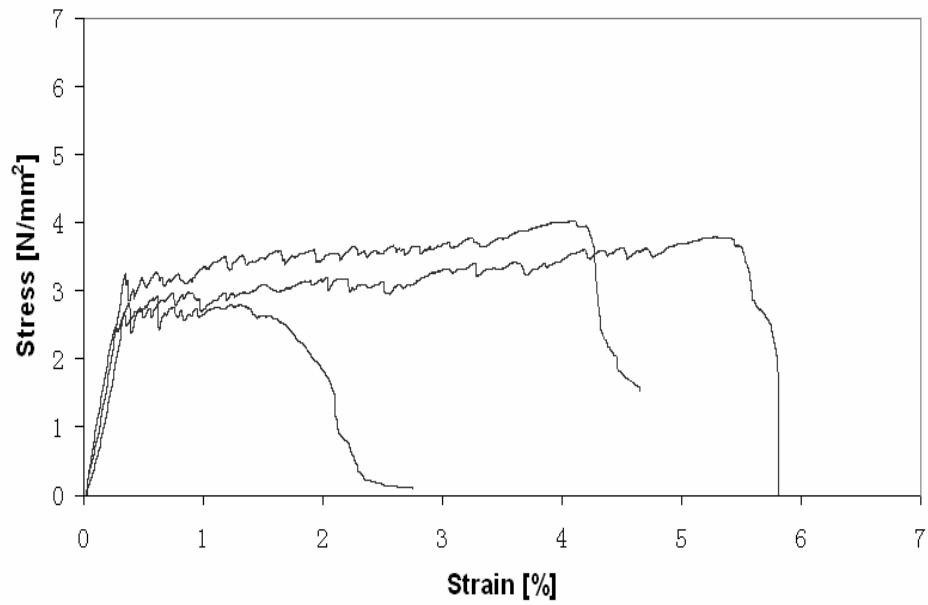

SF14

Table A Direct tension test result for SF14

		Tensile strength					Age on test
		ε_M [%]	σ_M [N/mm^2]	ε_U [%]	σ_U [N/mm^2]	ε_F [%]	
SF14	1	0.036	4.76	5.18	6.18	5.99	340
	2	0.470	3.84	3.92	5.87	4.30	
	3	0.610	4.07	3.21	5.72	3.96	
	4	0.430	4.20	3.26	5.00	3.94	
	AVG	0.387	4.22	3.89	5.69	4.55	

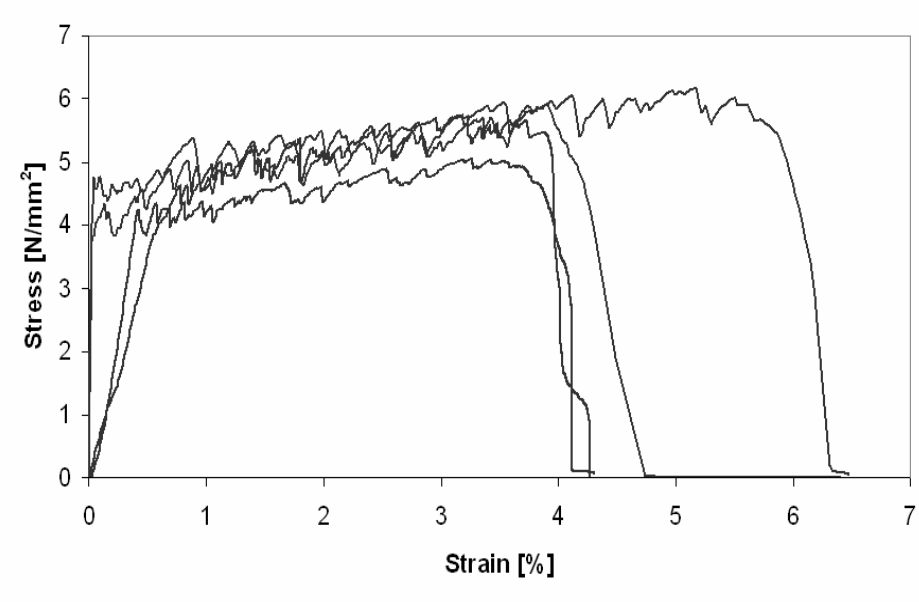

SF15

		Tensile strength					Bending MOR [N/mm²]	processing
		ε_M [%]	σ_M [N/mm²]	ε_U [%]	σ_U [N/mm²]	ε_F [%]		
SF15	1	0.058	1.33	1.17	1.63	2.46	4.91	Cast
	2	0.023	0.94	0.34	1.37	0.96	5.04	Cast
	3						4.97	Extruding
	4						5.25	Extruding
	AVG	0.041	1.13	0.75	1.50	4.66		

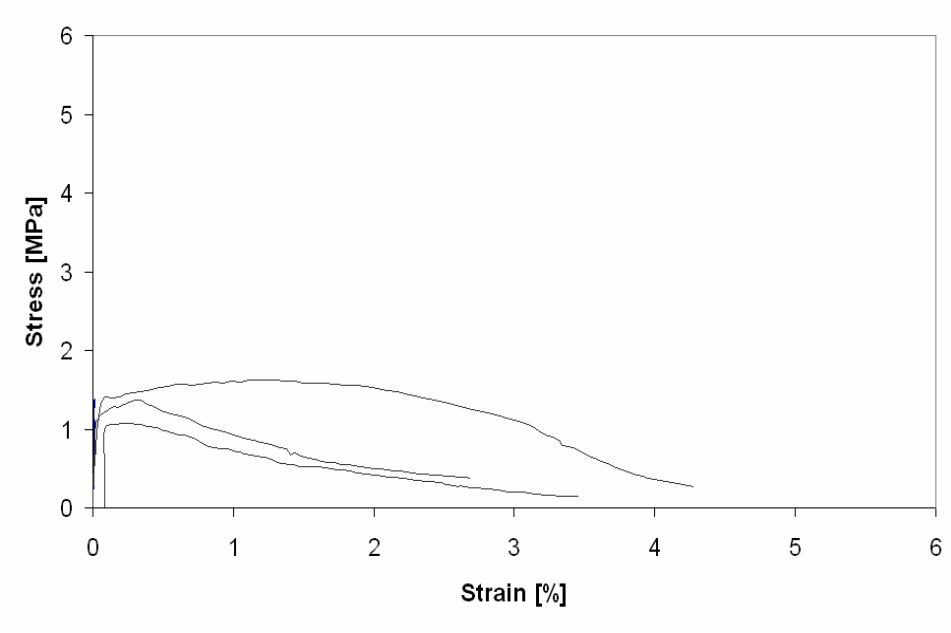

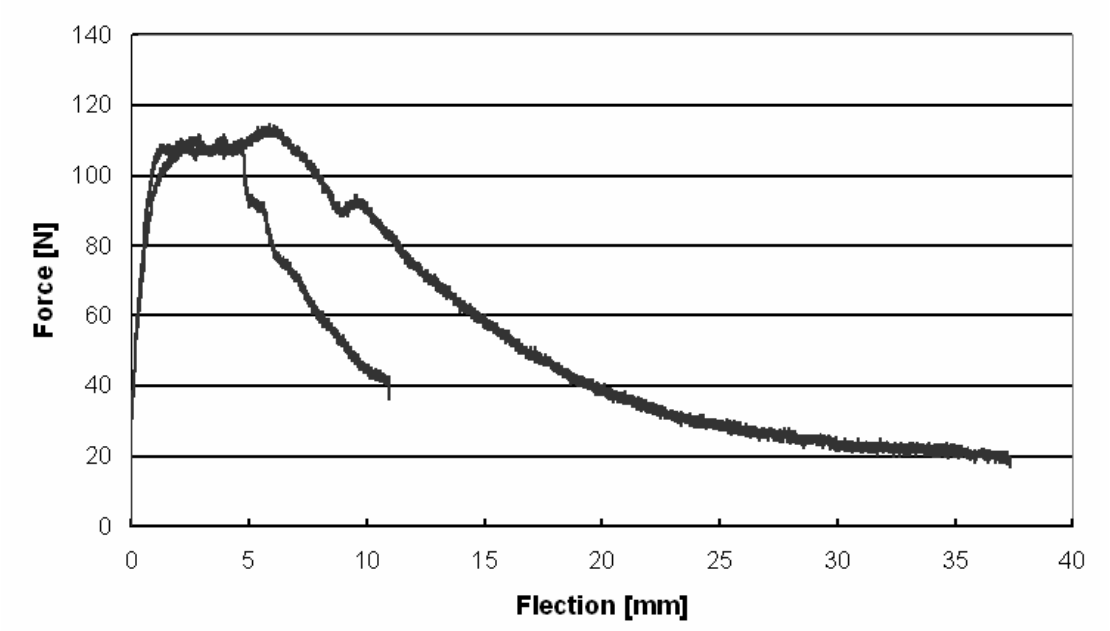

*Cast specimen bending behaviours

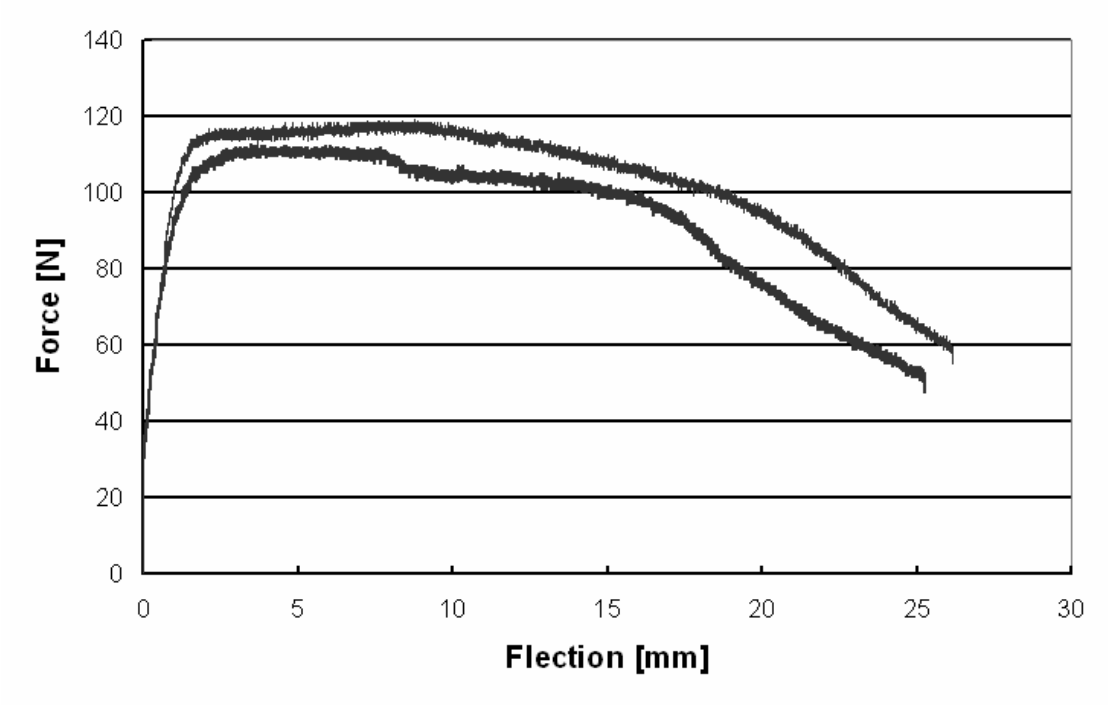

*Extrusion specimen bending behaviours

SF17A

		Tensile strength					Bending MOR [N/mm^2]	Age on test
		ε_M [%]	σ_M [N/mm^2]	ε_U [%]	σ_U [N/mm^2]	ε_F [%]		
SF17A	1	0.013	2.17	0.08	2.60	1.20	9.27	
	2	0.019	1.76	0.82	3.35	4.30	8.63	
	3	0.027	1.86	0.16	3.19	3.01	8.16	
	4	0.017	1.49	0.15	2.79	2.59		
	AVG	0.020	1.82	0.30	2.98	2.78		

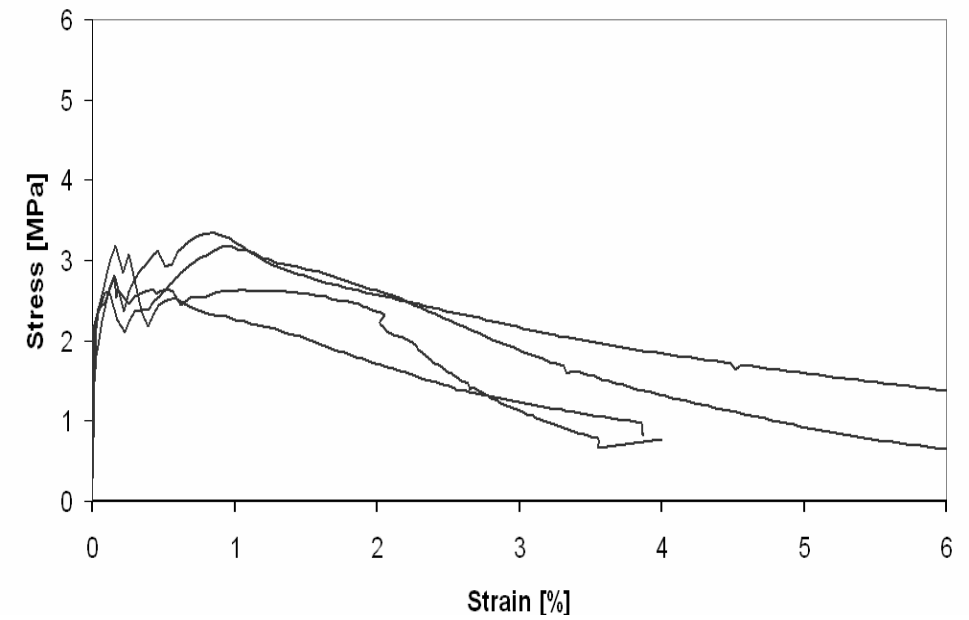

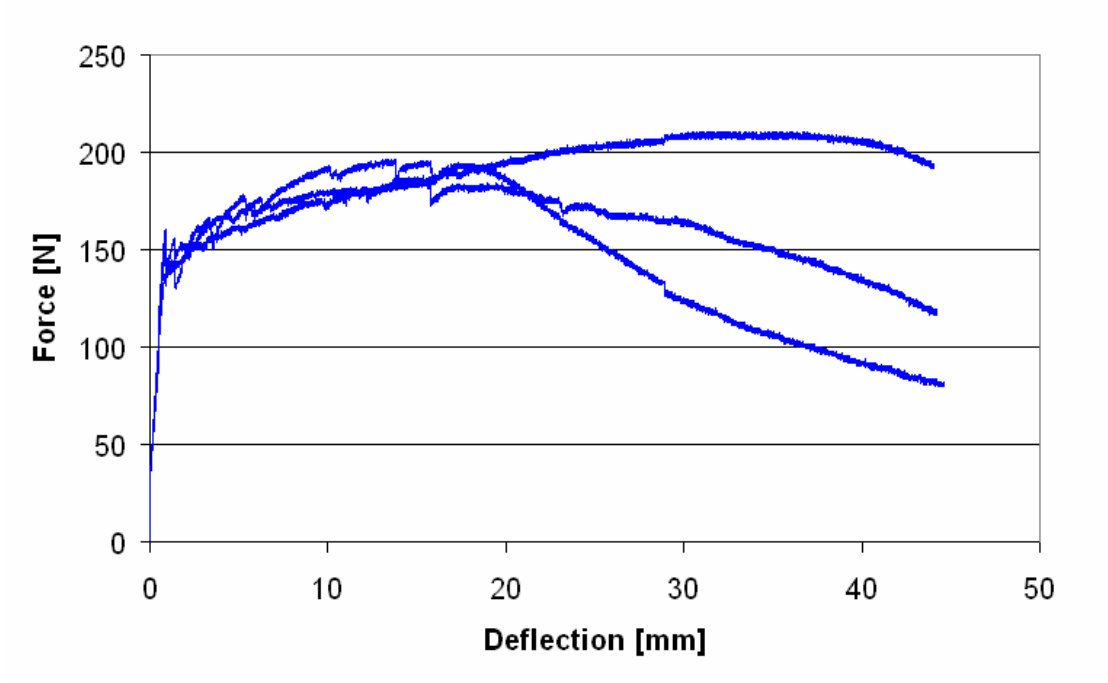
250
200
150
100
50
0
Force [N]
0
10
20
30
40
50
Deflection [mm]

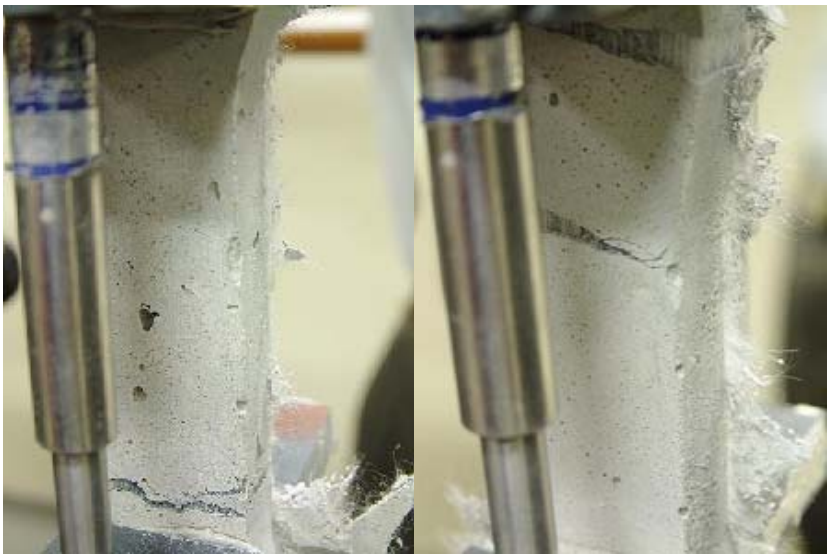

SF17B

		Tensile strength					Age on test
		ε_M [%]	σ_M [N/mm^2]	ε_U [%]	σ_U [N/mm^2]	ε_F [%]	
SF17B	1	0.020	2.90	0.20	3.86	0.93	225
	2	0.021	1.97	1.53	2.79	3.30	
	3	0.027	2.24	0.69	2.37	0.95	
	4						
	AVG	0.023	2.37	0.81	3.01	1.73	

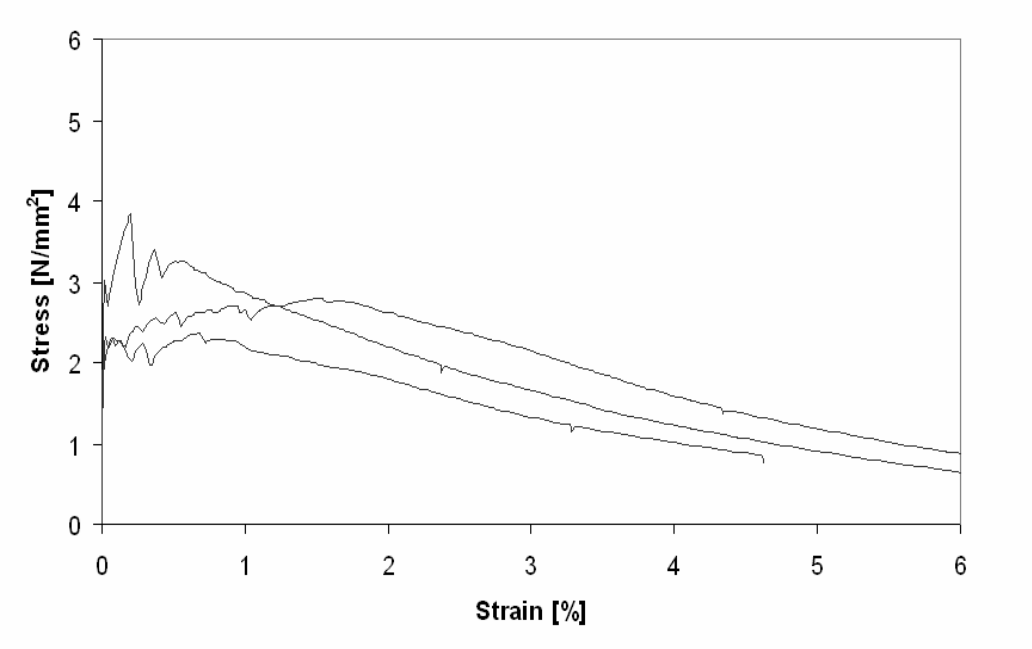

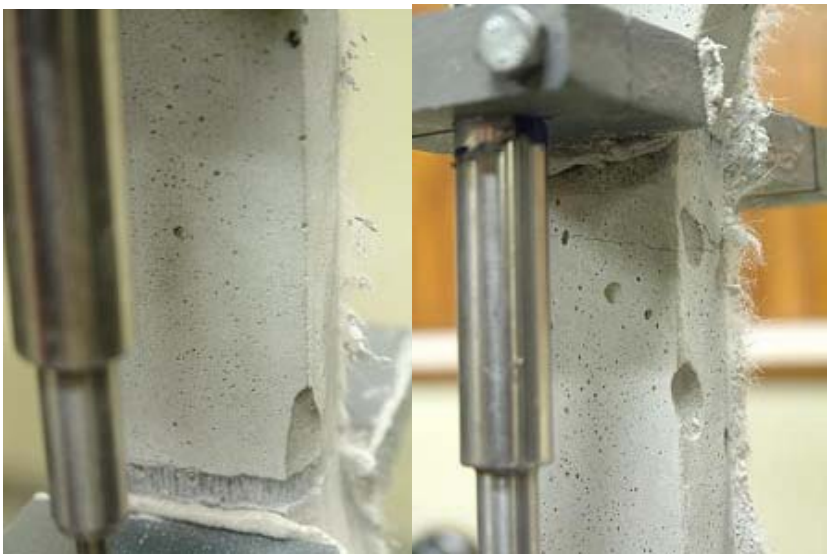

SF18

		Tensile strength					Age on test
		ε_M [%]	σ_M [N/mm^2]	ε_U [%]	σ_U [N/mm^2]	ε_F [%]	
SF18	1	0.021	3.57	0.10	5.37	0.34	21
	2	0.012	1.87	0.22	4.95	0.94	
	3	0.030	4.56	0.43	6.56	0.93	
	4	0.025	5.66	0.03	5.73	0.37	
	AVG	0.022	3.92	0.19	5.65	0.65	

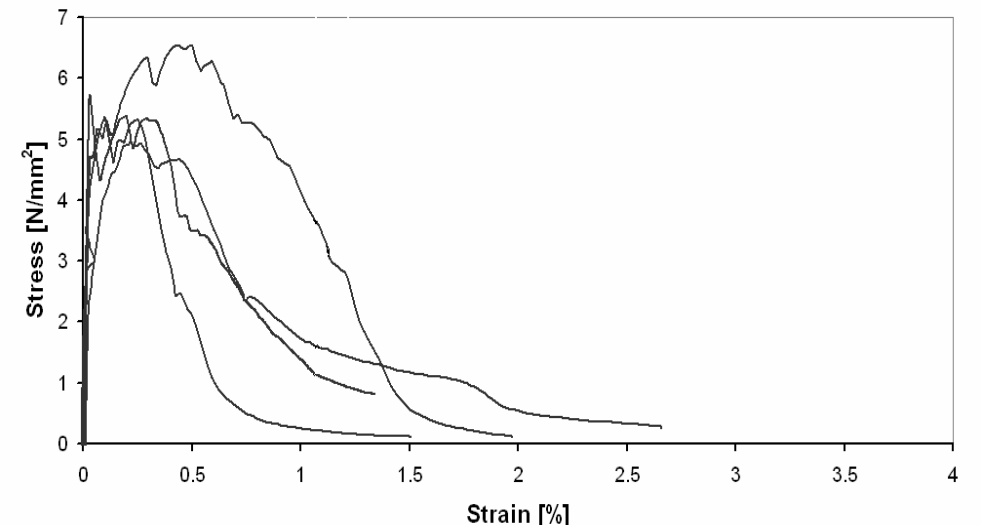

SF19

		Tensile strength					Bending MOR	Age on test
		ε_M [%]	σ_M [N/mm^2]	ε_U [%]	σ_U [N/mm^2]	ε_F [%]		
SF19	1	0.09	2.41	5.07	4.09	4.75		21
	2	0.1	1.44	2.67	2.50	5.18		
	3	0.061	1.80	1.68	2.23	3.34		
	4	0.11	2.00	5.25	3.53	5.51		
	AVG	0.090	1.91	3.67	3.09	4.69		

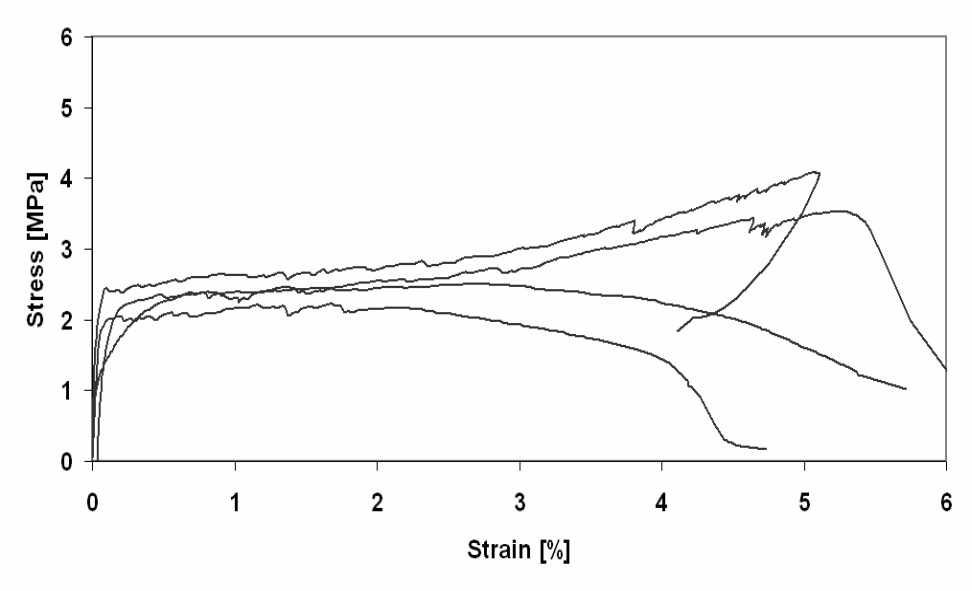
Stress [MPa]
Strain [%]
0
1
2
3
4
5
6

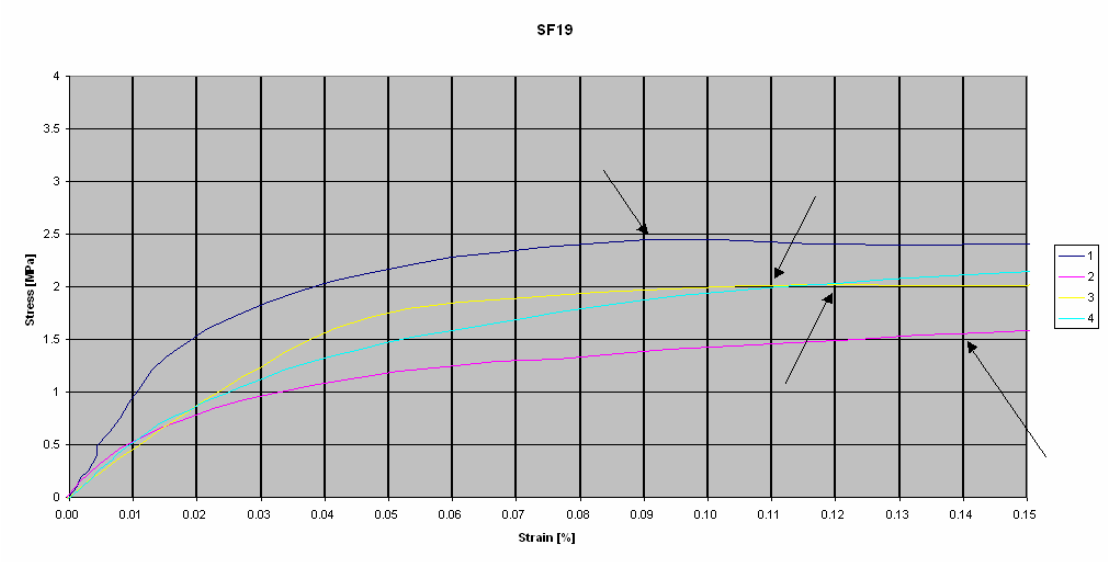
SF19
Stress [MPa]
Strain [%]
1
2
3
4

SF20

		Tensile strength					Bending MOR	Age on test
		ε_M [%]	σ_M [N/mm^2]	ε_U [%]	σ_U [N/mm^2]	ε_F [%]		
SF20	1	0.06	1.81	3.00	2.45	4.10		21
	2	0.06	1.85	4.50	2.92	4.02		
	3	0.07	1.42	1.88	1.73	2.94		
	4	0.06	1.70	4.22	2.58	5.49		
	AVG	0.063	1.70	3.40	2.42	4.14		

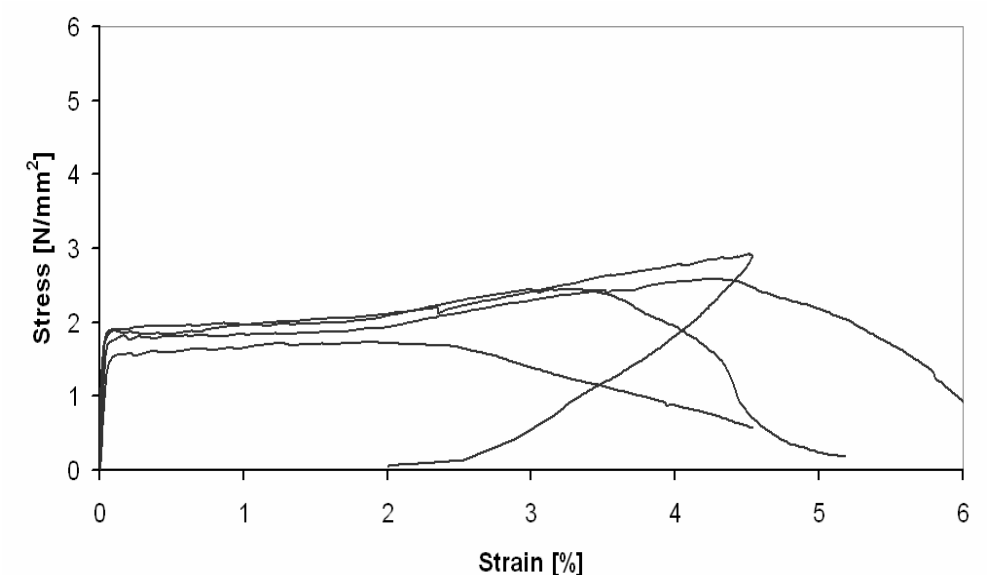

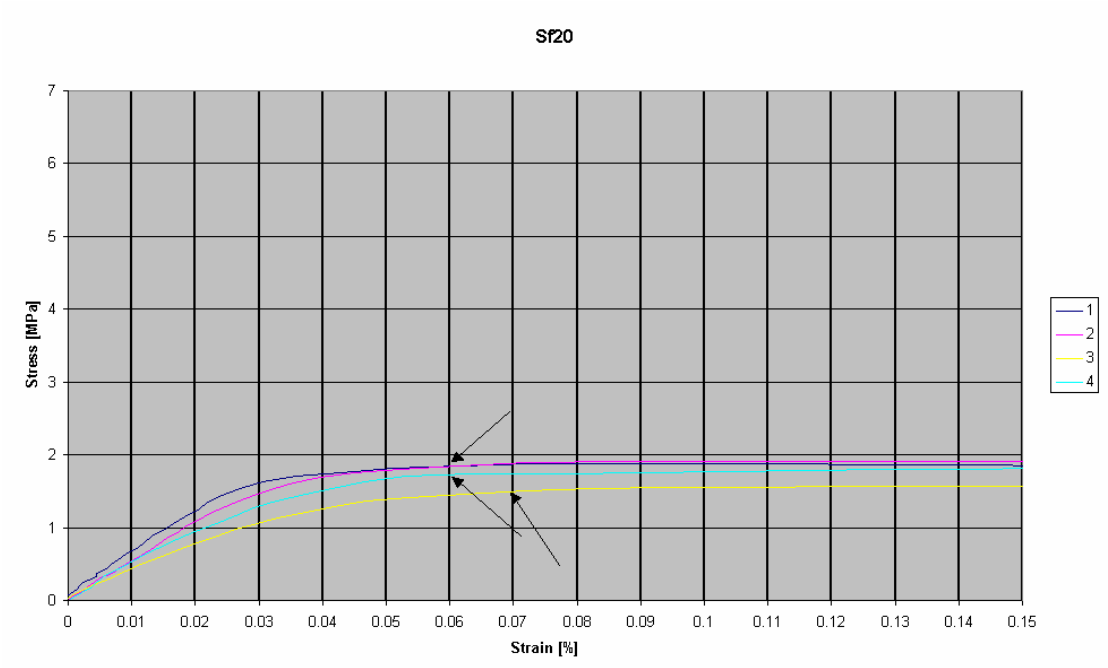

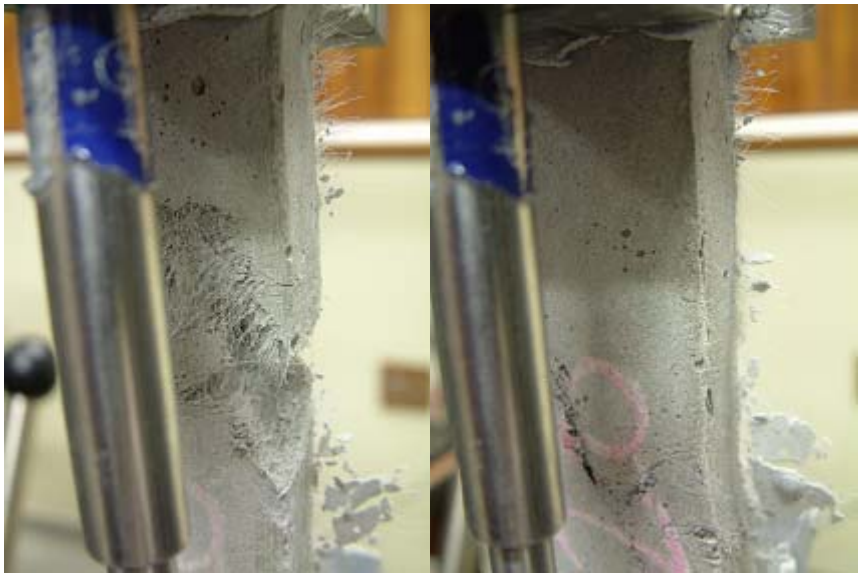

SF21

		Tensile strength					Bending MOR	Age on test
		ε_M [%]	σ_M [N/mm^2]	ε_U [%]	σ_U [N/mm^2]	ε_F [%]		
SF21	1	0.080	1.64	4.33	3.28	4.79		21
	2	0.060	1.97	3.63	2.78	4.51		
	3	0.050	1.61	3.58	2.81	4.08		
	4	0.060	1.92	4.39	2.86	4.87		
	AVG	0.063	1.78	3.98	2.93	4.56		

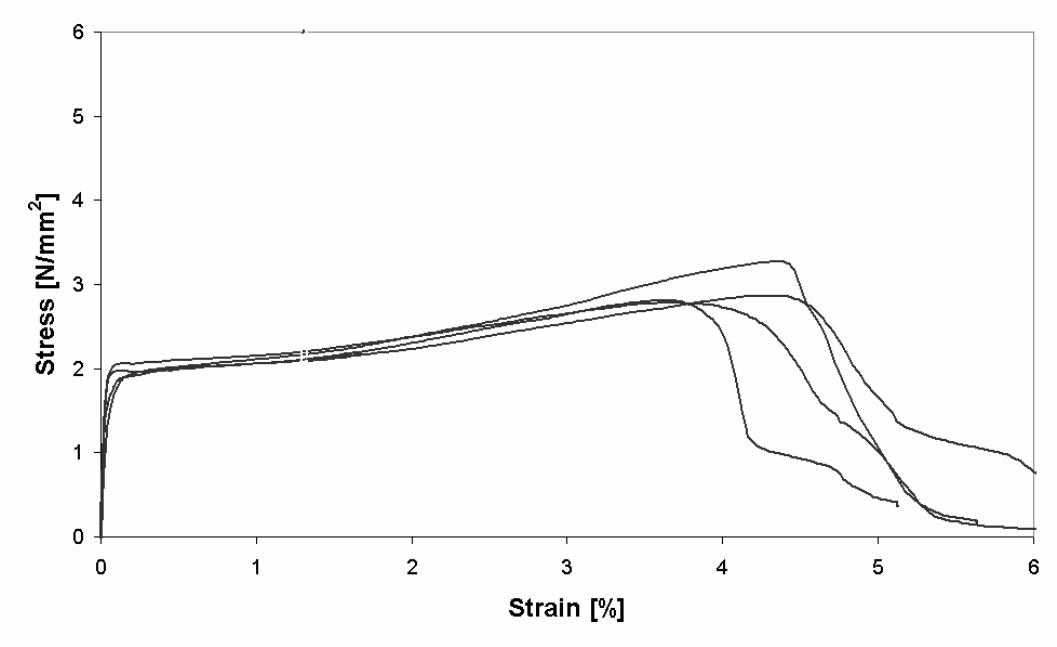
Stress [N/mm²]
Strain [%]
0
1
2
3
4
5
6

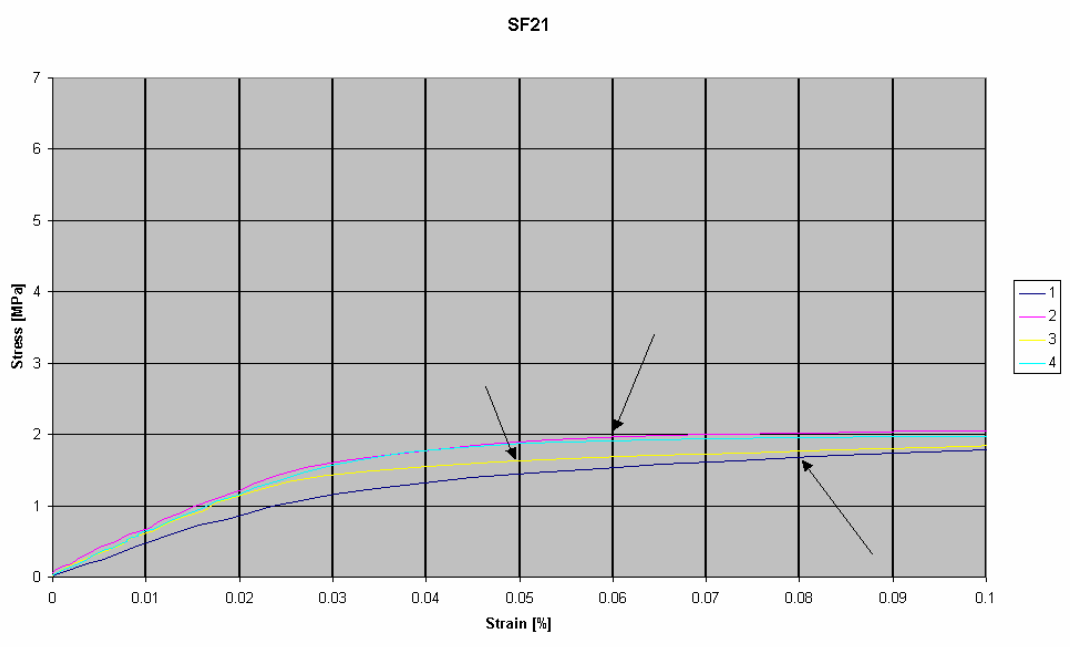
SF21
Stress [MPa]
Strain [%]
0
1
2
3
4
5
6
7
0.01
0.02
0.03
0.04
0.05
0.06
0.07
0.08
0.09
0.1
1
2
3
4

meng 5

		Tensile strength					Age on test
		ε_M [%]	σ_M [N/mm^2]	ε_U [%]	σ_U [N/mm^2]	ε_F [%]	
Meng5	1	0.29	3.27	0.49	6.07	0.93	21
	2	0.29	4.93	0.63	5.54	0.69	
	3	0.29	3.79	0.47	6.94	0.77	
	4	0.27	3.19	0.64	5.90	0.75	
	AVG	0.29	3.80	0.56	6.11	0.79	

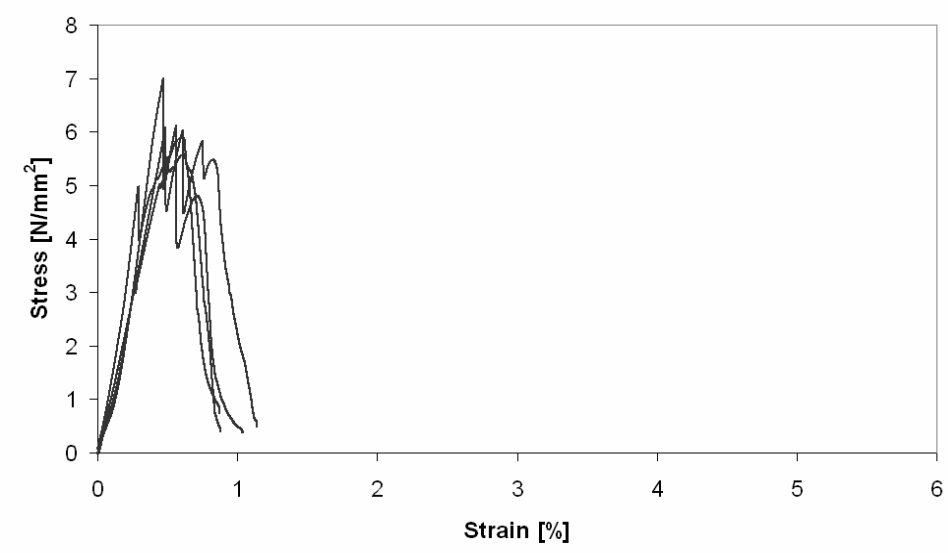

*The mix meng 5 was made by W.P. Boshoff

Compression test result

Compression test result			
Number	N/mm^2		N/mm^2
Steel fibre		PVA fibre	
GSF1	72.6	GSF8	30.3
	69.6		30.7
	71.1		30.2
			30.4
GSF2	80.7	GSF9A	16.6
	83		17.4
	98.8		17.5
	87.5		17.17
GSF4	92.7	GSF9B	9.7
	98.4		10.3
	96.4		10.3
	95.83		10.1
GSF5	142.1	GSF10	51.6
	133.9		51.6
	138.8		59.6
	138.27		54.27
GSF6	80	GSF11	39.2
	79.8		42.5
	79		51.7
	79.6		44.47
GAF7(3%Steelfibre)	51.8	GSF12	46.6
	51.3		45.4
	53.5		45.6
	52.2		45.87
GSS1	75.2	GSS2	45.8
30%Slag+30%FA	81.7	(70% Slag)	47.4
	80.8		44.7
	79.23		45.97